TECHNICAL UNIVERSITY OF CRETE

SCHOOL OF PRODUCTION ENGINEERING AND MANAGEMENT

Structure-Property Relationships and Stability Studies of Multi-Promoted Catalytic Systems for Nitrogen (NOx) and/or Nitrous (N₂O) Oxides Abatement

Thesis submitted for the partial fulfillment of the requirements for the degree of

Doctor of Philosophy (PhD)

by

ELENI PACHATOURIDOU

Associate Prof. Michalis Konsolakis (Supervisor, TUC)

Researcher B' Eleni Iliopoulou (Member of the advisory committee, CPERI/CERTH)
Prof. Ioannis Yentekakis (Member of the advisory committee, TUC)

Chania, Greece, July 2017

TECHNICAL UNIVERSITY OF CRETE

SCHOOL OF PRODUCTION ENGINEERING AND MANAGEMENT

Structure-Property Relationships and Stability Studies of Multi Promoted Catalytic Systems for Nitrogen (NOx) and/or Nitrous (N$_2$O) Oxides Abatement

by

ELENI PACHATOURIDOU

Advisory Committee
Michalis Konsolakis (Supervisor)
Associate Professor, School of Production Engineering and Management
Technical University of Crete (TUC)

Eleni Iliopoulou (Co-supervisor, member of the advisory committee)
Researcher B', Chemical Process and Energy Resources Institute (CPERI)
Centre for Research and Technology Hellas (CERTH)

Ioannis Yentekakis (Member of the advisory committee)
Professor, School of Environmental Engineering
Technical University of Crete (TUC)

Thesis Examination Committee
Georgios Marnellos
Associate Professor, Department of Mechanical Engineering
University of Western Macedonia (UOWM)

Konstantinos Triantafyllidis
Associate Professor, Department of Chemistry
Aristotle University of Thessaloniki (AUTH)

Spiros Papaefthimiou
Assistant Professor, School of Production Engineering and Management
Technical University of Crete (TUC)

Nikolaos Kallithrakas-Kontos
Professor, School of Mineral Resources Engineering
Technical University of Crete (TUC)

ΠΟΛΥΤΕΧΝΕΙΟ ΚΡΗΤΗΣ
ΣΧΟΛΗ ΜΗΧΑΝΙΚΩΝ ΠΑΡΑΓΩΓΗΣ ΚΑΙ ΔΙΟΙΚΗΣΗΣ

ΠΡΑΚΤΙΚΟ
ΤΗΣ ΕΠΤΑΜΕΛΟΥΣ ΕΞΕΤΑΣΤΙΚΗΣ ΕΠΙΤΡΟΠΗΣ
ΓΙΑ ΤΗΝ ΚΡΙΣΗ ΤΗΣ ΔΙΔΑΚΤΟΡΙΚΗΣ ΔΙΑΤΡΙΒΗΣ

της Ελένης Παχατουρίδου, του Παναγιώτη

ΔΙΠΛΩΜΑΤΟΥΧΟΥ/ΠΤΥΧΙΟΥΧΟΥ ΤΟΥ ΤΜΗΜΑΤΟΣ

Χημείας του Πανεπιστημίου Ιωαννίνων

Η εξεταστική επιτροπή που διορίσθηκε σύμφωνα με τις κείμενες διατάξεις και την απόφαση της Γενικής Συνέλευσης της Σχολής Μηχανικών Παραγωγής και Διοίκησης στη συνεδρίαση 10η/20.6.2017 για την κρίση της διδακτορικής διατριβής της **Ελένης Παχατουρίδου**, συνήλθε σε συνεδρίαση σήμερα την **Δευτέρα 10 Ιουλίου 2017** και παρακολούθησε την υποστήριξη της διατριβής με τίτλο:

«**Σχέση δομής-δραστικότητας και μελέτες σταθερότητας δομικά ή/και επιφανειακά ενισχυμένων καταλυτικών συστημάτων αποδόμησης οξειδίων (NO$_x$) ή/και υποξειδίου (N$_2$O) του αζώτου**»

Αγγλικός τίτλος: «**Structure-property relationships and stability studies of multi-promoted catalytic systems for nitrogen (NO$_x$) and/or nitrous (N$_2$O) oxides abatement**»

Μετά την ανάπτυξη της διατριβής, τα μέλη της εξεταστικής επιτροπής, έκαναν ερωτήσεις στην υποψήφια κα Ελένη Παχατουρίδου, τόσο γενικού περιεχομένου, όσο και σχετικές με το θέμα της διατριβής.

Στη συνέχεια, αποχώρησε η υποψήφια και ακολούθησε συζήτηση της επιτροπής.

Η επιτροπή, μετά από ψηφοφορία, έκρινε ότι η διατριβή της Ελένης Παχατουρίδου, είναι πρωτότυπη και αποτελεί ουσιαστική συμβολή στην επιστήμη, προτείνει δε προς τη Γενική Συνέλευση με ειδική σύνθεση της Σχολής, **ομόφωνα** να του απονείμει τον τίτλο του Διδάκτορος.

Η ΕΠΙΤΡΟΠΗ   **ΥΠΟΓΡΑΦΗ**

1. Μιχάλης Κονσολάκης, επιβλέπων, ΜΠΔ, Πολυτεχνείο Κρήτης

2. Ελένη Ηλιοπούλου, ΙΔΕΠ/ΕΚΕΤΑ

3. Ιωάννης Γεντεκάκης, ΜΗΠΕΡ, Πολυτεχνείο Κρήτης

4. Γεώργιος Μαρνέλλος, Πανεπ. Δυτ. Μακεδονίας

5. Κωνσταντίνος Τριανταφυλλίδης, ΑΠΘ

6. Σπύρος Παπαευθυμίου, ΜΠΔ, Πολυτεχνείο Κρήτης

7. Νικόλαος Καλλίθρακας-Κόντος, ΜΗΧΟΠ, Πολυτεχνείο Κρήτης

Στο πλαίσιο του εν λόγω ερευνητικού προγράμματος, συνεργάστηκαν στενά για την ολοκλήρωση του τα παρακάτω εργαστήρια:

- Εργαστήριο Περιβαλλοντικών Καυσίμων και Υδρογονανθράκων (ΕΠΚΥ/ΕΚΕΤΑ)
- Εργαστήριο Τεχνολογίας Περιβάλλοντος (Πανεπιστήμιο Δ. Μακεδονίας)
- Εργαστήριο Φυσικοχημείας και Χημικών Διεργασιών (Πολυτεχνείο Κρήτης)
- Εργαστήριο Εναλλακτικών Καυσίμων & Περιβαλλοντικής Κατάλυσης (ΤΕΙ Δ. Μακεδονίας)

Μεγάλο μέρος των ερευνητικών προσπαθειών του έργου οδήγησαν στην εκπόνηση των κάτωθι δύο διδακτορικών διατριβών:

(1) **«Σχέση δομής-δραστικότητας και μελέτες σταθερότητας δομικά ή/και επιφανειακά ενισχυμένων καταλυτικών συστημάτων αποδόμησης οξειδίων (NOx) ή/και υποξειδίου (N$_2$O) του αζώτου/Structure-property relationships and stability studies of multi-promoted catalytic systems for nitrogen (NOx) and/or nitrous (N$_2$O) oxides abatement»** υπό της **Ελένης Παχατουρίδου**.
Επιβλέπων: Αν. Καθηγητής Μιχάλης Κονσολάκης

(2) **«Ανάπτυξη καινοτόμων καταλυτικών συστημάτων μέσω της συνέργειας δομικών και επιφανειακών προωθητών για τον περιορισμό των εκπομπών υποξειδίου του αζώτου (N$_2$O)/Development of novel catalytic materials through the synergy of structure and surface promoters for the abatement of nitrous oxide (N$_2$O)»** υπό της **Ελένης Πάπιστα**.
Επιβλέπων: Αν. Καθηγητής Γεώργιος Μαρνέλλος

Λόγω των συγκεκριμένων πρακτικών και επιστημονικών στόχων του εν λόγω ερευνητικού έργου, οι εκπονηθείσες στα πλαίσια του διδακτορικές διατριβές είναι κατ' ανάγκην αλληλένδετες και συμπληρωματικές αλλά με σαφώς διακριτό φυσικό αντικείμενο/περιεχόμενο. Εξαιτίας της συμπληρωματικότητας των διατριβών, σε κάθε μια

από αυτές κρίθηκε σκόπιμη η παράθεση και παρουσίαση κάποιων αποτελεσμάτων της άλλης σε μικρότερη ή μεγαλύτερη έκταση, με σκοπό την επιστημονική τεκμηρίωση των ερευνητικών συμπερασμάτων αλλά και την επίδειξη της επίτευξης των συγκλινόντων στόχων των διατριβών. Ωστόσο, για να παραμείνει σαφές και αναλλοίωτο, πέραν πάσης αμφιβολίας, το χαρακτηριστικό της διακριτότητας του περιεχομένου και του υλοποιημένου φυσικού αντικείμενου των δυο διατριβών, στα σημεία εκείνα του περιεχομένου της κάθε μίας όπου φιλοξενούνται αποτελέσματα της άλλης, τονίζεται με σαφήνεια η πηγή προέλευσης των αποτελεσμάτων και γίνεται η σχετική παραπομπή (αναφορά).

ΕΥΧΑΡΙΣΤΙΕΣ

SUMMARY

The current thesis aims at exploring the impact of structural (CeO_2, La_2O_3) and surface (K) promoters on the solid state properties and the surface chemistry of Al_2O_3-based noble metal (Pt, Pd, Ir) catalysts, during nitrogen (NOx) and/or nitrous (N_2O) oxides abatement. Various characterization techniques, such as N_2 physisorption (BET method), X-ray diffraction (XRD), temperature programmed methods (TPR/TPD), microscopy methods (HRTEM, STEM) and infrared spectroscopy (FTIR, DRIFTS) were employed to gain insight into the impact of structural/surface promoters on the physicochemical characteristics, as well as on the activity and stability performance of the as-prepared catalysts. In any case, particular emphasis was devoted in the present thesis on the underlying mechanism of promoters and the establishment of structure-property relationships.

It is well documented in our days that NOx and N_2O are contributing in various environmental problems such as photochemical smog and acid rain, while they have a direct harmful effect on human health. N_2O was considered for many years as a relatively innocuous gas. However, in recent years, it has been recognized as a harmful pollutant, due to its contribution to the greenhouse effect and stratospheric ozone depletion, resulting in the destabilization of world climate. In this regard, the aim of the present thesis is the development of technologically advanced-in terms of design, composition, cost and efficiency-catalytic materials, which could abate N_2O and/or NOx from combustion flue gases.

The present PhD thesis is divided into the following chapters:

Chapter I describes the environmental problems associated with the NOx and N_2O emissions to the atmosphere, their sources, the current European legislation, as well as the currently suggested abatement technologies and the corresponding catalytic systems.

Chapter II describes the procedure followed to prepare the catalysts used in this study, the characterization techniques and the experimental devices employed to carry out the catalytic tests. The following four chapters (chapters III to VI) are dedicated to the presentation and discussion of experimental results.

Chapter III investigates the N_2O decomposition (de-N_2O) performance of unmodified and structurally/surface modified Al_2O_3-based noble metal (Pt, Pd, Ir) catalysts of low metal content (0.25, 0.5 and 1.0 % wt.). The catalytic results imply that the de-N_2O performance is in general increased upon increasing metal loading, a fact being more intense over Ir-based catalysts. Under oxygen excess conditions, a moderate degradation is observed with Ir and Pd catalysts, while Pt-based catalysts are almost fully depressed. The superior de-N_2O performance of Ir- and Pd-based catalysts can be mainly interpreted by taking into account the formation of metal oxide phases, not easily susceptible to oxygen poisoning. The modification of alumina support with structure promoters (i.e. Ce and La), was investigated in order to improve the de-N_2O performance of Pd, Pt and Ir catalytic materials, especially in the presence of excess oxygen. The obtained results revealed the superiority of CeO_2-promoted Ir/Al_2O_3 catalyst (0.5Ir/AlCe) in the presence of excess O_2. The establishment of a certain $Ir^{\delta+}/Ir^0$ ratio and oxygen vacant sites (V_o) concentration in ceria, around very small supported Ir particles, under oxidative reaction conditions seem to largely promote a sustainable N_2O adsorption and decomposition into N_2 and O_2 over the CeO_2-promoted Ir/Al_2O_3 catalyst. To this end, Ir was selected for further studies, by investigating the modification of Ir/Al_2O_3 catalyst with a surface promoter (K). It was revealed that alkali-doping (0.5% wt. K) under oxygen excess conditions favored the N_2O adsorption and its concomitant dissociation and the formation of IrO_2, in which desorption of adsorbed oxygen species is facilitated. Both factors operate together towards high N_2O decomposition rates under oxygen excess conditions. The catalysts evaluation was carried out at the Environmental Technology Laboratory (UOWM) by Eleni Papista. The following publications were derived from the above described results:

*(1) **E. Pachatouridou**, E. Papista, E.F. Iliopoulou, A. Delimitis, G. Goula, I.V. Yentekakis, G.E. Marnellos, M. Konsolakis, "Nitrous Oxide Decomposition over Al_2O_3 Supported Noble Metals (Pt, Pd, Ir): Effect of Metal Loading and Feed Composition", Journal of Environmental Chemical Engineering 3 (2015) 815-821.*

*(2) **E. Pachatouridou**, E. Papista, A. Delimitis, M.A. Vasiliades, A.M. Efstathiou, M.D. Amiridis, O.S. Alexeev, D. Bloom, G.E. Marnellos, M. Konsolakis, E. Iliopoulou, "N_2O*

decomposition over ceria-promoted Ir/Al₂O₃ catalysts: The role of ceria", Applied Catalysis B 187 (2016) 259-268.

*(3) E. Papista, **E. Pachatouridou**, M.A. Goula, G.E. Marnellos, E. Iliopoulou, M. Konsolakis, I.V. Yentekakis, "Effect of alkali promoters (K) on nitrous oxide abatement over Ir/Al₂O₃ catalysts", Topics in Catalysis 59 (2016) 1020-1027.*

Chapter IV is devoted on the impact of H_2 as an additional reducing agent on the selective catalytic reduction (SCR) of NO with propene in excess oxygen, over γ-Al_2O_3 supported noble metal (Pt, Pd, Ir) catalysts of low noble metal loadings (0.5% wt.). Three different reaction schemes were employed: (i) $NO+C_3H_6+O_2$ (R#1), (ii) $NO+C_3H_6+O_2+H_2$ (R#2), and (iii) $NO+H_2+O_2$ (R#3). The Pt-, Pd- and Ir-catalyzed C_3H_6-SCR of NOx are significantly promoted by H_2. These promotional effects are not limited to a specific temperature window, but are extended in the whole temperature interval investigated (T: 50-400°C). The H_2 assisted C_3H_6-SCR of NOx is more substantial on Pt, then on Ir and less on Pd. The influence of H_2 on the oxidation state of the noble metals is considered to be a key factor for this promotion: an enhanced ratio of the metallic state of noble metal surface is presumably present under H_2 co-feed, which tracks the enhanced activity during Pt-, Pd- and Ir-catalyzed H_2-C_3H_6-SCR of NOx. The catalysts evaluation was carried out at the Laboratory of Alternative Fuels and Environmental Catalysis (LAFEC), in the Technological Educational Institute of Western Macedonia, as well as at the Lab. of Physical Chemistry & Chemical Processes (TUC), during the project "Thales-CASANNO". The experiments were performed and analyzed by Prof. Maria Goula and Prof. Ioannis Yentekakis. The following publication describes the results of this study:

*(4) M.A. Goula, N.D. Charisiou, K.N. Papageridis, A. Delimitis, E. Papista, **E. Pachatouridou**, E.F. Iliopoulou, G. Marnellos, M. Konsolakis, I.V. Yentekakis, "A comparative study of the H_2-assisted selective catalytic reduction of nitric oxide by propene over noble metal (Pt, Pd, Ir)/γ-Al_2O_3 catalysts", Journal of Environmental Chemical Engineering 4 (2016) 1629-1641.*

Chapter V presents the impact of thermal treatment (calcination at 400°C, 600°C and 800°C) on the solid state properties and the N_2O decomposition performance of Ir/γ-Al_2O_3 catalysts. In all catalytic materials IrO_2 phase was detected, with crystallites of

similar size. No agglomeration of the Ir particles was observed, even at high calcination temperatures, despite the expected tendency of IrO_2 to aggregate at elevated temperatures. This is probably related with the low (0.5% wt.) Ir loading and the high surface area of Al_2O_3 carrier (187 m^2/g). The catalyst calcined at 400°C (IrAl_oxi400) presented the best catalytic performance for the decomposition of N_2O, both in the absence and presence of oxygen excess. The superiority of the catalyst was maintained even after being subjected to successive reaction cycles. The enhanced performance of IrAl_oxi400 catalyst can be ascribed to its lower content on inactive $IrAl_xO_y$ species, as compared to IrAl_oxi600 and IrAl_oxi800 catalysts, where the sub-surface $IrAl_xO_y$ phase is favored.

Chapter VI explores the influence of typical inhibitors (i.e. SO_2 and H_2O) on the de-N_2O performance of Ir/Al_2O_3 catalysts. It was found that the deactivation caused by SO_2 is irreversible and can be attributed to the formation of stable sulfates on the surface of the catalyst. On the other hand, the inhibition effect of H_2O was totally reversible and attributed to its competitive adsorption into the catalyst surface. Moreover, it was shown that the un-modified Ir catalyst (0.5Ir/Al) demonstrated a better resistance to sulfur poisoning, than the Ce-modified catalyst (0.5Ir/AlCe). Among the thermally treated catalysts, the IrAl_oxi400 exhibited the optimum resistance to poisoning, due to the largest population of IrO_x phase on the catalyst surface linked to the preferential localization of sulfur species into the alumina carrier.

The final chapter, **chapter VII** summarizes the major conclusions of the present work and proposes further research studies over the abatement of NO_x and N_2O oxides.

ΠΕΡΙΛΗΨΗ

Η παρούσα διδακτορική διατριβή καταπιάνεται με την επίδραση των δομικών (CeO_2, La_2O_3) και επιφανειακών (Κ) ενισχυτών στα φυσικοχημικά και καταλυτικά χαρακτηριστικά ευγενών μετάλλων (Pt, Pd, Ir) υποστηριγμένων σε φορέα Al_2O_3, κατά την επιτέλεση των αντιδράσεων αποδόμησης οξειδίων (NOx) ή/και υποξειδίου (N_2O) του αζώτου. Η επίδραση των ενισχυτών στα φυσικοχημικά χαρακτηριστικά, καθώς και στην καταλυτική δραστικότητα και σταθερότητα των προς μελέτη καταλυτικών συστημάτων, διερευνήθηκε εκτενώς μέσω ποικίλων τεχνικών χαρακτηρισμού, όπως είναι η φυσιορόφηση N_2 (μέθοδος ΒΕΤ), η περίθλαση ακτινών Χ (XRD), η θερμοπρογραμματιζόμενη αναγωγή/εκρόφηση (TPR/TPD), μικροσκοπία σάρωσης/διέλευσης (HRTEM/STEM) και φασματοσκοπία υπερύθρου (FTIR, DRIFTS). Απώτερο σκοπό της παρούσας διατριβής αποτελεί η κατανόηση σε θεμελιώδες επίπεδο της δράσης των ενισχυτών, καθώς και η ανάπτυξη σχέσεων δομής-δραστικότητας κατά τη διάσπαση του N_2O ή την αναγωγή των NOx σε υποστηριγμένους καταλύτες ευγενών μετάλλων.

Ο περιορισμός των εκπομπών NOx και N_2O αποτελεί θέμα μείζονος περιβαλλοντικής σημασίας, δεδομένου ότι οι ρύποι αυτοί συμβάλλουν δραστικά στην όξυνση σοβαρών περιβαλλοντικών προβλημάτων, όπως το φαινόμενο του θερμοκηπίου, η τρύπα του όζοντος, το φωτοχημικό νέφος και η όξινη βροχή. Προς την κατεύθυνση αυτή, στόχο της παρούσας διδακτορικής διατριβής αποτελεί η σύνθεση, ο χαρακτηρισμός και η αξιολόγηση καινοτόμων καταλυτικών συστημάτων αντιμετώπισης των εκπομπών NOx ή/και N_2O. Τα εν λόγω καταλυτικά συστήματα συνίστανται από ένα ευγενές μέταλλο σε πολύ χαμηλή φόρτιση (< 1% κ.β.) υποστηριγμένο σε φορέα γ-Al_2O_3, τα οποία είναι κατάλληλα ενισχυμένα και σταθεροποιημένα από δομικούς ή/και επιφανειακούς ενισχυτές χαμηλού κόστους.

Η παρούσα διδακτορική διατριβή αποτελείται από τα παρακάτω κεφάλαια:

Κεφάλαιο Ι: Το πρώτο κεφάλαιο παρουσιάζει τις πηγές εκπομπής, τις περιβαλλοντικές επιπτώσεις, την ισχύουσα Ευρωπαϊκή νομοθεσία, καθώς και τις διαθέσιμες προτεινόμενες τεχνολογίες και τα καταλυτικά συστήματα μείωσης των εκπομπών οξειδίων (NOx) και υποξειδίου (N_2O) του αζώτου.

Κεφάλαιο ΙΙ: Το δεύτερο κεφάλαιο περιγράφει τη διαδικασία που ακολουθήθηκε για την σύνθεση των καταλυτικών υλικών που χρησιμοποιήθηκαν στην παρούσα μελέτη, τις μεθόδους χαρακτηρισμού των υλικών και τις διατάξεις στις οποίες αξιολογήθηκαν ως προς την καταλυτική τους δραστικότητα.

Κεφάλαιο ΙΙΙ: Το τρίτο κεφάλαιο περιλαμβάνει τον χαρακτηρισμό, σε συνδυασμό με την καταλυτική αξιολόγηση των μη-τροποποιημένων, αλλά και των δομικά ή/και επιφανειακά τροποποιημένων καταλυτικών υλικών ως προς την διάσπαση του N_2O. Αύξηση του % ποσοστού (0.25, 0.5 και 1.0 % κ.β.) των ευγενών μετάλλων (Pt, Pd, Ir), αυξάνει την καταλυτική ενεργότητα των υλικών, ειδικά στην περίπτωση των καταλυτών ιριδίου. Παρουσία περίσσειας οξυγόνου, στους καταλύτες Ir/Al_2O_3 και Pd/Al_2O_3 παρατηρείται μια μικρή πτώση της δραστικότητας τους, σε αντίθεση με τον καταλύτη Pt/Al_2O_3, η δραστικότητα του οποίου μειώνεται ραγδαία. Η ανωτερότητα των καταλυτών Ir και Pd αποδίδεται στην παρουσία των οξειδίων των μετάλλων, τα οποία είναι πιο ανθεκτικά στην παρουσία οξυγόνου. Η τροποποίηση της αλουμίνας με δομικούς ενισχυτές (όπως CeO_2 and La_2O_3) διερευνήθηκε με σκοπό τη βελτίωση της δραστικότητας των καταλυτών Pd, Pt και Ir παρουσία O_2. Ο δομικά ενισχυμένος καταλύτης Ir (Ir/Al_2O_3-CeO_2) παρουσίασε την μεγαλύτερη δραστικότητα ως προς την διάσπαση του N_2O. Το γεγονός αυτό οφείλεται στην επίτευξη ενός συγκεκριμένου λόγου $Ir^{\delta+}/Ir^0$, καθώς και στην ύπαρξη κενών θέσεων οξυγόνου (V_o) στην Ce, γύρω από τα μικρού μεγέθους σωματίδια ιριδίου. Τα εν λόγω σωματίδια κάτω από οξειδωτικές συνθήκες φαίνεται να προωθούν την προσρόφηση και διάσπαση του N_2O σε N_2 και O_2. Λόγω της αυξημένης δραστικότητας του, το ιρίδιο (Ir/Al_2O_3) τροποποιήθηκε περαιτέρω με επιφανειακό ενισχυτή (K). Η επιφανειακή τροποποίηση του καταλύτη με 0.5% κ.β. K ενισχύει την προσρόφηση του N_2O και τη διάσπαση του, καθώς ευνοεί τον σχηματισμό IrO_2, στα οποία διευκολύνεται η εκρόφηση των προσροφημένων ειδών οξυγόνου. Η αξιολόγηση των καταλυτικών υλικών έλαβε χώρα στο Εργαστήριο Τεχνολογίας Περιβάλλοντος (Πανεπιστήμιο Δ. Μακεδονίας), από την υποψήφια Διδάκτωρ Ελένη Πάπιστα. Τα αποτελέσματα του κεφαλαίου ΙΙΙ δημοσιεύτηκαν στα παρακάτω επιστημονικά περιοδικά:

*(1) **E. Pachatouridou**, E. Papista, E.F. Iliopoulou, A. Delimitis, G. Goula, I.V. Yentekakis, G.E. Marnellos, M. Konsolakis, "Nitrous Oxide Decomposition over Al$_2$O$_3$*

Supported Noble Metals (Pt, Pd, Ir): Effect of Metal Loading and Feed Composition", Journal of Environmental Chemical Engineering 3 (2015) 815-821.

(2) **E. Pachatouridou**, E. Papista, A. Delimitis, M.A. Vasiliades, A.M. Efstathiou, M.D. Amiridis, O.S. Alexeev, D. Bloom, G.E. Marnellos, M. Konsolakis, E. Iliopoulou, "N_2O decomposition over ceria-promoted Ir/Al_2O_3 catalysts: The role of ceria", Applied Catalysis B 187 (2016) 259-268.

(3) E. Papista, **E. Pachatouridou**, M.A. Goula, G.E. Marnellos, E. Iliopoulou, M. Konsolakis, I.V. Yentekakis, "Effect of alkali promoters (K) on nitrous oxide abatement over Ir/Al_2O_3 catalysts", Topics in Catalysis 59 (2016) 1020-1027.

Κεφάλαιο IV: Το τέταρτο κεφάλαιο μελετά την αντίδραση εκλεκτικής αναγωγής (SCR) του NO με αναγωγικό μέσο το υδρογόνο (H_2) και το προπυλένιο (C_3H_6), παρουσία οξυγόνου (O_2) στην τροφοδοσία, πάνω σε καταλύτες Pt, Ir και Pd (0.5% κ.β.) στηριζόμενους σε μη-τροποποιημένη αλουμίνα. Μελετήθηκαν οι παρακάτω τρεις αντιδράσεις: (i) $NO+C_3H_6+O_2$ (R#1), (ii) $NO+C_3H_6+O_2+H_2$ (R#2) και (iii) $NO+H_2+O_2$ (R#3). Η παρουσία του H_2 ενίσχυσε την καταλυτική δράση και των τριών καταλυτικών υλικών κατά την επιτέλεση της αντίδρασης R#2. Η ενίσχυση παρατηρήθηκε σε όλο το θερμοκρασιακό εύρος που μελετήθηκε (T: 50-400°C). Μεγαλύτερη επίδραση του H_2 παρατηρήθηκε στους καταλύτες Pt, μετά στους καταλύτες Ir και λιγότερο στους καταλύτες Pd. Η παρουσία του H_2 επηρεάζει την οξειδωτική κατάσταση των μετάλλων, γεγονός το οποίο θεωρείται βασικός παράγοντας για την ενίσχυση της καταλυτικής δράσης των υλικών. Η αξιολόγηση των καταλυτών έλαβε χώρα στο Εργαστήριο Εναλλακτικών Καυσίμων και Περιβαλλοντικής Κατάλυσης (ΤΕΙ Δ. Μακεδονίας) και στο Εργαστήριο Φυσικοχημείας και Χημικών Διεργασιών (Πολυτεχνείο Κρήτης), από την ομάδα της Καθηγήτριας Μαρίας Γούλας και του Καθηγητή Ιωάννη Γεντεκάκη. Τα αποτελέσματα του κεφαλαίου αυτού, οδήγησαν στην δημοσίευση:

(4) M.A. Goula, N.D. Charisiou, K.N. Papageridis, A. Delimitis, E. Papista, **E. Pachatouridou**, E.F. Iliopoulou, G. Marnellos, M. Konsolakis, I.V. Yentekakis, "A comparative study of the H_2-assisted selective catalytic reduction of nitric oxide by propene over noble metal (Pt, Pd, Ir)/γ-Al_2O_3 catalysts", Journal of Environmental Chemical Engineering 4 (2016) 1629-1641.

Κεφάλαιο V: Στο πέμπτο κεφάλαιο διερευνήθηκε η επίδραση της θερμικής προ-κατεργασίας (πύρωση στους $400^{\circ}C$, $600^{\circ}C$ και $800^{\circ}C$) στα φυσικοχημικά χαρακτηριστικά και την καταλυτική δραστικότητα των καταλυτών Ir, ως προς την αντίδραση διάσπασης του N_2O. Σε όλα τα υλικά σχηματίστηκε η φάση του IrO_2, με παρόμοιο μέγεθος κρυσταλλιτών. Παρά την αναμενόμενη τάση που παρουσιάζουν οι κρυσταλλίτες IrO_2 προς συσσωμάτωση (σε υψηλές θερμοκρασίες), στην συγκεκριμένη περίπτωση δεν παρατηρήθηκε κάτι τέτοιο, πιθανώς λόγω της μικρής φόρτισης του Ir (0.5% κ.β.) σε ένα φορέα Al_2O_3 εκτεταμένης επιφάνειας (187 m^2/g). Ο οξειδωμένος καταλύτης στους $400^{\circ}C$ (IrAl_oxi400) παρουσίασε την μεγαλύτερη δραστικότητα ως προς τη διάσπαση του N_2O, τόσο απουσία όσο και παρουσία περίσσειας O_2. Η υπεροχή του καταλύτη διατηρήθηκε και μετά την υποβολή του σε διαδοχικούς κύκλους αντίδρασης. Η μειωμένη απόδοση των IrAl_oxi600 και IrAl_oxi800 αποδόθηκε στον σχηματισμό μη δραστικών υπο-επιφανειακών ειδών ιριδίου (υπό την μορφή $IrAl_xO_y$), των οποίων ο σχηματισμός ευνοείται με αύξηση της θερμοκρασίας.

Κεφάλαιο VI: Το τελευταίο κεφάλαιο παρουσιάζει την επίδραση των παρεμποδιστικών παραγόντων, όπως του SO_2 και του H_2O, στους καταλύτες Ir κατά τη διάσπαση του N_2O, απουσία και παρουσία O_2. Η απενεργοποίηση που λαμβάνει χώρα λόγω του SO_2 είναι μη αντιστρεπτή, με αποτέλεσμα ο καταλύτης να μην ανακτά την αρχική του δραστικότητα μετά την απομάκρυνση του SO_2 από το ρεύμα τροφοδοσίας. Το γεγονός αυτό οφείλεται στον σχηματισμό σουλφομάδων στην επιφάνεια του καταλύτη. Από την άλλη μεριά, η απενεργοποίηση λόγω της παρουσίας του H_2O είναι αντιστρεπτό φαινόμενο, λόγω της ανταγωνιστικής ρόφησης που λαμβάνει χώρα μεταξύ των μορίων H_2O και N_2O. Ο καταλύτης επανέρχεται στην αρχική του ενεργότητα μετά την απομάκρυνση του νερού από την τροφοδοσία. Ο μη-τροποποιημένος καταλύτης (0.5Ir/Al) παρουσιάζει μεγαλύτερη ανθεκτικότητα παρουσία SO_2, σε αντίθεση με τον δομικά τροποποιημένο καταλύτη (0.5Ir/AlCe). Μεταξύ των θερμικά επεξεργασμένων καταλυτών (Ir/Al_oxi400, Ir/Al_oxi600 και IrAl_oxi800), η βέλτιστη δραστικότητα και ανθεκτικότητα παρατηρήθηκε για τον καταλύτη Ir/Al_oxi400. Το γεγονός αυτό αποδίδεται στο μικρότερο πληθυσμό υπο-επιφανειακών, μη-δραστικών, ειδών ιριδίου ($IrAl_xO_y$)

καθώς και στην εκλεκτική συσσώρευση των θειικών ειδών στον φορέα της Al_2O_3 παρά στα ενεργά κέντρα του μετάλλου.

Τέλος, το τελευταίο κεφάλαιο (**κεφάλαιο VII**) συνοψίζει και παρουσιάζει τα κύρια συμπεράσματα, καθώς και προτάσεις για μελλοντική έρευνα.

CONTENTS

CHAPTER I

NOx & N_2O: Sources, Environmental Effects and Emission Control Strategies

CO$_2$

CH$_4$

N$_2$O
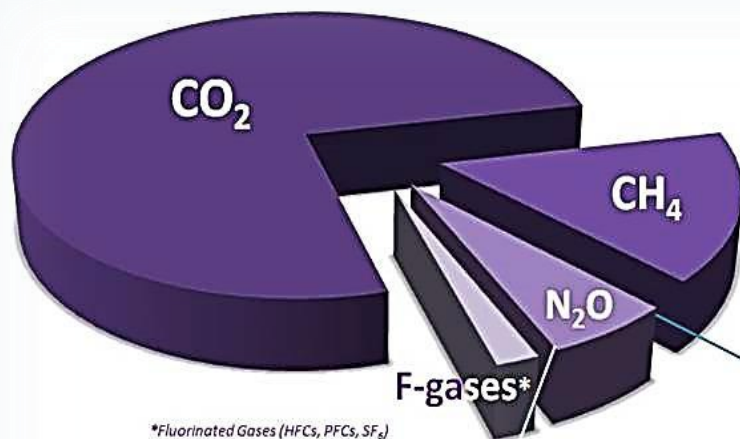
F-gases*

*Fluorinated Gases (HFCs, PFCs, SF$_6$)

Other

Manure Management

Transportation

Industry or Chemical Production

Stationary Combustion

Agricultural Soil Management
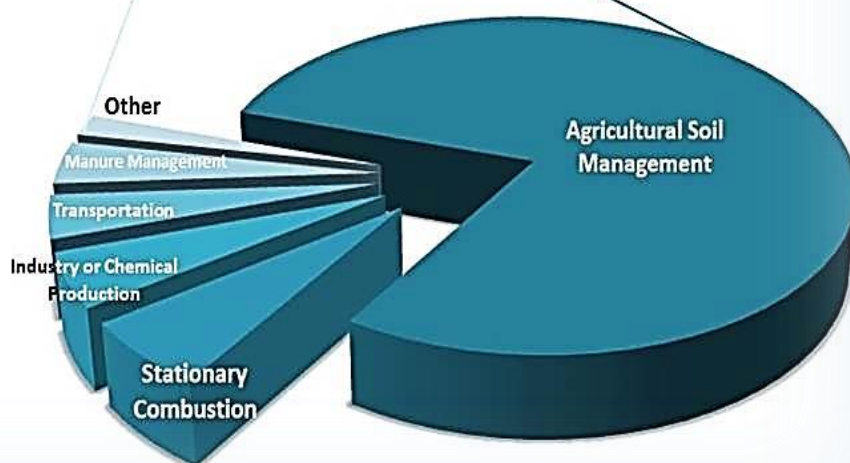
Chapter I provides an introduction to nitrogen (NOx) and nitrous (N_2O) oxides sources and their environmental consequences. The abatement of NOx and N_2O emissions has become one of the greatest challenges in environmental catalysis. This consice literature review describes the abatement technologies, as well as the catalytic systems (mainly noble metals-based catalysts) that have been employed so far by numerous groups, academics as well as industrial research laboratories.

I.1 NOx AND N$_2$O EMISSIONS AND ENVIRONMENTAL EFFECTS

Nitrogen oxides (NOx: NO or NO$_2$) and nitrous oxide (N$_2$O) are among the most important air polluting chemical compounds [1]. In this regard, the control of nitrogen oxides emissions has become one of the greatest environmental challenges [2].

Diatomic molecular nitrogen (N$_2$) is a relatively inert gas that makes up about 80% of the air we breathe. However, the chemical element nitrogen (N), as a single atom, can be reactive and have ionization levels from plus one to plus five [1]. Thus nitrogen can form several different oxides, like nitrogen oxides (NO, NO$_2$) and nitrous oxide (N$_2$O), ammonia (NH$_3$), nitrate (NO$_3^-$) and nitrite (NO$_2^-$). Figure I.1 presents the reactive forms of nitrogen [3].

Since 1970, EPA (Environmental Protection Agency) has tracked emissions of the six principal air pollutants: carbon monoxide (CO), lead (Pb), nitrogen oxides (NOx), particulate matter (PM), sulfur dioxide (SO$_2$) and volatile organic compounds (VOCs). Reducing emissions of NOx is a crucial component of EPA's strategy for cleaner air [4].
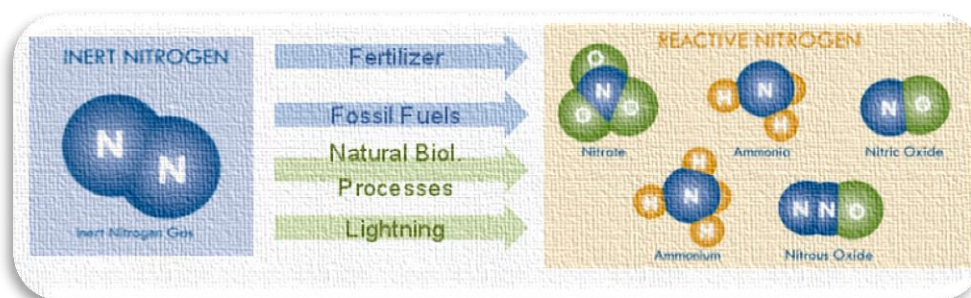
Figure I.1: Reactive forms of nitrogen [3].

NOx Emissions

Sources of troposphere NOx emissions can be anthropogenic, resulting from human activity, or biogenic, resulting from the activity of non-human organisms. Moreover, the production from livestock or agriculture can contribute to NOx emissions. However, anthropogenic sources contribute substantially more to NOx emissions than biogenic ones.

Anthropogenic NOx emissions are dominated by fossil fuel combustion processes, which release NOx in the form of NO and NO$_2$. Out of this total, emissions from all types of transportation account for ~56% of NOx, with on-road highway vehicles representing the major mobile source component. Roughly one half of these on-road emissions have diesel engine sources and one-half have gasoline engine sources [5]. Electric power plant boilers produce about 40% of the NOx emissions from stationary sources. Additionally, substantial emissions are added by anthropogenic sources such as industrial boilers, incinerators, gas turbines, reciprocating spark ignition and Diesel engines in stationary sources, iron and steel mills, cement manufacture, glass manufacture, petroleum refineries, and nitric acid manufacture. Biogenic or natural sources of nitrogen oxides include lightning, forest fires, grass fires, trees, bushes, etc. [1, 6, 7].

In all combustion processes there are three main routes toward NOx formation [8]:

i.   Thermal NOx: The concentration of "thermal NOx" is controlled by the nitrogen and oxygen molar concentrations and the temperature of combustion. Combustion at temperatures well below 1300°C hinders the formation of thermal NOx.

ii.   Fuel NOx: Fuels that contain nitrogen (e.g. coal) contribute to "fuel NOx" that results from oxidation of the already-ionized nitrogen contained in the fuel.

iii. Prompt NOx: Prompt NOx is formed from molecular nitrogen in the air combined with fuel under low-temperature or fuel-rich conditions. This atomic nitrogen is then oxidized along with the fuel and becomes NOx during combustion, just like fuel NOx.

NO is a major atmospheric pollutant. It has the ability to generate secondary contaminants through its interaction with other primary pollutants (like carbonyl molecules, alcohol radicals, etc.). NO plays a major role in the photochemistry of the troposphere and the stratosphere. It reacts with photochemical pollutants such as ozone, formaldehyde, organic hydroperoxides and peroxyacyl nitrates that are all very reactive, with very short lifetime. This fast reaction generates more nitrogen oxides and organic nitrates. The formed NO$_2$ contributes substantially to acid rain. Among the reactions involving ozone, the one with chlorofluorocarbons is very

dangerous, since it has a determining effect on the climate. The normal average content of ozone in the atmosphere is about 10^{-10} vol. % and its interaction with NO also contributes to its diminution. The chemical depletion of ozone, in an important part due to nitrogen oxide species, is a prolonged phenomenon [9]. Carcinogenic products are also formed during these reactions.

Hydrocarbons (HCs) in polluted air do not react among themselves under the action of sun radiations, not even to a very small extent, but show a high reactivity towards intermediate species such as peroxides RO_2 [10]. Such species react with the primary pollutants, NO, NO_2, O_3 and HC. The photochemical complex HC-NOx-Ox is formed during the HCs interactions in the photolytic cycle of NO; the mixture of products generated is called "photochemical smog'' and contains O_3, CO, peroxyacetyl nitrates, alkyl nitrates, ketones, etc. The photochemical cycle of nitrogen oxides initiates under sunlight. NO_2 is initially decomposed as follows [11]:

$$NO_2 + \textit{Sunlight} \rightarrow NO + O \qquad\qquad (1.1)$$
$$O + O_2 \rightarrow O_3 \qquad\qquad (1.2)$$
$$O_3 + NO \rightarrow NO_2 + O_2 \qquad\qquad (1.3)$$

Until a dynamic equilibrium is reached:

$$NO_2 + O_2 \xrightarrow{\textit{Sunlight}} NO + O_3 \qquad\qquad (1.4)$$

In the presence of oxygen, NO is oxidized very quickly to NO_2 which, as mentioned before, is partly responsible for the acid rain and the urban smog, which have negative effects in agriculture, but may also predispose to respiratory diseases by weakening the ability of the bronchopulmonary structures to function properly [12].

N_2O Emissions

Nitrous oxide (N_2O) is commonly known as "laughing gas" through its use as an anesthetic in surgery and dentistry, but it is also naturally present in trace amounts in the Earth's atmosphere. In view of this fact, it has been long considered as a

relatively harmless compound and has suffered from a lack of interest from scientists, engineers and politicians. However, during the last decade, N$_2$O has been recognized as the third most significant anthropogenic greenhouse gas and the largest stratospheric ozone depleting substance [13-15].

Thus, N$_2$O has received considerable attention as environmental pollutant, taking into account also its high global warming potential (GWP), which is approximately 310 times higher compared to CO$_2$, in conjunction to its ability to deplete ozone layer in a way similar to chlorofluorocarbons (CFCs) due to its long lifetime (114 years) in atmosphere. More worryingly, the anthropogenic N$_2$O emissions are rapidly increasing and projected to almost double by 2050 [1, 15, 16].

In particular, nitrous oxide affects the atmosphere at the troposphere level as well at the stratosphere level. N$_2$O is a relatively strong absorber of infrared radiation and is therefore implicated as an important contributor to the "Greenhouse Effect." It is estimated that a mere doubling of its concentration will result in a 0.28°C contribution to global warming [17]. Since N$_2$O is chemically stable in the troposphere, it can be transported to the stratosphere where it has also been responsible for ozone (O$_3$) depletion. In the stratosphere, N$_2$O is converted to NO, which is the primary substance responsible for the establishment of the equilibrium stratospheric O$_3$ concentration. It is estimated that by doubling the atmospheric N$_2$O concentration the total column of ozone will be decreased by ca. 12% [18].

On the other hand, N$_2$O is emitted from both natural and anthropogenic sources. The anthropogenic sources include agricultural activities, industrial chemical production, fuel and biomass combustion, and sewage treatment operations. Globally, the relative contributions from the various sources has remained steady over the years, with agricultural activities being the largest contributor (60%), followed by industrial processes and fuel combustion, each contributing about 10% [19].

Emissions from synthetic fertilizers, manure and crop residues are mainly involved in agricultural N$_2$O emissions. N$_2$O emissions from biomass are mostly derived from forest fires, crop residue burning and biomass combustion for heating and cooking. The industrial and fossil fuel combustion sector includes N$_2$O emissions from nitric and adipic acid production, as well as emissions from stationary and mobile

combustion sources, however the current emissions are 15% of the total gross human sources. These emissions are expected to be increased. Nitric and adipic acid production are the main N_2O industrial sources. Nitric acid is the major feedstock in manufacturing processes related to the production of explosives, nitrogen-based fertilizers, adipic acid, and so forth. Moreover, N_2O is released as a byproduct during the Pt catalyzed ammonia oxidation process. The amount of the formed N_2O depends on the catalyst type and age, as well as on the combustion conditions in the oxidizing unit. The formation of N_2O at nitric acid plants can be considered as the result of the following reactions [15, 20, 21]:

$$2NH_3 + 2O_2 \rightarrow N_2O + 3H_2O \qquad\qquad (1.5)$$
$$2NH_3 + 8NO \rightarrow 5N_2O + 3H_2O \qquad\qquad (1.6)$$
$$4NH_3 + 4NO + 3O_2 \rightarrow 4N_2O + 6H_2O \qquad\qquad (1.7)$$
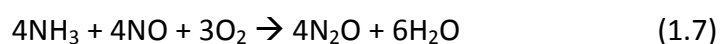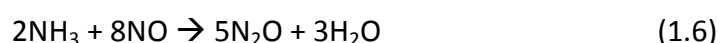
The emissions of N_2O from stationary combustion facilities (public and industrial power plants and other facilities burning fossil fuels) are strongly dependent on fuel characteristics, the type of combustion technology, the temperature of combustion, and the type of emission control technologies possibly applied. Thermal decomposition of N_2O is rapid and emissions are negligible for combustion temperatures significantly above 900^oC. The N_2O emission rates are highest when combustion temperature is in the range $500\text{-}900^oC$. Measurements show that N_2O emissions are low from conventional stationary combustion units, but relatively high from bubbling, re-circulating and pressurized fluidized bed units. The relatively high N_2O emissions from fluidized bed combustors are primarily due to the lower temperature of combustion ($500\text{-}600^oC$) [21, 22].

N_2O emissions from mobile sources are released primarily by three-way catalytic converters (TWCs), which are worldwide employed to simultaneously abate nitrogen oxides (NOx), carbon monoxide (CO) and hydrocarbons (HCs). The amount of N_2O released by the transportation sector is mainly affected by the adopted control technology, the driving cycle, the TWC operating temperature as well as by the TWC composition and aging. N_2O is a byproduct of the reactions taking place in TWCs and its formation is notably favored during the "cold start" and "intermediate

temperature" periods. Additionally, N$_2$O emissions are in general increased as a result of catalyst deactivation and as the fuel sulfur is increased [15, 21, 23].

In summary, the first potential environmental consequence of excess N in the environment was acid rain (1860s). This discovery was followed by NOx-induced ozone contributing to smog (1950s), the fresh and coastal water quality aspects (1970s), and N$_2$O-induced impacts on stratospheric ozone (1980s). Then in the early 2000s, it was proposed that all of the effects were linked by the nitrogen cascade, which is essentially driven by the fact that once N$_2$ is converted to N species, that nitrogen will continue to be active in the environment with the potential to contribute to all effects in sequence until it is back to N$_2$ [24, 25]. Figure I.2 presents some of the environmental impacts of nitrogen oxides species [7].
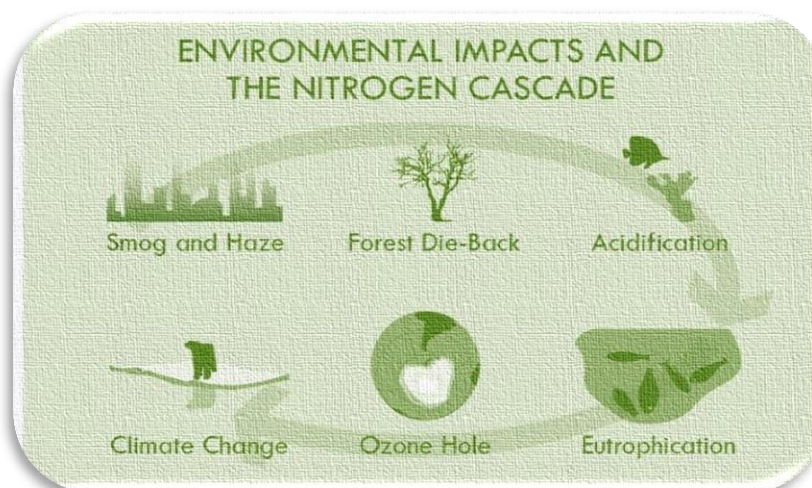
Figure I.2: Effect of nitrogen oxides (NO, NO$_2$, N$_2$O) on environment [7].

I.2 LEGISLATION (EURO 6)

The "Euro Standards" regulate emissions of nitrogen oxides (NOx), hydrocarbons (HCs), carbon monoxide (CO), particulate matter (PM) and particle numbers (PN). There are separate regulations for light vehicles (fewer than 3.5 tons) and heavy-duty vehicles. The standards for both light and heavy vehicles are designated "Euro" and followed by a number (usually Arabic numerals for light vehicles: Euro 1, 2, 3..., and Roman numerals for heavy vehicles: Euro I, II, III...). Non-compliant vehicles

cannot be sold in the EU, but the new standards do not apply to vehicles that are already on the roads. Euro standards also exist for two and three-wheeled vehicles (motorcycles and mopeds) and for engines for non-road machinery [26].

Since 1992, when the first Euro 1 legislation was introduced for trucks and buses, the European Commission has regulated the amount of pollutants coming out of the tail-pipe of a diesel engine. Figure I.3 presents the Euro emissions standards for diesel passenger cars since the first Euro. In particular, the Commission identified two key constituents within the exhaust stream - Oxides of Nitrogen (NOx) and Particulate Matter (PM) - as being harmful, and needing to be controlled and reduced.

Over the past 20 years (Fig. I.3) European engine makers have invested heavily in developing new technology, which has seen the levels of NOx and PM (as well as other elements such as unburnt hydrocarbons) in the exhaust of all new diesel-engine trucks and buses falling dramatically, with a consequent improvement in air-quality [26].
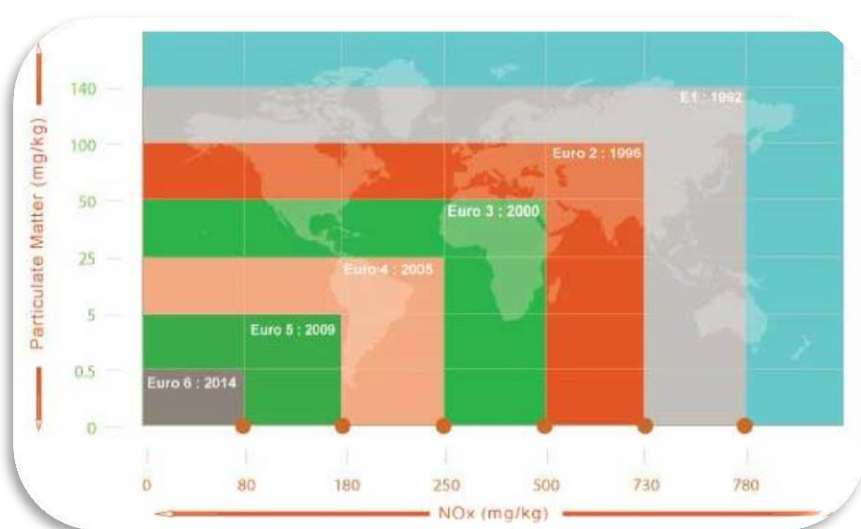
Figure I.3: Euro emissions standards for diesel passenger cars.

NH_3 and N_2O emissions are not regulated for Euro 5 vehicles in Europe. Nonetheless, NH_3 has a regulatory limit of 10 ppm weighted average over the type approval cycle applicable for Euro 6 [27]. Furthermore, U.S. Environmental Protection Agency (EPA) has recently developed a GHG emissions program, under the Clean Air Act, that includes N_2O emission standards of 0.10 g/bhp-h (0.133 g/kWh) measured over the

Heavy-Duty Engine FTP cycle [28]. This limit is applicable in the US since 2014 for compression ignition heavy-duty engines and from 2016 for spark ignition engines [29].

The arrival of future Euro 7 automotive legislation is anticipated to involve a further reduction of NOx emissions compared to EURO 6 standards. To comply with the anticipated EURO 7 standard, for a typical diesel exhaust composition, approximately 200 ppm NO has to be reduced to 10 ppm NO in competition with an excess of 5% vol. O$_2$, 5% vol. CO$_2$ and 5-10% vol. H$_2$O. This means that extremely effective exhaust-emission after-treatment technologies will be required [30].

I.3 NOx AND N$_2$O ABATEMENT TECHNOLOGIES

The reduction of nitrogen (NOx) and nitrous (N$_2$O) oxides emissions has become one of the greatest challenges in environmental protection. Different categories of catalysts have been tested so far by numerous research groups, applying different methods for their abatement.

NOx Abatement

The use of such a large number of catalysts to eliminate NO is mainly associated to the different remediation reactions for NO abatement, which can be categorized as follows [2, 31, 32]:

i. The selective catalytic reduction of NO with ammonia (NH$_3$-SCR), typical of chemical plants and stationary power stations;

ii. The catalytic reduction of NO in the presence of CO (CO-SCR), typical of automotive pollution control;

iii. The selective catalytic reduction of NO in the presence of hydrocarbons (HCs-SCR) and more particularly methane (CH$_4$-SCR). This method has not yet reached industrial use, but can be applied for automotive pollution control and in various industrial plants;

iv. The direct decomposition of NO into N$_2$ and O$_2$, which is a goal worth striving for since it eliminates the need for reductants, and the products N$_2$ and O$_2$ are harmless.

The first method, NH_3-SCR, is in practical use for NOx emissions control from large-scale boilers, and can be, in general, applied to oxygen rich exhaust streams. However, the use of NH_3 as a reductant is difficult for vehicle applications. The CO-SCR on the other hand, is more attractive from a practical point of view, since CO is already contained in vehicle exhausts and can be relatively more easily produced by engine operation. In addition, H_2-SCR is an interesting alternative, since it proceeds at relatively low temperatures. H_2-SCR is an attractive approach to the efficient removal of NOx in the exhaust of lean-burn and diesel engines, the temperature of which has become lower due to the improvement of engine thermal efficiency. Hydrogen can be formed by reforming of hydrocarbon fuels. H_2-SCR is also a promising approach for NOx treatment emitted from future hydrogen fueled vehicles [31, 33, 34].

HCs-SCR: The HCs-SCR is believed to be the most promising way to eliminate nitrogen oxide. The main advantage of this reaction is the use of a gas mixture very similar to that found in exhausts [2, 31]. In this regard, a great number of studies have been conducted on the use of hydrocarbons as the reductant for the HC-SCR in oxygen-rich atmospheres. This catalytic process was first experimented on copper ion-exchanged zeolites by Iwamoto et al. [35, 36] and Held et al. [37], independently. They showed that the catalytic activity of Cu/ZSM-5 could be greatly enhanced by small amounts of hydrocarbons in the presence of excess oxygen. Soon afterwards, Hamada et al. [38, 39] found that H-zeolites and alumina were also active in the selective reduction of NO; however the required temperatures were much higher. Examining ion-exchanged zeolites, Iwamoto et al. [40] reported that both MFI and mordenite structures were active. Similarly, Hall et al. [41] conducted investigations in the same direction and found that an MFI structure was most favorable, while ferrierite structure could also be considered.

Supported transition metals and metal oxide-type catalysts such as Ni/Al_2O_3 [39], Ag/Al_2O_3 [43] and La_2O_3 [44] were found to be also active [45, 46]. Supported noble metals have been proved very active in HC-SCR of NOx, but within very narrow temperature windows. Their efficiency of HC-SCR of NOx is only slightly affected by the presence of water, but it is quite sensitive to sulphur dioxide poisoning [47]. Compared to noble metals, metal oxides exhibit moderate activities, but the

operation temperatures are higher. Their activities are however strongly subjected to deactivation by sulphur dioxide and to thermal ageing due to the loss of specific area [32].

Concerning the reaction mechanism of the HC-SCR process, it is still a matter of debate. Thus, at present, three kinds of reaction schemes can be proposed [48]:

(a) Decomposition of NO proceeds to yield N$_2$, while the hydrocarbons clean up the surface oxygen species; moreover the reaction of hydrocarbon with oxygen can adjust the oxidation state of active sites [as shown in reactions (1.8) and (1.9)];

(b) Some reaction intermediates (HC∗) formed during the oxidation of the hydrocarbon has the ability to reduce NO selectively [reactions (1.10) and (1.11)];

(c) Nitrogen oxides generated from NO and O$_2$, for example NO$_2$, can preferentially react with the hydrocarbon [reactions (1.12) and (1.13)].

$$\text{(a) } 2NO \rightarrow N_2 + 2O_{ads} \qquad (1.8)$$
$$HC + O_{ads} \rightarrow CO_2 + H_2O \qquad (1.9)$$
$$\text{(b) } HC + O_2 \text{ (or NOx)} \rightarrow HC* + CO_2 + H_2O \qquad (1.10)$$
$$HC* + NOx \rightarrow N_2 + CO_2 + N_2O \qquad (1.11)$$
$$\text{(c) } NO + 1/2O_2 \rightarrow NO_2 \qquad (1.12)$$
$$HC + NO_2 \rightarrow N_2 + CO_2 + H_2O \qquad (1.13)$$
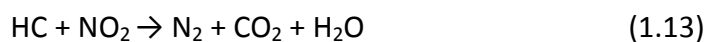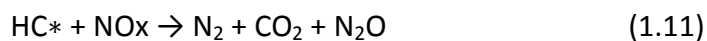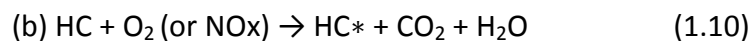
N$_2$O Abatement

On the other hand, the N$_2$O abatement can be also achieved by employing after-treatment technologies. The choice of the approach is strongly dependent on N$_2$O source and its particular "exhaust" characteristics as well as on relevant economic aspects. Hence, taking into account the diffuse character of N$_2$O emissions from the agricultural sector and non-controlled biomass burning, the employment of end-of-pipe technologies should be considered unfeasible. In this case, the first approach (i.e., lowering of N$_2$O formation) is the best solution to reduce N$_2$O emissions [15, 49]. On the other hand, the control of N$_2$O emissions from chemical and energy industries require after-treatment technologies, which can be classified in four categories [7, 15, 49, 50]:

i.   Thermal decomposition;

ii.   Non-selective catalytic reduction (NSCR);

iii.   Selective catalytic reduction (SCR);

iv.   Direct catalytic decomposition (De-N$_2$O).

Among all technologies, the N$_2$O catalytic decomposition is one of the most promising methods for controlling N$_2$O emissions, due to its simplicity, high efficiency, and low energy requirements [7, 15, 47]. For this reason, significant research efforts have been lately focused on the development of novel catalytic materials for N$_2$O abatement.

_De-N$_2$O:_ N$_2$O decomposition is an exothermic reaction, which can proceed either catalytically or thermally. Catalytically, the required temperatures are above 600°C in order to initiate the N$_2$O decomposition: 2N$_2$O → 2N$_2$ + O$_2$, $\Delta_R H^{\ominus}_{m\ [T=298K]}$ =-163 kJ/mol (1.14). Thermally, N$_2$O decomposition requires much higher temperatures (T: 800-1000°C), due to the considerably high value of the activation energy [51-53].

The dominant mechanism is dictated by the operating temperature and the catalyst used, with both paths being important in the intermediate range [50]. Figure I.4 presents N$_2$O molecule structure, indicating its bond properties.
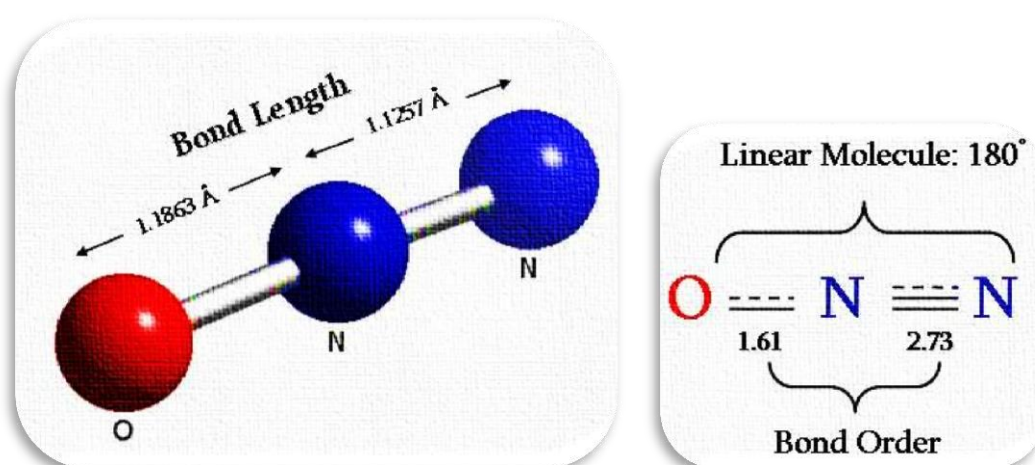
Figure I.4: N$_2$O molecule structure.

N$_2$O molecule is quite stable at room temperature. In the asymmetric N-N-O molecule, the N-N bond is stronger than the N-O bond; thus the N-O bond is the most probable to be first broken. The activation energy for N-O bond break is 250-270 kJ/mol. The N$_2$O decomposition catalytic reaction can be simply described as the

followings: (a) absorption of N$_2$O at the active site (*); (b) formation of N$_2$ and surface oxygen; (c) desorption of surface oxygen by combination with another oxygen atom; and (d) direct reaction of surface oxygen with another N$_2$O [54].

$$N_2O + * \leftrightarrow N_2O* \qquad\qquad (1.15)$$

$$N_2O* \rightarrow N_2 + O* \qquad\qquad (1.16)$$

$$2O* \leftrightarrow O_2 + 2* \qquad\qquad (1.17)$$

$$N_2O + O* \rightarrow N_2 + O_2 + * \qquad\qquad (1.18)$$

The catalytic decomposition of N$_2$O to nitrogen and oxygen has been examined over a wide variety of catalysts, which can be generally classified into noble metal catalysts, metal oxides, perovskites and zeolite-based catalysts. The N$_2$O decomposition on perovskites was reviewed by Swamy and Christopher in 1992 [55]. Subsequently, in 2001, the chemical structure and performance of perovskite-type materials was extensively covered by Peña and Fierro [56]. The de-N$_2$O performance of hydrotalcite-type materials was comprehensively summarized by Kannan in 1996 [57]. In the same year (1996), Kapteijn et al. [49] published a survey study on N$_2$O decomposition over metal-based catalysts, bare or mixed oxides, as well as on zeolitic systems. Several aspects on the reaction mechanism and kinetics as well as on the inhibiting role of several substances, such as O$_2$, H$_2$O and NO were addressed. A comprehensive survey on the application of clay derived catalysts for the removal of nitrogen oxides (de-NOx) was given by Serwicka in 2001 [58]. In 2003, Centi et al. [59] reported on the catalytic reduction of N$_2$O over highly active Rh-based catalysts. It was revealed that Rh catalysts supported over a modified zirconia–alumina carrier are among the most effective catalysts for the deN$_2$O process [59].

NOx and N$_2$O: Simultaneous Abatement

In spite of the intense research activity for nitrogen oxides abatement, only few studies are dealing with the simultaneous abatement of N$_2$O and NOx, although both pollutants coexist in the flue gases of chemical and combustion processes, as presented in Table I.1.

Table I.1: Typical composition of flue gases derived from various emission sources [15, 49, 60].

SOURCE	FLUE GASES COMPOSITION (%)					
	N_2O	NOx	O_2	CO	H_2O	SO_2
ADIPIC ACID UNIT	20-50	0.7	4	0.03	2-3	-
NITRIC ACID UNIT	0.03-0.35	0.01-0.35	1-4	-	0.3-2	-
FOSSIL FUELS COMBUSTION	0.05-0.5	0.05-0.5	2-10	> 0.1	~ 10	< 0.2
THREE-WAY CATALYTIC CONVERTERS	0-0.1	0-0.2	> 0.1	0-0.4	~ 10	> 0.01

Kögel et al. [61] have studied in detail, the simultaneous catalytic reduction of N_2O and NO by C_3H_8 over Fe/MFI zeolitic catalysts and found that while N_2O and C_3H_8 can be completely removed at temperatures higher than 400^oC, the maximum NO conversion reached only 50%. In a similar work, Li and Armor [62] noticed that Co/ZSM5 catalyst can be utilized for the simultaneous removal of NO and N_2O using CH_4 and C_3H_8 as reducing agents, without however achieving total conversion. Gassan-Zedeh and Seyidbayova [63] examined the simultaneous reduction of N_2O and NO using CO as reducing agent over a Cu/Co_2O_4 catalyst. NO presence was found to inhibit the reaction between N_2O and CO, as both N_2O and NO compete for the same surface active sites. Remarkable is the work of van den Brink et al. [64], which reports the use of a dual catalytic bed (first Co/ZSM-5 and then Pd/Fe-ZSM-5) for the simultaneous reduction of N_2O and NO. Eighty percent (80%) N_2O and NO conversions were obtained at temperatures higher than 300^oC in the absence of inhibiting gases (i.e. excess of O_2, H_2O, SO_2). Significant research efforts in this field have been also realized by Figueiredo et al. [65, 66] over bimetallic catalysts supported on activated carbon. Among all materials studied the Pt/K catalysts exhibited the optimum catalytic performance, a behavior that was attributed to the preservation of Pt sites in reduced state due to K presence. However, in spite of these encouraging results an insufficient stability was observed, since after 3h testing the activity was dramatically decreased. In addition, the simultaneous catalytic reduction of NO_X and N_2O in excess O_2 was studied using propylene as the reducing agent in the presence and absence of 10% vol. H_2O and 50 ppm SO_2. The reaction was carried out in a dual bed catalytic reactor consisting of In/Al_2O_3 (first

bed) and Ru/Al$_2$O$_3$ (second bed). However, long-term stability experiments in the presence of SO$_2$ led to a notable catalyst deactivation, eliminating as a result N$_2$O conversion, while NO$_X$ conversion was also significantly reduced [67].

I.4 CATALYTIC SYSTEMS BASED ON NOBLE METALS CATALYSTS

Among the different groups of catalysts that have been tested in order to reduce N$_2$O and/or NO emissions, noble metal supported catalysts (NMs) exhibit satisfactory activity [2, 31, 34, 48, 49, 68-71]. Among noble metals, Rh and Ru-based catalysts were studied a lot [68-71]. In the present study, the catalytic performance of Pt, Pd and Ir is comparatively explored.

In addition, support seems to play an important role on the catalytic performance, due to its ability to disperse as active phase but mainly due to the metal-support interactions that can be developed. Alumina is a suitable support as it provides high specific area, crush strength and stability. On the other hand, textural modifiers help maintain high metal and support surface areas at the high temperatures that are required. Rare-earths are used to stabilize γ-alumina against temperature induced phase transitions. La, Ce, Pr, Ca, Ba, Sr and Mg have been described in the literature as alumina's thermal stabilizers [72]. Among these, cerium oxide (CeO$_2$) is by far the most frequently used material, due to its unique acid-base and redox properties which can enhance both the catalytic activity of metal sites and the stability of support materials [73]. Although the main promoting effect of cerium oxide has been ascribed to its high oxygen storage capacity (OSC), recent studies are also focused on the influence of ceria to the electronic state and the concomitant catalytic activity of metal sites interfaced with CeO$_2$ [73-77]. La$_2$O$_3$ is also considered as a promising promoter/stabilizer in several catalytic systems since it has shown significant improvements on the stabilization of Al$_2$O$_3$ support and on the noble metals dispersion and their catalytic activity [78]. In the present study, bare γ-Al$_2$O$_3$, or modified with (20% wt.) CeO$_2$ or (20% wt.) Ce$_{0.8}$La$_{0.2}$O$_{1.9}$, were selected as supporting materials for the decomposition of N$_2$O.

In the following sections I.4.1 and I.4.2, a literature review about the catalytic systems that have been studied for NOx and N_2O abatement over Rh, Pt, Pd and Ir-based catalysts is presented.

I.4.1 *Rh-, Pt- and Pd-Based Catalysts*

Supported precious metals are widely used to catalyze industrial petroleum and chemical reactions. A fundamental concern in metal-catalyzed reactions is the relationship between catalytic activity and the dispersion of the metal in the supported catalysts [79]. Three noble metals -rhodium (Rh), platinum (Pt) and palladium (Pd) - have been dispersed, stabilized and promoted in different ways over the years to achieve extraordinary advances in performance and durability of the catalysts. It is a story that parallels the tremendous growth in many areas of catalysis research and development over the past 40 years [80]. Research on noble metal catalysts began early on, in recognition of their excellent thermal stability and their lower tendency (compared to the base metals) to react with support materials. Perhaps the most important factor culling the list of candidate platinum group metals was the recognition that Ru, Ir, and Os form volatile oxides. Thus, Rh, Pt and Pd were left as clear choices for the oxidation catalysts employed during the first phase of catalytic emission controls (i.e. reduction of NO, oxidation of CO and HCs) beginning in US in 1975 [81].

<u>TWC:</u> In the earlier 1980s, the automotive manufacturer had to include exhaust after treatment control systems for four-stroke passenger car gasoline engines by three-way catalytic converter (TWC), which is capable of simultaneously reducing hydrocarbons (HCs), carbon monoxide (CO) and nitrogen oxides emissions (NOx) [82]. In the last few years, the most dominant catalyst form has been the monolith or honeycomb structure catalyst. This catalyst consists of a cordierite skeleton coated with a highly porous washcoat of about 90% γ-Al_2O_3 and a mixture of alkaline-earth metals, oxides etc. and last the noble metals, which are fixed in the washcoat surface [83]. Rhodium (Rh), Platinum (Pt) and Palladium (Pd) are preferred among the noble metals for oxidation reactions. As compared to them, all other noble metals exhibited undesirable higher volatility due to high temperatures and high velocity of the gases encountered during exhaust gas treatment [84, 85].

The commercially used three way catalytic converters formulations contain Pt/Rh, Pt/Pd/Rh (trimetal), Pd-only and Pd/Rh noble metal combinations [86, 87]. Palladium has higher specific activity than Pt for oxidation of CO, olefins and methane. For the oxidation of aromatics, Pd and Pt have similar activity while for the oxidation of paraffin hydrocarbon (higher than propane) Pt is more active than Pd. Palladium has a lower sintering tendency than Pt at high temperatures of about 980°C in the oxidizing atmosphere. The NO reduction activity of noble metals is in the order Rh>Pd>Pt. When simultaneous conversion of CO, HC and NOx is desired in the 3-way catalytic converters, a mixture of Pt + Pd is used, with Rh in a ratio of 5:1 to 10:1 [88, 89].

Rh-based Catalysts: Regardless the support, Rh is the most active noble metal among the three noble metals (Rh, Pt and Pd). Rh catalysts are active for N$_2$O decomposition from 200°C to 250°C, depending on the support, while a complete conversion is reached in the range 300-400°C. In contrast, Pd and Pt catalysts become active only above 400°C [90]. Interestingly, Rh$_2$O$_3$ has been recently identified as a highly active phase for N$_2$O decomposition by experimental [69] and theoretical studies [70]. It has been reported that Rh oxide (Rh$^{\delta+}$) was more active that Rh^0 for N$_2$O decomposition [69]. DFT calculations indicated that Rh$_2$O$_3$ phases exhibit high reactivity towards N$_2$O decomposition, which is mainly associated to high Lewis acidity of the Rh$_2$O$_3$ surface [70]. The activity of the noble metal catalyst for N$_2$O decomposition is closely related to the support type, as was mentioned above. Kim et al. [91] compared the activity of Rh/CeO$_2$ and Rh/Al$_2$O$_3$ for the decomposition of N$_2$O. Rh/CeO$_2$ exhibited complete conversion of N$_2$O at 350°C, whereas only about 40% conversion was obtained over Rh/Al$_2$O$_3$. Activity of Rh catalyst depended on the interactions between Rh and the support material. The most active sites for N$_2$O decomposition are reported to be located at the RhOx-ceria interface [92, 93]. Rhodium is also widely used for NOx reduction [94]. Nováková [95] compared the activities of CO and H$_2$ for NO reduction over Pt, Pd, and Rh supported on NaX zeolite, and found that Rh showed the best activity for NO-CO, while the worst for NO-H$_2$. Similar results were also reported by Kobylinski and Taylor [96]. Their investigations even inferred that CO shows higher activity than H$_2$ for NO reduction

over Rh. Experimental investigations by Chambers et al. [97] revealed that H_2 manifests similar onset temperature as CO for NO reduction over rhodium.

Pt-based Catalysts: Another metal mostly studied among the platinum group metal (PGM) catalysts is Pt, where much research has been done on it [98-104]. In 1971, Jones et al. [98] pointed out that H_2 can react preferentially with NO over O_2 in the reaction system of H_2-NO-O_2 on commercially supported Pt catalysts, suggesting the possibility of selective catalytic reaction in the presence of H_2 (H_2-SCR), although the reaction was not performed in excess oxygen conditions. Burch and Coleman [102, 104] systematically examined platinum-group metals (Pt, Pd, Rh, and Ir) on Al_2O_3 and SiO_2 for the NO reduction in the presence of a large excess of O_2 (500 ppm NO, 2000 ppm H_2, 6 vol. % O_2). NO was reduced effectively over Pt/Al_2O_3 catalyst (50% conversion at 140∘C) and 1% wt. Pt/SiO_2 (75% conversion at 90∘C). It was noted that N_2O is also formed in large amounts in addition to N_2 by H_2-SCR over Pt catalysts. The selectivity to N_2O was sensitive to reaction conditions; N_2O formation is increased in the presence of H_2O and decreased with increasing temperature.

Pd-based Catalysts: Although, Pd supported on conventional metal oxides appears to be inactive for the reduction of NO with H_2 in the presence of O_2 at temperatures lower than 200∘C, it presents significant activity when supported on more complex supports such as zeolites [105] and aluminosilicates (clays) [106]. Wen [105] reported that the activity of Pd towards the $NO/H_2/O_2$ reaction increases dramatically, when MFI is used as a support. In particular, the author showed that Pd/MFI presents high activity in the 50-250∘C low temperature range with selectivity values towards N_2 up to 70%. Yang et al. [107] have reported that Pd based catalysts, prepared by impregnation, show great activity (80-97%) and selectivity towards N_2 (80-95%), at low temperatures (140-250∘C), with the use of mixed metal oxides as supports (Al_2O_3, TiO_2, V_2O_5).

Li et al. [108] reported on the H_2-SCR of Pd on K_2O-$6TiO_2$ nanowires, prepared by alkali treatment of TiO_2. Although NO conversion on 1% wt. Pd/K_2O-$6TiO_2$ was intermediate (maximum 40%), it is accompanied by high N_2 selectivity of 80% and low H_2 conversion (ca. 11%). On the other hand, Pd/Al_2O_3 and Pd/TiO_2 exhibited maximum NO conversion values of about 50-60% at 100-130∘C, with N_2 selectivity less than 40%. In situ DRIFT spectroscopy revealed surface-fixed nitrates and Pd-

bound NO, but no NHx ad-species. It was concluded that the beneficial effect of the K$_2$O-6TiO$_2$ support is due to the stabilization of highly dispersed Pd with enhanced concentration of Pd^0-NO intermediates, as well as to the support basicity towards enhancing nitrate fixation.

HC-SCR over Pt-, Pd-, Rh-based Catalysts: In addition, noble metals (Pt, Pd, Rh) based catalysts have been extensively studied for the selective catalytic reduction of NO in the presence of hydrocarbons (HC-SCR), due to their low temperature activity and their stability in the presence of water vapor and sulfur compounds [109-121]. For example, Pt/Si-MCM-41 [112], Rh/TiO$_2$ [113], Pt/Al$_2$O$_3$ [114], are promising due to their high activity at low temperatures and good sulfur resistance and tolerance to steam. Obuchi and co-workers [115] prepared a series of alumina-supported Pt, Pd, Rh and Ru catalysts and obtained high NO conversion, in the presence of C$_3$H$_6$, at low temperature range (200-350°C). Kotsifa et al. [116] developed a 0.5% wt. Pt/ZrO$_2$ catalyst, which exhibited 40% NO conversion in the presence of C$_3$H$_6$ at 260°C. However, quite different mechanisms have been proposed for those catalysts. Some suggested surface nitrate species as the main intermediates in the HC-SCR reactions [117, 118], while others recommended the dissociation of NO over noble metal sites [119-121].

De-N$_2$O over Pt-, Pd-, Rh-based Catalysts: Noble metals, i.e. Pt, Pd and Rh, referred above, are used also for N$_2$O decomposition. However, a very important factor, which has to be considered, is the support. Pt catalysts are drastically hindered by adsorbed oxygen, leading to complete deactivation on a fully oxidized Pt surface [122, 123]. To this end, considerable efforts have been recently focused on enhancing the catalytic properties of noble metals by surface or structural modifiers such as alkalis (i.e. K, Na, etc.) [124-127] and REOs (i.e. CeO$_2$, La$_2$O$_3$, etc.) [128, 129]. Konsolakis et al. [77] investigated the impact of lanthanide oxides as support additives on N$_2$O decomposition. The de-N$_2$O efficiency of Pt/Al$_2$O$_3$ washcoated monoliths was greatly enhanced by incorporation of CeO$_2$-La$_2$O$_3$ mixed oxides into Al$_2$O$_3$ support; complete conversion of N$_2$O was attained over Pt/Al$_2$O$_3$-(CeO$_2$-La$_2$O$_3$) catalysts at ca. 500°C and a Gas Hourly Space Velocity (GHSV) of 10,000 h^{-1} even in the presence of excess O$_2$, in opposite to the unmodified Pt/Al$_2$O$_3$ catalyst, which achieved N$_2$O conversion less than ~20% at 600°C. Based on in situ diffuse

reflectance infrared Fourier transform spectroscopic (DRIFTS) measurements, the superior catalytic performance of modified samples was attributed to the formation of electron enriched Pt sites ($Pt^{\delta-}$), located at metal-support interfacial area, which are highly active towards N_2O decomposition.

However, besides structural modifiers, electropositive promoters, such as alkalis or alkaline earths, have also been reported to play a key role on de-N_2O process, over several catalytic systems e.g. [124, 130]. In a similar way highly effective and thermally stable Pt-based three way converters (TWCs) were developed in an effort to avoid the use of rare Rh in TWCs [131, 132]. This was accomplished through a synergistic structural and surface promotion by modifying the TWC washcoat with 20% wt. of $Ce_{0.8}La_{0.2}O_{1.9}$ (structural promoter) and sodium (surface promoter): $Pt(Na)/Al_2O_3$-$(CeO_2 + La_2O_3)$ [132].

The surface and catalytic properties of Pd/Al_2O_3 catalysts during the N_2O decomposition in the presence of hydrocarbons can be substantially altered by potassium (K), which was supplied either electrochemically [133] or conventionally [134] onto the catalyst surface. In particular, it was found that potassium strongly enhances the N_2O decomposition rate, resulting in notably lower N_2O light-off temperatures (of about 100^oC), as compared to the un-promoted catalyst. Based on a surface characterization study [134], it was revealed that the electronic properties of Pd/Al_2O_3 catalyst can be substantially modified by potassium addition, which in turn affects the reactants' chemisorptive bonds and consequently the deN_2O activity.

I.4.2 Ir-Based Catalysts

For a long time Ir catalysts have received little attention. The limited use of Ir (like in injection engines from Mitsubishi) can be attributed to several factors. Among them the scarcity of Ir, the formation of volatile iridium chlorides and oxychlorides, and its underestimated catalytic potential may be the most crucial ones [135]. Only recently, Ir catalysts have been gaining more and more interest. Tauster and Murrell [136] were the first to use CO as reducing agent in the reduction of NO over Ir. They showed that on Ir/Al_2O_3 the reaction between NO and CO was favored instead of the reaction of CO with O_2. These results were also confirmed by Taylor and Schlatter

[137]. The high conversions for NO were ascribed to the strong ability of Ir to adsorb and dissociate NO in the presence of excess oxygen. A significant advantage of Ir-based catalysts, as compared to Pt-based catalysts, is the high selectivity toward N$_2$ formation. In a similar manner, Wögerbauer et al. [138] reported on the high N$_2$ yield of unsupported iridium catalysts. Ogura et al. [139] showed that CO could be a selective reducing agent for NO, under oxidizing conditions, over several different supported Ir catalysts. Wang et al. [140, 141] reported that among Pt, Pd, Rh and Ir catalyst, Ir/ZSM-5 catalyst exhibits the highest activity for the NO reduction by CO, in the presence of excess O$_2$ and H$_2$O. Haneda et al. [142-144] discovered that Ir/SiO$_2$ shows marked catalytic activity for the NO reduction with CO, in the presence of O$_2$, H$_2$O and SO$_2$. Furthermore, Fujitani et al. [145] investigated the adsorption/activation of NO over the clean Ir (111) surfaces and found that the adsorbed NO dissociates to N$_2$ at 200°C and 300°C. Chen et al. [146, 147] studied the adsorption and decomposition of NO on the clean and O-covered planar Ir (210) and nanofaceted Ir (210). They found that both Ir (210) surfaces are very active for the NO decomposition, with high selectivity to N$_2$.

Concerning N$_2$O decomposition, Ir metal has been rarely investigated although its activity is expected to be similar to that of Rh [49]. Ir/Al$_2$O$_3$ was reported to be a promising representative [148, 149]. However, the catalyst exhibited relatively lower initial activity at low temperatures, in high-concentration N$_2$O decomposition for propulsion applications and was gradually deactivated at high temperatures due to the sintering of iridium, which greatly constrains its practical application. One effective strategy is to find a suitable support, capable of stabilizing Ir particles and efficiently facilitating the decomposition of N$_2$O, like addition of promoters to alumina support, in order to prevent the catalyst sintering and stabilize the metal. Yentekakis et al. [150] showed that in the case of Ir catalysts supported on γ-Al$_2$O$_3$, rapid and extensive sintering occurred, while over doped alumina or mixed oxides (i.e. ceria-zirconia- alumina or gadolinia-ceria) negligible sintering was observed. This resistance to sintering is considered in terms of oxygen spillover from support to nanoparticles and discussed with respect to the alternative mechanisms of Ostwald ripening versus nanoparticle diffusion.

Although there are some concerns about the volatility of iridium at elevated temperatures, its adequate performance in conjunction with its satisfactory stability at intermediate temperatures [151], render Ir-based catalysts as possible alternatives for NO, as well N_2O abatement in practical applications. The key factor for these reactions seems to be the crystallite size of iridium particles and the oxidation state of Ir. At the same time, the pretreatment plays also an important role in order to achieve the active phase of iridium. It was shown that inactive Ir catalysts could be activated by on-stream conditioning [152], by other hydro-thermal pretreatment [153, 154], by high temperature pretreatments [140, 155, 156] or by in situ activation during catalytic tests [157, 158]. These methods led to crystallite growth and a coexistence of Ir and IrO_2 [157, 159], which are consider as the key factors for the abatement of both NOx and/or N_2O.

According to Wögerbauer et al. [157], crystallite size and oxidation state of Ir is crucial for the NO reduction behavior of Ir/H-ZSM-5. Under reaction conditions Ir was present as Ir^0 and IrO_2, where the metallic Ir was considered as the active phase for high De-NOx activity. The ratio of Ir^0/Ir^{4+} was found to depend on the size of Ir-containing crystallites, with larger crystallites to contain predominantly Ir^0. Haneda et al. [160] studied the selective reduction of NO with CO in the presence of O_2 and SO_2 over Ir/SiO_2 and showed that larger iridium crystallites are more difficult to be oxidized and much easier to be reduced under reaction conditions; resulting in the formation of stable iridium metal sites, on which NO reduction occurs. Larger crystallites (catalysts with lower metal dispersion) were found to exhibit significantly higher N_2 yields [135, 154], which could be related -in the case of iridium- to a change in the relative adsorption properties of O_2 and NO on its surface [135]. Iojoiu et al. [158] on the other hand, supported that during SCR of NO by propene under lean-burn conditions, the surface of initially oxidized Ir particles progressively reduced with increasing temperatures into partially reduced $Ir^{\delta+}$ surface species, allowing the adsorption of both CO and NO [158].

For the direct N_2O decomposition, the most crucial problem arises from the poisoning of the catalytic surface by the strongly adsorbed oxygen atoms, as well as by the presence of H_2O and NO, that typically coexist with N_2O in an exhaust gas stream. In this regard, the development of stable and active catalysts for N_2O

decomposition under industrial conditions is still required. Ohnishi et al. [161] investigated the direct decomposition of nitrous oxide on iridium catalyst supported on alumina. One of the important factors for high catalytic activity of the present catalyst is the large crystallite size of iridium. It is rather surprising to know that desorption of oxygen from the bulk of IrO$_2$ started at much lower temperature than desorption of oxygen from the surface of Ir metal particles. These results indicate that removal of oxygen atoms formed by N$_2$O decomposition requires relatively high temperatures. The catalytic activity was improved by increasing the crystallite size of iridium species. Small particles of metal Ir expose kinks and steps on the surface and it is reasonable to assume that the oxygen atoms adsorbed on these defect sites are quite difficult to be desorbed. Therefore, the catalyst with a small crystallite size of iridium has a low steady-state activity, even though it has a larger metal surface area.

In the case of Ir-based catalysts structural promoters prevent iridium sintering and stabilize iridium particles. Among them, CeO$_2$ has been widely investigated due to the oxygen storage capacity, which affects the oxidation state of the supported elements [162, 77]. The beneficial role of structure modifiers, based on CeO$_2$, is mainly related to its ability of increasing dispersion of supported metals, changing metal oxidation state, promoting several reactions, as well as capturing or releasing O$_2$ depending on the conditions used [73].

I.5 EFFECT OF INHIBITORS (SO$_2$, H$_2$O)

In the previous section an overview of the noble metal-based catalytic systems for NOx and N$_2$O abatement was presented. However, the co-existence of various inhibitors, such as SO$_2$ and H$_2$O, in the exhaust stream require the development of catalytic materials that possess good activity and stability under real exhaust conditions.

Amiridis et al. [163] reviewed the catalytic activity of supported noble metals for the abatement of NO in the presence of various poisons, summarizing the experimental results over different catalysts and the proposed reaction mechanisms. They noticed that the presence of water and SO$_2$ in the feed gas stream can inhibit the NO

reduction, while the formation of undesirable gas products such as N_2O and SO_3 was also noticed. However, over Pt/Al_2O_3 catalyst, Zhang et al. [164] reported that the presence of SO_2 improved both the activity and selectivity of these catalysts for the reduction of NO. These results were attributed to an inhibiting effect of SO_2 on propylene combustion and the preferential poisoning by sulfur of the sites responsible for N_2O formation. Nakatsuji et al. [165] further suggested that the activity of a Pt/Al_2O_3 catalyst is enhanced by SO_2 only below the temperature of maximum NO conversion, while the opposite is observed at higher temperatures. Oxidation of SO_2 to SO_3 is also expected to take place on supported Pt catalysts under realistic diesel exhaust conditions, leading to the formation of unwanted sulfated particles. The same was observed over Rh-based catalysts for the abatement of NO and N_2O [166-168]. Efthimiadis et al. [166, 167] observed that the presence of SO_2 in the NO + C_3H_6 + O_2 gas mixture increased the activity of Rh/Al_2O_3 catalysts for NO reduction, because of the formation of sulfates. In addition, low concentration of SO_2 does not significantly affect the conversion of N_2O to N_2 and O_2 [168].

Moreover, Ir/SiO_2 shows excellent activity with respect to NO reduction with CO in the presence of O_2 and SO_2. On the other side, Ir over Al_2O_3 support was slightly affected by the presence of SO_2. Thus, SiO_2 appears to be more effective support than Al_2O_3 for NO reduction with CO in the presence of O_2 and SO_2 [169]. The inhibiting effect of SO_2 was observed over Pd/Al_2O_3 catalyst for the decomposition of N_2O. SO_2 addition in the feed stream results in an irreversible deactivation, ascribed to the creation of Brönsted acid sites on alumina support; this in turns results, via metal-support interactions, to highly oxidized Pd species, which are inactive for N_2O decomposition [170]. Although the deactivation of supported metal catalysts by SO_2 is a well-known phenomenon, there still exists an extended discrepancy in the literature concerning the mechanism of this deactivation. The deactivation induced by SO_2 can be mainly ascribed to the formation of inactive metal-SOx species [171]. On the other hand, several studies over metal supported catalysts on sulfating (like Al_2O_3) supports reveal that the deactivation should be primarily assigned to the sulfation of support [172].

Water has also an inhibiting effect to the catalyst's activity. However, this inhibition is completely reversible and the catalyst's initial activity is restored after removing H$_2$O from the feed [170, 173-176]. Marnellos et al. [173] reported that the addition of water shifted the experimental curves to higher temperatures and the concentration of H$_2$O in the feed did not affect the catalytic activity. The inhibition caused by the presence of water is attributed to the competitive adsorption of H$_2$O with N$_2$O on the catalyst surface. Konsolakis et al. [170] presented that H$_2$O does not have any permanent effect on catalyst surface acidity, justifying the recovery of de-N$_2$O efficiency after H$_2$O removal, in contrast with SO$_2$, which permanently affects the catalytic activity.

I.6 AIM OF THE PRESENT PhD THESIS

The aim of the present PhD thesis is the development of technologically advanced-in terms of design, composition, cost and efficiency-catalytic materials, which could abate N$_2$O and/or NOx from combustion flue gases. Both NOx and N$_2$O have been recognized as extremely harmful pollutants, contributing among others to ozone depletion and the greenhouse effect. It is therefore essential to develop efficient processes for their abatement. The novel, in terms of synthesis and design, the materials of the present study, will also contribute significantly to its innovative character, since the intrinsic catalytic characteristics will be adjusted via the synergy of structure and surface promoters. The as prepared catalysts will be characterized by low cost, since the amount of noble metal (Pt, Pd, Ir) will be lower than 1% wt., avoiding at the same time the use of rare and expensive Rh. From a fundamental research point of view, the proposed thesis directly promotes the innovation, since the mechanism of both structure/surface promoters, as well as their synergy, will be investigated in depth through the use of advanced characterization techniques. In this direction, the obtained results are expected to contribute significantly to the understanding of the promotion phenomena in environmental catalysis.

REFERENCES

[1] Clean Air Technology Center, "Nitrogen Oxides (NOx), Why and How They Are Controlled", November (1999).

[2] Pârvulescu V.I., Grange P., Delmon B., "Catalytic Removal of NO", Catalysis Today 46 (1998) 233-316.

[3] Galloway J.N., Townsend A.R., Erisman J.W., Bekunda M., Cai Z., Freney J.R., Martinelli L.A., Seitzinger S.P., Sutton M.A., "Transformation of the Nitrogen Cycle: Recent Trends, Questions, and Potential Solutions", Science 320 (2008) 889-892.

[4] Clean Air Technology Center, "NOx-How Nitrogen Oxides Affect the Way we Live and Breathe", September (1998).

[5] Sawyer R.F., Harley R.A., Cadle S.H., Norbeck J.M., Slott R., Bravo H.A., "Mobile sources critical review: 1998 NARSTO assessment", Atmospheric Environment 34 (2000) 2161-2181.

[6] Vitousek P.M., Aber J., Howarth R.W., Likens G.E., Matson P.A., Schindler D.W., Schlesinger W.H., Tilman G.D., "Human Alteration of the Global Nitrogen Cycle: Causes and Consequences", Issues in Ecology 1 (1997).

[7] http://www.n-print.org/Background "The Formation of Reactive Nitrogen".

[8] Cheng W.C., Kim G., Peters A.W., Zhao X., Jagopalan K.R., Ziebarth M.S., Pereira C.J., "Environmental Fluid Catalytic Cracking Technology", Catalysis Reviews: Science and Engineering 40 (1998) 39-79.

[9] Manney G.L., Froidevaux L., Waters J.W., Zurek R.W., Read W.G., Elson, Kumer J.B., Mergenthaler J.L., Roche A.E., O'Nelll A., Harwood R.S., MacKenzie I., Swinbank R., "Chemical depletion of ozone in the Arctic lower stratosphere during winter 1992–93", Nature 370 (1994) 429.

[10] Armor J.N., "Environmental Catalysis", Applied Catalysis B: Environmental 1 (1992) 221-256.

[11] Stern A.C., Wohlers H.C., Boubel R.W., Lowry W.P., "Fundamental of Air Pollution", Academic Press, New York (1973).

[12] Maric D., Burrows J.P., "Formation of N_2O in the photolysis/photoexcitation of NO, NO_2 and air", Journal of Photochemistry and Photobiology A: Chemistry 66 (1992) 291-312.

[13] Perez-Ramirez J., Kapteijn F., Schöffel K., Moulijn J.A., "Formation and control of N$_2$O in nitric acid production-Where do we stand today?", Applied Catalysis B: Environmental 44 (2003) 117-151.

[14] Ravishankara A.R., Sutton M.A., Davidson E.A., Kanter D., Daniel J.S., "Drawing Down N$_2$O: To Protect Climate and the Ozone Layer", UNEP Synthesis Report, Chapter 1: Introduction, (2013).

[15] Konsolakis M., "Recent Advances on Nitrous Oxide (N$_2$O) Decomposition over Non-Noble-Metal Oxide Catalysts: Catalytic Performance, Mechanistic Considerations, and Surface Chemistry Aspects, ACS Catalysis 5 (2015) 6397-6421.

[16] Daniel J.S., Holland E., Ravishankara A.R., Boering K., Sharma P., "Drawing Down N$_2$O: To Protect Climate and the Ozone Layer", UNEP Synthesis Report, Chapter 2: N$_2$O-Its Role in Climate Change and Ozone Layer Depletion, (2013).

[17] Weiss R.F., "The Temporal and Spatial Distribution of Tropospheric Nitrous Oxide", Journal of Geophysical Research 86 (1981) 7185-7195.

[18] Lyon R.K., Kramlich J.C., Cole J.A., "Nitrous Oxide: Sources, Sampling, and Science Policy", Environmental Science and Technology 23 (1989) 392-393.

[19] Li L., Xu J., Hu J., Han J., "Reducing Nitrous Oxide Emissions to Mitigate Climate Change and Protect the Ozone Layer", Environmental Science and Technology 48 (2014) 5290-5297.

[20] Davidson E., Kanter D., Suddick E., Sutharalingam P., "Drawing Down N$_2$O: To Protect Climate and the Ozone Layer", UNEP Synthesis Report, Chapter 3: N$_2$O-Sources, Inventories, Projections, (2013).

[21] Wiesen P., Wallington T.J., Winiwarter W., "Drawing Down N$_2$O: To Protect Climate and the Ozone Layer", UNEP Synthesis Report, Chapter 5: Reducing N$_2$O Emissions from Industry and Fossil Fuel Combustion (2013).

[22] Tsupari E., Monni S., Tormonen K., Pellikka T., Syri S., "Estimation of Annual CH$_4$ and N$_2$O Emissions from Fluidised Bed Combustion: An Advanced Measurement-based Method and its Application to Finland", International Journal of Greenhouse Gas Control 1 (2007) 289–297.

[23] Odaka M., Koike N., Suzuki H., "Influence of Catalyst Deactivation on N$_2$O Emissions from Automobiles", Chemosphere: Global Change Science 2 (2000) 413-423.

[24] Galloway J.N., Leach A.M., Bleeker A., Erisman J.W., "A Chronology of Human Understanding of the Nitrogen Cycle", Philosophical Transactions of the Royal Society 368 (2013).

[25] Galloway J.N., Aber J.D., Erisman J.W., Seitzinger S.P., Howarth R.W., Cowling E.B., Cosby B.J., "The Nitrogen Cascade", Bioscience 53 (2003) 341-356.

[26] Lindqvist K., "Emission standards for light and heavy road vehicles", AirClim Factsheet-EU Regulation, no: 25 (2012).

[27] European Commission, 25.6.2011. Commission regulation (EU) No 582/2011 of 25 May 2011 implementing and amending regulation (EC) No 595/2009 of the European Parliament and of the council with respect to emissions from heavy duty vehicles (Euro VI) and amending annexes I and III to directive 2007/46/EC of the European Parliament and of the council. Official J. Eur. Union L 167, 1-168.

[28] U.S. Environmental Protection Agency, 2015. Phase 2 Greenhouse Gas Emissions Standards and Fuel Efficiency Standards for Medium- and Heavy-duty Engines And Vehicles. Available from: http://www3.epa.gov/otaq/climate/regs-heavy-duty.htm.

[29] Suarez-Berto R., Mendoza-Villafuerte P., Bonnel P., Lilova V., Hill L., Perujo A., Astorga C., "On-road measurement of NH_3 and N_2O emissions from a Euro V heavy-duty vehicle", Atmospheric Environment 139 (2016) 167-175.

[30] Wang Y., Posthuma de Boer J., Kapteijn F., Makkee M., "Next generation automotive DeNOx catalysts: Ceria what else?", Chemcatchem 8 (2016) 102-105.

[31] Burch R., Breen J.P, Meunier F.C., "A review of the selective reduction of NOx with hydrocarbons under lean-burn conditions with non-zeolitic oxide and platinum group metal catalysts", Applied Catalysis B: Environmental 39 (2002) 283–303.

[32] Fritz A., Pitchon V., "Review-The current state lean of research on automotive NOx catalysis", Applied Catalysis B: Environmental 13 (1997) 1-25.

[33] Liu Z., Woo S.I., "Recent Advances in Catalytic DeNOx Science and Technology", Catalysis Reviews 48 (2006) 43-89.

[34] Hamada H., Haneda M., "A review of selective catalytic reduction of nitrogen oxides with hydrogen and carbon monoxide", Applied Catalysis A: General 421– 422 (2012) 1– 13.

[35] Iwamoto M., "Chapter II.3 Catalytic Decomposition of Nitrogen Monoxide", Studies in Surface Science and Catalysis 54 (1990) 121–143.

[36] Inui T., Kojo S., Shibata M., Yoshida T., Iwamoto S., "NO Decomposition on Cu-Incorporated A-Zeolites under the Reaction Condition of Excess Oxygen with a Small Amount of Hydrocarbons", Studies in Surface Science and Catalysis 69 (1991) 355–364.

[37] Held W., Konig A., Richter T., Puppe L., "Catalytic NOx Reduction in Net Oxidizing Exhaust Gas", SAE Technical Paper 900 (1990) 496.

[38] Hamada H., Kintaichi Y., Sasaki M., Ito T., Tabata M., "Highly selective reduction of nitrogen oxides with hydrocarbons over H-Form zeolite catalysts in oxygen-rich atmosphers", Applied Catalalysis 64 (1990) L1–L4.

[39] Kintaichi Y., Hamada H., Tabata M., Sasaki M., Ito T., "Selective reduction of nitrogen oxides with hydrocarbons over solid acid catalysts in oxygen-rich atmospheres", Catalysis Letters 6 (1990) 239–244.

[40] Sato S., Hirabayashi H., Yahiro H., Mizuno N., Iwamoto M., "Iron ion exchanged Zeolite: the most active catalyst at 473 K for selective reduction of nitrogen monoxide by ethene in oxidizing atmosphere", Catalysis Letters 12 (1992) 193–200.

[41] Witzel F., Sill G.A., Hall W.K., "Reaction Studies of the Selective Reduction of NO by Various Hydrocarbons", Journal of Catalysis 149 (1994) 229–237.

[42] Loginov A.Yu., Chapayeva A.Yu., Chokayev H.K., Ikonnikov I.A., "Development of the rare earth-transition metal oxide catalysts active surface for industrial gas detoxication", Catalysis Today 17 (1993) 85–93.

[43] Miyadera T., "Alumina-supported silver catalysts for the selective reduction of nitric oxide with propene and oxygen-containing organic compounds", Applied Catalysis B 2 (1993) 199–205.

[44] Zhang X., Waiters A.B., Vannice M.A., "NOx decomposition and reduction by methane over La$_2$O$_3$", Applied Catalysis B: Environmental 4 (2-3) (1994) 237–256.

[45] Tabata M., Hamada H., Suganuma F., Yoshinari Y., Tsuchida H., Kintaichi Y., Sasaki M., lto T., "Promotive effect of Sn on the catalytic activity of Al$_2$O$_3$ for the selective reduction of NO by methanol", Catalysis Letters 25 (1-2) (1994) 55–60.

[46] Bethke K.A., Alt D., Kung M.C., "NO reduction by hydrocarbons in an oxidizing atmosphere over transition metal-zirconium mixed oxides", Catalysis Letters 25 (1994) 37–48.

[47] Tran K-Q., Kilpinen P., Kumar N., "In-situ catalytic abatement of NOx during fluidized bed combustion—A literature study", Applied Catalysis B: Environmental 78 (2008) 129–138.

[48] Savva P.G., Costa C.N., "Hydrogen Lean-DeNOx as an Alternative to the Ammonia and Hydrocarbon Selective Catalytic Reduction (SCR)", Catalysis Reviews: Science and Engineering 53 (2011) 91–151.

[49] Kapteijn F., Rodriguez-Mirasol J., Moulijn J.A., "Review Heterogeneous Catalytic Decomposition of Nitrous Oxide", Applied Catalysis B: Environmental 9 (1996) 25-64.

[50] Galle M., Agar D.W., Watzenberger O., "Thermal N_2O decomposition in regenerative heat exchanger reactors", Chemical Engineering Science 56 (2001) 1587-1595.

[51] Bamford C.H., Tipper C.F.H., "Reactions of non-metallic inorganic compounds", Amsterdam: Elsevier 6 (1972) 65-75.

[52] Dindi H., Tsai H., Branch M.C., "Combustion Mechanism of Carbon Monoxide-Nitrous Oxide Flames", Combustion and Flame 87 (1991) 13-20.

[53] Miller J.A., Bowman C.T., "Mechanism and modeling of nitrogen chemistry in combustion", Progress in Energy Combustion Science 15 (1989) 287.

[54] Lee D.H., Kim T., "N_2O Decomposition by Catalyst-Assisted Cold Plasma".

[55] Swamy C.S., Christopher J., "Decomposition of N_2O on Perovskite-Related Oxides", Catalysis Reviews 34 (1992) 409–425.

[56] Peña M.A., Fierro L.G., "Chemical Structures and Performance of Perovskite Oxides", Chemical Reviews 101 (2001) 1981–2017.

[57] Kannan S., Viswanathan, B., "Selected Studies in Heterogeneous Catalysis", Indian Institute of Technology: Madras, India (1996) 62–85.

[58] Serwicka, E. M., "Clays as catalysts for the removal of nitrogen oxides", Polish Journal of Chemistry 75 (2001) 307–328.

[59] Centi G., Perathoner S., Rak Z. S., "Reduction of greenhouse gas emissions by catalytic processes", Applied Catalysis B 41 (2003) 143–155.

[60] Dramlic D.M., Jrsic Z.J., Popovic M.M, "Possibility of the detection of a low concentration hydrogen sulphide gas using the semiconducting gas sensors of the SNO_2 type", Journal of Environmental Protection and Ecology 3 (2002) 519.

[61] Kögel M., Mönnig R., Schwieger W., Tissler A., Turek T., "Simultaneous catalytic removal of NO and N$_2$O using Fe-MFI", Journal of Catalysis 182 (1999) 470.

[62] Li Y., Armor J.N., "Catalytic combustion of methane over palladium exchanged zeolites", Applied Catalysis B: Environmental 3 (1994) 275.

[63] Gassan-Zedeh G.Z., Seyidbayova S.F., "The heterogeneous catalytic reduction of NO and N$_2$O mixture by carbon monoxide", Applied Catalysis B: Environmental 42 (2003) 359.

[64] Van den Brink R.W., Booneveld S., Verhaak M.J.F.M., de Bruijn F.A., "Selective catalytic reduction of N$_2$O and NOx in a single reactor in the nitric acid industry", Catalysis Today 75 (2002) 227.

[65] Gonçalves F., Figueiredo J.L.,"Development of carbon supported metal catalysts for the simultaneous reduction of NO and N$_2$O", Applied Catalysis B: Environmental 50 (2004) 271.

[66] Goncalves F., Figueiredo J.L., "Synergistic effect between Pt and K in the catalytic reduction of NO and N$_2$O", Applied Catalysis B: Environmental 62 (2006) 181.

[67] Marnellos G.E., Efthimiadis E.A., Vasalos I.A., "Simultaneous Catalytic Reduction of NOx and N$_2$O in an In/Al$_2$O$_3$-Ru/Al$_2$O$_3$ Dual-Bed Reactor in the Presence of SO$_2$ and H$_2$O", Industrial & Engineering Chemistry Research 43 (2004) 2413.

[68] Centi G., Galli A., Montanari B., Perathoner S., Vaccari A., "Catalytic decomposition of N$_2$O over noble and transition metal containing oxides and zeolites. Role of some variables on reactivity", Catalysis Today 35 (1997) 113-120.

[69] Bueno-Lopez A., Such-Basanez I., Salinas-Martinez de Lecea C., "Stabilization of active Rh$_2$O$_3$ species for catalytic decomposition of N$_2$O on La-, Pr-doped CeO$_2$", Journal of Catalysis 244 (2006) 102-112.

[70] Scherson Y.D., Aboud S.J., Wilcox J., Cantwell B.J., "Surface Structure and Reactivity of Rhodium Oxide", Journal of Physical Chemistry C 115 (2011) 11036–11044.

[71] Komvokis V.G., Marnellos G.E., Vasalos I.A., Triantafyllidis K.S., "Effect of pretreatment and regeneration conditions of Ru/g-Al$_2$O$_3$ catalysts for N$_2$O decomposition and/or reduction in O$_2$-rich atmospheres and in the presence of NOx, SO$_2$ and H$_2$O", Applied Catalysis B 89 (2009) 627.

[72] Alvarez-Galvan M.C., Navarro R.M., Rosa F., Bricen Y., Gordillo Alvarez F., Fierro J.L.G., "Performance of La,Ce-modified alumina-supported Pt and Ni catalysts for the oxidative reforming of diesel hydrocarbons", International Journal of Hydrogen Energy 33 (2008) 652–663.

[73] Trovarelli A., "Catalytic Properties of Ceria and CeO_2-Containing Materials", Catalysis Reviews, Science and Engineering 38 (1996) 439.

[74] Riguetto B.A., Damyanova S., Gouliev G., Marques C.M.P., Petrov L., Bueno J.M.C., "Surface behavior of alumina-supported Pt catalysts modified with cerium as revealed by X-ray diffraction, X-ray photoelectron spectroscopy, and Fourier transform infrared spectroscopy of CO adsorption", Journal of Physical Chemistry B 108 (2004) 5349.

[75] Martinez-Arias A., Coronado J.M., Cataluna R., Conesa J.C., Soria J., " Influence of mutual platinum-dispersed ceria interactions on the promoting effect of ceria for the CO oxidation reaction in a $Pt/CeO_2/Al_2O_3$ catalyst", Journal of Physical Chemistry B 102 (1998) 4357.

[76] Matsouka V., Konsolakis M., Lambert R.M., Yentekakis I.V., "In situ DRIFTS study of the effect of structure (CeO_2–La_2O_3) and surface (Na) modifiers on the catalytic and surface behaviour of Pt/g-Al_2O_3 catalyst under simulated exhaust conditions", Applied Catalysis B 84 (2008) 715.

[77] Konsolakis M., Drosou C., Yentekakis I.V., "Support mediated promotional effects of rare earth oxides (CeO_2 and La_2O_3) on N_2O decomposition and N_2O reduction by CO or C_3H_6 over Pt/Al_2O_3 structured catalysts", Applied Catalysis B: Environmental 123– 124 (2012) 405- 413.

[78] Schaper H., Doesburg E.B.M., van Reijen L.L., "The influence of lanthanum oxide on the thermal stability of gamma alumina catalyst supports", Applied Catalysis 7 (1983) 211–20.

[79] Kim M.H., Ebner J.R., Friedman R.M., Vannice M.A., "Dissociative N_2O adsorption on supported Pt", Journal of Catalysis 204 (2001) 348-357.

[80] Gandhi H.S., Graham G.W., McCabe R.W., "Automotive exhaust catalysis", Journal of Catalysis 216 (2003) 433–442.

[81] Kummer J.T., "Use of noble metals in automobile exhaust catalysts", Journal of Physical Chemistry 90 (1986) 4747.

[82] Faiz A.,Weaver C.S., Walsh M.P., "Air Pollution from Motor Vehicles. Standards and Technologies for Controlling Emissions", The World Bank Washington, D.C. (1996).

[83] Leman A.M., Jajuli A., Feriyanto D., Rahman F., Zakaria S., "Advanced Catalytic Converter in Gasoline Enginer Emission Control: A Review", MATEC Web of Conferences 87 (2017).

[84] Choudhary T.V., Banerjee S., Choudhary V.R., "Catalysts for combustion of methane and lower alkanes", Applied Catalysts A: General 234 (2002) 1-23.

[85] Arai H., Machida M., "Recent progress in high-temperature catalytic combustion", Catalysis Today 10 (1991) 81-94.

[86] Shelef M., McCabe R.W., "Twenty-five years after introduction of automotive catalysts: what next?", Catalysis Today 62 (2000) 35-50.

[87] Chauhan S., "Noble metal catalysts for monolithic converters", Journal of Chemical and Pharmaceutical Research 2(4) (2010) 602-611.

[88] Nishita Y., Mizuki J., Tanka H., Uenishi M., Kimura M., "Self regeneration of palladium-perovskite catalysts in modern automobile?", Journal of Physics and Chemistry of Solids 66 (2005) 274-282.

[89] Pardiwala J.M., Patel F., Patel S., "Review paper on Catalytic Converter for Automotive Exhaust Emission", Institute of Technology, NIRMA UNIVERSITY, AHMEDABAD (2011).

[90] Liu Z., He F., Ma L., Peng S., "Recent Advances in Catalytic Decomposition of N$_2$O on Noble Metal and Metal Oxide Catalysts", Catalysis Surveys from Asia (2016) 1-12.

[91] Kim S.S., Lee S.J., Hong S.C., "Effect of CeO$_2$ Addition to Rh/Al$_2$O$_3$ Catalyst on N$_2$O Decomposition", Chemical Engineering Journal 169 (2011) 173.

[92] Parres-Esclapez S., Such-Basanẽz I., Illan-Gomez M.J., De Lecea C.S.M., Bueno-Lopez A., "Study by isotopic gases and in situ spectroscopies (DRIFTS, XPS and Raman) of the N$_2$O decomposition mechanism on Rh/CeO$_2$ and Rh/γ-Al$_2$O$_3$ catalysts", Journal of Catalysis 276 (2010) 390.

[93] Rico-Pèrez V., de Lecea C.S.M., Bueno-Lòpez A., "Preparation of RhOx/Ce$_y$Pr$_{1-y}$O$_2$ N$_2$O decomposition catalysts by rhodium nitrate impregnation with different solvents", Applied Catalysis A 472 (2014) 134.

[94] Srinivasan A., Depcik C., "Review of chemical reactions in the no reduction by co on rhodium/alumina catalysts", Catalysis Reviews 52 (2010) 462.

[95] Nováková J., "Reduction of NO by hydrogen versus reduction by CO over Pt, Pd and Rh clusters in NaX zeolite", Applied Catalysis B 30 (2001) 445.

[96] Kobylinski T.P., "The catalytic chemistry of nitric oxide. II. Reduction of nitric oxide over noble metal catalysts", Journal of Catalysis 33 (1974) 376.

[97] Chambers D.C., Angove D.E., Cant N.W., "The formation and hydrolysis of isocyanic acid during the reaction of NO, CO, and H_2 mixtures on supported platinum, palladium, and rhodium", Journal of Catalysis 204 (2001) 11.

[98] Jones J.H., Kummer J.T., Otto K., Shelef M., Weaver E.E., "Selective catalytic reaction of hydrogen with nitric oxide in the presence of oxygen", Environmental Science and Technology 5 (1971) 790–798.

[99] Lamb A., Tollefson E.L., "Catalytic reduction of nitric oxide in the presence of oxygen in low concentration high velocity gas streams", The Canadian0 Journal of Chemical Engineering 53 (1975) 68–73.

[100] Wildermann A., Ph.D. Thesis, University of Erlangen, Nurnberg, 1994.

[101] Yokota K., Fukui M., Tanaka T., **"**Catalytic removal of nitric oxide with hydrogen and carbon monoxide in the presence of excess oxygen", Applied Surface Science 121-122 (1997) 273–277.

[102] Burch R., Coleman M.D., "An investigation of promoter effects in the reduction of NO by H_2 under lean-burn conditions", Journal of Catalysis 208 (2002) 435–447.

[103] Frank B., Emig G., Renken A., "Kinetics and mechanism of the reduction of nitric oxides by H2 under lean-burn conditions on a Pt-Mo-Co/α-Al$_2$O$_3$ catalyst", Applied Catalysis B 19 (1998) 45–57.

[104] Burch R., Coleman M.D., "An investigation of the NO/H_2/O$_2$ reaction on noble-metal catalysts at low temperatures under lean-burn conditions", Applied Catalysis B 23 (1999) 115–121.

[105] Wen B., "NO reduction with H_2 in the presence of excess O_2 over Pd/MFI catalyst", Fuel 81 (2002) 1841–1846.

[106] Qi G., Yang R.T., Thompson L.T., "Catalytic reduction of nitric oxide with hydrogen and carbon monoxide in the presence of excess oxygen by Pd supported on pillared clays", Applied Catalysis A: General 259 (2004) 261–267.

[107] Qi G., Yang R.T., Rinaldi F.C., "Selective catalytic reduction of nitric oxide with hydrogen over Pd-based catalysts", Journal of Catalysis 237 (2006) 381–392.

[108] Li L., Zhang F., Guan N., Schreier E., Richter M., "NO selective reduction by hydrogen on potassium titanate supported palladium catalyst", Catalysis Communications 9 (2008) 1827–1832.

[109] Zhang Z., Chen M., Jiang Z., Shangguan W., "Performance and mechanism study for low-temperature SCR of NO with propylene in excess oxygen over Pt/TiO$_2$ catalyst", Journal of Environmental Sciences 2010, 22(9) 1441–1446.

[110] Mrad R., Aissat A., Cousin R., Courcot D., Siffert S., "Catalysts for NOx selective catalytic reduction by hydrocarbons (HC-SCR)", Applied Catalysis A: General 504 (2015) 542–548.

[111] Amiridis M.D., Mihut C., Maciejewski M., Baiker A., "The selective catalytic reduction of NO by hydrocarbons over Pt- and Ir-based catalysts", Topics in Catalysis 28 (2004) 141.

[112] Shen S.C., Kawi S., "Mechanism of selective catalytic reduction of NO in the presence of excess O$_2$ over Pt/Si-MCM-41 catalyst", Journal of Catalysis 203 (2003) 241-250.

[113] Halkides T.I., Kondarides D.I., Verykios X.E., "Mechanistic study of the reduction of NO by C$_3$H$_6$ in the presence of oxygen over Rh/TiO$_2$ catalysts", Catalysis Today 73 (2002) 213-221.

[114] Captain D.K., Amiridis M.D., "In situ FTIR studies of the selective catalytic reduction of NO by C$_3$H$_6$ over Pt/Al$_2$O$_3$", Journal of Catalysis 184 (1999) 377-389.

[115] Obuchi A., Ohi A., Nakamura M., Ogata A., Mizuno K., Ohuchi H., "Performance of platinum-group metal catalysts for the selective reduction of nitrogen oxides by hydrocarbons", Applied Catalysis B: Environmental 2 (1993) 71-80.

[116] Kotsifa A., Kondarides D.I., Verykios X.E., "Comparative study of the chemisorptive and catalytic properties of supported Pt catalysts related to the selective catalytic reduction of NO by propylene", Applied Catalysis B: Environmental 72 (2007) 136-148.

[117] Flores-Moreno J.L., Delahay G., Figueras F., Coq B., "DRIFTS study of the nature and reactivity of the surface compounds formed by co-adsorption of NO, O$_2$ and

propene on sulfated titania-supported rhodium catalysts", Journal of Catalysis 236 (2005) 292-303.

[118] Kantcheva M., "Identification, stability, and reactivity of NOx species adsorbed on titania-supported manganese catalysts", Journal of Catalysis 204 (2001) 479-494.

[119] Brown W.A., King D.A., "NO chemisorption and reactions on metal surfaces: a new perspective", Journal of Physical Chemistry B 104 (2000) 2578-2595.

[120] Burch R., Millington P.J., Walker A.P., "Mechanism of the selective reduction of nitrogen monoxide on platinumbased catalysts in the presence of excess oxygen", Applied Catalysis B: Environmental 4(1) (1994) 65-94.

[121] Burch R., Millington P.J., "Selective reduction of NOx by hydrocarbons in excess oxygen by alumina- and silica supported catalysts", Catalysis Today 29 (1996) 37-42.

[122] Burch R., Daniells S.T., Breen J.P., Hu P., "A combined transient and computational study of the dissociation of N_2O on platinum catalysts", Journal of Catalysis 224 (2004) 252.

[123] Burch R., Daniells S.T., Breen J.P., Hu P., "The effect of H_2 and the presence of hot-O-(ads) during the decomposition of N_2O on platinum", Catalysis Letters 94 (2004) 103.

[124] Pasha N., Lingaiah N., Reddy P.S.S., Prasad P.S.S., "An investigation into the effect of Cs promotion on the catalytic activity of NiO in the direct decomposition of N_2O", Catalysis Letters 118 (2007) 64-68.

[125] Zasada F., Stelmachowski P., Maniak G., Paul J.F., Kotarba A., Sojka Z., "Potassium promotion of cobalt spinel catalyst for N_2O decomposition-accounted by work function measurements and DFT modelling", Catalysis Letters 127 (2009) 126.

[126] Stelmachowski P., Maniak G., Kotarba A., Sojka Z., "Strong electronic promotion of Co_3O_4 towards N_2O decomposition by surface alkali dopants", Catalysis Communications 10 (2009) 1062.

[127] Haber J., Nattich M., Machej T., "Alkali-metal promoted rhodium-on-alumina catalysts for nitrous oxide decomposition", Applied Catalysis B 77 (2008) 278.

[128] Granger P., Leclercq G., "Reduction of N_2O by CO over ceria-modified three-way Pt-Rh catalysts: kinetic aspects", Journal of Physical Chemistry C 111 (2007) 9905.

[129] Li X., Zhang C., He H., Teraoka Y., "Catalytic decomposition of N$_2$O over CeO$_2$ promoted Co$_3$O$_4$ spinel catalyst", Applied Catalysis B 75 (2007) 167.

[130] Parres-Esclapez S., Lopez-Suarez F.E., Bueno-Lopez A., Illan-Gomez M.J., Ura B., Trawczynski J., "Rh-Sr/Al$_2$O$_3$ catalyst for N$_2$O decomposition in the presence of O$_2$", Topics in Catalysis 52 (13-20) (2009) 1832-1836.

[131] Collins N.R., Twigg M.V., "Three-way catalyst emissions control technologies for spark-ignition engines-recent trends and future developments", Topics in Catalysis 42-43 (2007) 323-332.

[132] Papavasiliou A., Tsetsekou A., Matsouka V., Konsolakis M., Yentekakis I.V., Boukos N., "Synergistic structural and surface promotion of monometallic (Pt) TWCs: effectiveness and thermal aging tolerance", Applied Catalysis B 106 (2011) 228–241.

[133] Pekridis G., Kaklidis N., Konsolakis M., Athanasiou C., Yentekakis I.V., Marnellos G.E., "A comparison between electrochemical and conventional catalyst promotion: the case of N$_2$O reduction by alkanes or alkenes over K-modified Pd catalysts", Solid State Ionics 192 (2011) 653-658.

[134] Pekridis G., Kaklidis N., Konsolakis M., Iliopoulou E.F., Yentekakis I.V., Marnellos G.E., "Correlation of surface characteristics with catalytic performance of potassium promoted Pd/Al$_2$O$_3$ catalysts: The case of N$_2$O reduction by alkanes or alkenes", Topics in Catalysis 54 (2011) 1135-1142.

[135] Wögerbauer C., Maciejewski M., Baiker A., "Structure sensitivity of NO reduction over iridium catalysts in HC-SCR", Journal of Catalysis 205 (2002) 157-167.

[136] Tauster S.J., Murrell L.L., "The NO-CO reaction in the presence of excess O2 as catalyzed by iridium", Journal of Catalysis 41 (1976) 192.

[137] Taylor K.C., Schlatter J.C., "Selective Reduction of Nitric Oxide over Noble Metals", Journal of Catalysis 63 (1980) 53.

[138] Wögerbauer C., Maciejewski M., Baiker A., "Reduction of nitrogen oxides over unsupported iridium: effect of reducing agent", Applied Catalysis B: Environmental 34 (2001) 11-27.

[139] Ogura M., Kawamura A., Matsukata M., Kikuchi E., "Catalytic activity of Ir for NO–CO reaction in the presence of SO$_2$ and excess oxygen", Chemistry Letters 29 (2000) 146–147.

[140] Wang A.Q., Liang D.B., Xu C.H., Sun X.Y., Zhang T., "Catalytic reduction of NO over in situ synthesized Ir/ZSM-5 monoliths", Applied Catalysis B: Environmental 32 (2001) 205–212.

[141] Wang A.Q., Ma L., Cong Y., Zhang T., Liang D.B., "Unique properties of Ir/ZSM-5 catalyst for NO reduction with CO in the presence of excess oxygen", Applied Catalysis B: Environmental 40 (2003) 319–329.

[142] Haneda M., Yoshinari T., Sato K., Kintaichia Y., Hamada H., "Ir/SiO$_2$ as a highly active catalyst for the selective reduction of NO with CO in the presence of O$_2$ and SO$_2$", Chemical Communications (2003) 2814–2815.

[143] Haneda M., Pusparatu, Kintaichia Y., Nakamura I., Sasaki M., Fujitani T., Hamada H., "Promotional effect of SO$_2$ on the activity of Ir/SiO$_2$ for NO reduction with CO on the oxygen-rich condition", Journal of Catalysis 229 (2005) 197–205.

[144] Haneda M., Hamada H., "Promotional role of H$_2$O in the selective catalytic reduction of NO with CO over Ir/WO$_3$/SiO$_2$ catalyst", Journal of Catalysis 273 (2010) 39-49.

[145] Fujitani T., Nakamura I., Kobayashi Y., Takahashi A., Haneda M., Hamada H., "Adsorption and reactions of NO on clean and CO-precovered Ir(111)", The Journal of Physical Chemistry B 109 (2005) 17603–17607.

[146] Chen W.H., Madey T.E., Stottlemyer A.L., Chen J.G., Kaghazchi P., Jacob T., "Structure sensitivity in adsorption and decomposition of NO on Ir", Journal of Physical Chemistry C 112 (2008) 19113–19120.

[147] Chen W.H., Stottlemyer A.L., Chen J.G., Kaghazchi P., Jacob T., Madey T.E., Bartynski R.A., "Adsorption and decomposition of NO on O-covered planar and faceted Ir(210)", Surface Science 603 (2009) 3136–3144.

[148] Wallbank J.R., Sermon P.A., Baker A.M., Courtney L., Sambrook R.M., "Nitrous oxide as a green monopropellant for small satellites", The 2nd International Conference on Green Propellants for Space Propulsion 557 (2004) 125.

[149] Mary S., Kappenstein C., Balcon S., Rossignol S., Gengembre E., "Monopropellant decomposition catalysts. I. Ageing of highly loaded Ir/Al$_2$O$_3$ catalysts in oxygen and steam. Influence of chloride content", Applied Catalysis A: General 182 (1999) 317–325.

[150] Yentekakis I.V., Goula G., Panagiotopoulou P., Kampouri S., Taylor M.J., Kyriakou G., Lambert R.M., "Stabilization of catalyst particles against sintering on oxide supports with high oxygen ion lability exemplified by Ir-catalyzed decomposition of N$_2$O", Applied Catalysis B: Environmental 192 (2016) 357-364.

[151] Jehn H., Volker R., Ismail M.I., "Iridium losses during oxidation", Platinum Metals Review 22 (1978) 92-97.

[152] Wögerbauer C., Maciejewski M., Baiker A., Göbel U., in: Preprints of the Fifth International Congress on Catalysis and Automotive Pollution Control, Vol. 1, Brussels, 2000, p. 203.

[153] Nawdali M., Praliaud H., Primet M., in: Preprints of the Fifth International Congress on Catalysis and Automotive Pollution Control, Vol. 2, Brussels, 2000, p. 107.

[154] Nakatsuji T., "Studies on the structural evolution of highly active Ir-based catalysts for the selective reduction of NO with reductants in oxidizing conditions", Applied Catalysis B: Environmental 25 (2000) 163-179.

[155] Nawdali M., Iojoiu E., Gelin P., Praliaud H., Primet M., "Influence of the pre-treatment on the structure and reactivity of Ir/Al$_2$O$_3$ catalysts in the selective reduction of nitric oxide by propene", Applied Catalysis A: General 220 (2001) 129-139.

[156] Nawdali M., Praliaud H., Primet M., "SCR of NO over Ir/Al$_2$O$_3$ catalysts. Importance of the activation procedure and influence of the dispersion", Topics in Catalysis 16 (2001) 199-204.

[157] Wögerbauer C., Maciejewski M., Baiker A., Gobel U., "Ir/H-ZSM-5 catalysts in the selective reduction of NOx with hydrocarbons", Topics in Catalysis 16 (2001) 181-186.

[158] Iojoiu E., Gelin P., Praliaud H., Primet M., "Reduction of NO by propene over supported iridium catalysts under lean-burn conditions: an in situ FTIR study", Applied Catalysis A: General 263 (2004) 39–48.

[159] Wögerbauer C., Maciejewski M., Baiker A., Gobel U., "Structural Properties and Catalytic Behavior of Iridium Black in the Selective Reduction of NO by Hydrocarbons", Journal of Catalysis 201 (2001) 113–127.

[160] Haneda M., Fujitani T., Hamada H., "Effect of iridium dispersion on the catalytic activity of Ir/SiO$_2$ for the selective reduction of NO with CO in the presence of O$_2$ and SO$_2$", Journal of Molecular Catalysis A: Chemical 256 (2006) 143-148.

[161] Ohnishi C., Iwamoto S., Inoue M., "Direct decomposition of nitrous oxide in the presence of oxygen over iridium catalyst supported on alumina", Chemical Engineering Science 63 (2008) 5076-5082.

[162] Liu S., Cong Y., Huang Y., Zhao X., Zhang T., "TiO$_2$ promoted Ir/Al$_2$O$_3$ catalysts for direct decomposition of N$_2$O", Catalysis Today 175 (2011) 264-2.

[163] Amiridis M.D., Zhang T., Farrauto R.J., "Selective catalytic reduction of nitric oxide by Hydrocarbons", Applied Catalysis B 10 (1996) 203.

[164] Zhang G., Yamaguchi T., Kawakami H., Suzuki T., "Effects of sodium modification, different reductants and SO$_2$ on NO reduction by Rh/Al$_2$O$_3$ catalysts at excess O$_2$ conditions", Applied Catalysis B 1 (1992) L15.

[165] Nakatsuji T., Shimizu H., Yasukawa R., Nagano K., Nakahira K., Yoshimoto M., International Forum on Environmental Catalysis, Tokyo, Japan (1993).

[166] Efthimiadis E.A., Christoforou S.C., Nikolopoulos A.A., Vasalos I.A., "Selective catalytic reduction of NO with C$_3$H$_6$ over Rh/alumina in the presence and absence of SO$_2$ in the feed", Applied Catalysis B 22 (1999) 91-106.

[167] Efthimiadis E.A., Lionta G.D., Christoforou S.C., Vasalos I.A., "The effect of CH$_4$, H$_2$O and SO$_2$ on the NO reduction with C$_3$H$_6$", Catalysis Today 40 (1998) 15-26.

[168] Dann T.W., Schulz K.H., Mann M., Collings M., "Supported rhodium catalysts for nitrous oxide decomposition in the presence of NO, CO$_2$, SO$_2$ and CO",Applied Catalysis B: Environmental 6 (1995) 1-10.

[169] Haneda M., Yoshinary T., Sato K., Kintaichi Y., Hamada H., "Ir/SiO$_2$ as a highly active catalyst for the selective reduction of NO with CO in the presence of O$_2$ and SO$_2$", Chemical Communication (2003) 2814-2815.

[170] Konsolakis M., Yentekakis I.V., Pekridis G., Kaklidis N., Psarras A.C., Marnellos G.E., :Insights into the role of SO$_2$ and H$_2$O on the surface characteristics and de-N$_2$O efficiency of Pd/Al$_2$O$_3$ catalysts during N$_2$O decomposition in the presence of CH$_4$ and O$_2$ excess", Applied Catalysis B: Environmental 138-139 (2013) 191-198.

[171] Corro G., Cano C., Fierro J.L.G., "A study of Pt–Pd/γ-Al$_2$O$_3$ catalysts for methane oxidation resistant to deactivation by sulfur poisoning", Journal of Molecular Catalysis A 315 (2010) 35.

[172] Colussi S., Arosio F., Montanari T., Busca G., Groppi G., Trovarelli A., "Study of sulfur poisoning on Pd/Al$_2$O$_3$ and Pd/CeO$_2$/Al$_2$O$_3$ methane combustion catalysts", Catalysis Today 155 (2010) 59.

[173] Marnellos G.E., Efthimiadis E.A., Vasalos I.A., "Effect of SO$_2$ and H$_2$O on the N$_2$O decomposition in the presence of O$_2$ over Ru/Al$_2$O$_3$", Applied Catalysis B: Environmental 46 (2003) 523-539.

[174] Komvokis V.G., Marnellos G.E., Vasalos I.A., Triantafyllidis K.S., "Effect of pretreatment and regeneration conditions of Ru/γ-Al$_2$O$_3$ catalysts for N$_2$O decomposition and/or reduction in O$_2$-rich atmospheres and in the presence of NOx, SO$_2$ and H$_2$O", Applied Catalysis B: Environmental 89 (2009) 627-634.

[175] Salem I., Courtois X., Corbos E.C., Marecot P., Duprez D., "NO conversion in presence of O$_2$, H$_2$O and SO$_2$: Improvement of a Pt/Al$_2$O$_3$ catalyst by Zr and Sn, and influence of the reducer C$_3$H$_6$ or C$_3$H$_8$", Catalysis Communications 9 (2008) 664-669.

[176] Haneda M., Hamada H., "Promotional role of H$_2$O in the selective catalytic reduction of NO with CO over Ir/WO$_3$/SiO$_2$ catalyst", Journal of Catalysis 273 (2010) 39-49.

CHAPTER II
Experimental:
Materials Preparation, Characterization and Catalytic Evaluation Studies
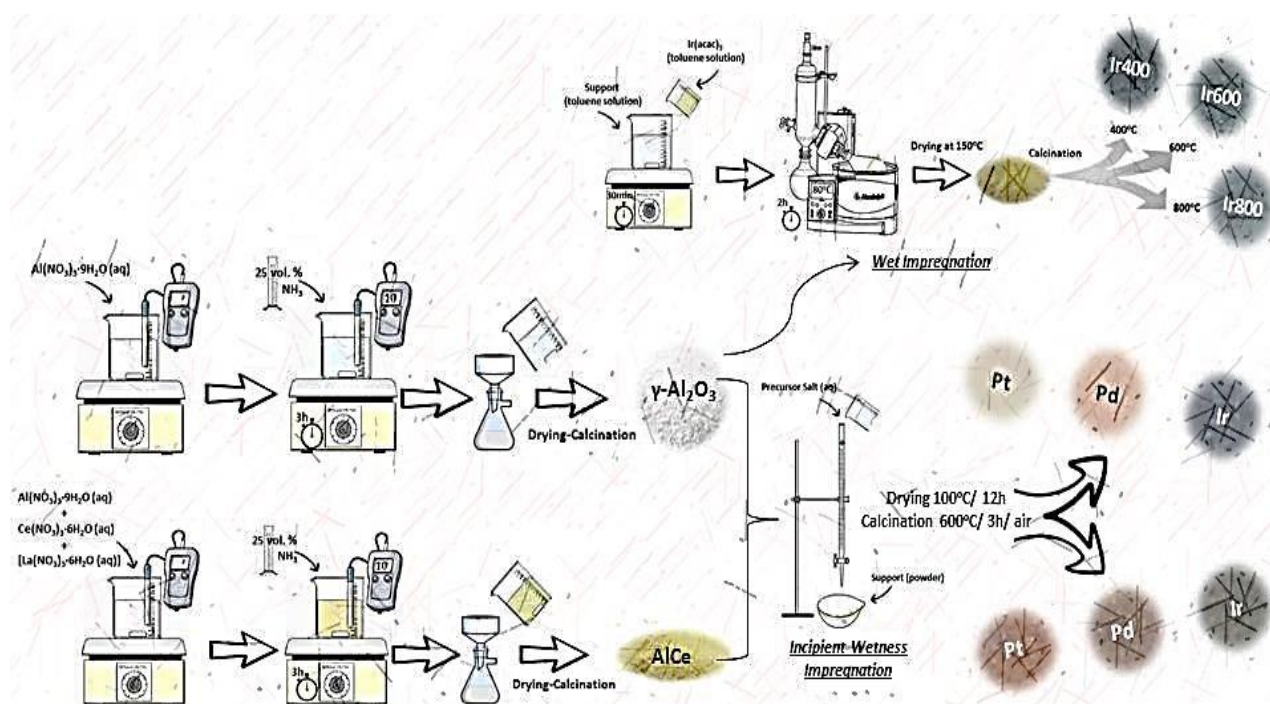
Chapter II presents the preparation procedure, which was followed for the synthesis of bare γ-Al$_2$O$_3$ or modified γ-Al$_2$O$_3$ supports and the incorporation of the noble metals (Pt, Pd, Ir) over the alumina-based supports. All the catalytic materials were characterized via several methods in order to gain an insight into their surface/structural characteristics, and evaluated for their de-N$_2$O performance under different reaction conditions.

II.1 MATERIALS PREPARATION

II.1.1 *Preparation of Bare and Structurally (CeO$_2$, Ce$_{0.8}$La$_{0.2}$O$_{1.9}$) Promoted γ-Al$_2$O$_3$ Carrier*

All support materials were prepared by the co-precipitation method. During this procedure, the solutions containing the metal salt precursor are contacted, under stirring with a base in order to precipitate as hydroxides. After washing, the derived pastes can be transformed to oxides by heating. Many variables have to be controlled: efficient mixing is very important, the procedure and order of addition of the different solutions, the temperature, the aging time of the precipitate (which may help filtration by converting a gelatinous precipitate in a more crystalline one), the filtering and washing procedure. Moreover, since we are dealing with a multicomponent system, the pH has to be carefully controlled in order to avoid precipitation of the component at a different sequence, thus affecting the final structure of the solid [1].
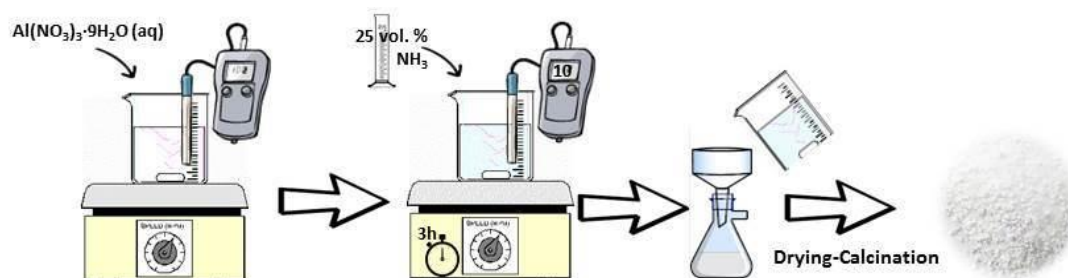
Figure II.1: Co-precipitation method for the preparation of γ-Al$_2$O$_3$.

For the preparation of bare γ-Al$_2$O$_3$, a precipitating agent (25% vol. NH$_3$ solution) was added at room temperature to a continuously stirred solution containing the desirable amount of Al(NO$_3$)$_3$·9H$_2$O (98.5% purity, supplied by Chem-Lab), until the pH of the solution reached the value of ~10. Then the pH remained stable at this value for additional 3h. Following co-precipitation, the resulting precipitate was filtered, dried overnight at 110°C and then calcined at 600°C for 2h in air flow. The preparation of bare γ-Al$_2$O$_3$ is presented in Figure II.1.

The CeO$_2$-promoted γ-Al$_2$O$_3$ was prepared following a similar method, using Al(NO$_3$)$_3$·9H$_2$O (98.5% purity, supplied by Chem-Lab) and Ce(NO$_3$)$_3$·6H$_2$O (99% purity, supplied by Fluka) as precursor salts. After mixing the aqueous solutions of the precursors, the preparation procedure is continued as described above. The amount of CeO$_2$ was 20% wt. and the CeO$_2$-promoted γ-Al$_2$O$_3$ will be denoted hereinafter as AlCe. Finally, Ce- and La-promoted (molar ratio of Ce/La=4) γ-Al$_2$O$_3$ was prepared using the corresponding nitrate solutions, including the one for lanthanum (La(NO$_3$)$_3$·6H$_2$O, 99% purity, supplied by Fluka).
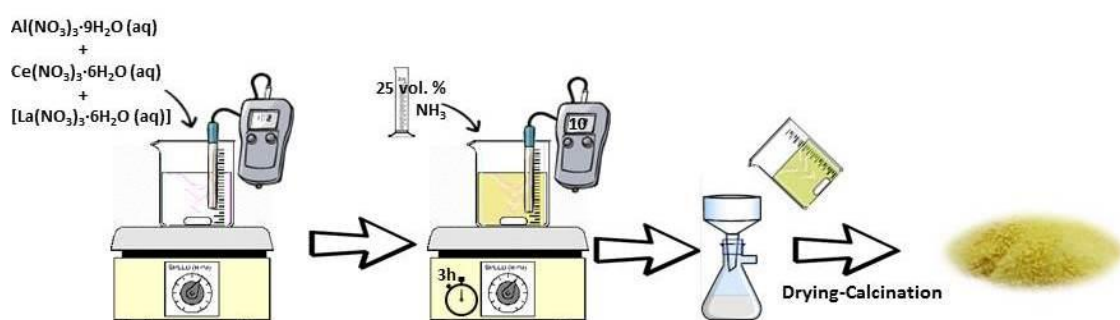
Figure II.2: Co-precipitation method for the preparation of Ce- and La-promoted γ-Al$_2$O$_3$ (AlCe, AlCeLa).

The desirable amount of Ce$_{0.8}$La$_{0.2}$O$_{1.9}$ over γ-Al$_2$O$_3$ support was 20% wt., and herein is labeled as AlCeLa support. The preparation steps of structurally promoted γ-Al$_2$O$_3$ are presented in Figure II.2.

An extra support of bare CeO$_2$ was prepared for comparison reasons. Once again the same procedure was followed, as for the preparation of bare γ-Al$_2$O$_3$, with the exception that only Ce(NO$_3$)$_3$·6H$_2$O was used as the precursor salt.

II.1.2 *Preparation of Noble Metals (Pt, Pd, Ir)-based Catalysts*

The incorporation of noble metals over the oxide supports was conducted by applying the incipient wetness impregnation method, where the volume of the solution containing the precursor does not exceed the pore volume of the support. In principle this method appears to be simple, economic (especially when using solutions of costly active components) and able to give a reproducible metal loading, which is however limited by the solubility of the metal precursor. Nevertheless,

when higher concentration of the metal is required, this limitation can be overcome by carrying out consecutive impregnation steps [1].

Initially, a series of Pt-, Pd- and Ir-based catalysts supported on bare γ-Al_2O_3 were prepared in three different metal loadings (0.25%, 0.5% and 1% wt.). Incorporation of the Pt, Pd and Ir actives phases was accomplished by using $H_2PtCl_6·6H_2O$ (40% wt. Pt, supplied by Merck), $Pd(NO_3)_2·xH_2O$ (99.9% purity, supplied by Alfa-Aesar) and $IrCl_3·H_2O$ (98% purity, supplied by Merck) as the precursor salts, respectively. Aqueous solutions of the corresponding metal salts were impregnated on γ-Al_2O_3 support, in successive stages, with intermediate drying in an oven at $100^{o}C$ for 30 min. The derived samples were dried at 100°C overnight and finally calcined, under air flow at 600°C for 3 h. The as prepared composites are herein labeled as xM/Al, where x is the metal loading and M is the metal type.

The impregnation of structurally promoted supports with noble metals was also carried out at the percentage of 0.5% wt. The same procedure was followed as above and the catalytic materials will be denoted as 0.5M/AlCe or 0.5M/AlCeLa (where M is the metal type). Schematic presentation of the procedure is presented in Figure II.3.
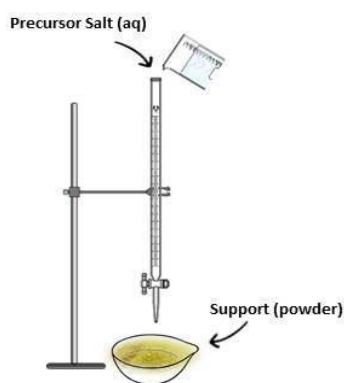
Figure II.3: Incipient wetness impregnation method for the incorporation of Pt-, Pd-, Ir- over the oxide supports.

II.1.3 Preparation of Surface (K)-Promoted Ir Catalysts

Surface promotion with alkali, took place only for the case of Ir-based catalysts. According to the results of evaluation tests, iridium catalysts presented the best catalytic performance, when compared with Pt- and Pd-based catalysts. To this end, Ir was selected for further study and promotion of its catalytic performance.

The preparation of supports (γ-Al$_2$O$_3$, AlCe) was carried out according to the method described above (section II.1.1). The addition of the active phase (Ir) and alkali promoter (K) was conducted sequentially, using the incipient wetness impregnation method (Fig. II.3). Initially, the incorporation of iridium (0.5% wt.) to γ-Al$_2$O$_3$ support took place, using an aqueous solution of IrCl$_3$·H$_2$O. The derived sample was dried overnight at 100°C and calcined at 600°C, for 3h, under air flow. In the sequence potassium was added, using KNO$_3$ (99% pure, supplied by Strem Chemicals) as the precursor material, using the appropriate concentrations, in order to achieve the desirable loading, varying between 0-1% wt. An identical impregnation procedure was followed as before. The resulted suspension was dried (at 100°C overnight) and calcined at 600°C for 3h under air flow. The as prepared samples are herein labeled as 0.5Ir(xK)/Al and 0.5Ir(xK)/AlCe, where x is the potassium loading (x= 0, 0.25%, 0.5% and 1% wt. K).

II.1.4 Preparation of Ir/ γ-Al$_2$O$_3$ Catalysts by Different Synthesis Routes

A second series of 0.5Ir/Al catalytic materials was prepared following a different synthesis route. The γ-Al$_2$O$_3$ support was initially prepared as described and presented above in Figure II.1, via the co-precipitation method (section II.1.). The addition of Ir phase was conducted via the wet impregnation method, using iridium acetylacetonate [Ir(O$_2$C$_5$H$_7$)$_3$ or Ir(acac)$_3$, purity 97%, supplied by Sigma-Aldrich] as a precursor salt. This type of impregnation, involves the use of an excess of solution with respect to the pore volume of the support. The system is left to age for a certain time under stirring and then filtered and dried. This procedure is applied especially, when a precursor-support interaction is desired. Therefore, the concentration of the metal precursors on the support will depend not only on the concentration of the solution and on the pore volume of the support, but also on the type and/or concentration of adsorbing sites existing at the surface [1].

Ir(acac)$_3$ was diluted in toluene, due to its insolubility in water and at the same time γ-Al$_2$O$_3$ was also diluted in toluene. The two solutions were mixed and kept under stirring in room temperature for 30 min and then, the mixture was dried in a vacuumed rotary evaporator for 2h at 80°C. The formed material was dried at 150°C

for 12h and was divided into three parts, each receiving a different pretreatment procedure (Figure II.4).

In detail, the pretreatment conditions were the following:

    i.   Calcination at $400^{o}C$ for 3 h under air flow.

    ii.   Calcination at $600^{o}C$ for 3 h under air flow.

    iii.   Calcination at $800^{o}C$ for 3 h under air flow.
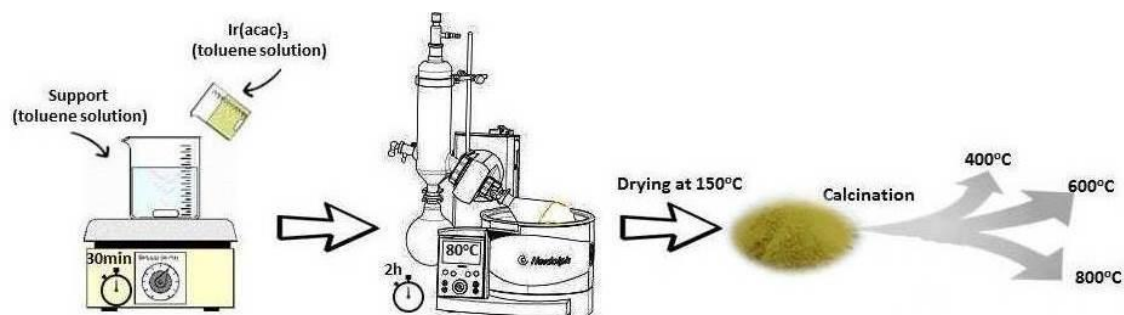
Figure II.4: Wet impregnation method for the incorporation of Ir over γ-Al$_2$O$_3$.

The as prepared catalytic materials are herein labeled as 0.5IrAl_oxi_T, where *oxi* means oxidized, and *T* is the temperature of pretreatment. Table II.1 summarize all the catalytic materials, which were used in the present study, as well as the preparation method, the precursor salt, the pretreatment conditions and the code name for each material.

Table II.1: List of catalytic materials used in the present thesis.

Materials (Code Name)	Preparation Method	Pretreatment Conditions	Loading (wt. %)	Precursor Salt
γ-Al$_2$O$_3$-Based Noble Metals				
γ-Al$_2$O$_3$	Co-precipitation	600°C/2h/air	-	Al(NO$_3$)$_3$·9H$_2$O
0.25Pt/Al	Incipient Wetness Imp.	600°C/3h/air	0.25	H$_2$PtCl$_6$·6H$_2$O
0.5Pt/Al	Incipient Wetness Imp.	600°C/3h/air	0.50	H$_2$PtCl$_6$·6H$_2$O
1Pt/Al	Incipient Wetness Imp.	600°C/3h/air	1.00	H$_2$PtCl$_6$·6H$_2$O
0.25Pd/Al	Incipient Wetness Imp.	600°C/3h/air	0.25	Pd(NO$_3$)$_2$·xH$_2$O
0.5Pd/Al	Incipient Wetness Imp.	600°C/3h/air	0.50	Pd(NO$_3$)$_2$·xH$_2$O
1Pd/Al	Incipient Wetness Imp.	600°C/3h/air	1.00	Pd(NO$_3$)$_2$·xH$_2$O
0.25Ir/Al	Incipient Wetness Imp.	600°C/3h/air	0.25	IrCl$_3$·H$_2$O
0.5Ir/Al	Incipient Wetness Imp.	600°C/3h/air	0.50	IrCl$_3$·H$_2$O
0.5Ir(0.25K)/Al	Incipient Wetness Imp.	600°C/3h/air	Ir: 0.50 K: 0.25	IrCl$_3$·H$_2$O KNO$_3$
0.5Ir(0.5K)/Al	Incipient Wetness Imp.	600°C/3h/air	Ir: 0.50 K: 0.50	IrCl$_3$·H$_2$O KNO$_3$
0.5Ir(1K)/Al	Incipient Wetness Imp.	600°C/3h/air	Ir: 0.50 K: 1.00	IrCl$_3$·H$_2$O KNO$_3$
0.5IrAl_oxi400	Wet Impregnation	400°C/3h/air	0.50	*Ir(acac)$_3$
0.5IrAl_oxi600	Wet Impregnation	600°C/3h/air	0.50	Ir(acac)$_3$
0.5IrAl_oxi800	Wet Impregnation	800°C/3h/air	0.50	Ir(acac)$_3$
1Ir/Al	Incipient Wetness Imp.	600°C/3h/air	1.00	IrCl$_3$·H$_2$O

*Ir(acac)$_3$: Iridium Acetylacetonate- Ir(O$_2$C$_5$H$_7$)$_3$.

Structurally/ Surface Promoted Materials				
AlCe	Co-precipitation	600°C/2h/air	80 wt. % γ-Al_2O_3 20 wt. % CeO_2	$Al(NO_3)_3 \cdot 9H_2O$, $Ce(NO_3)_3 \cdot 6H_2O$
0.5Pt/AlCe	Incipient Wetness Imp.	600°C/3h/air	0.50	$H_2PtCl_6 \cdot 6H_2O$
0.5Pd/AlCe	Incipient Wetness Imp.	600°C/3h/air	0.50	$Pd(NO_3)_2 \cdot xH_2O$
0.5Ir/AlCe	Incipient Wetness Imp.	600°C/3h/air	0.50	$IrCl_3 \cdot H_2O$
0.5Ir(0.25K)/AlCe	Incipient Wetness Imp.	600°C/3h/air	Ir: 0.50 K: 0.25	$IrCl_3 \cdot H_2O$ KNO_3
0.5Ir(0.5K)/AlCe	Incipient Wetness Imp.	600°C/3h/air	Ir: 0.50 K: 0.50	$IrCl_3 \cdot H_2O$ KNO_3
0.5Ir(1K)/AlCe	Incipient Wetness Imp.	600°C/3h/air	Ir: 0.50 K: 1.00	$IrCl_3 \cdot H_2O$ KNO_3
AlCeLa	Co-precipitation	600°C/2h/air	80 wt. % γ-Al_2O_3 20 wt. % $Ce_{0.8}La_{0.2}O_{1.9}$	$Al(NO_3)_3 \cdot 9H_2O$, $Ce(NO_3)_3 \cdot 6H_2O$, $La(NO_3)_3 \cdot 6H_2O$
0.5Pt/AlCeLa	Incipient Wetness Imp.	600°C/3h/air	0.50	$H_2PtCl_6 \cdot 6H_2O$
0.5Pd/AlCeLa	Incipient Wetness Imp.	600°C/3h/air	0.50	$Pd(NO_3)_2 \cdot xH_2O$
0.5Ir/AlCeLa	Incipient Wetness Imp.	600°C/3h/air	0.50	$IrCl_3 \cdot H_2O$
CeO_2	Co-precipitation	600°C/2h/air	-	$Ce(NO_3)_3 \cdot 6H_2O$
0.5Ir/Ce	Incipient Wetness Imp.	600°C/3h/air	0.50	$IrCl_3 \cdot H_2O$

II.2 CHARACTERIZATION TECHNIQUES

The physicochemical characteristics of as-synthesized materials were evaluated by various complimentary techniques. In brief, Inductively Coupled Plasma (ICP) was employed to determine the actual amount of metal loading, N_2 physisorption (BET method) in order to gain insight into the textural properties (surface area, pore volume), X-ray Diffraction (XRD) and Transmission Electron Microscopy (HRTEM/STEM) analysis to provide most definitive structural/morphological information, Temperature Programmed Techniques (H_2-TPR, CO_2-TPD, NH_3-TPD, etc.) to produce a detailed picture in relation to redox properties of the investigated catalysts, Fourier Transform Infrared Spectroscopy with Pyridine (FTIR-Pyridine), to determine the acidity characteristics of the materials and Diffuse Reflectance Infrared Fourier Transform Spectroscopy with CO (CO-DRIFTS), as an effort to investigate the oxidation state of the metals. The experimental apparatus and the procedure followed for each characterization method is presented in detail below.

II.2.1 Textural and Structural Characterization (BET, XRD)

The total metal loading (% wt.) of the final catalysts was determined by the Inductively Coupled Plasma Atomic Emission Spectroscopy (ICP-AES -on a Perkin-Elmer Optima 4300DV apparatus). Determination of the % percent of metal on Ir-based catalysts was not possible tentatively, due to the insolubility of the formed IrO_2 phase.

The textural characteristics of the as prepared catalysts were determined by the N_2 adsorption–desorption isotherms at -196°C (Nova 2200e Quantachrome flow apparatus). Specific surface areas (m^2g^{-1}) were obtained according to the Brunauer-Emmett-Teller (BET) method at relative pressures in the 0.05-0.30 range. The specific pore volume (cm^3g^{-1}) was calculated based on the highest relative pressure, whereas the average pore size diameter (d_p, nm) was determined by the Barrett-Joyner-Halenda (BJH) method. Prior to measurements the samples were degassed at 350°C for 5h under vacuum.

The crystalline structure of the catalysts was determined by powder X-ray diffraction (XRD) on a Siemens D 500 diffractometer operated at 40 kV and 30 mA with Cu Kα

radiation (λ=0.154 nm). Diffractograms were recorded in the 5-80° 2θ range and at a scanning rate of 0.01^o s^{-1}. The Scherrer equation was employed to determine the primary particle size of a given crystal phase based on the most intense diffraction peak.

A part of BET experiments were carried out at the Lab. of Physical Chemistry and Chemical Processes, of the Technical University of Crete (TUC), while the ICP, XRD and the rest BET analysis were performed at the Laboratory of Analysis and Characterization of Solids (LACS), in the Chemical Process and Energy Resources Institute (CPERI), of the Center for Research and Technology Hellas (CERTH).

II.2.2 *Redox-Acidity-Basicity Characterization (TP Methods)*

Temperature programmed methods were performed in a TP unit, which is presented schematically in Figure II.5. The unit basically consists of an oven, a quartz fixed bed reactor, the gas lines connected with the flowmeters and the mass spectrometer (MS), which record the effluent gases.

Hydrogen temperature-programmed reduction (H$_2$-TPR) experiments were performed after loading 0.1 g of sample in the reactor, coupled with mass spectrometer (MS). A flow (50 cm^3/min) of 5% vol. H$_2$/He gas mixtures was used, while the temperature of the solid catalyst was increased to 700°C at the rate of 5°C/min. The effluent gas from the reactor was analysed using the MS detector (m/z=2 was used for H$_2$). Prior reduction, the as prepared sample was loaded to the reactor and pre-treated at 300°C for 1h under He flow (heating rate of 3°C/min from 30 to 300°C). The catalyst sample was then cooled in He gas flow to room temperature, before recording the H$_2$-TPR trace.
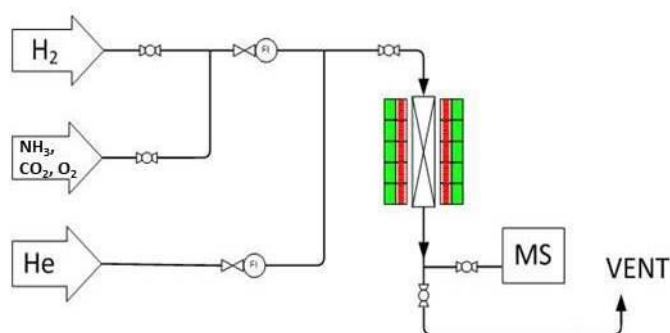
Figure II.5: Schematic diagram of Temperature Programmed Unit.

Additional, TP methods were also used in order to measure the acidity and basicity of the catalysts via NH_3 temperature-programmed desorption (NH_3-TPD) and CO_2 temperature-programmed desorption (CO_2-TPD) technique. After the pre-treatment procedure under He flow, follows the sorption step (of NH_3 or CO_2) at constant temperature for 1h. Then, the purging of the material surface takes place (under He flow) followed at the end by the desorption step. The effluents of the final step are recorded with the MS detector (m/z=44 for CO_2 and m/z= 15 for NH_3).

Table II.2 presents in more detail the steps and experimental conditions of all TP methods used at the present study.

Table II.2: Experimental conditions of temperature programmed techniques.

TP Method	Pre-treatment	Experiment		m/z (MS-detector)
		1st Step	2nd Step	
H_2-TPR	RT → 300°C Heating Rate: 3°C/min Gas: 50cc/min He	RT → 700°C Heating Rate: 5°C/min Gas: 50cc/min 5 vol.% H_2/He	-	2 (H_2)
CO_2-TPD	RT → 600°C Heating Rate: 10°C/min Gas: 50cc/min He	Sorption at 30°C- Gas: 50cc/min 10 vol.% CO_2/He Flashing at 30°C Gas: 50cc/min He for 2h	Desorption 30°C → 700°C H.R.: 10°C/min Gas: 50cc/min He	44 (CO_2)
NH_3-TPD	RT → 600°C Heating Rate: 10°C/min Gas: 50cc/min He	Sorption at 100°C- Gas: 50cc/min 5 vol.% NH_3/He Flashing at 100°C-overnight Gas: 30cc/min He	Desorption 100°C → 950°C H.R.: 10°C/min Gas: 50cc/min He	15 (NH_3)
SO_2-TPD	-	-	Desorption RT → 900°C H.R.: 10°C/min Gas: 50cc/min He	64 (SO_2)

Besides fresh catalysts, "used" catalysts (i.e. catalysts after de-N_2O reaction in the absence/presence of O_2, SO_2 etc.), were also characterized via Hydrogen temperature-programmed reduction (H_2-TPR), as well as via temperature programmed desorption of SO_2 (SO_2-TPD, see conditions at Table II.2).

These experiments were carried out at the Laboratory of Environmental Fuels and Hydrocarbons (LEFH), in the Chemical and Energy Resources Institute (CPERI) of the Center for Research and Technology Hellas (CERTH). Series of TPR experiments (not presented here) were also realized at the Lab. of Physical Chemistry and Chemical Processes, of the Technical University of Crete (TUC).

II.2.3 *Acidity Measurements (FTIR-Pyridine)*

For the Fourier Transform Infrared Spectroscopy (FTIR-Pyridine) experiments, the IR spectra were collected with a resolution of 4 cm^{-1}, using a Nicolet 5700 spectrometer equipped with a homemade stainless steel IR cell, with CaF$_2$ windows. The infrared cell, loaded with self-supporting wafers (~15 mg/cm^2), is connected to a high vacuum line consisting of turbomolecular and diaphragm pumps; both sample holder and vacuum line are heated to avoid pyridine condensation (Fig. II.6).
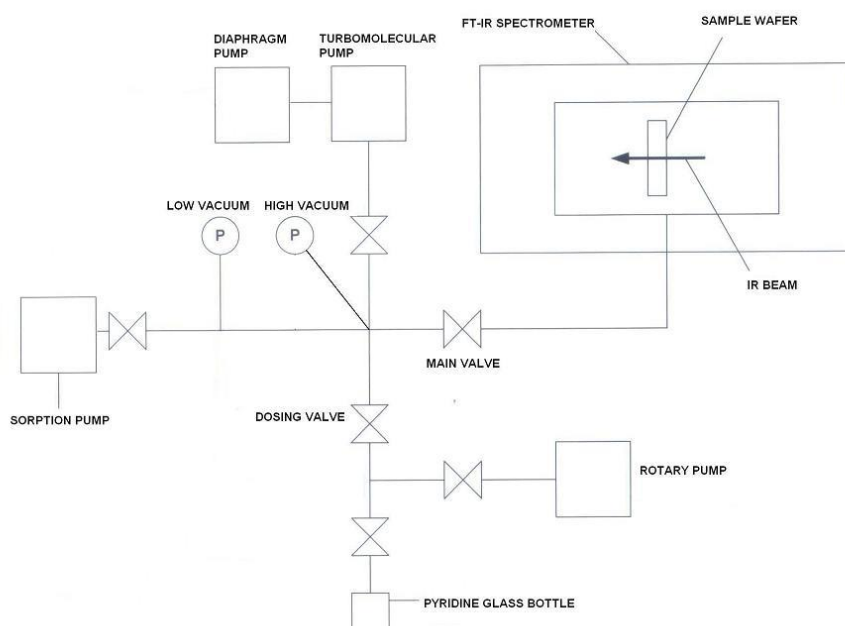
Figure II.6: Schematic diagram of FTIR-Pyridine unit.

Before IR spectra acquisition, samples were heated at 450°C under vacuum (10^{-6} mbar) for 1h to desorb any physisorbed species. Then the reference spectrum of each sample is collected at 150°C. Spectra of adsorbed pyridine were obtained at 150°C and 1 mbar by equilibrating the catalyst wafer with the probe vapour, added

in pulses for 1h. In order to evaluate the strength of the acid sites, three more spectra were collected at 250°C, 350°C and 450°C, representing the weak, medium and strong acid sites. The concentration of acid sites was calculated using the Lambert-Beer's law and the appropriate molar extinction coefficients. During pyridine adsorption we focused in two bands; one at 1450 cm^{-1} attributed to pyridine coordinated to Lewis sites and a second one at 1545 cm^{-1} assigned to protonated pyridine on Brönsted acid sites. These bands are considered as most representative for the quantification of Lewis and Brönsted acid sites [2-4].

These experiments took place at the Laboratory of Analytical Services Unit (ASU), in the Chemical Process and Energy Resources Institute (CPERI) of the Center for Research and Technology Hellas (CERTH).

II.2.4 *Morphological Studies (HRTEM, STEM, EELS)*

Samples for electron microscopy (HRTEM, HAADF-STEM, EELS) characterization were prepared by gently grinding the catalyst powder in high-purity ethanol using an agate pestle and mortar. A drop of the solution was subsequently deposited onto a lacey carbon film supported on a Cu grid and allowed to evaporate under ambient conditions.

Electron microscopy experiments were carried out in a JEOL 2011 high resolution transmission electron microscope (HRTEM), operating at 200 kV, with a point resolution of 0.23 nm. Elemental analysis was performed by means of energy-dispersive X-ray spectroscopy (EDS) using an Oxford Instruments spectrometer (INCAx-sight liquid nitrogen cooled detector with an ultrathin window). High resolution transmission electron microscopy (HRTEM) was performed using a JEOL 2100F 200kV FEG-STEM/TEM spectrometer equipped with a CEOS Cs corrector on the illumination system. The geometrical aberrations were measured and controlled to provide a less than $\pi/4$ phase shift of the incoming electron wave over the probe-defining aperture of 17.5 mrad. High angle annular dark-field (HAADF-STEM) images were acquired on a Fischione Model 3000 HAADF detector with a camera length such that the inner cut-off angle of the detector was 50 mrad. The scanning acquisition was synchronized to the 60 Hz AC electrical power to minimize 60 Hz noise in the images and using a pixel dwell time of 15.8 μs. EELS spectra were

acquired in a probe-corrected 300 kV FEI Titan 3 G2 60-300 microscope with an X-FEG Schottky field emission electron source, equipped with a Gatan GIF Quantum ERS spectrometer.

Scanning transmission electron microscopy (STEM) experiments in combination with EELS analysis were performed in a probe-corrected FEI Titan 3 G2 60-300 microscope at 300 kV, equipped with a Schottky field emission electron source (X-FEG). EEL spectra were acquired with a Gatan GIF Quantum ERS spectrometer attached to the microscope. A convergence semi-angle of 19.6 mrad was used. For EELS analysis the spectrum image approach was applied, where a focused electron beam was scanned across the region of interest (nanoparticle) and EEL spectra were acquired at each pixel. The step size of the EEL spectrum images ranged from 0.15-0.30 nm with an exposure time of 10 ms per pixel, while the energy dispersion was 0.5 eV/channel. Using the dual EELS method, low loss spectra including the Zero-Loss, which consists of elastically scattered electrons, were acquired simultaneously to correct the data in terms of possible energy shifts.

HRTEM analysis was performed at the Laboratory of Analysis and Characterization of Solids (LACS), in the Chemical Process and Energy Resources Institute (CPERI) of the Center for Research and Technology Hellas (CERTH). STEM and EELS analysis carried out at the TU of Graz, under the supervision of F. Schmidt, W. Grögger and F. Hofer in collaboration with Andreas Delimitis, as well as in Electron Microscopy Center of University of South Carolina, in Columbia (USA), under the supervision of M. Amiridis and O. Alexeev.

II.2.5 Metal Oxidation State (CO-DRIFTS)

In situ diffuse reflectance infrared Fourier transform spectroscopy (DRIFTS) experiments were carried out in a Perkin-Elmer/Frontier FT-IR spectrometer equipped with an MCT detector and a high-temperature/high-pressure controllable DRIFTS cell (Harrick Scientific), loaded with ~100 mg of catalyst sample (fine powder). Before DRIFT spectra acquisition, the as synthesized sample was pre-treated according to the following gas sequence: (i) 20 vol. % O_2/ Ar (30 cm^3/min) at 600°C for 1h (oxidation step), (ii) decrease of temperature to 300°C in Ar flow, (iii) H_2 (1 bar) at 300°C for 1h (reduction step), and (iv) Ar purge at 300°C, 10 min.

Background spectra were recorded under Ar flow at desired temperatures (needed for CO desorption studies). CO chemisorption took place at 30°C for 30 min with 1% vol. CO/ He (30 cm^3/min) gas mixture, whereas desorption of CO was performed in Ar flow (30 cm^3/min). DRIFT-CO spectra during the desorption step were recorded after 2 min the catalyst sample reached the selected desorption temperature.

In situ DRIFTS experiments were carried out at the Laboratory of Heterogeneous Catalysis at the University of Cyprus, under the supervision of Professor Angelos M. Efstathiou.

II.3 CATALYTIC EVALUATION STUDIES

A part of the catalytic experiments were performed in the bench-scale De-NOx unit, which is presented in Fig. II.7a. It basically consists of the feed gas system, a fixed bed reactor (o.d.: 1.9 cm) made of quartz (Fig. II.7b), one zone furnace controlled by PID controllers and the on-line gas analysis system, which comprised a N_2O analyzer. Reaction temperature is measured by a thermocouple placed inside the catalytic bed. The bench-scale unit is equipped with a gas feed system, capable to supply the following gas components: He, N_2O, NO, O_2, SO_2 and HCs. The volume flow rates of individual components, at the laboratory temperature, are monitored by calibrated mass flows. Water, when included in the feed mixture, are added to the blend of the other gases using a saturation bath at controlled temperature conditions of the He flow.

In a typical light-off N_2O decomposition experiment the fixed bed reactor was loaded with 0.6 g of catalyst, with 0.3 g of quartz. The total gas flow rate was 900 cm^3 (STP)/min, corresponding to a Gas Hourly Space Velocity (GHSV) of ~40,000 h^{-1}. The composition of the feed was 1000 ppm N_2O (absence of O_2) or 1000 ppm N_2O and 2% vol. O_2 (presence of O_2). In addition, the effect of H_2O content (0, 5 and 10% vol. H_2O in He) was studied on N_2O decomposition. The N_2O conversion was monitored in the 200-600°C range (in an increasing temperature mode) and was held constant at each temperature for ~30 min prior taking measurements. The composition of the effluent gas from the reactor was analyzed using the N_2O analyzer (VIA-510, Horiba).

The resistance of catalytic materials to inhibitors, like SO_2 and H_2O was studied performing step-change experiments, where N_2O is continuously monitored, while the feed composition is switched from poison-free to poison-containing mixtures. The feed mixtures were containing 1000 ppm N_2O, 2% vol. O_2 and 50 ppm SO_2 or 5% vol. H_2O. Stability of catalyst's performance (time-on-stream) was tested at 600^oC for 9h, under different feed composition (Chapters V, VI).

Experiments took place at the Laboratory of Environmental Fuels and Hydrocarbons (LEFH), in the Chemical Process Engineering Research Institute (CPERI), of the Center for Research and Technology Hellas (CERTH).
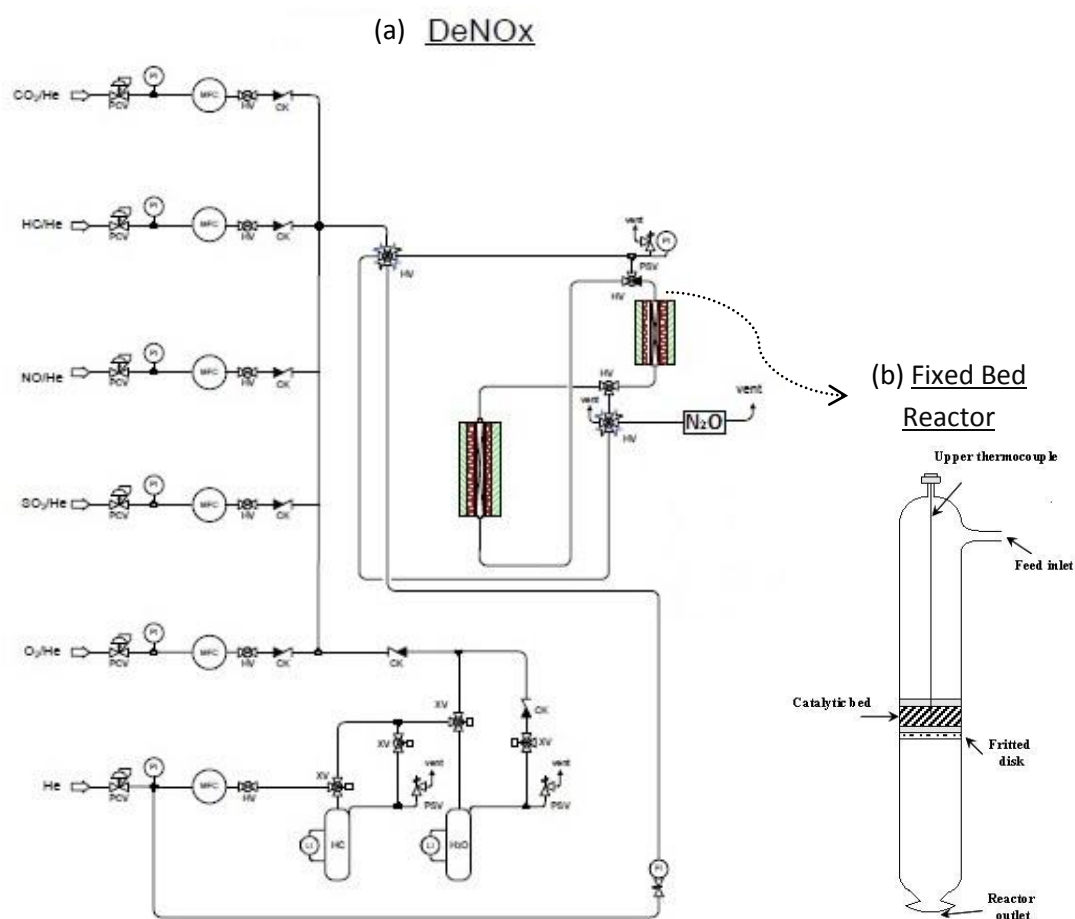
Figure II.7: Schematic diagram of (a) DeNOx unit and (b) fixed bed reactor in CPERI/CERTH.

Besides the catalysts evaluation that took place in CPERI, significant part of the catalytic experiments (Chapter III) was carried out at the Environmental Technology

Laboratory, in the University of Western Macedonia, during the project "Thales-CASANNO". The experiments were performed and analyzed by Eleni Papista [5].

Experimental Conditions: N_2O catalytic decomposition activity experiments carried out in a cylindrical quartz U-shape fixed-bed reactor (inner diameter of 8 mm). The reactor was loaded with 0.1 g of catalyst (less than 0.3 mm in size) diluted with 0.05 g of quartz. The total gas flow rate was 150 cm^3 (STP)/min, corresponding to a Gas Hourly Space Velocity (GHSV) of $\sim$ 40,000 h^{-1}. The feed composition was 1000 ppm N_2O or 1000 ppm N_2O + 2% vol. O_2, balanced with He. Before catalytic activity measurements, the fresh calcined sample was pretreated in He flow (100 cm^3/min) for 1h at 600°C before cooled in He flow to the lowest reaction temperature. The N_2O conversion was monitored in the 200-600°C range (in an increasing solid catalyst temperature mode). The composition of the effluent gas from the reactor was analyzed using a gas chromatograph (Shimadzu 14B) equipped with a thermal conductivity detector (TCD) and a combination of Porapak QS and Molecular Sieve 5A columns.

In addition, catalysts evaluation for the Selective Catalytic Reduction of NO by C_3H_6 in the presence of H_2 (Chapter IV), were carried out at the Laboratory of Alternative Fuels and Environmental Catalysis (LAFEC), in the Technological Educational Institute of Western Macedonia, as well as at the Lab. of Physical Chemistry and Chemical Processes, of the Technical University of Crete, during the project "Thales-CASANNO". The experiments were performed and analyzed by Prof. Maria Goula and Prof. Ioannis Yentekakis.

Experimental Conditions: Catalysts' performance evaluation under the desired reaction conditions was performed in a continuous flow, fixed-bed, single pass, tubular quartz reactor, with an inner diameter of 10 mm. The reactor loading was 335 mg catalyst powder, diluted with 165 mg of quartz particles, while the total gas flow rate was 500 cm^3 (STP)/min corresponding to a Gas Hourly Space Velocity (GHSV) of 40,000 h^{-1}. The feed composition was consisted of 1000 ppm NO, 1000 ppm C_3H_6 and 2% vol. O_2 during the reaction NO+C_3H_6+O_2 (R#1), 1000 ppm NO, 1000 ppm C_3H_6, 2% vol. O_2 and 0.5% vol. H_2 for reaction NO+C_3H_6+O_2+H_2 (R#2), and 1000ppm NO, 0.5% vol. H_2, 2% vol. O_2 in the case of reaction NO+H_2+O_2 (R#3), balanced with Ar. Prior to catalytic evaluation experiments, all catalyst samples were

pretreated in Ar flow (100 cm^3/min) for 1h at 400 ^{o}C. Then the reaction mixture was fed into the reactor, the temperature was decreased stepwise between 400-50°C, remaining 20 min at each step in order to ensure operation at steady state conditions, and the reactants' conversions as well as the concentration of reaction products were recorded versus temperature (light-off experiments). The composition of the reactants and products gas streams were continuously monitored by an analysis system involving an FTIR analyzer (Gasmet DX 4000) for the analysis of H_2O, CO, CO_2, CH_4, N_2O, NO, NO_2, C_3H_6, C_3H_8. N_2 was calculated by means of the N-containing species balance in the reactor effluent gas; notably NH_3 was detected only in limited cases (Pt-based catalysts and presence of H_2 in the feed) and only in traces.

REFERENCES

[1] Pinna F., "Supported metal catalysts preparation", Catalysis Today 41 (1998) 129-137.

[2] Travert A., Vimont A., Sahibed-Dine A., Daturi M., Lavalley J-C., "Use of pyridine CH(D) vibrations for the study of Lewis acidity of metal oxides", Applied Catalysis A 307 (2006) 98.

[3] Lercher J.A., Jentys A., "Infrared and raman spectroscopy for characterizing zeolites", Studies in Surface Science and Catalysis 168 (2007) 435.

[4] Emeis C.A., "Determination of integrated molar extinction coefficients for infrared adsorption bands of pyridine adsorbed on solid acid catalysts", Journal of Catalysis 141 (1993) 347.

[5] Papista E., PhD Thesis, University of Western Macedonia, Greece (in progress).

Effect of Structural/Surface Promoters on γ-Al$_2$O$_3$ Supported Noble Metals Catalysts
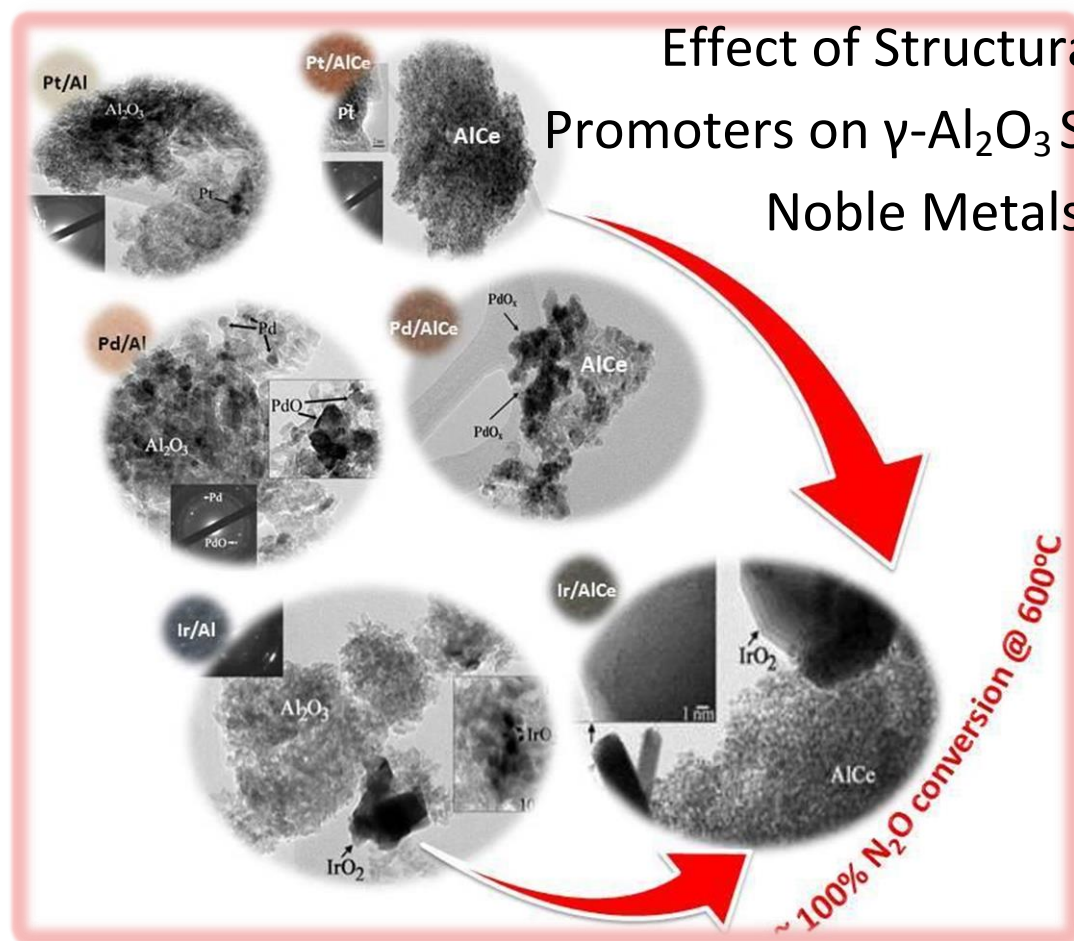
Chapter III deals with the effect of promoters (structural and surface) on the solid state properties and the de-N$_2$O performance of Al$_2$O$_3$ supported noble metal catalysts. Initially, the effect of structural promoters (i.e. Ce and La) over Pt-, Pd- and Ir-catalysts is investigated. Iridium based catalysts demonstrated the optimum de-N$_2$O performance as compared to Pt- and Pd-based catalysts. Hence, Ir-based materials were also subjected to surface promotion by means of alkali (K) modifiers and their performance was investigated for the decomposition of N$_2$O in the absence as well as in the presence of O$_2$.

III.1 EFFECT OF CeO$_2$ AND La$_2$O$_3$ PROMOTERS ON Pt- AND Pd-BASED CATALYSTS

INTRODUCTION

The recent advances in the field of N$_2$O abatement over noble metal (NM) catalysts has been extensively presented in the introduction section. Herein, a short overview is presented, mainly in relation to the fine-tuning of NMs surface chemistry by means of structural/surface modifiers, which is the main subject of the present chapter.

Various types of catalysts have been investigated for the de-N$_2$O process. Among these, NMs supported catalysts exhibit satisfactory activity, even at low temperatures [1-3]. However, their high cost represents an important obstacle toward practical applications. Hence, from a practical and economical point of view, it is of particular importance to develop catalytic materials with low noble metal content. These catalysts can be subsequently subjected to structural and/or electronic promotion to further enhance their de-N$_2$O performance, as recently revealed [2, 4-7].

Regardless the support, Rh is among the most active NMs for N$_2$O decomposition. Rh catalysts are active for N$_2$O decomposition from 200°C to 250°C, depending on the support used, and the complete conversion is reached in the range 300-400°C. In contrast, Pd and Pt catalysts are active only above ca. 400°C [8]. However, Pt is one of the most investigated NMs both for NO [9-15] and N$_2$O [16-25] abatement. On the other hand, Pt catalysts are drastically hindered by adsorbed oxygen leading to complete deactivation on a fully oxidized Pt surface [26, 27]. To this end, considerable efforts have been recently focused on enhancing the catalytic properties of noble metals by structural modifiers such as rare earth oxides (REOs), i.e. CeO$_2$, La$_2$O$_3$, etc. [25, 28, 29]. Konsolakis et al. [28] investigated the impact of lanthanide oxides as support additives on N$_2$O decomposition. Unmodified Pt/Al$_2$O$_3$ catalyst offered N$_2$O conversion less than ~20% at 600°C, while incorporation of CeO$_2$-La$_2$O$_3$ mixed oxides into Al$_2$O$_3$ support led to complete conversion of N$_2$O over Pt/Al$_2$O$_3$-(CeO$_2$-La$_2$O$_3$) catalysts at ca. 500°C even in the presence of excess O$_2$.

In a similar manner, the surface and catalytic properties of Pd/Al$_2$O$_3$ catalysts during the N$_2$O decomposition in the presence of hydrocarbons can be substantially altered by potassium (K), which was supplied either electrochemically [30] or conventionally [31] onto the catalyst surface. In particular, it was found that potassium strongly enhances the N$_2$O decomposition rate, resulting in notably lower N$_2$O light-off temperatures (of about 100°C) compared to the un-promoted catalyst. Based on a surface characterization study [31], it was revealed that the electronic properties of Pd/Al$_2$O$_3$ catalyst can be substantially modified by potassium addition, which in turn affects the reactants' chemisorptive bonds and consequently the de-N$_2$O activity.

In the present Chapter, the influence of 20% wt. CeO$_2$ (AlCe) and of 20% wt. Ce$_{0.8}$La$_{0.2}$O$_{1.9}$ (AlCeLa), as Al$_2$O$_3$ support modifiers, on the physicochemical characteristics and the deN$_2$O performance of Pt- and Pd- based catalysts is investigated. In addition, the effect of metal loading (0.25-1.00% wt.) was investigated over Al$_2$O$_3$ based samples.

III.1.1 Experimental

Material Synthesis

The catalysts used in this chapter (0.25, 0.5, 1% wt. Pt, Pd/ γ-Al$_2$O$_3$, 0.5Pt/AlCe, 0.5Pt/AlCeLa, 0.5Pd/AlCe, 0.5Pd/AlCeLa) were obtained using the preparation process described previously in chapter II.1 (Materials Preparation). The catalytic materials of this section are presented in Table III.1.

Characterization Techniques

The textural characteristics of the as prepared catalysts were determined by the BET and BJH method, while the determination of the percentage of metal over the supports by Inductively coupled plasma method (ICP). The structure of the catalysts was determined by powder X-ray diffraction (XRD) and electron microscopy techniques (HRTEM). The reducibility of the catalysts was analyzed by hydrogen temperature-programmed reduction (H$_2$-TPR) experiments. The experimental conditions of each technique are described in chapter II.2 (Characterization Techniques).

III.1.2 Results

Characterization Results

Table III.1 summarizes the textural and redox characteristics of Pt- and Pd/Al$_2$O$_3$ catalysts of different metal loading (0.25, 0.50 and 1% wt.), as well as that of structurally (Ce, La) modified samples. The textural characteristics (surface area, pore volume and pore size) of all samples are more or less similar (ca. 163.2- 188.1 m^2/g). However, differences are obtained in NMs particle size, upon the modification of alumina support with rare earth dopants. These differences are further verified by HRTEM analysis (analysed below).

Table III.1: Textural and redox characteristics of Pt- and Pd-supported catalysts.

Catalyst	S$_{BET}$ (m^2/g)	Pore Volume (cm^3/ g)	Pore Size (nm)	Mean NMs' Particle Size (nm)^a	ICP (%)	T$_{max}$ (^{o}C)^b
0.25Pt/Al	185.1	0.32	7.00	-	0.15	-
0.5Pt/Al	187.3	0.30	6.44	< 8	0.51	-
1Pt/Al	188.1	0.32	6.40	-	0.67	-
0.5Pt/AlCe	169.6	0.25	5.95	-	0.42	230, 650
0.5Pt/AlCeLa	182.1	0.27	6.04	< 6	0.52	230, 650
0.25Pd/Al	164.3	0.33	7.99	-	0.29	62, 450
0.5Pd/Al	163.2	0.33	8.16	11	0.49	61, 450
1Pd/Al	165.2	0.33	7.93	-	1.13	60, 450
0.5Pd/AlCe	180.0	0.28	6.16	13.3	0.46	240, 700
0.5Pd/AlCeLa	178.9	0.29	6.46	7.5	0.50	240, 700

^{a} Evaluated by HRTEM; ^{b} Temperature at maximum reduction rate (H$_2$-TPR);

The temperature at maximum reduction rate (T$_{max}$) for each catalyst during H$_2$-TPR experiments are also given in Table III.1, while the TPR profiles are presented in Figure III.1 (a-d). Bare alumina did not show any peak during the reduction, as it was expected. The addition of rare earths (Ce, La) to alumina support changed the TPR profiles due to the reduction of CeO$_2$. TPR profile of AlCe (Fig. III.1a) results in three

reduction peaks: the first one is centered at 360°C, and the two other peaks at 570°C and 810°C, respectively. This reductive behavior can be attributed to changes in the extent and the nature of the interaction between the CeO$_2$ and the Al$_2$O$_3$. In accordance with the TPR literature addressing ceria-alumina systems, the peaks observed can be assigned, respectively, to: (i) the reduction of the most easily reducible surface oxygen of highly dispersed ceria species; (ii) the removal of oxygen from bulk ceria and (iii) the reduction of dispersed ceria species, with the formation of a CeAlO$_3$ phase. The only difference between AlCe and AlCeLa profiles was the absence of the reduction peak at 360°C, ascribed to surface ceria reduction, which indicates the lower degree of dispersion of CeO$_2$ entities on the AlCeLa support with respect to the AlCe support. The support containing lanthanum (AlCeLa) did not show any reduction phenomena associated with lanthanum species [32, 33].

Pd catalysts based on γ-Al$_2$O$_3$ exhibit a negative peak at ~60°C, which is characteristic of the decomposition of β-PdH phase (Fig. III.1b). According to Berry et al. [34], Pd on alumina support is oxidized to PdO by calcination at 450°C. However, this is reduced to β-palladium hydride, when the TPR apparatus is flushed with a H$_2$/N$_2$ mixture at room temperature, before the start of each experiment. It is noteworthy, that no PdO characteristic peaks were observed at the corresponding TPR patterns, since the reduction of PdO species highly dispersed on Al$_2$O$_3$ is occurring between 0-25°C [35]. However, at 450°C a broad reduction peak is observed for Pd/Al samples, which can be attributed to the reduction of small Pd oxides particles present on alumina support. The existence of Pd oxides was confirmed by XRD and HRTEM analysis (see below). On the other side, H$_2$ consumption peaks in TPR profile of Pt/Al catalyst were not practically observed. This most probably reflects the fact that Pt nanoparticles mainly exist in the metallic form (Pt^0), not accessible for further reduction (as was confirmed by the HRTEM analysis, see below).

Incorporation of Pt and Pd over the modified supports shifted the CeO$_2$ reduction peaks to lower temperatures (Table III.1 and Fig. III.1 c, d). The addition of noble metals facilitates the reduction of ceria surface due to metal-support interactions that were developed. The TPR profiles of structurally-modified Pd catalysts are presented in Fig. III.1c. The absence of the negative peak of β-PdH probably indicates that Pd occupies the lattice sites as Pd^{+2} or/and Pd^{+4} ions, as was confirmed by

HRTEM analysis. Two broad peaks were observed with maximum temperatures at 240°C and 700°C (for both of the modified supports). The low temperature peak is related with the reduction of ceria surface, which is facilitated by the incorporation of Pd to the modified supports. More or less the same observations came out for the modified platinum catalysts.
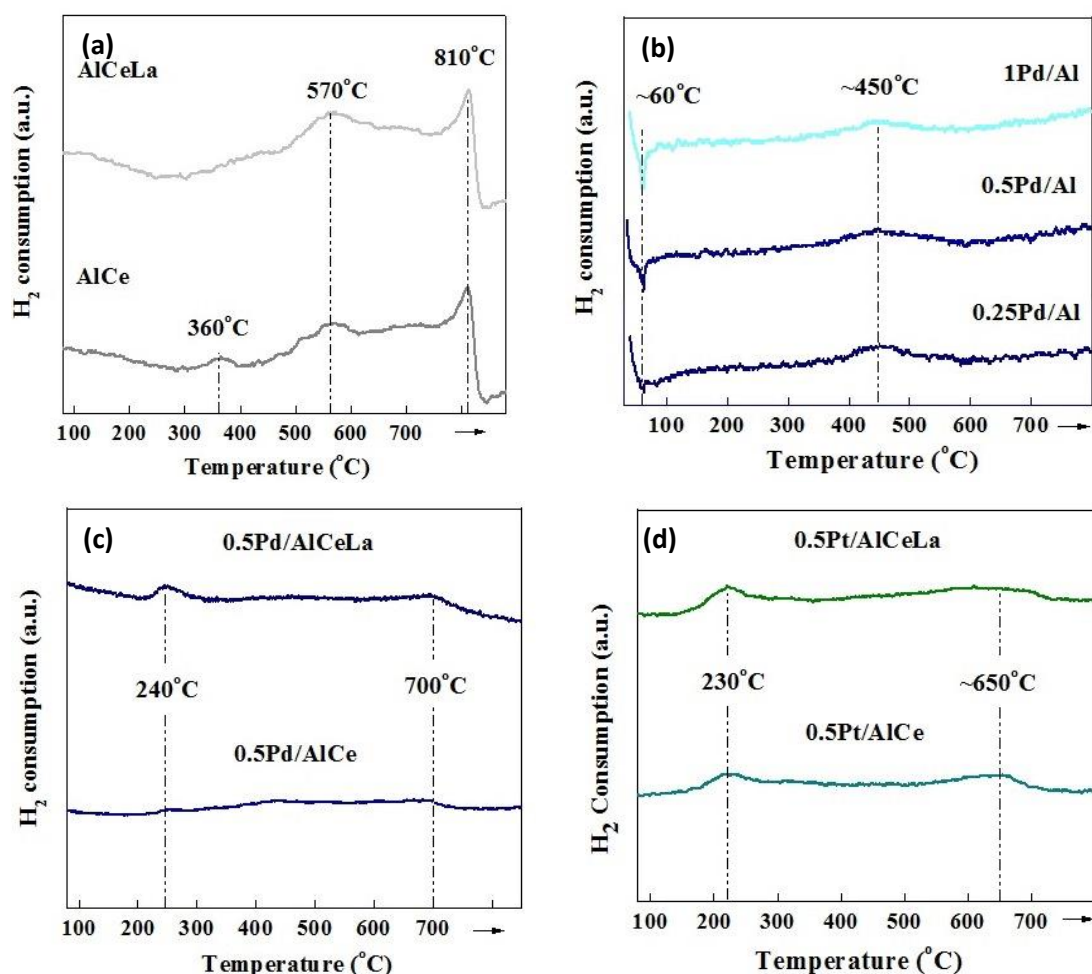
Figure III.1: H_2-TPR profiles of: (a) Modified γ-Al_2O_3 supports, (b) Pd/Al catalysts, (c) 0.5Pd/AlCe, AlCeLa catalysts and (d) 0.5Pt/AlCe, AlCeLa catalysts.

Representative XRD patterns of bare supports are shown in Fig. III.2a. As expected, bare alumina exhibits characteristic peaks predominately located at 2θ: 37.7°, 46° and 67° [37], which are also preserved in the Al_2O_3-supported catalysts. AlCe and AlCeLa diffractograms exhibit besides the peaks already observed in bare Al_2O_3, strong reflections of CeO_2 phase at 2θ: 33.3°, 47.5°, 56.4° and 76.5° [36, 37]. Not any diffraction peak due to La_2O_3 was observed, probably due to the high dispersion of

lanthanum entities over the surface of the AlCeLa calcined support [32]. The diffraction patterns of 0.5% and 1.0% wt. Pt-, Pd/ alumina are shown in Fig. III.2b. 0.5Pd/Al showed low intensity peaks for PdO ($2\theta= 33.8°$, $54.7°$), that could be attributed to small crystallite sizes of this oxide phase [38].
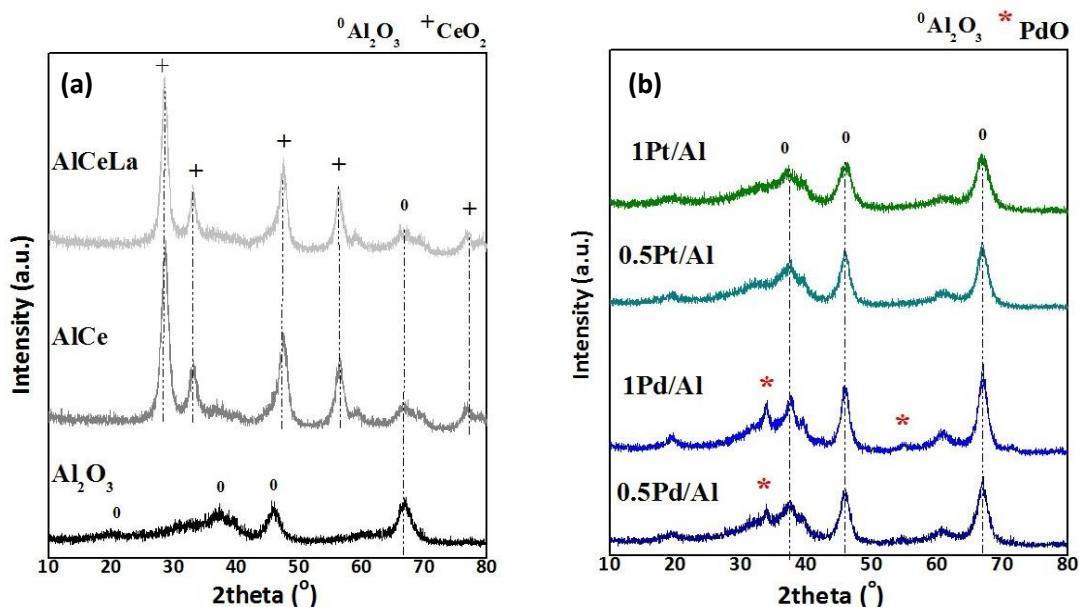
Figure III.2: Powder X-ray diffraction patterns of: (a) Bare supports and (b) Pt-, Pd/ γ-Al₂O₃ catalysts.

The intensity of the peak is increasing, while the percentage of Pd is increased (1Pd/Al). However, palladium XRD patterns over AlCe and AlCeLa did not evidence any peak of Pd oxides, due to the overlapping of PdO peaks with the intense and high crystalline CeO_2 peaks. In contrast to Pd/Al samples, in the diffractogram of 0.5Pt/Al and 1Pt/Al catalysts no diffraction peaks related with platinum oxides or metallic Pt (at $2\theta=39.8^o$, 46.2^o) were observed [39]. The latter can be tentatively ascribed to the existence of very small Pt particles, as indeed confirmed by HRTEM (see below). This is not surprising in terms of the well-known trend of Pt to form very small Pt particles (< 10 nm) at this or even higher loadings [40].

Representative HRTEM images of un-promoted and Ce, La promoted catalysts is depicted in Fig. III.3 (a-e). The samples comprise of the Al₂O₃ supported nanoparticles, which adopt a densely agglomerated morphology, as evidenced by the spotty rings in the Selected Area Diffraction (SAD) pattern inset in Fig. III.3a. The

presence of catalyst particles is resolved, exhibiting distinct morphologies and phases in each sample.

0.5Pd/Al catalyst is mainly in nanoparticle form, as illustrated in Fig. III.3a, with sizes ranging from 5 nm up to 20 nm, while the mean particle size is 11 nm. The oxidation state of Pd was predominately verified by SAD experiments, and complemented by HRTEM observations.
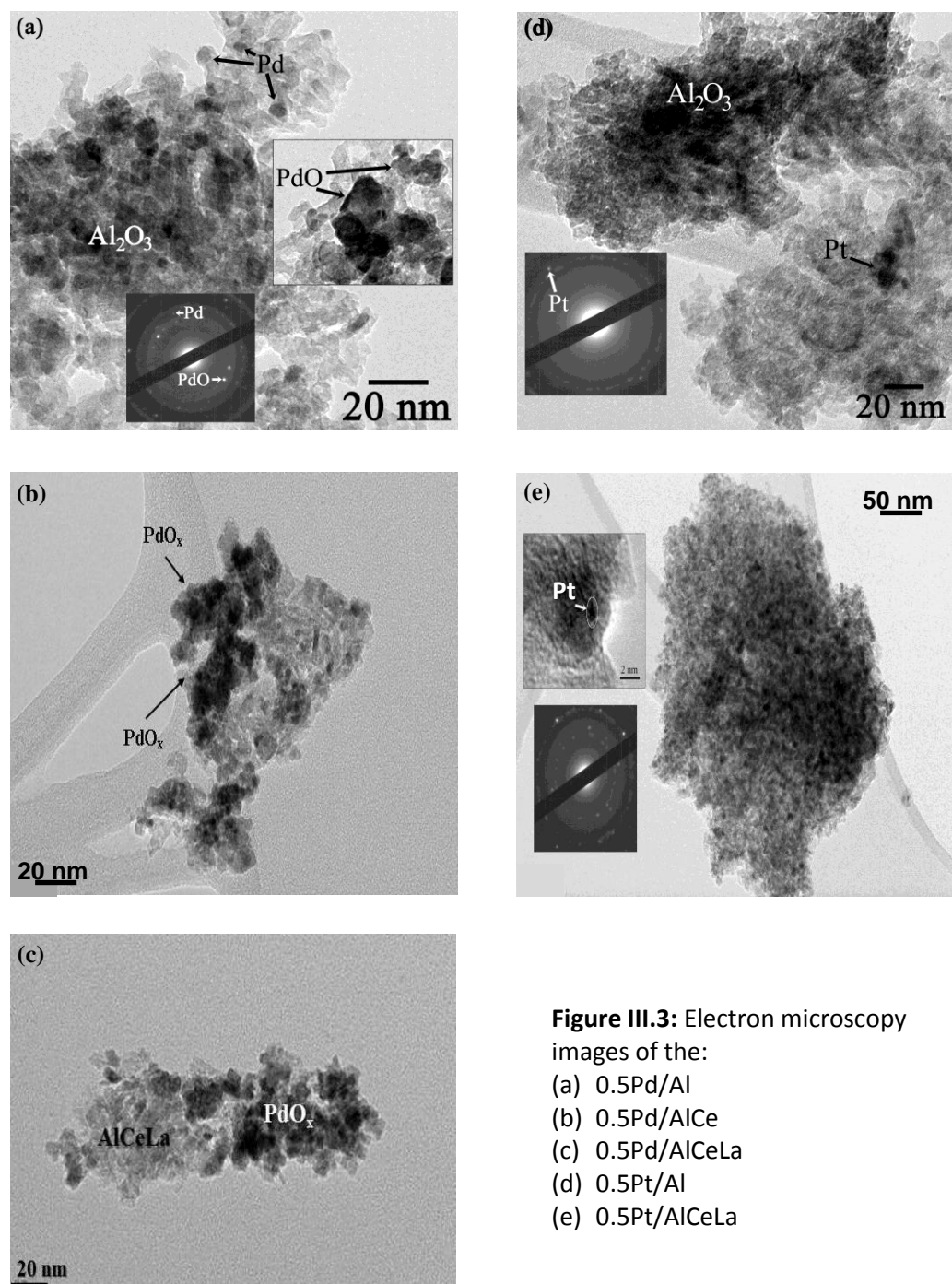
Figure III.3: Electron microscopy images of the:
(a) 0.5Pd/Al
(b) 0.5Pd/AlCe
(c) 0.5Pd/AlCeLa
(d) 0.5Pt/Al
(e) 0.5Pt/AlCeLa

Measurements of the lattice fringe spacing resolved yielded d_1=0.263 nm and d_2=0.305 nm, which correspond to the (002) and (100) crystal planes of tetragonal PdO. The particle is also viewed along its [010] zone axis. Although Pd particles were predominately in oxide form, few smaller size catalyst nanoparticles were also detected, which comprised of metallic Pd as shown in Fig. III.3a. Their size and percentage in the sample may well account for the metallic Pd peaks absence at the XRD pattern of the corresponding sample. The addition of structural modifiers reduced the dispersion of Pd on the supports. As a result, aggregates were created, which were consisting of PdO$_x$ (Pd^{+2} or/and Pd^{+4}) particles, without any metallic character (Fig. III.3, a-c). However, the addition of CeO$_2$ to alumina support increased slightly the mean particle size of PdO$_x$ (~13.3 nm). On the other hand, in the case of AlCeLa support, Pd particles were decreased around 7.5 nm.

The existence of metallic Pt phase in 0.5Pt/Al was hardly resolved during TEM experiments and best clarified by EDS, which confirms the catalyst high dispersion. Only occasionally small Pt nanoparticles, up to 8 nm in size, were observed on top of the Al$_2$O$_3$ support, as shown in Fig. III.3d. Analysis at typical SAD patterns, such as the one shown as inset in the same figure, revealed that these nanoparticles comprise of metallic Pt. The same was also observed in the case of 0.5Pt/AlCeLa catalytic material, with even smaller mean particle size (< 6 nm) (Fig. III.3e).

Catalytic Activity Results

The effect of the NMs percentage (%) over γ-Al$_2$O$_3$ on the de-N$_2$O activity of supported Pt- and Pd- catalysts, as well the effect of structural modification of alumina support were studied by Papista Eleni in the University of Western Macedonia. Papista et al. [41] demonstrated that at high temperatures (600°C) the highest the noble metals loading, the highest the N$_2$O conversion performance, following the order Pd > Pt. The superior catalytic performance of Pd/Al catalysts in comparison to Pt/Al catalysts is observed both in absence and presence of oxygen. Pt-based catalysts are drastically hindered by oxygen species originated either from gas phase (presence of O$_2$) or from N$_2$O decomposition (absence of O$_2$) [6, 28].

The effect of Ce and La over Pt and Pd based over γ-Al$_2$O$_3$, is presented in Fig. III.4. Addition of rare earth oxides to γ-Al$_2$O$_3$ support enhances the catalytic performance

of both noble metals. In the absence of oxygen, 0.5Pt/AlCeLa presented the double N$_2$O conversion at 600°C, in contrast with the unmodified catalyst. Pd catalysts maintain the superior performance, with 0.5Pd/AlCe reaching > 80% N$_2$O conversion at 600°C (in the absence and presence of O$_2$) [41].
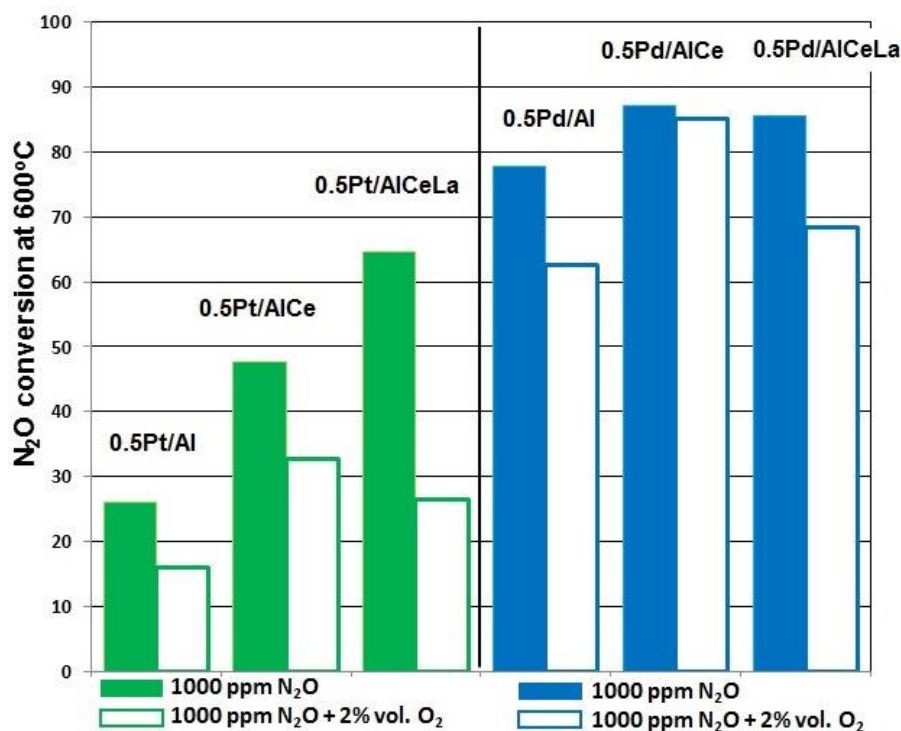
Figure III.4: Effect of structural promoters over Pt/γ-Al$_2$O$_3$ and Pd/γ-Al$_2$O$_3$ for deN$_2$O.

Based on the obtained characterization results, it can be argued that unmodified Pt catalysts are not active towards N$_2$O decomposition, most probably due to the sensitivity of metallic Pt^0 sites to oxygen poisoning. However, according with recent studies [28], incorporation of Ce and La on γ-Al$_2$O$_3$ results in significant increase of Pt dispersion and the formation of Pt sites with exceptional electron density, located on the metal-support interfacial area. Konsolakis et al. [28], based on in situ CO-DRIFTS measurements, attributed the superior catalytic performance of modified samples to the formation of electron enriched Pt sites (Pt$^{\delta-}$), located at metal-support interfacial area, which are highly active towards N$_2$O decomposition.

Pd/Al catalysts on the other hand, are only slightly depressed by the O$_2$ in the reaction feed. This is probably related with the existence of the metal oxide phase (PdO), which is active towards N$_2$O decomposition under these conditions. The

addition of Ce and La reduced the dispersion and created aggregates of PdO$_x$ (Pd^{+2} or/and Pd^{+4}). The oxidation state of Pd and the interaction of noble metal-modified alumina supports, enhance the de-N$_2$O performance of Pd catalysts, especially of the 0.5Pd/AlCe catalyst sample.

III.1.3 *Conclusions*

The incorporation of structural promoters (Ce, La) into γ-Al$_2$O$_3$-supported noble metal (Pt, Pd) catalysts was investigated, with particular emphasis on their impact on the structural and surface characteristics. In addition, all the catalytic materials were tested for the decomposition of N$_2$O in the absence and presence of oxygen. The obtained results revealed the superiority of Pd-based samples both in the presence and absence of oxygen. The unmodified Pt catalysts demonstrated an inferior performance, probably related with the metallic state of Pt (Pt^0), which is sensitive to oxygen poisoning. Incorporation of structural modifiers enhances the catalytic performance of both metals, either in the presence or absence of oxygen, by stabilizing the active entities for N$_2$O activation. Metal oxide phase of Pd (PdO) seem to be active towards de-N$_2$O, while the incorporations of Ce and La enhance even more the de-N$_2$O performance due to the creation of PdO$_x$ aggregates (Pd^{+2} or/and Pd^{+4}).

III.2 EFFECT OF CeO$_2$ AND La$_2$O$_3$ ON Ir-BASED CATALYSTS

INTRODUCTION

Ir has comparatively received little attention up to now and was usually used in multicomponent systems [42, 43]. The limited use of Ir (injection engines from Mitsubishi) can be attributed to several factors: the scarcity of Ir, problems with Ir loss due to the formation of volatile iridium chlorides and oxychlorides, and iridium's underestimated catalytic potential, among others [44]. However, its adequate performance in conjunction with its satisfactory stability at intermediate temperatures [45], render Ir-based catalysts as an exceptional catalyst for various processes, involving among others: the reforming of hydrocarbons [46, 47], the selective (in excess of O$_2$) catalytic reduction (SCR) of NOx (SCR-NOx) [48-57], the hydrocarbons and CO deep oxidation [58-60] as well as the N$_2$O decomposition (de-N$_2$O) [61-63].

The catalytically active phase of iridium (iridium metal, IrO$_2$ or a certain steady-state Ir^0/IrO$_2$ ratio) may strongly depend on the reaction system and the specific operational conditions used. The initial, as prepared, morphology and oxidation state of iridium particles are always of essential significance for its catalytic behavior, not only for the first few hours of operation until a steady-state to be reached, but also for its overall performance.

Wögerbauer et al. [54-57] have shown that the Ir crystallite size determines the time needed for the catalyst to reach steady-state during the SCR of NO by HCs: the larger the crystallite size, the faster steady-state of the reaction is achieved, at which a certain Ir^0/IrO$_2$ ratio is considered to be established, with an essential role on the N-containing products distribution (therefore on N$_2$-selectivity). In a similar manner, Haneda et al. [64], showed that, for the SCR of NO by CO in the presence of O$_2$ and SO$_2$, larger iridium crystallites dispersed on SiO$_2$ supports are more difficult to be oxidized and much easier to be reduced under reaction conditions, resulting in the formation of stable iridium metal sites, on which NO reduction occurs. Primet and co-workers [52], on the other hand, conclude that during SCR of NO by propene under lean-burn conditions, the surface of initially oxidized Ir particles is

progressively reduced with increasing temperatures into partially reduced Ir$^{\delta+}$ surface, allowing the efficient adsorption of both CO and NO.

For the direct N$_2$O decomposition, the most crucial problem arises in the poisoning of the catalytic surface by the strongly adsorbed oxygen atoms [65]. For instance, Ohnishi et al. [61] have shown that among noble metal catalysts supported on alumina, iridium offered the optimal performance for the N$_2$O decomposition in excess oxygen. This was mainly attributed to the facile desorption of adsorbed oxygen atoms from IrO$_2$ crystallites which are present under reaction conditions. On the other hand, small Ir particles expose kinks and steps sites on the surface that do not favor desorption of oxygen atoms [61]. Similarly, particle size and oxidation state of the active phase, as well as metal-support interactions have shown to determine the Ir-catalyzed direct N$_2$O decomposition in the absence or presence of excess O$_2$ [62].

In the present section the impact of 20 wt. % CeO$_2$ (AlCe) and 20 wt. % Ce$_{0.8}$La$_{0.2}$O$_{1.9}$ (AlCeLa) structural modifiers on 0.5Ir/Al$_2$O$_3$ catalysts is explored. Structural and morphological characterizations (including a detailed and advanced electron microscopy characterization, i.e. HRTEM, HAADF-STEM, EDS and EELS methods), were employed in order to gain insight into the effect of REOs on the physicochemical properties and the deN$_2$O performance.

III.2.1 Experimental

Material Synthesis

The catalysts used in this chapter (0.5Ir/Al, 0.5Ir/Ce, 0.5Ir/AlCe and 0.5Ir/AlCeLa) were obtained using the preparation process described previously in chapter II.1 (Materials Preparation). Table III.2 presents all catalytic materials, which were used for this study.

Characterization Techniques

The textural characteristics of the as prepared catalysts were determined by the BET and BJH method. The structure of the catalysts was determined by powder X-ray diffraction (XRD) and electron microscopy techniques (HRTEM, HAADF-STEM, EELS,

EDS). The reducibility of the catalysts were analyzed by hydrogen temperature-programmed reduction (H_2-TPR) experiments and the determination of the oxidation state of iridium was accomplished by in situ diffuse reflectance infrared Fourier transform spectroscopy (CO-DRIFTS) experiments. The corresponding experimental conditions are described in chapter II.2 (Characterization Techniques).

III.2.2 Results

Characterization Results

Table III.2 provides the textural characteristics (surface area, specific pore volume and pore size) of the 0.5Ir/Al, 0.5Ir/Ce, 0.5Ir/AlCe and 0.5Ir/AlCeLa solids. It is obvious that alumina-based samples (0.5Ir/Al, 0.5Ir/AlCe and 0.5Ir/AlCeLa) possess similar textural characteristics. However, ceria-modified Ir catalyst (0.5Ir/AlCe and 0.5Ir/AlCeLa) presents a five-fold larger mean particle size of IrO_2, as verified by XRD and HRTEM analyses to be presented next. This difference will be further discussed based on characterization and catalytic activity evaluation studies.

Table III.2: Textural and redox (H_2-TPR) characteristics of Ir-based catalysts.

Catalyst	S_{BET} (m^2/g)	Pore Volume (cm^3/ g)	Pore Size (nm)	Mean Ir particle size (nm)		T_{max} (^{o}C)[a] IrO_2	H_2 consumption (μmol/g)[b]
				XRD	TEM		
0.5Ir/Al	182	0.32	6.9	27	31	223	19.6
0.5Ir/Ce	27	0.06	8.3	-	27	216	89.7
0.5Ir/AlCe	170	0.26	6.2	137	155[c]	222	25.5
0.5Ir/AlCeLa	176	0.26	6.0	-	236	226	22.8

[a] Temperature at maximum reduction rate (H_2-TPR); [b] H_2 consumption as determined by H_2-TPR in the low-T range of 150-250°C (1st reduction peak); [c] Significant number density of tiny Ir clusters was also observed on top of IrO_2 and AlCe surfaces.

On the other hand, ceria-based sample (0.5Ir/Ce) presents the lowest BET area with a significantly lower pore volume as compared to the other two catalysts. Moreover,

0.5Ir/Al and 0.5Ir/Ce samples demonstrate a similar IrO$_2$ mean particle size according to HRTEM analyses (see below).

Powder XRD patterns of iridium supported on unmodified and modified γ-Al$_2$O$_3$ catalysts, as well of the bare supports, are presented in Fig. III.5. The presence of IrO$_2$ phase is confirmed by the XRD peaks at 2θ: 28°, 34.7° (main peak) and 54° in the 0.5Ir/Al, 0.5Ir/AlCe and 0.5Ir/AlCeLa samples [58]. In the case of Ce and La modified alumina, the IrO$_2$ peak at 2θ=28° overlaps with the intense peak at 2θ=28.5° of CeO$_2$. The remaining diffraction peaks are characteristic of pure γ-Al$_2$O$_3$ (2θ: 37.7°, 46°, 67°) and CeO$_2$ (2θ: 33.3°, 47.5°, 56.4°, 76.5°) phases, as revealed by their corresponding XRD diffractograms [36]. No diffraction peak was observed for La$_2$O$_3$, probably due to the high dispersion of lanthanum entities over the surface of the AlCeLa calcined support [32].

The XRD pattern of 0.5Ir/Ce catalyst did not show diffraction peaks due to IrO$_2$. Only the diffraction peaks of bare ceria with the fluorite structure were recorded. The absence of IrO$_2$ diffraction lines is tentatively related with the large density of small in size IrO$_2$ particles compared to that of large in size IrO$_2$ particles, deposited on the surface of CeO$_2$ support, given also the low metal loading (0.5% wt. Ir) used, resulting, therefore, in very low-intensity diffraction peaks (Fig. III.5). To this end, the broadening of diffraction peaks, due to particle size effects, also contributed to the absence of IrO$_2$ diffraction peaks. It is worth mentioning that the IrO$_2$ phase was clearly identified by powder XRD only in 0.5Ir/Al, 0.5Ir/AlCe and 0.5Ir/AlCeLa samples, apparently due to the favorable distribution of IrO$_2$ particle size, as verified by HRTEM analysis. Measurements of the IrO$_2$ mean particle size (employing the Scherrer equation) resulted in 27 and 137 nm for the 0.5Ir/Al and 0.5Ir/AlCe catalysts, respectively, in good agreement with the TEM particle size analyses performed (31 and 155 nm, respectively). Despite the fact that the 0.5Ir/Ce powder XRD pattern did not show clear diffraction lines due to IrO$_2$ (main peak at 34.7°), the existence of this phase was verified by HRTEM analysis. The mean particle size of IrO$_2$ was similar to that of 0.5Ir/Al catalyst (Table III.2).
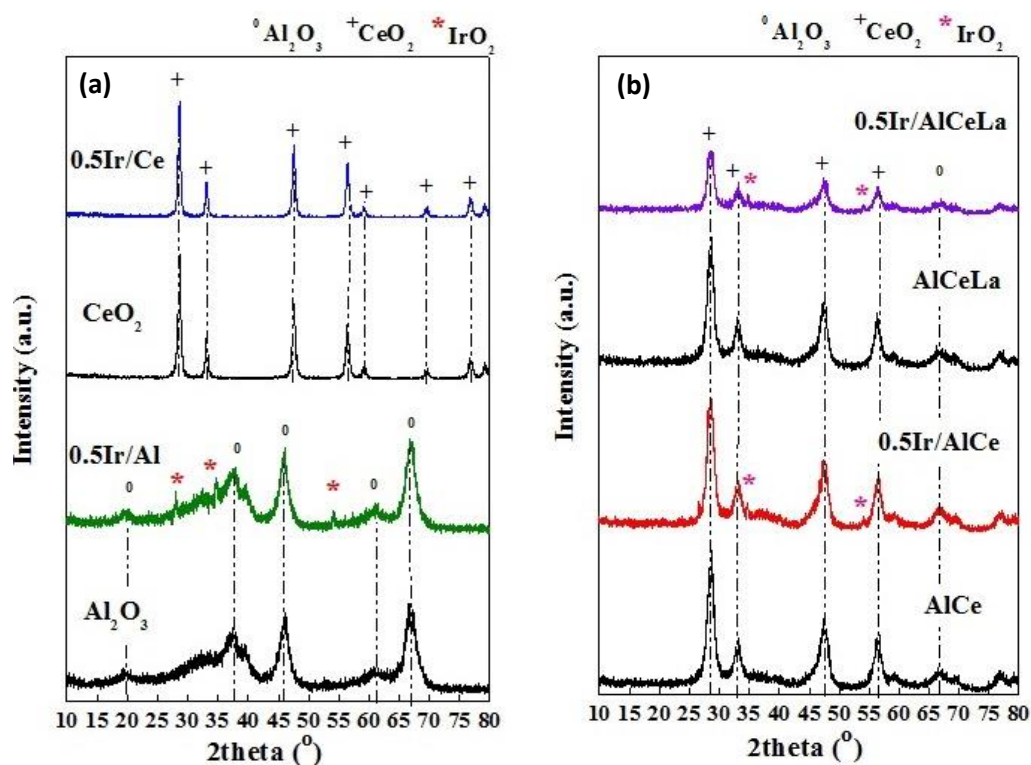
Figure III.5: Powder X-ray diffraction patterns of: (a) Ir based over γ-Al$_2$O$_3$, CeO$_2$ and (b) Ir based over AlCe, AlCeLa.

The morphology, crystalline structure and particle size distribution of Ir supported metal catalysts were evaluated by means of HRTEM and STEM studies. Typical images of the 0.5Ir/Al sample are depicted in Fig. III.6 (a, b). The alumina support comprises of small primary crystallites with sizes up to 20 nm, and a moderate degree of crystallinity, as shown by the rings in the selected area diffraction (SAD) pattern (Fig. III.6a, inset I). On top of γ-Al$_2$O$_3$, large IrO$_2$ particles are observed (black arrows, Fig. III.6a) with sizes up to 70 nm and a typical rectangular shape. The IrO$_2$ crystalline structure of these particles was proved by the discrete spots shown in the SAD pattern (inset I), where the main reflections for the tetragonal IrO$_2$ structure are indexed. The IrO$_2$ phase was also confirmed by EELS measurements (Fig. III.6c), where a typical spectrum in the low loss regime (0-100 eV) is presented.

The experimental peaks assigned to IrO$_2$ are located at 20.5, 28, 53.5 and 67 eV. Comparison with the theoretical EELS spectrum of IrO$_2$, superimposed at the same image, shows good agreement between the experimental peaks and those labeled as B, C, D and E in the theoretical spectrum, which confirms the presence of IrO$_2$. Besides the large crystalline IrO$_2$ particles, IrO$_2$ also appears as dense aggregates of

smaller crystallites (inset II, Fig. III.6a) with up to 10 nm in size as proved by SAD experiments in such regions. Measurements of the particle sizes of the two discrete IrO$_2$ morphologies over TEM micrographs (bimodal particle size distribution) resulted in a mean Ir particle size of 31 nm (see Table III.2), which is in good agreement with that estimated from the XRD analysis.
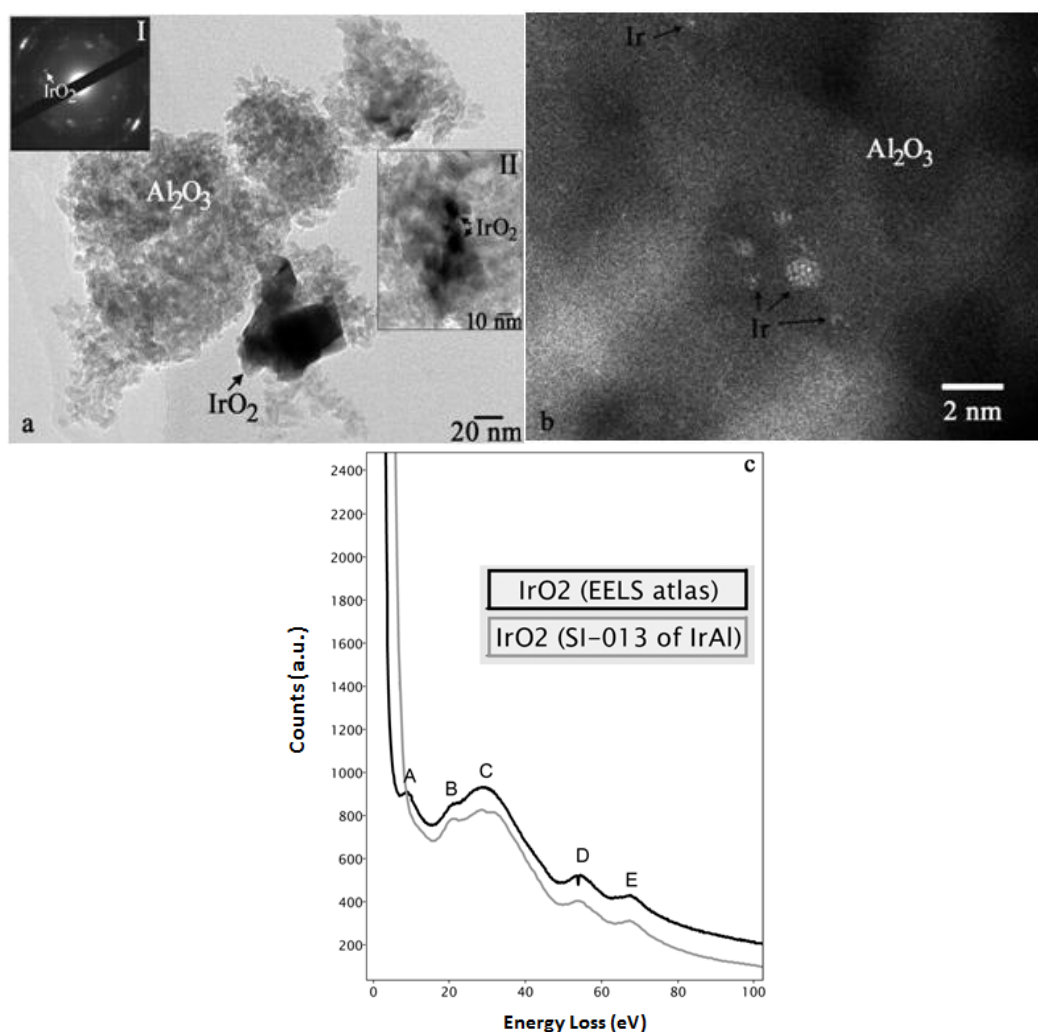
Figure III.6: (a) Electron microscopy images of 0.5Ir/Al catalyst, where a typical TEM BF image showing the IrO$_2$ discrete particles morphology is presented; (b) HAADF-STEM image, where isolated Ir metallic species are denoted with black arrows; (c) representative EELS spectrum of a large IrO$_2$ particle in the 0.5Ir/Al catalyst sample (grey line). The theoretical spectrum for IrO$_2$ [EELS Atlas by C.C. Ahn & O.L. Krivanek, Gatan (1983)] is also shown for comparison.

To further elucidate the morphology of Ir particles in the calcined 0.5 wt. % Ir/Al sample, HAADF-STEM experiments were carried out. A typical image is presented in Fig. III.6b. It is shown that part of the Ir phase is widely dispersed on the γ-Al$_2$O$_3$

support and appears either as isolated particles, or as tiny clusters of Ir (up to 1.5 nm in size). HAADF imaging experiments proved that both entities have pure metallic character, in contrast to distinct IrO_2 particles formed in other regions of the sample. This result is in good agreement with the H_2-TPR studies (described below), where multiple oxidation states of Ir were evidenced.

Table III.3: Morphological characteristics of supported Ir catalysts.

Catalyst	Particles morphology			
	IrO₂		Metallic Ir	
0.5Ir/Al	Large Crystallites (up to 70 nm)	Small Crystallites (up to 10 nm) in dense aggregate	Isolated Particles	Tiny Clusters (up to 1.5 nm)
0.5Ir/Ce	Large Crystallites (up to 90 nm)	Small Crystallites (up to 15 nm) in dense aggregates	-	-
0.5Ir/AlCe	Large Crystallites (up to 500 nm)	-	Isolated Particles	-
0.5Ir/AlCeLa	Large Crystallites (up to 600 nm)	-	-	-

TEM imaging experiments coupled with EDS were also carried out on the calcined 0.5 wt. % Ir/CeO$_2$ catalyst (not shown for brevity's sake). The results revealed a similar Ir particle morphology and distribution with the 0.5Ir/Al material. The 0.5Ir/Ce catalyst comprises of small -up to 15 nm- IrO$_2$ particles, densely aggregated on top of CeO$_2$, and larger (75-90 nm in size) IrO$_2$ particles. The latter, usually found isolated on CeO$_2$, are in somehow lower percentage in Ir/Ce compared with the 0.5Ir/Al solid.

Features of the morphology of the calcined 0.5 wt. % Ir/AlCe solid are presented in Fig. III.7. TEM image shows several IrO$_2$ large particles dispersed on the AlCe support. The latter comprises of single crystalline nanoparticles with sizes in the 3-9 nm range. On the other hand, the IrO$_2$ particles are significantly larger than those of support, having mean sizes of about 155 nm (larger sizes up to 500 nm were also observed). They are crystalline materials, as confirmed by the HRTEM image in Fig. III.7a (inset), where the (110) crystal planes of IrO$_2$ are resolved with an average d spacing of 0.317 nm. The termination of lattice planes almost up to its free surface clearly denotes particle's perfect crystal structure. Segregation of smaller IrO$_2$

particles into dense aggregates has not been extensively observed in this sample; only very few cases were encountered with small IrO$_2$ nanoparticles, densely aggregated on the AlCe support.

The existence of any possible additional Ir structural entities in the 0.5Ir/AlCe material has been evaluated by means of HAADF-STEM imaging (Fig. III.7b). Besides IrO$_2$ large secondary particles as described above, very small isolated Ir particles are readily observed, which are widely dispersed all over the AlCe support's surface. Furthermore, these very small Ir particles do not show a tendency for cluster formation as in the 0.5Ir/Al sample, but they mainly appear as discrete entities, distributed either on top of the AlCe support or the large IrO$_2$ particles.
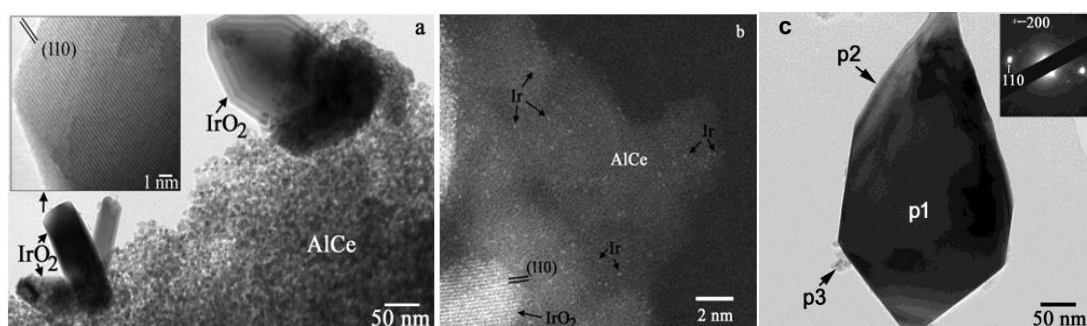
Figure III.7: Electron microscopy images: (a) TEM/HRTEM image revealing large IrO$_2$ particles of the 0.5Ir/AlCe catalyst; (b) HAADF-STEM image revealing isolated very small Ir metallic particles (black arrowed) of the 0.5Ir/AlCe catalyst, widely dispersed on top of the AlCe support and IrO$_2$ particles; (c) TEM/HRTEM image revealing very large IrO$_2$ particle of the 0.5Ir/AlCeLa catalyst.

0.5Ir/AlCeLa on the other side, basically presented very large IrO$_2$ particles (Fig. III.7c)-up to 600 nm-, without any smaller particles into dense aggregates or nanoparticles aggregated on the AlCeLa support. Unfortunately, no STEM analysis of this catalyst took place, in order to investigate the existence of isolated or tiny clusters of Ir^0. However, according with the characterization results with H$_2$-TPR and CO-DRIFTS (which are presented below) we can assume that the addition of La into the Al$_2$O$_3$-CeO$_2$ support did not influence in an important degree the physicochemical properties, as well as the catalytic performance for the N$_2$O decomposition reaction.

It is important to mention here that the small Ir (of metallic character) particles/ clusters identified in 0.5Ir/Al and 0.5Ir/AlCe solids have persisted conversion into

IrO_2 after calcination at 600°C. The above described findings indicate that the surface characteristics of the co-precipitated CeO_2 and Al_2O_3 phases are responsible for the formation of both large IrO_2 crystallites and very small Ir particles on the surface of 0.5Ir/AlCe solid. Jóźwiak and Maniecki [66] have reported on the mechanism of $IrCl_3.3H_2O$ thermal decomposition under oxidative conditions. The entire process can be divided into three not overlapped temperature regions [66]: dehydration (50-400°C), dechlorination-reoxidation (650-750°C) and dissociative deoxidation of IrO_2 above 900°C. It is speculated that the temperature range of dechlorination-reoxidation could vary in the case of supported $IrCl_3.3H_2O$ phase, as in the present work. Therefore, the presence of Ir^0 phase may not be a surprise. The main morphological characteristics of the three solid catalysts are summarized in Table III.3.

Further analysis by EELS at the large IrO_2 particles revealed a quite interesting finding. Figure III.8(a) and (b) show two HAADF images from the edge of two different IrO_2 particles and their corresponding EEL spectra, both focused on the O K edge at 525 eV. The presence of this peak up to the very outmost surface of the particle in Fig. III.8(a) demonstrates its oxidized nature, as anticipated. On the other hand, there are IrO_2 particles at the 0.5Ir/Al catalyst where their surface region is covered by a metallic Ir layer. Such a case is presented in Figure III.8(b), where the edge of an IrO_2 particle is shown, along with its EEL spectrum from its surface.

The absence of the O K peak proves the metallic Ir layer of this particle, whose thickness is below the 1 nm range. EELS measurements in other large IrO_2 particles confirmed this finding for the 0.5Ir/Al sample. On the other hand, 0.5Ir/AlCe catalyst did not show the presence of metallic Ir adlayers in IrO_2 surface regions (Fig. III.9a, b).

H_2-TPR profiles of supported Ir catalysts are presented in Fig. III.10, whereas Table III.2 reports the corresponding H_2 consumption (μmol H_2 g^{-1}) in the low-T range of 150-250°C and the peak maximum temperature (T_{max}) of the main reduction peak.
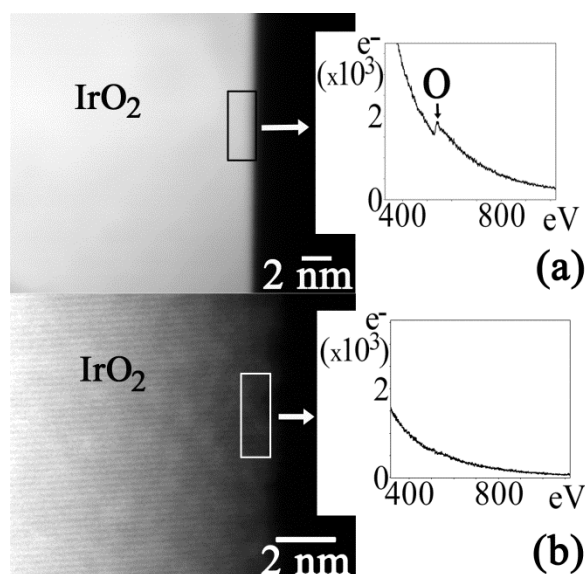
Figure III.8: (a) & (b) HAADF images from the edges of two distinct large IrO$_2$ particles and corresponding EEL spectra, focused at the O K edge in the 0.5Ir/Al catalyst. An absence of the O K peak in (b) is outlined, confirming the metallic Ir character of the surface in such IrO$_2$ particles.

The non-promoted catalyst (0.5Ir/Al) presents a well-defined reduction peak centered at ~223°C. This peak is attributed to the reduction of IrO$_2$ phase [36, 70-74]. However, besides the reduction peak of iridium oxide, the H$_2$-TPR profile of 0.5Ir/Al catalyst exhibits also a broad reduction peak (350-500°C), which can be attributed to the reduction of smaller IrO$_2$ particles present on the alumina support, as revealed by TEM and HAADF-STEM analyses (Fig. III.6a, inset II).

Modification of the 0.5Ir/Al with CeO$_2$ results in three reduction peaks: the first one is centered at 222°C, and the two other broad peaks at 340 and 655°C. The first low-T peak is largely related with the reduction of larger IrO$_2$ particles; reduction of surface Ce^{4+} to Ce^{3+} within few lattice constants around the Ir-CeO$_2$ interface cannot be excluded. The second broad peak at 340°C can be assigned to further reduction of surface ceria facilitated by the presence of Ir. It has been reported [75] that incorporation of Ir metal on the CeO$_2$ support facilitates reduction of ceria surface due to metal-support interactions developed, resulting in H$_2$-TPR peaks at temperatures lower than 400°C. Moreover, this peak could also be assigned to highly dispersed IrO$_2$ phase in close interaction with the support [76].
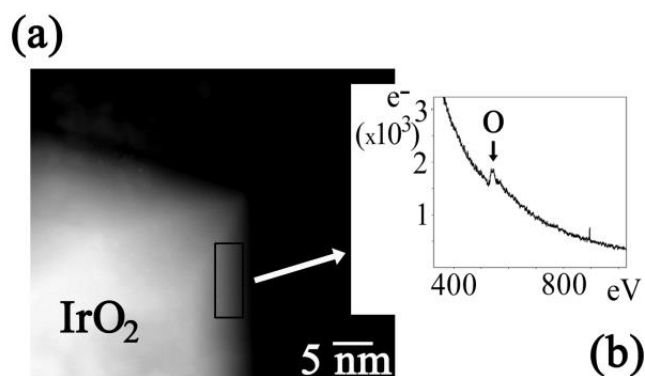
Figure III.9: (a) Experimental EEL spectrum from a large IrO_2 particle in the 0.5Ir/AlCe catalyst. (b) HAADF image and corresponding EEL spectrum, focused at the O K peak from the edge of a large IrO_2 particle in the same sample.

This finding is in line with the HAADF-STEM results (Fig. III.7), which indicate the formation of very small Ir particles on the AlCe surface. The third broad reduction peak at high temperatures (ca. 655°C) is related with the removal of bulk lattice oxygen from the CeO_2 matrix [76, 77]. The addition of La with Ce to alumina support did not influence the redox properties of Ir/AlCeLa catalyst. It presented the same TPR profile with the Ir/AlCe catalyst.

The Ir/CeO_2 catalyst (0.5Ir/Ce) exhibits three reduction peaks (ca. 216^oC, 330^oC and 707^oC). The first peak is attributed (see above) to the reduction of larger IrO_2 particles as in the case of the other two catalyst samples, but also to the ceria surface reduction around the IrO_2 particles. The second reduction peak is related with the reduction of small in size IrO_2 particles and ceria surface reduction, whereas the third high-T peak corresponds to the reduction of bulk ceria [76, 77].

To gain further insight into the impact of CeO_2 on the redox properties of the catalysts, the H_2 consumption in the low-temperature range was estimated, where reduction of larger IrO_2 particles mainly occurs, and this is reported in Table III.2. The non-promoted catalyst (0.5Ir/Al) was found to consume 19.6 μmol H_2 g^{-1}, which corresponds to 37.7% reduction of the IrO_2 phase (0.5% wt. Ir). The corresponding percentage on Ir/AlCe is 49%. These results could imply either the promoting effect of CeO_2 towards the formation/reduction of more IrO_2 particles or the facilitation of surface ceria reduction in the presence of Ir.
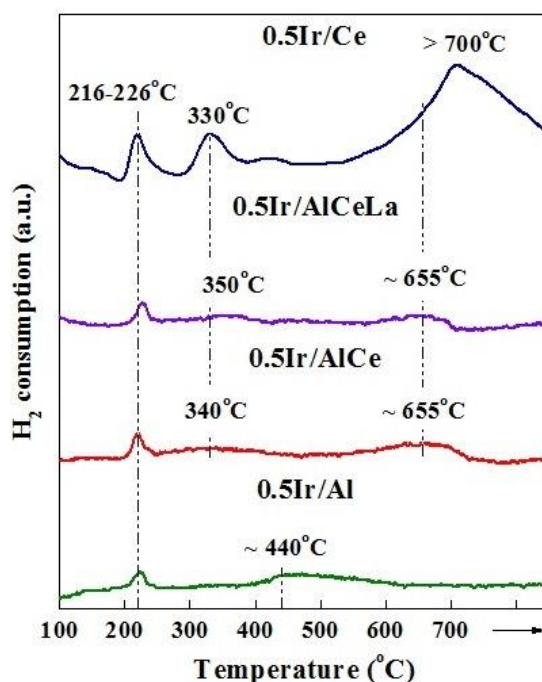
Figure III.10: H$_2$-TPR profiles of non-promoted (0.5Ir/Al), CeO$_2$-promoted (0.5Ir/AlCe) and Ir/CeO$_2$ (0.5Ir/Ce) catalysts.

The hydrogen consumption for the 0.5Ir/Ce sample considerably exceeds the theoretical value required for complete reduction of IrO$_2$ (52 μmol H$_2$ g^{-1}). This was found to be 89.7 μmol g^{-1}, a value that clearly implies the contribution from surface CeO$_2$ reduction (first peak at 216°C), in line with relevant literature studies [77, 78]; partial surface reduction of CeO$_2$, through H$_2$ spillover from the Ir metal to the support surface.

To reveal the impact of La and/or Ce-induced modifications on the surface chemistry of 0.5Ir/AlCeLa and 0.5Ir/AlCe catalyst, *in situ* DRIFTS-CO chemisorption studies were carried out. Figure III.11 shows DRIFT spectra recorded in the vC-O stretching vibrational mode region for the 0.5Ir/Al, 0.5Ir/Ce and CeO$_2$-promoted alumina (0.5Ir/AlCe) catalysts, following CO adsorption (30 min) and Ar purge (5 min) at 30°C. The 0.5Ir/Al and 0.5Ir/Ce catalysts present one main infrared absorption band centered at 2060 cm^{-1}, which is assigned to linearly adsorbed CO (L-CO) on Ir^0 (reduced) sites [71, 76, 79-85], whereas an infrared band centered at 1860 cm^{-1} was only observed in the case of 0.5Ir/Ce catalyst (Fig. III.11).
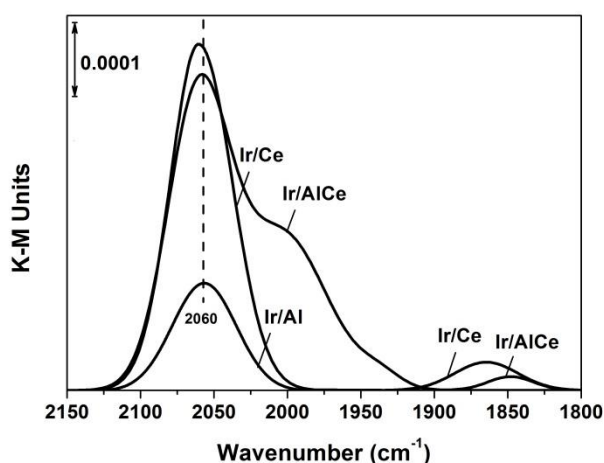
Figure III.11: In situ DRIFTS-CO spectra recorded on 0.5Ir/Al, 0.5Ir/Ce and 0.5Ir/AlCe catalysts following 30-min CO adsorption (1 vol. % CO/He) at 30°C and a 5-min Ar purge.

The latter IR band is associated with bridged CO species (B-CO) [71, 76-78, 82]. Taking into account the fact that no oxidized Ir species were identified by CO-DRIFTS, as opposed to the 0.5Ir/AlCe catalyst (see below), this could imply that after hydrogen reduction at 300°C and CO treatment at 30°C, Ir^0 (reduced) sites prevail on the catalyst surface of 0.5Ir/Al and 0.5Ir/Ce solids, leading only to the formation of L-CO species (IR band at 2060 cm^{-1}). The latter is in harmony with the CO-DRIFTS results reported by Iojoiu et al. [81] on Ir/γ-Al$_2$O$_3$ after oxidation followed by hydrogen reduction.

La and/or Ce modification of γ-Al$_2$O$_3$ support (0.5Ir/AlCe and 0.5Ir/AlCeLa catalysts) results in significant alterations in the CO chemisorption behavior of iridium surface. In particular, two infrared bands can be observed for the both catalysts, namely: an intense band at 2064 cm^{-1} with a shoulder in the 2000-2010 cm^{-1} range, and an extra one for 0.5Ir/AlCe catalyst at 1847 cm^{-1}. The first band has been already assigned to L-CO species on Ir^0 (reduced) sites, whereas the shoulder is attributed to gem-dicarbonyl adsorbed CO on partially oxidized iridium (Ir$^{\delta+}$(CO)$_2$, G-CO) on very small particles [82]. It was reported [82] that the main difference between single-crystal studies and supported Ir catalysts is the presence of G-CO either alone or in the presence of L-CO species. The ratio between the intensities of the IR bands of the L-CO and G-CO depends on several parameters such as the metal loading, the nature of the support and the reduction temperature [82]. It has to be mentioned here that

G-CO species provides two IR bands, the symmetric (~2070-2080 cm^{-1}) and antisymmetric (~2010 cm^{-1}) dicarbonyl vibrations [76, 77]. The IR band centred at 2064 cm^{-1} is, therefore, the overlap of the ν(L-CO) and ν(G-CO)s bands. The IR band centred at 1847 cm^{-1} is assigned to bridged CO species (B-CO) [71, 82, 85]. The slight shift of this band to lower wavenumbers, with respect to that observed in the Ir/Ce solid, might be explained due either to a surface coverage difference, or to an inherent small C-O binding energy difference between the two B-CO species populated on 0.5Ir/Ce and 0.5Ir/AlCe solids.

It is worth mentioning that after hydrogen reduction treatment carried out prior to CO chemisorption, the ceria-promoted 0.5Ir/AlCe and 0.5Ir/AlCeLa catalysts exhibit oxidized Ir species as opposed to the non-promoted 0.5Ir/Al and the 0.5Ir/Ce catalysts, in which iridium largely exists in metallic state (G-CO species were hardly observed, Fig.III.11). These results in conjunction with the TEM/STEM and H$_2$-TPR analyses imply the formation of oxidized Ir crystallites in the 0.5Ir/AlCe and 0.5Ir/AlCeLa catalysts samples, which persist hydrogen reduction at 300°C. According to the HAADF-STEM results previously presented and discussed, the AlCe support surface promoted the formation of a large number density of very small Ir particles of metallic character, as in the case of bare Al support. However, these very small Ir particles appear to possess Ir$^{\delta+}$ sites in the case of 0.5Ir/AlCe, very likely at the Ir-CeO$_2$ support interface, which persist H$_2$ reduction. Such sites couldn't be identified by the electron spectroscopy techniques used here. The very small Ir particles appeared in 0.5Ir/AlCe are likely strongly bound on the Ce support surface via oxygen-bridging (Ce-O-Ir). The latter was previously related to the second H$_2$-TPR peak (350-500°C range).

The above mentioned view of Ir$^{\delta+}$ sites formation finds strong support in the DRIFTS-CO chemisorption studies (Fig. III.11). It is very interesting to note here that the formation of such very small Ir particles in the AlCe and AlCeLa supports is the result of the co-precipitation synthesis method applied. The existence of some surface interaction between the ceria and alumina particles, which might have created specific sites for Ir deposition in very small particles, cannot be excluded.

Figure III.12 shows DRIFTS-CO spectra recorded at 30, 200 and 400°C under Ar gas flow during TPD over the 0.5Ir/AlCe catalyst. It is clearly indicated that L-CO (2064

cm^{-1}) is less thermally stable than the G-CO (2004 cm^{-1}) and B-CO (1847 cm^{-1}), where the L-CO desorbs completely at T ~ 400°C while the latter two species persist even at 400°C.
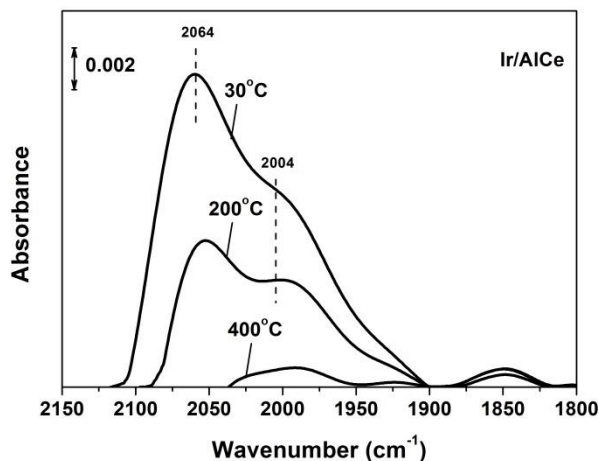
Figure III.12: In situ DRIFTS-CO spectra recorded on 0.5Ir/AlCe catalyst in Ar gas flow at 30°C (following 1 vol. % CO/He gas treatment at 30°C) and after TPD at 200 and 400°C.

This result is in agreement with previous reports [78, 82], where stable G-CO adsorbed species (~2000 cm^{-1}) were observed at high-T on Ir containing solids. In Fig. III.12, the symmetric G-CO band (~2070-2080 cm^{-1} overlapped with the L-CO at 2064 cm^{-1}) and that of v(G-CO)as recorded at 30°C have shifted to lower wavenumbers at 400°C due to the significant decrease in the surface coverage of G-CO species. Similar DRIFTS-CO TPD spectra were also recorded on the 0.5Ir/Al and 0.5Ir/Ce solids. It was found that the ratio of L-CO (T)/L-CO (30°C) was 0.51 and 0.25 at 200°C for the 0.5Ir/Ce and 0.5Ir/Al catalyst, respectively, whereas this ratio was found to be 0.25 and 0.12 at 400°C. This important result probes for the different adsorption and desorption characteristics of the Ir^o sites in the two catalytic surfaces. Due to the overlapping of v(L-CO) and v(G-CO)s in the 0.5Ir/AlCe solid, it was difficult to obtain a reliable value for the same L-CO (T)/L-CO (30°C) ratio in this catalytic system.

Catalytic Activity Results

The effect of structural promoters on the de-N$_2$O activity of supported Ir catalysts in terms of N$_2$O conversion at 600°C, is presented in Fig. III.13. These results were obtained by Papista Eleni in the University of Western Macedonia and revealed that

in the absence of O$_2$ in the feed stream (1000 ppm N$_2$O/He), the incorporation of Ce and La in the γ-Al$_2$O$_3$ support composition does not practically affect the N$_2$O decomposition activity behavior [41]. The N$_2$O conversion is almost complete at ca. 600°C. An inferior activity was obtained for the 0.5Ir/Ce catalyst, where ~ 85% N$_2$O conversion was attained at 600°C. However, under excess O$_2$ reaction conditions (1000 ppm N$_2$O/2% vol. O$_2$/He), a completely different behavior is obtained. The de-N$_2$O activity of both the 0.5Ir/Al and 0.5Ir/Ce catalysts is largely decreased by the presence of oxygen. On the contrary, the de-N$_2$O efficiency of Ce and La-promoted catalysts (0.5Ir/AlCe, 0.5Ir/AlCeLa) is only slightly affected by the presence of oxygen in the feed stream, with 0.5Ir/AlCe still being the best one among the two structurally promoted catalysts. These results indicate the existence of a synergistic effect between CeO$_2$ and Al$_2$O$_3$ upon Ir (0.5% wt.) addition [41].
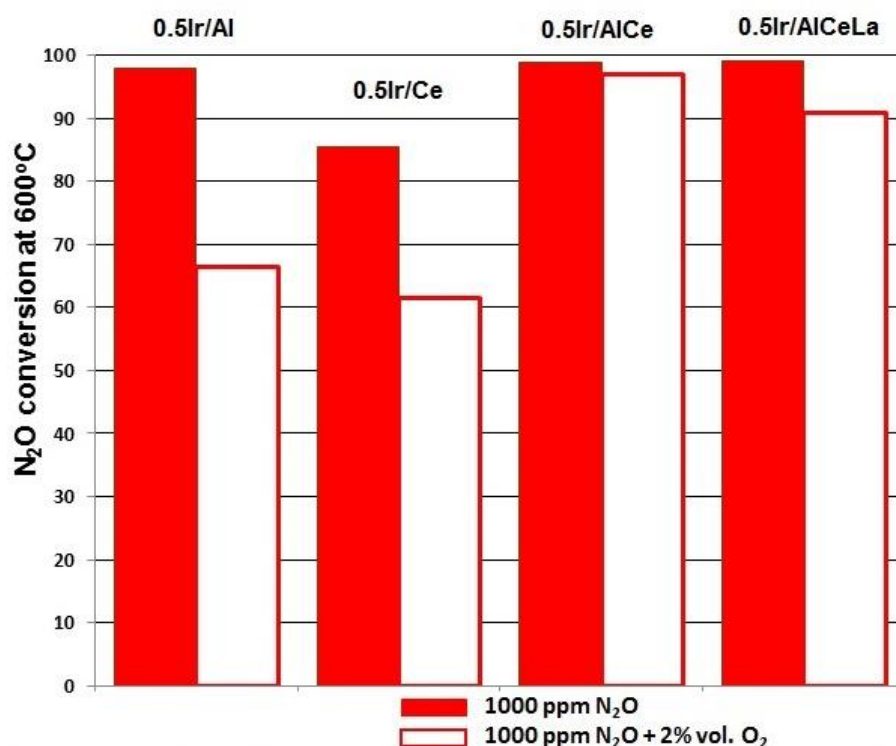

Figure III.13: Effect of structural promoters over Ir/γ-Al$_2$O$_3$ catalysts for de-N$_2$O.

In light of the above findings it can be deduced that structural promotion effects by CeO$_2$ incorporation to Al$_2$O$_3$ supports resulted in significant modifications in Ir catalyst surface. The remarkable resistance towards the loss of de-N$_2$O activity in the

presence of oxygen and the characterization analysis over 0.5Ir/AlCe catalyst can be summarized in the following:

(i)   0.5Ir/AlCe contains a large density of very small particles of Ir deposited on the ceria surface (HAADF-STEM studies), the latter being oxidized by the ceria support according to the CO-DRIFTS experimental results (Figs. III.11 and III.12). It should be re-emphasized at this point that these partially oxidized $Ir^{\delta+}$ species resist towards their full reduction in hydrogen, a fact that was observed only in the La and/or Ce promoted Al_2O_3 and not in the other catalytic systems. The probability that in the case of 0.5Ir/CeO_2 catalyst, some Ir is in the oxidized state ($Ir^{\delta+}$) under N_2O/O_2 reaction conditions cannot be excluded, in spite of the fact that these sites are reduced in hydrogen at $300^{\circ}C$, according to the CO-DRIFTS results.

(ii)   The rate of N_2O decomposition seems to be largely determined by a significant number of $Ir^{\delta+}$ sites formed along the Ir-ceria interface, which provide a favorable pathway for N_2 formation, thus possessing higher site reactivity. This mechanistic route is not available in the case of 0.5Ir/Al catalyst, the activity of which is largely reduced in the presence of O_2. In the case of Ir/Ce catalyst, the lower availability of $Ir^{o}/Ir^{\delta+}$ redox pairs (revealed by CO-DRIFTS, Fig. III.11) seems to be detrimental for the N_2O decomposition activity, on the basis of the redox mechanism proposed.

(iii)   In the case of 0.5Ir/AlCe, the available electron density in oxygen vacant (V_O) site per Ir atom, at the iridium-ceria interface, is likely to be larger compared to that in 0.5Ir/Ce.

Hong et al. [83] have reported a very interesting work on the effect of Ir loading on the selective hydrogenation of crotonaldehyde over Ir/SiO_2 catalysts. The authors concluded that the low-loading (1% wt. Ir/SiO_2) catalyst contained predominantly surface $Ir^{\delta+}$ species, whereas higher Ir loadings (3-5% wt.) contained a mixture of Ir^{o} and $Ir^{\delta+}$ species, the latter being twice as active than those formed in the low-loading catalysts. The authors concluded that a proper $Ir^{\delta+}/Ir^{o}$ ratio may be suitable for the chemisorption and activation of the crotonaldehyde molecule. In a similar manner, it

was found that the activity of Ir-based catalysts is notably enhanced after high-temperature treatment, which results in the establishment of an optimal Ir$^{\delta+}$/Ir^0 ratio [5]. It has been recently revealed by means of XPS and Raman studies that addition of Ir to ceria leads to the formation of surface oxygen vacancies, thus to a reduced ceria, where Ir^{x+}-O^2-Ce^{3+} surface entities in the ceria crystallites were suggested [86]. Moreover, it has been demonstrated my means of oxygen storage capacity measurements that oxygen uptake (due to the oxygen vacancies formed) is increased by 2-3 times, upon the incorporation of Ir in ceria [87, 88].

In the light of the discussion offered above, it could be stated that the design of an efficient supported Ir catalyst may require the formation of very small Ir particles with an optimum Ir$^{\delta+}$/Ir^0 atom ratio in order to achieve a high and stable de-N$_2$O performance under oxidizing conditions.

III.2.3 Conclusions

The effect of Ce and La in the Al$_2$O$_3$-20% wt. CeO$_2$ and Al$_2$O$_3$-20% wt. Ce$_{0.8}$La$_{0.2}$O$_{1.9}$ support prepared by the co-precipitation method on the Ir particle size, morphology and oxidation state were investigated. The catalysts were tested for the decomposition of N$_2$O in the absence and presence of O$_2$. The obtained results revealed the superiority of CeO$_2$-promoted Ir/Al catalyst (0.5Ir/AlCe) in the presence of excess O$_2$ (1000 ppm N$_2$O/2% vol. O$_2$/He). The superiority of the latter catalytic composition was interpreted on the basis of HAADF-STEM, H$_2$-TPR and CO-DRIFTS experiments. The establishment of a certain Ir$^{\delta+}$/Ir^0 ratio and oxygen vacant sites (V$_O$) concentration in ceria, around very small supported Ir particles, under oxidative reaction conditions seem to largely promote a sustainable N$_2$O adsorption and decomposition into N$_2$ and O$_2$ over the CeO$_2$-promoted Ir/Al catalyst. The addition of La into the Al$_2$O$_3$-CeO$_2$ support did not influence in an important degree the physicochemical properties of the catalyst, as well as the catalytic performance for the N$_2$O decomposition. A small decrease was observed during the decomposition of N$_2$O in the presence of O$_2$, as compared to 0.5Ir/AlCe catalyst. In the case of 0.5Ir/Al, a different deN$_2$O decomposition mechanism occurs, where the site reactivity of Ir$^{\delta+}$/Ir^0, established under oxidizing conditions, is reduced significantly.

III.3 EFFECT OF POTASSIUM (K) ON Ir-BASED CATALYSTS: SURFACE VS. STRUCTURAL PROMOTION

INTRODUCTION

Recently particular emphasis is given on the modification of catalysts surface chemistry by structural modifiers, like Ce, La (which was presented in section III.1 and III.2) or electropositive surface modifiers, such as alkalis or alkaline earths (i.e. K, Na, etc.) [5-7, 16-19, 28-31, 89]. Alkali metals can substantially affect the electronic properties of oxide catalysts, due to their low ionization potentials [90].

Extensive research studies by Konsolakis and Yentekakis on the SCR of NO by propene over Pt/Al_2O_3 [91-93] showed that alkali and alkaline earth metals could promote the adsorption of NO (electron-acceptor) on the catalyst surface by acting as electronic promoters. The N-O bond was weakened at the same time, thus facilitating NO dissociation. Haber et al. [94] reported that doping with alkali metals could influence the dispersion of rhodium on Al_2O_3, and then influence its catalytic activity for the decomposition of N_2O. The promotion effects of alkali or alkaline earth metals on the catalytic decomposition of N_2O have also been observed by other researchers. For instance, Farris et al. [95] found in a scale-up process that an appropriate amount of residual Na is very important for the catalytic activity of Co-Al hydrotalcite in N_2O decomposition. Ohnishi et al. [96] reported that alkali and alkaline earth metals could promote the activity of a Co_3O_4 catalyst for N_2O decomposition.

Xue et al. [97-99] revealed the improved redox ability of active sites (Co^{2+}), which is induced by residual K and supposed to be the main reason for the high catalytic activity of the catalyst (Co/CeO_2) for the catalytic decomposition of N_2O. The presence of ceria in this catalyst was very important, because it could also improve the cobalt catalyst's activity even in the presence of residual K. However, the promotion effect of alkali metals was much greater than that of ceria.

Konsolakis et al. [6] examined also the synergistic promotion of potassium with REOs on the Pt/Al_2O_3-catalyzed N_2O decomposition, under both lean and O_2 excess conditions. The doubly-promoted $Pt(K)/Al_2O_3$-$(CeO_2+La_2O_3)$ catalysts attained complete elimination of N_2O, at 45-60°C lower temperatures versus those obtained

over K-free catalysts. The pronounced effect of potassium on de-N$_2$O performance can be mainly ascribed to the strengthening of the chemisorption bond of N$_2$O with the electron enriched Pt sites associated with the potassium ions. Independently of the K-loading, the de-N$_2$O efficiency of the doubly-promoted catalysts is strongly affected by the feed stream composition. In addition, K-modification (either electrochemically or conventionally) on Pd/Al$_2$O$_3$ catalysts enhanced the N$_2$O decomposition in the presence of hydrocarbons [19, 30, 31].

The impact of alkali modifiers over Ir-based catalysts has not been studied to a similar extent as in the case of platinum and palladium catalysts. Hence, in the present section the impact of K (0-1.0% wt.) on the physicochemical properties and the de-N$_2$O performance of 0.5% wt. Ir/γ-Al$_2$O$_3$ is investigated. At the same time, a comparison between structural (section III.2) and surface promotion is taking place.

III.3.1 *Experimental*

Material Synthesis

The catalysts used in this chapter (0.5Ir(xK)/Al; where x= 0-1% wt. K) were obtained using the preparation process already described in chapter II.1 (Materials Preparation). The as prepared catalytic materials are presented in Table III.4.

Characterization Techniques

The textural characteristics of the as prepared catalysts were determined by the BET and BJH method. The structure of the catalysts was determined by powder X-ray diffraction (XRD) and electron microscopy technique (HRTEM). The reducibility of the catalysts were analyzed by hydrogen temperature-programmed reduction (H$_2$-TPR) experiments and the determination of the acidity of all the catalytic materials were accomplished by Fourier transform infrared spectroscopy of pyridine adsorption (FTIR-pyridine) experiments. The experimental conditions are described in chapter II.2 (Characterization Techniques).

III.3.2 Results

Characterization Results

The textural and redox characteristics of the as prepared catalysts are presented in Table III.4. A decrease in the total surface area of alumina is observed upon the addition of iridium and even less upon the addition of potassium. The pore volume is more or less similar for the as prepared catalytic materials, but the average of pore diameter differs from one sample to the other, with 0.5Ir(0.5K)/Al catalyst to present the higher value.

Table III.4: Textural and redox characteristics of K-doped catalytic materials.

Catalyst Code	K Content (wt.%)	K/Ir Atomic Ratio	K Coverage $(\Theta_K)^a$	S_{BET} (m^2/g)	Pore Volume (cm^3/g)	Av. Pore Diameter (nm)	TPR Peaks $(^oC)^b$
Al_2O_3	0	0	0	179.6	0.36	8.1	-
0.5Ir(0K)/Al	0	0	0	160.3	0.34	8.6	233
0.5Ir(0.25K)/Al	0.25	2.46	1.8	155.8	0.34	8.7	238
0.5Ir(0.5K)/Al	0.50	4.92	3.6	153.3	0.35	9.1	245
0.5Ir(1K)/Al	1.00	9.84	7.2	153.6	0.34	8.9	253

^{a} Assuming a potassium anionic radius of 1.51×10^{-10} m and a uniform distribution of alkali over the entire surface area; ^{b} Indicated by H_2-TPR experiments.

Catalysts characterization via H_2-TPR revealed one main and well defined reduction peak, centered at 233-253°C (Table III.4). This peak is attributed to the reduction of IrO_2 [72], which shifts to higher temperatures with the increase of K content. Therefore the increase in reduction temperature of iridium oxides in the present case, most probably reflects a strengthening in the Ir-O bond due to K interaction with iridium particles (note that the oxygen is an electron acceptor adsorbate [93]). The presence of Ir oxide phase was confirmed by XRD patterns (Figure III.14a), with the characteristic diffraction peaks at 28°, 34.7^o and 54° (2θ) [58]. The XRD patterns did not reveal any new peak related to K, only a small decrease of the intensities of IrO_2 phase was observed, in relation to the K-free sample.

Figure III.14b and Table III.5 present the acidity of the catalytic materials via NH$_3$-TPD and FTIR-pyridine techniques, respectively. NH$_3$-TPD profiles gave a qualitative estimation of acidity, while FTIR-pyridine provided also quantitative characterization. The K-free catalyst exhibits a desorption peak of NH$_3$ at around 370°C, which can be attributed to Lewis acid sites. The addition of 0.25% wt. K shifts this peak to a lower temperature (~300°C), indicating that the strength of surface acid sites is notably decreased by potassium.
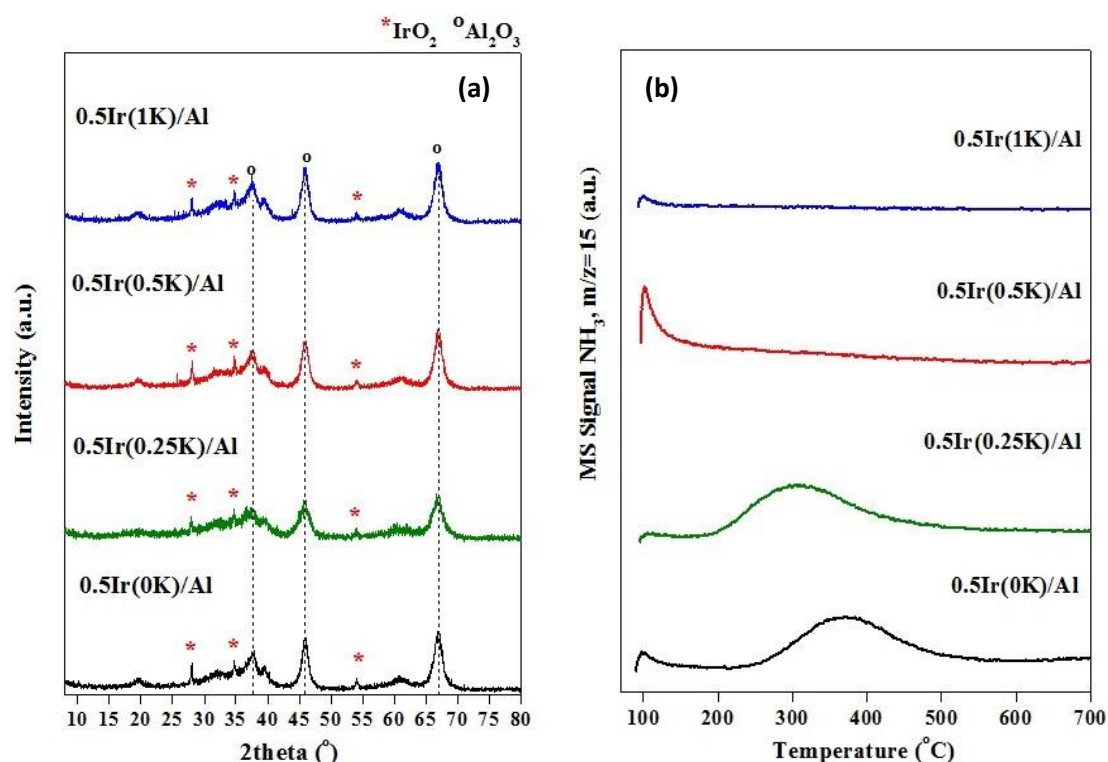
Figure III.14: K-free and K-doped 0.5Ir/Al catalysts: (a) XRD patterns and (b) NH$_3$-TPD profiles.

Further increase of K loading (0.5-1.0% wt.), resulted in a significant attenuation of Lewis acid sites. However, FTIR-pyridine can provide a more accurate estimation of surface acidity. The total surface acidity for all catalysts, as well as the discrimination of the acidity to very weak, weak, medium and strong acid sites, as estimated by the FTIR-pyridine measurements, is presented in Table III.5.

All the catalysts presented only Lewis and no Brönsted acidity, as expected. K-free Ir/Al catalyst exhibits significant Lewis acidity (115 μmol/g), with a high concentration of strong acid sites (25.9 μmol/g). The addition of potassium is

detrimental for the Lewis acidity, as also observed by NH_3-TPD. At high K loadings (0.50-1.00% wt.), the level of strong acid sites is decreasing by more than 90%, in comparison with the un-doped sample. Interestingly, an almost linear decrease in acidity is obtained upon increasing K loading. These findings are in agreement with previous studies, reporting that alkaline ions increase the basic strength of catalyst surface, while eliminating the Lewis acidity [31, 100-102].

Table III.5: Acidity of K-free and K-doped Ir/Al catalysts.

Catalyst Code	Strength of Lewis Acid Sites $(\mu mol/g)^a$				Total Lewis Acidity $(\mu mol/g)^a$
	Very Weak	Weak	Medium	Strong	
0.5Ir(0K)/Al	41.3	30.2	17.6	25.9	115.0
0.5Ir(0.25K)/Al	47.7	25.2	12.7	8.7	94.3
0.5Ir(0.5K)/Al	36.2	21.3	8.4	2.5	68.4
0.5Ir(1K)/Al	25.3	7.5	1.0	1.9	35.7

[a] Estimated by FTIR-Pyridine experiments.

Catalytic Activity Results

The effect of the potassium over 0.5Ir/Al on the de-N_2O activity was studied by Papista Eleni in the University of Western Macedonia. Papista et al. [41] revealed the pronounced effect of K addition, under oxygen excess conditions (2% vol. O_2) choosing an optimal loading of 0.5% wt. K. In opposite, the de-N_2O performance was negatively affected upon increasing K loading, under oxygen deficient conditions. Figure III.15 depicts the effect of alkali promotion on N_2O decomposition at 600°C for both reaction conditions (absence and presence of O_2). By comparing the bars, it is evident that the de-N_2O behavior of 0.5Ir/Al catalyst under oxidizing conditions is remarkably enhanced by K addition, while in the absence of oxygen the system is less sensitive to alkali promotion. A superior behavior is presented by 0.5Ir(0.5K)Al catalyst, in the presence and absence of O_2 [41].

TPR results clearly indicated that K addition suppressed the reduction of iridium species, shifting their reduction to higher temperatures. Acidity measurements

indicated that K eliminated the Lewis acidity of the catalyst surface, increasing at the same time the basicity.
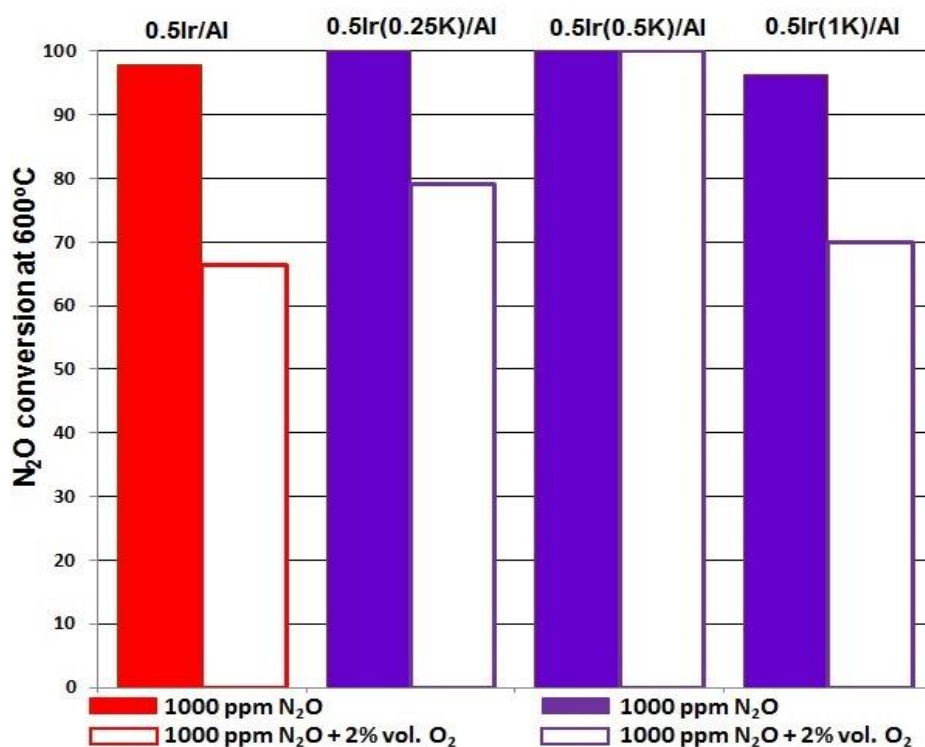
Figure III.15: Effect of surface promoters over 0.5Ir/γ-Al$_2$O$_3$ catalysts for de-N$_2$O.

In addition, morphological studies over K-free catalyst (presented in section III.2), revealed that 0.5Ir/Al comprises of large IrO$_2$ particles (with sizes up to 70nm), of dense aggregates of smaller crystallites (up to 10nm) and of Ir phase dispersed on the alumina either as isolated particles or as tiny clusters of Ir (up to 1.5nm in size). At the same time, at the edge of the large IrO$_2$ particles a metallic Ir adlayer (thickness below 1 nm) revealed. The optimum K-doped catalyst 0.5Ir(0.5K)/Al, on the other side, did not show any metallic layer to IrO$_2$ particles outermost surface layers, as proved by EELS analysis. In general, larger IrO$_2$ particles (with maximum and mean IrO$_2$ particle size, around ~200 nm and ~120 nm, respectively) were detected on K-doped catalyst, in comparison with the K-free catalyst (Fig. III.16a). In addition, Ir nanoclusters and isolated atoms were detected, which are presented in Fig. III.16b. The morphological study revealed more or less similar results with the

CeO$_2$-doped catalyst (0.5Ir/AlCe), which was presented in Chapter III.2 and discussed further below.
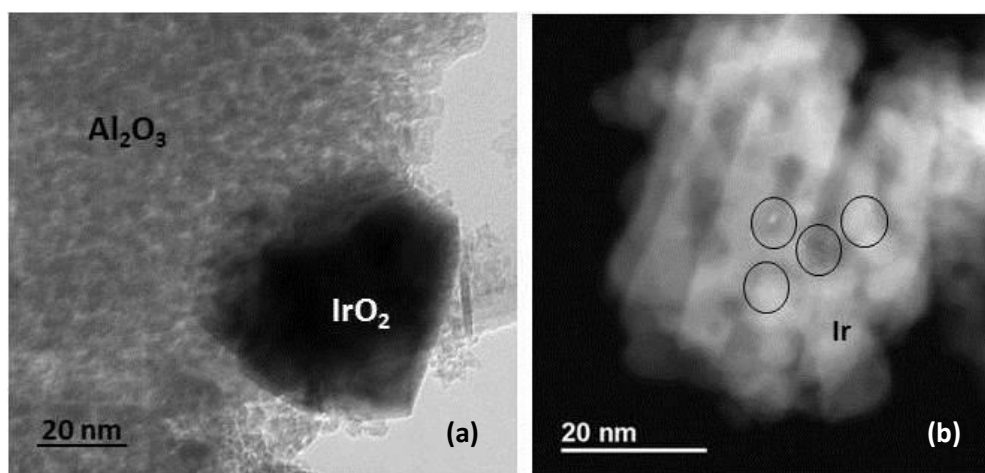
Figure III.16: Electron microscopy images of 0.5Ir(0.5K)/Al catalyst: (a) TEM/HRTEM image revealing large IrO$_2$ particles; (b) HAADF-STEM image revealing isolated very small Ir metallic particles (black circled).

Combining the characterization and evaluation results of the catalytic materials, the metallic Ir sites over 0.5Ir/Al are relatively active for N$_2$O decomposition, but progressively deactivated by accumulation of surface oxygen ad-species. In opposite, the alkali-doping, under oxygen excess conditions, promotes the oxidation of Ir^0 to Ir$^{\delta+}$ species, in which desorption of adsorbed oxygen species is facilitated [5]. Therefore, the pronounced effect of K under oxygen excess conditions can be attributed to the enhancement of N$_2$O adsorption and its concomitant dissociation due to the increase of catalyst's surface basicity, as well as to the facilitation of oxygen desorption from Ir$^{\delta+}$ sites. In a similar manner, it has been reported that the activity of Ir-based catalysts is notably enhanced after high temperature treatment, which results to the establishment of a certain Ir$^{\delta+}$/Ir^0 ratio [50].

III.3.3 Conclusions

Surface vs. Structural Promotion over 0.5Ir/Al Catalyst

Both surface and structural promotion were performed over 0.5Ir/Al catalyst, in order to enhance its catalytic performance for N$_2$O decomposition, in the excess of oxygen. Both promoters increase the % N$_2$O conversion in the presence of 2% vol. O$_2$

at 600°C, from ~66% for the un-promoted 0.5Ir/Al catalyst to ~97% and ~100% for the structurally promoted with Ce (0.5Ir/AlCe) and surface promoted with K (0.5Ir(0.5K)/Al) catalysts, respectively [41]. Figure III.17 presents the surface versus structural promotion as well as their combined impact.
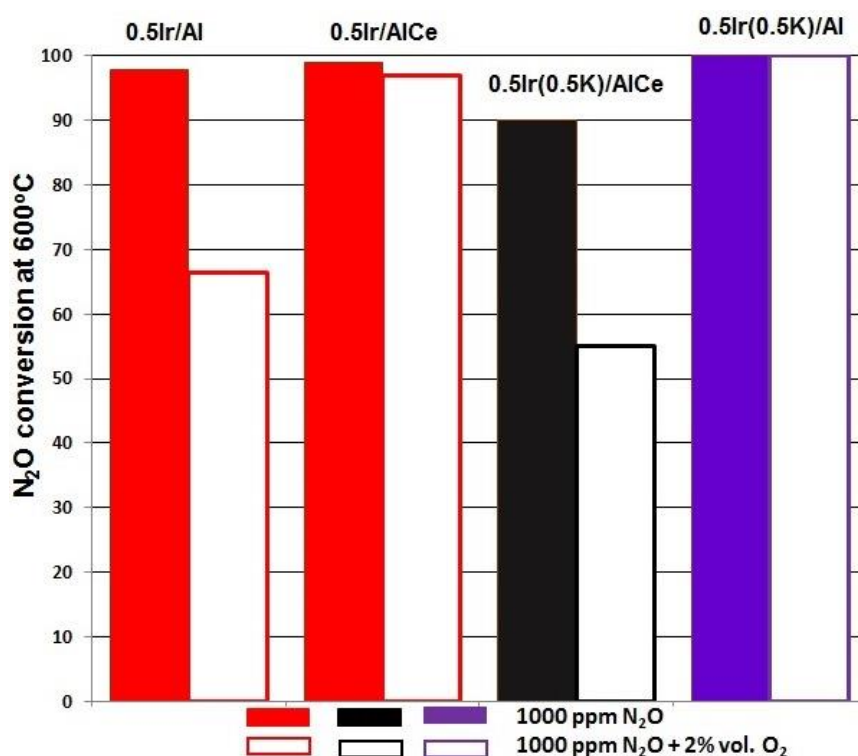
Figure III.17: Surface vs. structural promotion over 0.5Ir/Al catalyst.

Both promotion methods can notably affect the de-N$_2$O performance. In particular, the addition of Ce to 0.5Ir/Al catalyst (0.5Ir/AlCe) led to the establishment of a certain Ir$^{\delta+}$/Ir^0 ratio and oxygen vacant sites (Vo) concentration in ceria around very small supported Ir particles, which under oxidative reaction conditions seems to largely promote a sustainable N$_2$O adsorption and decomposition into N$_2$ and O$_2$. On the other hand, the addition of K to 0.5Ir/Al (0.5Ir(0.5K)/Al) in combination with oxygen excess, enhances the N$_2$O adsorption and its concomitant dissociation, whereas it promotes the formation of Ir$^{\delta+}$ species, in which desorption of adsorbed oxygen species is facilitated. However, no further promotion can be achieved by combining structural and surface promoters, implying that the optimum surface chemistry, and in turn de-N$_2$O performance, can be achieved either by surface or structural modifiers.

REFERENCES

[1] Pârvulescu V.I., Grange P., Delmon B., "Catalytic Removal of NO", Catalysis Today 46 (1998) 233-316.

[2] Kapteijn F., Rodriguez-Mirasol J., Moulijn J.A., "Review Heterogeneous Catalytic Decomposition of Nitrous Oxide", Applied Catalysis B: Environmental 9 (1996) 25-64.

[3] Centi G., Galli A., Montanari B., Perathoner S., Vaccari A., "Catalytic decomposition of N_2O over noble and transition metal containing oxides and zeolites-Role of some variables on reactivity", Catalysis Today 35 (1997) 113-120.

[4] Konsolakis M., Drosou C., Yentekakis I.V., "Support mediated promotional effects of rare earth oxides (CeO_2 and La_2O_3) on N_2O decomposition and N_2O reduction by CO or C_3H_6 over Pt/Al_2O_3 structured catalysts", Applied Catalysis B 123 (2012) 405-413.

[5] Bueno-Lopez A., Such-Basanez I., Salinas-Martinez de Lecea C., "Stabilization of active Rh_2O_3 species for catalytic decomposition of N_2O on La-, Pr-doped CeO_2", Journal of Catalysis 244 (2006) 102-112.

[6] Konsolakis M., Aligizou F., Goula G., Yentekakis I.V., "N_2O decomposition over doubly-promoted $Pt(K)/Al_2O_3$-(CeO_2-La_2O_3) structured catalysts: on the combined effects of promotion and feed composition", Chemical Engineering Journal 230 (2013) 286-295.

[7] Luo J., Gao F., Kim D.H., Peden C.H.F., "Effects of potassium loading and thermal aging on $K/Pt/Al_2O_3$ high-temperature lean NOx trap catalysts", Catalysis Today 231 (2014) 164-172.

[8] Liu Z., He F., Ma L., Peng S., "Recent Advances in Catalytic Decomposition of N_2O on Noble Metal and Metal Oxide Catalysts", Catalysis Surveys from Asia (2016) 1-12.

[9] Jones J.H., Kummer J.T., Otto K., Shelef M., Weaver E.E., "Selective catalytic reaction of hydrogen with nitric oxide in the presence of oxygen", Environmental Science and Technology 5 (1971) 790–798.

[10] Lamb A., Tollefson E.L., "Catalytic reduction of nitric oxide in the presence of oxygen in low concentration high velocity gas streams", The Canadian Journal of Chemical Engineering 53 (1975) 68–73.

[11] Wildermann A., Ph.D. Thesis, University of Erlangen, Nurnberg, 1994.

[12] Yokota K., Fukui M., Tanaka T., "Catalytic removal of nitric oxide with hydrogen and carbon monoxide in the presence of excess oxygen", Applied Surface Science 121-122 (1997) 273-277.

[13] Burch R., Coleman M.D., "An investigation of promoter effects in the reduction of NO by H$_2$ under lean-burn conditions", Journal of Catalysis 208 (2002) 435–447.

[14] Frank B., Emig G., Renken A., "Kinetics and mechanism of the reduction of nitric oxides by H2 under lean-burn conditions on a Pt-Mo-Co/α-Al$_2$O$_3$ catalyst", Applied Catalysis B 19 (1998) 45–57.

[15] Burch R., Coleman M.D., "An investigation of the NO/H$_2$/O$_2$ reaction on noble-metal catalysts at low temperatures under lean-burn conditions", Applied Catalysis B 23 (1999) 115–121.

[16] Pasha N., Lingaiah N., Reddy P.S.S., Prasad P.S.S., "An investigation into the effect of Cs promotion on the catalytic activity of NiO in the direct decomposition of N$_2$O", Catalysis Letters 118 (2007) 64-68.

[17] Zasada F., Stelmachowski P., Maniak G., Paul J.F., Kotarba A., Sojka Z., "Potassium promotion of cobalt spinel catalyst for N$_2$O decomposition-accounted by work function measurements and DFT modelling", Catalysis Letters 127 (2009) 126.

[18] Stelmachowski P., Maniak G., Kotarba A., Sojka Z., "Strong electronic promotion of Co$_3$O$_4$ towards N$_2$O decomposition by surface alkali dopants", Catalysis Communications 10 (2009) 1062.

[19] Haber J., Nattich M., Machej T., "Alkali-metal promoted rhodium-on-alumina catalysts for nitrous oxide decomposition", Applied Catalysis B 77 (2008) 278.

[20] Granger P., Leclercq G., "Reduction of N$_2$O by CO over ceria-modified three-way Pt-Rh catalysts: kinetic aspects", Journal of Physical Chemistry C 111 (2007) 9905.

[21] Li X., Zhang C., He H., Teraoka Y., "Catalytic decomposition of N$_2$O over CeO$_2$ promoted Co$_3$O$_4$ spinel catalyst", Applied Catalysis B 75 (2007) 167.

[22] Perez-Ramirez J., Kapteijn F., "Effect of NO on the SCR of N$_2$O with propane over Fe-zeolites", Applied Catalysis B 47 (2004) 177.

[23] Parres-Esclapez S., Lopez-Suarez F.E., Bueno-Lopez A., Illan-Gomez M.J., Ura B., Trawczynski J., "Rh-Sr/Al$_2$O$_3$ catalyst for N$_2$O decomposition in the presence of O$_2$", Topics in Catalysis 52 (13-20) (2009) 1832-1836.

[24] Collins N.R., Twigg M.V., "Three-way catalyst emissions control technologies for spark-ignition engines-recent trends and future developments", Topics in Catalysis 42-43 (2007) 323-332.

[25] Papavasiliou A., Tsetsekou A., Matsouka V., Konsolakis M., Yentekakis I.V., Boukos N., "Synergistic structural and surface promotion of monometallic (Pt) TWCs: effectiveness and thermal aging tolerance", Applied Catalysis B 106 (2011) 228-241.

[26] Burch R., Daniells S.T., Breen J.P., Hu P., "A combined transient and computational study of the dissociation of N_2O on platinum catalysts", Journal of Catalysis 224 (2004) 252.

[27] Burch R., Daniells S.T., Breen J.P., Hu P., "The effect of H_2 and the presence of hot-O-(ads) during the decomposition of N_2O on platinum", Catalysis Letters 94 (2004) 103.

[28] Konsolakis M., Drosou C., Yentekakis I.V., "Support mediated promotional effects of rare earth oxides (CeO_2 and La_2O_3) on N_2O decomposition and N_2O reduction by CO or C_3H_6 over Pt/Al_2O_3 structured catalysts", Applied Catalysis B: Environmental 123-124 (2012) 405-413.

[29] Matsouka V., Konsolakis M., Lambert R.M., Yentekakis I.V., "In situ DRIFTS study of the effect of structure (CeO_2–La_2O_3) and surface (Na) modifiers on the catalytic and surface behaviour of Pt/g-Al_2O_3 catalyst under simulated exhaust conditions", Applied Catalysis B 84 (2008) 715.

[30] Pekridis G., Kaklidis N., Konsolakis M., Athanasiou C., Yentekakis I.V., Marnellos G.E., "A comparison between electrochemical and conventional catalyst promotion: the case of N_2O reduction by alkanes or alkenes over K-modified Pd catalysts", Solid State Ionics 192 (2011) 653-658.

[31] Pekridis G., Kaklidis N., Konsolakis M., Iliopoulou E.F., Yentekakis I.V., Marnellos G.E., "Correlation of surface characteristics with catalytic performance of potassium promoted Pd/Al_2O_3 catalysts: The case of N_2O reduction by alkanes or alkenes", Topics in Catalysis 54 (2011) 1135-1142.

[32] Navarro R.M., Alvarez-Galvan M.C., Rosa F., Fierro J.L.G., "Hydrogen production by oxidative reforming of hexadecane over Ni and Pt catalysts supported on Ce/La-doped Al_2O_3", Applied Catalysis A: General 297 (2006) 60-72.

[33] Navarro R.M., Alvarez-Galvan M.C., Sanchez-Sanchez M.C., Rosa F., Fierro J.L.G., "Production of hydrogen by oxidative reforming of ethanol over Pt catalysts supported on Al$_2$O$_3$ modified with Ce and La", Applied Catalysis B: Environmental 55 (2005) 229-241.

[34] Berry F.J., Smart L.E., Sai Prasad P.S., Lingaiah N., Kanta Rao P., "Microwave heating during catalyst preparation: influence on the hydrodechlorination activity of alumina-supported palladium-iron bimetallic catalysts", Applied Catalalysis A: General 204 (2000) 191-201.

[35] Zhou R., Zhao B., Yue B., "Effects of CeO$_2$-ZrO$_2$ present in Pd/Al$_2$O$_3$ catalysts on the redox behavior of PdOx and their combustion activity", Applied Surface Science 254 (2008) 4701-4707.

[36] Hou T., Lei Y., Zhang S., Zhang J., Cai W., "Ethanol dry reforming for syngas production over Ir/CeO$_2$ catalyst", Journal of Rare Earths 33 (2015) 42.

[37] Huang S., Zhang C., He H., "Complete oxidation of o-xylene over Pd/Al$_2$O$_3$ catalyst at low temperature", Catalysis Today 139 (2008) 15-23.

[38] Babu N.S., Lingaiah N., Gopinath R., Reddy S., Sai Prasad P.S., "Characterization and Reactivity of Alumina-Supported Pd Catalysts for the Room-Temperature Hydrodechlorination of Chlorobenzene", Journal of Physical Chemistry C 111 (2007) 6447-6453.

[39] Chiang K.C., Chen K.L., Chen C.Y., Huang J.J., Shen Y.H., Yeh M.Y., Wong F.F., "Recovery of spent alumina-supported platinum catalyst and reduction of platinum oxide via plasma sintering technique", Journal of the Taiwan Institute of Chemical Engineers 42 (2011) 158-165.

[40] Yentekakis I.V., Konsolakis M., Lambert R.M., Macleod N., Nalbandian L., "Extraordinary effective promotion by sodium in emission control catalysis: NO reduction by propene over Na-promoted Pt/γ-Al$_2$O$_3$", Applied Catalysis B 22 (1999) 123-133.

[41] Papista E., PhD Thesis, University of Western Macedonia, Greece (in progress).

[42] Nakatsuji T., Yasukawa R., Tabata K., Ueda K., Niwa M., "A highly durable catalytic NOx reduction in the presence of SOx using periodic two steps, an operation in oxidizing conditions and a relatively short operation in reducing conditions", Applied Catalysis 21 (1999) 121.

[43] Takami A., Takemoto T., Iwakuni H., Yamada K., Shigetsu M., Komatsu K., "Zeolite-supported precious metal catalysts for NOx reduction in lean burn engine exhaust", Catalysis Today 35 (1997) 75.

[44] Wögerbauer C., Maciejewski M., Baiker A., "Structure sensitivity of NO reduction over iridium catalysts in HC-SCR", Journal of Catalysis 205 (2002) 157-167.

[45] Jehn H., Volker R., Ismail M.I., "Iridium losses during oxidation", Platinum Metals Review 22 (1978) 92-97.

[46] Ashcroft A.T., Cheetham A.K., Green M.L.H., Vernon P.D.F., "Partial oxidation of methane to synthesis gas using carbon dioxide", Nature 352 (1991) 225-226.

[47] Yentekakis I.V., Goula G., Panagiotopoulou P., Katsoni A., Diamadopoulos E., Mantzavinos D., Delimitis A., "Dry reforming of methane: Catalytic performance and stability of Ir catalysts supported on γ-Al$_2$O$_3$, Zr$_{0.92}$Y$_{0.08}$O$_{2-\delta}$ (YSZ) or Ce$_{0.9}$Gd$_{0.1}$O$_{2-\delta}$ (GDC) supports", Topics in Catalysis 58 (2015) 1228-1241.

[48] Burch R., Breen J.P., Meunier F.C., "A review of the selective reduction of NOx with hydrocarbons under lean-burn conditions with non-zeolitic oxide and platinum group metal catalysts", Applied Catalysis B 39 (2002) 283-303.

[49] Granger P., Parvulescu V.I., "Catalytic NO$_x$ abatement systems for mobile sources: from three-way to lean burn after-treatment technologies", Chemical Reviews 111 (2011) 3155-3207.

[50] Amiridis M.D., Mihut C., Maciejewskiv M., Baiker A., "The selective catalytic reduction of NO by hydrocarbons over Pt- and Ir-based catalysts", Topics in Catalysis 28 (2004) 141-150.

[51] Nawdali M., Iojoiu E., Gelin P., Praliaud H., Primet M., "Influence of the pre-treatment on the structure and reactivity of Ir/Al$_2$O$_3$ catalysts in the selective reduction of nitric oxide by propene", Applied Catalysis A: General 220 (2001) 129–139.

[52] Iojoiu E., Gelin P., Praliaud H., Primet M., "Reduction of NO by propene over supported iridium catalysts under lean-burn conditions: an in situ FTIR study", Applied Catalysis A: General 263 (2004) 39–48.

[53] Wögerbauer C., Maciejewski M., Baiker A., Gobel U., "Structural Properties and Catalytic Behavior of Iridium Black in the Selective Reduction of NO by Hydrocarbons", Journal of Catalysis 201 (2001) 113–127.

[54] Wögerbauer C., Maciejewski M., Baiker A., "Structure sensitivity of NO reduction over iridium catalysts in HC-SCR", Journal of Catalysis 205 (2002) 157-167.

[55] Wögerbauer C., Maciejewski M., Baiker A., Gobel U., "Ir/H-ZSM-5 catalysts in the selective reduction of NOx with hydrocarbons", Topics in Catalysis 16 (2001) 181–186.

[56] Wögerbauer C., Maciejewski M., Baiker A., "Reduction of nitrogen oxides over unsupported iridium: effect of reducing agent", Applied Catalysis B: Environmental 34 (2001) 11-27.

[57] Wögerbauer C., Maciejewski M., Schubert M.M., Baiker A., "Effect of sodium on the catalytic properties of iridium black in the selective reduction of NOx by propene under lean-burn conditions", Catalysis Letters 74 (2001) 1-7.

[58] Iliopoulou E.F., Efthimiadis E.A., Nalbandian L., Vasalos I.A., Barth J.O, Lercher J.A., "Ir-based additives for NO reduction and CO oxidation in the FCC regenerator: Evaluation, characterization and mechanistic studies", Applied Catalysis B 60 (2005) 277-288.

[59] Okumura M., Nasuyama N., Konishi E., Ichikawa S., Akita T., "CO Oxidation below Room Temperature over Ir/TiO$_2$ Catalyst Prepared by Deposition Precipitation Method", Journal of Catalysis 208 (2002) 485-489.

[60] Nakagawa, Ikenaga N., Suzuki T., Kobayashi T., Haruta M., "Partial oxidation of methane to synthesis gas over supported iridium catalysts", Applied Catalysis A: General 169 (1998) 281-290.

[61] Ohnishi C., Iwamoto S., Inoue M., "Direct decomposition of nitrous oxide in the presence of oxygen over iridium catalyst supported on alumina", Chemical Engineering Science 63 (2008) 5076-5082.

[62] Yentekakis I.V., Goula G., Panagiotopoulou P., Kampouri S., Taylor M.J., Kyriakou G., Lambert R.M., "Stabilization of catalyst particles against sintering on oxide supports with high oxygen ion lability exemplified by Ir-catalyzed decomposition of N$_2$O", Applied Catalysis B: Environmental 192 (2016) 357-364.

[63] Shen Q., Li L., Hao Z., Xu Z.P., "Highly active and stable bimetallic Ir/Fe-USY catalysts for direct and NO-assisted N$_2$O decomposition", Applied Catalysis B 84 (2008) 734–741.

[64] Haneda M., Fujitani T., Hamada H., "Effect of iridium dispersion on the catalytic activity of Ir/SiO_2 for the selective reduction of NO with CO in the presence of O_2 and SO_2", Journal of Molecular Catalysis A 256 (2006) 143-148.

[65] Konsolakis M., "Recent Advances on Nitrous Oxide (N_2O) Decomposition over Non-Noble-Metal Oxide Catalysts: Catalytic Performance, Mechanistic Considerations, and Surface Chemistry Aspects", ACS Catalysis 5 (2015) 6397-6421.

[66] Jóźwiak W.K., Maniecki T.P., "Influence of atmosphere kind on temperature programmed decomposition of noble metal chlorides", Thermochimica Acta 435 (2005) 151-161.

[67] Hong X., Li B., Wang Y., Lu J., Hu G., Luo M., "Stable Ir/SiO_2 catalyst for selective hydrogenation of crotonaldehyde", Applied Surface Science 270 (2013) 388– 394.

[68] De Leitenburg C., Trovarelli A., Kaspart J., "A Temperature-Programmed and Transient Kinetic Study of CO_2 Activation and Methanation over CeO_2 Supported Noble Metals", Journal of Catalysis 166 (1997) 98-107.

[69] Cai W., Wang F., Daniel C., van Veen A.C., Schuurman Y., Descorme C., Provendier H., Shen W., Mirodatos C., "Oxidative steam reforming of ethanol over Ir/CeO_2 catalysts: A structure sensitivity analysis", Journal of Catalysis 286 (2012) 137-152.

[70] Wang F., Cai W., Tana, Provendier H., Schuurman Y., Descorme C., Mirodatos C., Shen W., "Ageing analysis of a model Ir/CeO_2 catalyst in ethanol steam reforming", Applied Catalysis B: Environmental 125 (2012) 546-555.

[71] Chen P., Lu J., Xie G., Zhu L., Luo M., "Characterizations of Ir/TiO_2 catalysts with different Ir contents for selective hydrogenation of crotonaldehyde", Reaction Kinetics Mechanism and Catalysis 106 (2012) 419-434.

[72] Vicerich M.A., Benitez V.M., Especel C., Epron F., Pieck C.L., "Influence of iridium content on the behavior of $Pt-Ir/Al_2O_3$ and $Pt-Ir/TiO_2$ catalysts for selective ring opening of naphthenes", Applied Catalysis A: General 453 (2013) 167-174.

[73] Carnevillier C., Epron F., Marecot P., "Controlled preparation and characterization of plurimetallic Pt-Sn and $Pt-Ir-Sn/Al_2O_3$ reforming catalysts", Applied Catalysis A: General 275 (2004) 25-33.

[74] Tian H., Zhang T., Sun X., Liang D., Lin L., "Performance and deactivation of Ir/γ-Al$_2$O$_3$ catalyst in the hydrogen peroxide monopropellant thruster", Applied Catalysis A: General 210 (2001) 55-62.

[75] Haneda M., Hamada H., "Promotional role of H$_2$O in the selective catalytic reduction of NO with CO over Ir/WO$_3$/SiO$_2$ catalyst", Journal of Catalysis 273 (2010) 39–49.

[76] López-De Jesús Y.M., Vicente A., Lafaye G., Marécot P., Williams C.T., "Synthesis and Characterization of Dendrimer-Derived Supported Iridium Catalysts", Journal of Physical Chemistry C 112 (2008) 13837-13845.

[77] Solymosi F., Novák É., Molnár A., "Infrared spectroscopic study on carbon monoxide-induced structural changes of iridium on an alumina support", Journal of Physical Chemistry 94 (1990) 7250-7255.

[78] Alexeev O., Gates B.C., "Iridium Clusters Supported on γ -Al$_2$O$_3$: Structural Characterization and Catalysis of Toluene Hydrogenation", Journal of Catalysis 176 (1998) 310.

[79] Erdohelyi A., Fodor K., Suru G., "Reaction of carbon monoxide with water on supported iridium catalysts", Applied Catalysis A: General 139 (1996) 131-147.

[80] Rojas H., Diaz G., Martinez J.J., Castaneda C., Gomez-Cortes A., Arenas-Alatorre J., "Hydrogenation of α,β-unsaturated carbonyl compounds over Au and Ir supported on SiO$_2$", Journal of Molecular Catalysis A: Chemical 363 (2012) 122-128.

[81] Iojoiu E., Gelin P., Praliaud H., Primet M., "Reduction of NO by propene over supported iridium catalysts under lean-burn conditions: an in situ FTIR study", Applied Catalysis A: General 263 (2004) 39-48.

[82] Bourane A., Nawdali M., Bianchi D., "Heats of adsorption of the linear CO species adsorbed on a Ir/Al$_2$O$_3$ catalyst using in situ FTIR spectroscopy under adsorption equilibrium ", Journal of Physical Chemistry B 106 (2002) 2665-2671.

[83] Hong X., Li B., Wang Y., Lu J., Hu G., Luo M., "Stable Ir/SiO$_2$ catalyst for selective hydrogenation of crotonaldehyde", Applied Surface Science 270 (2013) 388-394.

[84] Chen P., Lu J.-Q., Xie G.-Q., Hu G.-S., Zhu L., Luo L.-F., Huang W.-X., Luo M.-F., "Effect of reduction temperature on selective hydrogenation of crotonaldehyde over Ir/TiO$_2$ catalysts", Applied Catalysis A: General 433-434 (2012) 236-242.

[85] Nguyen T.-S., Morfin F., Aouine M., Bosselet F., Rousset J.-L., Piccolo L., "Trends in the CO oxidation and PROX performances of the platinum-group metals supported on ceria", Catalysis Today 253 (2015) 106-114.

[86] Nguyen T.-S., Postole G., Loridant S., Bosselet F., Burel L., Aouine M., Massin L., Gelin P., Morfin F., Piccolo L., "Ultrastable iridium–ceria nanopowders synthesized in one step by solution combustion for catalytic hydrogen production", Journal of Materials Chemistry A 2 (2014) 19822-19832.

[87] Mikulová J., Barbier Jr. J., Rossignol S., Mesnard D., Duprez D., Kappenstein C., "Wet air oxidation of acetic acid over platinum catalysts supported on cerium-based materials: Influence of metal and oxide crystallite size", Journal of Catalysis 251 (2007) 172-181.

[88] Sadovskaya E.M., Ivanova Y.A., Pinaeva L.G., Grasso G., Kuznetsova T.G., van Veen A., Mirodatos C., "Kinetics of Oxygen Exchange over CeO_2–ZrO_2 Fluorite-Based Catalysts", Journal of Physical Chemistry A 111 (2007) 4498.

[89] Okumura K., Motohiro T., Sakamoto Y., Shinjoh H., "Effect of combination of noble metals and metal oxide supports on catalytic reduction of NO by H2", Surface Science 603 (2009) 2544-2550.

[90] Kotarba A., Adamski G., Sojka Z., Mariadassou G.D., "Potassium surface stability and electronic promotion in K-$NbN_{0.9}O_{0.1}$ catalysts", Applied Surface Science 161 (2000) 105-108.

[91] Konsolakis M., Yentekakis I.V., "Strong promotional effects of Li, K, Rb and Cs on the Pt-catalyzed reduction of NO by propene", Applied Catalysis B 29 (2001) 103-113.

[92] Konsolakis M., Yentekakis I.V., "The reduction of NO by propene over Ba-promoted Pt/γ-Al_2O_3 catalysts", Journal of Catalysis 198 (2001) 142-150.

[93] Yentekakis I.V., Tellou V., Botzolaki G., Rapakousios I.A., "A comparative study of the C_3H_6+NO+O_2, C_3H_6+O_2 and NO+O_2 reactions in excess oxygen over Na-modified Pt/γ-Al_2O_3 catalysts", Applied Catalysis B 56 (2005) 229-239.

[94] Haber J., Machej T., Janas J., Nattich M., "Catalytic decomposition of N_2O", Catalysis Today 90 (2004) 15-19.

[95] Farris T.S., Li Y., Armor J.N., Braymer T.A., "Method for Decomposing N$_2$O Utilizing Catalysts Comprising Calcined Anionic Clay Minerals", US005472677A, Engelhard Corporation: Iselin, NJ1995.

[96] Ohnishi C., Asano K., Iwamoto S., Chikama K., Inoue M., "Alkali-doped Co$_3$O$_4$ catalysts for direct decomposition of N$_2$O in the presence of oxygen", Catalysis Today 120 (2007) 145-150.

[97] Xue L., Zhang C., He H., Teraoka Y., "Promotion effect of residual K on the decomposition of N$_2$O over cobalt-cerium mixed oxide catalyst", Catalysis Today 126 (2007) 449-455.

[98] Xue L., Zhang C., He H., Teraoka Y., "Catalytic decomposition of N$_2$O over CeO$_2$ promoted Co$_3$O$_4$ spinel catalyst", Applied Catalysis B 75 (2007) 167-174.

[99] Xue L., He H., Liu C., Zhang C., Zhang B., "Promotion Effects and Mechanism of Alkali Metals and Alkaline Earth Metals on Cobalt-Cerium Composite Oxide Catalysts for N$_2$O Decomposition", Environmental Science Technology 43 (2009) 890-895.

[100] Damon J.P., Scokart P.O., "Acid-base Properties of Alkali Promoted Chromia alumina Catalysts", Chemistry Letters 3 (1980) 327-330.

[101] Abello M.C., Gomez M.F., Cadus L.E., "Selective oxidation of propane on MgO/-Al$_2$O$_3$-supported molybdenum catalyst: influence of promoters", Catalysis Letters 53 (1998) 185-192.

[102] Wang Y., Liu H.H., Wang S.Y., Luo M.F., Lu J.Q., "Remarkable enhancement of dichloromethane oxidation over potassium-promoted Pt/Al$_2$O$_3$ catalysts", Journal of Catalysis 311 (2014) 314-324.

CHAPTER IV
H_2-Assisted Selective Catalytic Reduction of NO by C_3H_6 on γ-Al_2O_3 Supported Noble Metals Catalysts
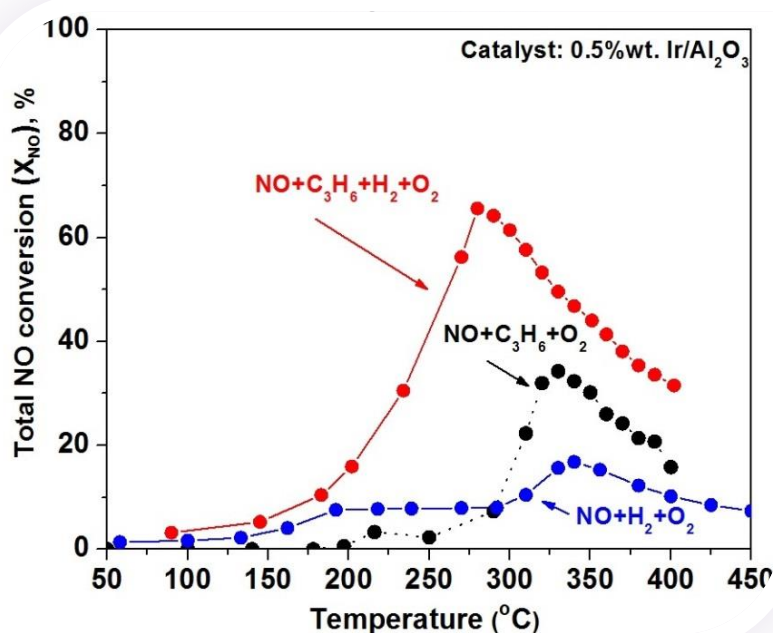
The impact of H_2 as an additional reducing agent on the selective catalytic reduction (SCR) of NO with propene in excess oxygen, was comparatively explored over γ-Al_2O_3 supported noble metal (Pt, Pd, Ir) catalysts of low noble metal (NM) loadings (0.5% wt.). Three different reaction schemes were employed: (i) NO+C_3H_6+O_2 (R#1), (ii) NO+C_3H_6+O_2+H_2 (R#2), and (iii) NO+H_2+O_2 (R#3).

IV H$_2$-ASSISTED SELECTIVE CATALYTIC REDUCTION OF NO BY C$_3$H$_6$ ON γ-Al$_2$O$_3$ SUPPORTED NOBLE METALS CATALYSTS

INTRODUCTION

Non-stoichiometric lean-burn engines have recently gained considerable attention, due to their advantages in relation to fuel efficiency and CO$_2$ emissions. Consequently, significant research efforts have been devoted to the SCR of NOx by hydrocarbons under lean-burn conditions [e.g. 1-4]. However, the three-way catalytic converters (TWCs), which are highly efficient in controlling NO, CO and hydrocarbon emissions from conventional gasoline-fueled vehicles that operate close to stoichiometric conditions, have been found to be insufficient under conditions of excess oxygen [e.g. 1-8].

Supported noble metal catalysts -typically bimetallic Pt/Rh and Pd/Rh constitutions supported on (BaO, CeO$_2$, La$_2$O$_3$, etc.)- enriched Al$_2$O$_3$ carrier- remain till today the best active phases among many other alternatives in TWC technology. This situation is attributed to their adequate three-way activity (simultaneous removal of CO, NO and HCs), good hydro-thermal stability and high tolerance to sulfur poisoning [7, 8]. Supported noble metal catalysts have also gained considerable attention in the field of SCR of NOx under lean-burn conditions, in the view of their application in lean-burn gasoline or diesel engines, as well as in stationary fuel combustion processes [1-8]. The NH$_3$-SCR process, which is currently the best choice for de-NOx processes in stationary power applications and chemical plants [4-6], experiences drawbacks related to the storage and slip of ammonia, although it may be pointed out that urea (as an NH$_3$ carrier)-SCR process is now commercially available for use on diesel truck and some lighter vehicles. This reality motivates significant efforts for the development of novel catalytic systems, capable for the efficient lean NOx reduction using in principle the gases, which already exist in the effluents as reducing agents, e.g., unburned hydrocarbons, H$_2$ or CO [1-25]. Most of these studies are once again concentrated on the use of supported Pt-group metal catalysts (in particular Pt), due to their typically high thermal/chemical stability and good de-NOx activity.

To this end, the lean propene-SCR of NOx on Pt-group metals supported on alumina, appeared to be efficient only in a very narrow temperature window (ΔT~100°C) with

NO conversion values typically being below than 60%, and N$_2$-selectivity values at the maximum NO conversion less than ~40%. These achievements are far away from those required for practical applications. More specifically, the active de-NOx windows of both Pt and Pd appear at similar temperatures (typically close to 250-300°C) and suffer by low N$_2$-selectivities, whereas, the lean deNOx activity of Ir-based catalysts is taking place at higher temperatures (ca. 400-600°C), accompanied, however, by better N$_2$-selectivity values [e.g., 2, 20-22]. In addition, Pt and Pd forms N$_2$ only in the presence of a reductant, in contrast to Ir where N$_2$ is formed under conditions, where the reducing agent is completely consumed [2, 20-26]. The Pt-catalysed NO+C$_3$H$_6$+excess O$_2$ reaction has been found to be subjected to promotional effects (by alkalis), that substantially improve the de-NOx performance [9, 10, 12]. The same promoter species, however, were found to inhibit the Ir-catalysed reaction [11, 25].

Another interesting trend of the Pt-group metals catalysing lean NOx reduction, that gained considerable interest in the last years, is the use of H$_2$ or more importantly, the employment of both H$_2$+CO as reducing agents [27-42]. Most of the studies were once again concentrated on Pt, until the pioneering work of Lambert and co-workers [37-41], who turned the interest on Pd-based catalysts as well; they revealed that Pd is very efficient for the lean NOx reduction by H$_2$+CO, overcoming some of the intrinsic catalytic weaknesses of Pt, as for example the poisoning influence of CO at high CO:H$_2$ ratios. Support-mediated promotional effects induced by TiO$_2$ incorporation onto the γ-Al$_2$O$_3$ support of the Pd/Al$_2$O$_3$ catalyst was the key point for this effective catalysis [40, 41]. Later on, Konsolakis et al. [42] further improved the performance of Pd on this process, by developing a doubly-promoted Pd(K)/Al$_2$O$_3$-(TiO$_2$) catalyst, which successfully combines, in a synergistic manner, support-mediated promotion (by TiO$_2$) with surface induced promotion (by K). The resulted benefits with this novel, doubly-promoted catalyst were the high NOx conversion (ca. 85%) accompanied by promising N$_2$-selectivities (ca. 85%) in a wide temperature window (ca. 150-350°C) [42].

Apart from the aforementioned efforts on the lean NOx reduction by H$_2$+CO, and to the best of our knowledge, the study of the Pt-group metals catalysed SCR of NOx with hydrocarbons and H$_2$ as the reducing agent mixture is absent. Only few studies

concerning the H_2-assisted, lean SCR of NOx with hydrocarbons (mainly propene, propane or octane), focused on Ag catalysts, can be found in the relevant literature [e.g. 43-47].

The purpose of the present work is to investigate for the first time, and in a comparative manner, the lean NOx reduction by propene, H_2 as well as by propene and H_2 over supported (on γ-Al_2O_3), low loading (0.5% wt.), Pt, Pd and Ir catalysts. Catalyst performance evaluation was carried out in a wide temperature range (50-400^oC), under the following reaction conditions: $NO+C_3H_6+O_2$ (R#1), $NO+C_3H_6+O_2+H_2$ (R#2) and $NO+H_2+O_2$ (R#3). The evaluation experiments were performed and analyzed at the Laboratory of Alternative Fuels and Environmental Catalysis (LAFEC), in the Technological Educational Institute of Western Macedonia, as well as at the Lab. of Physical Chemistry and Chemical Processes (TUC).

IV.1 Experimental

Material Synthesis

The catalysts used in this chapter (0.5Ir/Al, 0.5Pd/Al, 0.5Pt/Al) were obtained using the preparation process already described in chapter II.1 (Materials Preparation). The catalytic materials of this section are presented in Table IV.1.

Characterization Techniques

Complementary characterization studies involving N_2 physisorption (BET method), hydrogen temperature programmed reduction (H_2-TPR), X-ray diffraction (XRD) and electron microscopy techniques [transmission (TEM) and scanning transmission (STEM)] were carried out to gain insight into the H_2-induced enhancement on C_3H_6-SCR of NOx over Pt-group metals.

IV.2 Results

Characterization Results

Table IV.1 summarizes the textural, morphological and redox characteristics of the as prepared catalysts. Detailed analysis of characterization results for the current

catalytic materials was presented in chapter III.1. However, a brief overview of the obtained results is presented below.

Table IV.1: Textural and redox properties of Pt-, Pd- and Ir/Al_2O_3 catalysts.

Catalyst	S_{BET} (m²/g)	Pore Volume (cm³/ g)	Mean NMs' Particle Size (nm)[a]	T max (°C)[b]
0.5Ir/Al	182	0.32	30	223 (IrO₂)
0.5Pd/Al	163	0.33	11	60 (β-PdH)
0.5Pt/Al	187	0.30	< 8	-

[a] Evaluate by HRTEM and/or Scherrer analysis of the XRD; [b] Temperature at maximum reduction rate (H₂-TPR).

The textural characteristics (BET area and pore volume) of all samples are more or less similar (ca. 163-187 m²/g). However, significant differences are obtained in NMs particle size as estimated by employing the Scherrer's equation, indicating a different dispersion trend of each metal entity. The latter is verified by XRD and TEM measurements, presented below.

The XRD patterns of γ-Al_2O_3 carrier, 0.5Pt/Al, 0.5Pd/Al and 0.5Ir/Al catalysts are depicted in Fig. IV.1. The characteristic peaks of Al_2O_3 at 2θ= 37.7°, 46° and 67°, are present in all samples. No diffraction peaks related with PtO₂ (expected at 2θ= 33.3° and 55.9°) are observed at the 0.5Pt diffractogram. This is not surprising in terms of the well-known trend of Pt to form very small Pt particles (<~ 10 nm) at this or even higher loadings [9, 48].
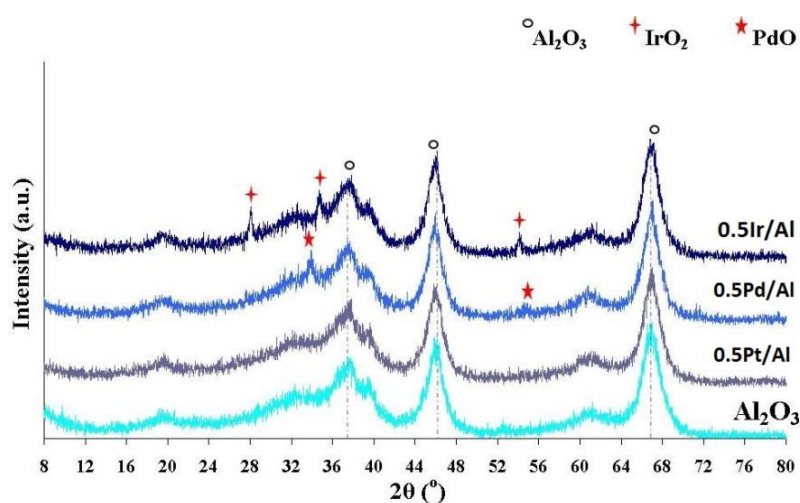

Figure IV.1: XRD patterns of Al_2O_3, 0.5Pt/Al, 0.5Pd/Al and 0.5Ir/Al samples.
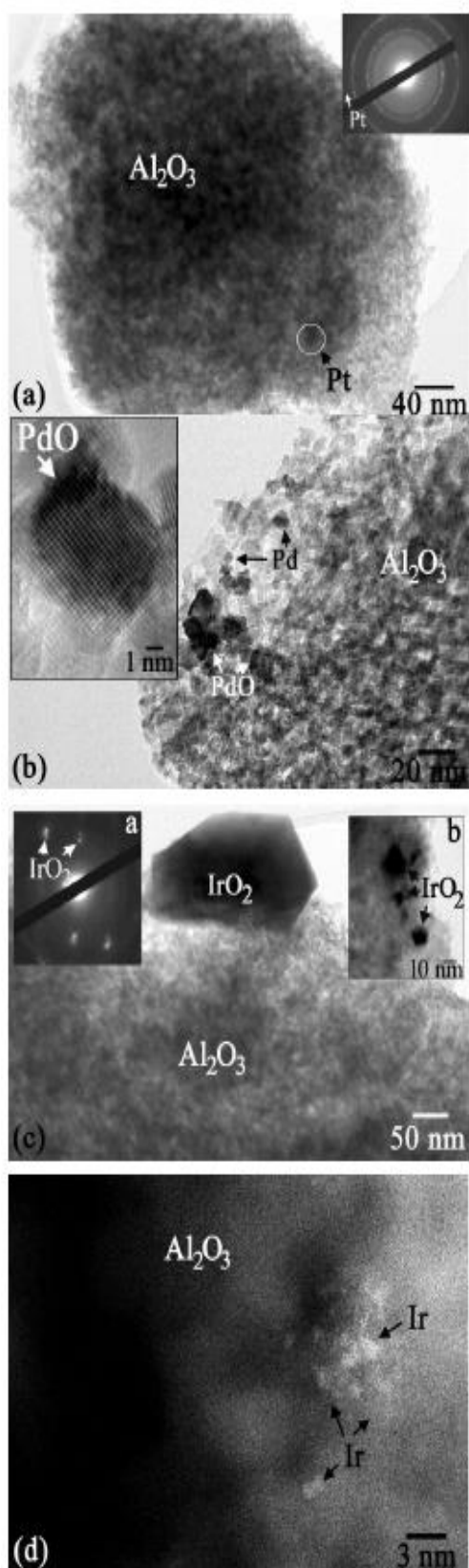
Figure IV.2: Representative TEM images of 0.5Pt/Al (a), 0.5Pd/Al (b) and 0.5Ir/Al (c) and a STEM image of 0.5Ir/Al (d) catalyst.

On the other hand, low intensity peaks at $2\theta=$ 34.7^o and 54.8^o are observed at the 0.5Pd/Al diffractogram attributed to small crystallite sizes of the metal oxide phase, PdO [59]. Characteristic diffraction peaks of high crystalline, large particles of IrO_2, at $2\theta=$ 28°, 34.7° and 54° [50], are clearly evidenced at the 0.5Ir/Al spectrum. Scherrer analysis of the mean crystal size of 0.5Ir/Al catalyst indicates a value of 27 nm of IrO_2 species. No other catalytic phases, metallic or oxide, were identified by the XRD analysis.

Representative TEM images of the 0.5Pt/Al, 0.5Pd/Al and 0.5Ir/Al catalysts are depicted in Fig. IV.2. The morphological results were analysed in detail in chapter III.1. Small Pt nanoparticles, up to 8 nm in size, were observed for 0.5Pt/Al catalyst (Fig. IV.2a). 0.5Pd/Al catalyst is mainly in nanoparticle form with Pd particles predominately in oxide form, as well as few, smaller size catalyst nanoparticles were also detected, which comprised of metallic Pd (Fig. IV.2b). The dominant phase in the 0.5Ir catalyst is IrO_2 (Fig. IV.2c), with sizes of up to 70 nm, or a smaller particles one, densely aggregated on top of Al_2O_3. These two morphologies result in a mean size of ~30 nm, which is in full agreement with the Scherrer analysis results provided above. The formation of large iridium agglomerates is a result of the high

calcinations temperature at oxidizing conditions (at 600 ^{o}C, for 3 h under air flow) used during preparation of the 0.5Ir/Al catalyst and the weak metal-support interactions between iridium particles and alumina. This propensity to sintering of IrO$_2$ particles is well known in the literature and becomes significant only at higher temperatures (typically > 450°C) [51, 52]; at reducing conditions Ir particles are very stable [51]. It must be noted as well that no iridium mass loss is expected during operation of the 0.5Ir/Al catalyst, in the temperature window of 50-600°C used here; IrOx volatility becomes significant only at very high temperatures and is practically negligible at temperatures less than 600°C [53].

However, the existence of distinct Ir species, other than pure oxide ones, has been reported on previous studies [19, 22, 24, 25] on the SCR of NO. According to these studies and, in line with the existence of both metallic Pd and PdO at the 0.5Pd/Al catalyst, the existence of additional Ir-based phases was further investigated employing HAADF imaging experiments on a HRSTEM. A typical STEM image from the catalyst is depicted in Fig. IV.2d, where the presence of Ir-based nanoentities is confirmed. The Ir species adopt a cluster or isolated atoms morphology, with sizes not more than 2 nm. Their character is shown to be purely metallic, as estimated by their difference in contrast compared to the faint Al$_2$O$_3$ particles in the HAADF image.

H$_2$ consumption peaks in TPR profile of 0.5Pt/Al catalyst were not practically observed. This most probably reflects the fact that Pt nanoparticles mainly exist in the metallic form (Pt^0), not accessible for further reduction (as was confirmed by the TEM image in Fig. IV.2a). Only 0.5Ir/Al catalyst exhibits a well-defined reduction peak at 223°C, which is attributed to the reduction of IrO$_2$ [54]. In the case of 0.5Pd/Al catalyst, no PdO characteristic peak was observed at the corresponding TPR pattern, since the reduction of PdO species is occurring between 0-25°C and this TPR apparatus does not have a cooling system. In opposite, its TPR profile presents a negative peak at ~60°C, which is characteristic of the decomposition of β-PdH phase [55]. According with Berry et al. [56], Pd on alumina support is oxidized to PdO by calcination at 450°C. However, this is reduced to β-palladium hydride, when the TPR apparatus is flushed with a H$_2$/N$_2$ mixture at room temperature, before the start of the experiment.

Catalytic Performance Evaluation

Fig. IV.3a depicts the effect of temperature (in the interval of 50-400°C) on NO and propene conversions (X_{NO} and X_{C3H6}) for the reactions NO + C_3H_6 + O_2 (R#1) and NO + C_3H_6 + O_2 + H_2 (R#2) over the 0.5Pt/Al catalyst. Catalyst loading in the reactor is ~335 mg and the total flow rate 500 cm^3/min, which corresponds to GHSV ~40,000 h^{-1}.The experimental conditions are the following:

R#1: 1000 ppmv NO + 1000 ppmv C_3H_6 + 2% vol. O_2, balanced with Ar;

R#2: 1000 ppmv NO + 1000 ppmv C_3H_6 + 2% O_2 + 0.5% vol. H_2 balanced with Ar.

Fig. IV.3b presents the corresponding distribution of the NO conversion to various N-containing products (N_2, N_2O, NO_2) and the selectivity toward N_2, which is defined as:

$$S_{N_2}\ (\%) = 100\ \times [\frac{NO\ conv.to\ N_2}{NO\ conv.to\ N_2 + NO\ conv.to\ N_2O + NO\ conv.to\ NO_2}]$$

Moreover, Fig. IV.3c represents the distribution of the propene conversion derived species, namely CO_2, CO, CH_4 and C_3H_8. Focusing first on R#1 (NO + C_3H_6 + O_2), the ignition temperature for propene oxidation is about 200°C, followed by a sharp increase, achieving complete conversion at 260°C. NO conversion (to N_2 and N_2O), follows a volcano type behavior with a maximum of ca. 35% at T ~234°C, which approximately corresponds to X_{C3H6}~50-60% (Fig. IV.3a). N_2 yield ($X_{NO \to N2}$) is maximized at ca. 220°C while N_2O yield is maximized at a slightly higher temperature, T= 241°C. At maximum NO conversion (T= 234°C) the N-containing products distribution is $X_{NO \to N2}$= 20% and $X_{NO \to N2O}$= 15%, providing a N_2- selectivity of S_{N2}= 57% (Fig. IV.3b). In respect to the N_2-selectivity behavior, it can be seen that at low temperatures NO is dominantly converted to N_2, thus resulting to N_2-selectivity values as high as >~90% (Fig. IV.3b). This picture is however significantly altered upon increasing temperature: N_2O formation significantly competes that of N_2 (Fig. IV.3b), until the temperature of complete propene conversion. Thereinafter, NO oxidation to NO_2 begins and is fully dominated at T > ~300°C (Fig. IV.3b). The above described features are more or less well known in the literature, since the Pt-catalyzed NO + C_3H_6 + excess O_2 reaction is widely used to simulate lean-burn or diesel exhaust conditions [e.g., 1-4, 12-19].

Of significant importance is the impact of H_2 on the conversion and the selectivity behavior. Note that H_2 can be present in off-gases of most combustion processes, whereas it is often considered as a reducing agent during the selective catalytic reduction of NOx [e.g. 27-45]. Lately, the NOx reduction by H_2 has been proposed as an efficient industrial technology for the NOx control [32].

The addition of 0.5% vol. H_2 in the feed (i.e., R#2: NO + C_3H_6 + excess O_2 + H_2) significantly alters the behavior of the system; a considerable enhancement of both NO and propene conversions in the whole temperature range is induced by H_2 co-presence. A two-maxima curve has now appeared in both NO and propene conversion profiles, instead of the high temperature maximum under R#1 (NO + C_3H_6 + O_2) conditions. The new maxima in NO and propene conversion profiles are located at low temperatures, T= ~110-125°C and correspond to 88% and 40% NO and propene conversions, respectively. On the other hand, the high temperature maxima during the NO + C_3H_6 + O_2 reaction (X_{NO}= 35%, T= 233°C) is still observed under R#2 conditions, being however increased and downshifted (X_{NO}= 50%, T= 225°C). This H_2-induced assistance in both NO and propene conversions, extended in the whole temperature range investigated, is of great interest. Indeed, although H_2 is a competitive to propene reducing agent, an about 15°C shift of propene conversion profile to lower temperatures is clearly revealed in Fig. IV.3a (that is promotion of propene oxidation). The selectivity toward N_2 follows the same trend in both cases (R#1 and R#2), as shown in Fig. IV.3b.

In Fig. IV.3c the distribution of propene conversion derived species is depicted, in order to gain insight into the origin of the low temperature (T= 125°C) maximum, which is obtained under R#2 conditions. It is evident that at temperatures higher than 175°C the main product is CO_2. Within the detection limits of our instrumentation, only traces of CO and CH_4 were observed, mainly at the region of the sharp increase of propene conversion (ca. 200-260°C). However, in the low temperature range, propene is almost exclusively converted to hydrogenation products, i.e. propane, justifying the low temperature maximum. The production of alkane (C_3H_8), however, in the presence of H_2, is taking place only at the low temperature region (100-175°C) and is not detected at higher temperatures (Fig. IV.3c).
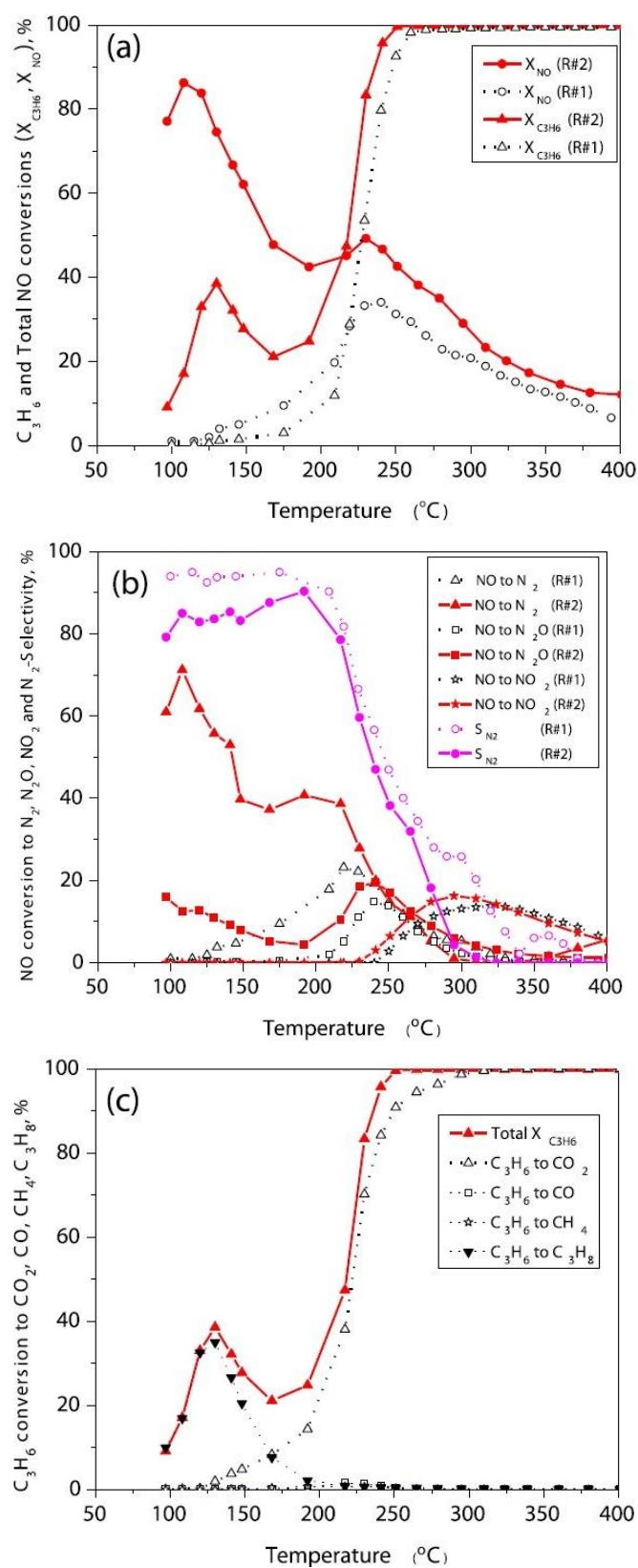
Figure IV.3: (a) The effect of temperature on the propene and total NO conversion performance of 0.5Pt/Al catalyst under R#1 and R#2 reactions; (b) the corresponding conversions and N$_2$-selectivity; (c) C-containing products distribution of propene conversion under R#2.

Fig. IV.4 shows similar results for the reactions NO + C_3H_6 + O_2 (R#1) and NO + C_3H_6 + O_2 + H_2 (R#2), over 0.5Pd/Al_2O_3 catalyst. Some differences in respect to the behavior of the 0.5Pt/Al_2O_3 catalyst are observed: propene conversion profile demonstrates again similar behavior upon increasing temperature, achieving however complete conversion at lower temperatures (ca. 225°C) in comparison to Pt.

Figure IV.4: (a) The effect of temperature on the propene and total NO conversion performance of 0.5Pd/Al catalyst under R#1 and R#2; (b) the corresponding conversions and N_2-selectivity.

The conversion of NO is also maximized at the temperature window of sharp increase in propene oxidation, but its maximum (X_{NO}= 20%) is less than that of platinum catalyst. That is, Pd is more effective than Pt on hydrocarbon oxidation, since it achieves 100% conversion at a temperature that is lower by ~40°C; however,

it is less efficient on NO conversion, since it appears a maximum value of about 15 percentage units lower than that of Pt (Figs. IV.3a and IV.4a). Moreover, the H_2-induced promotional effect on NO reduction and propene oxidation is obvious, although inferior in comparison to Pt/Al catalyst (Fig. IV.3). Although the NO conversion is enhanced by H_2 in the whole temperature interval (50-400°C), the low temperature maximum corresponds to only X_{NO}~30%, compared to the much higher value of X_{NO}~90% over Pt/Al catalyst. This temperature region of NO conversion obeys selectivity values at the level of only 30%, since the NO conversion to N_2O is prevailing (Fig. IV.4b).

In Fig. IV.5 the performance of 0.5Ir/Al catalyst is depicted during the reactions R#1 and R#2. For the NO + C_3H_6 + excess O_2 reaction (R#1), iridium exhibits the inferior performance in respect to the other noble metals (Pt and Pd) on hydrocarbon oxidation, since it achieves 100% propene conversion at temperatures as high as ~340°C. Maximum NO conversion is achieved at around this temperature as well and has a value of X_{NO}= 33%, i.e., similar to that of Pt and slightly higher to that of Pd. The activation of Ir-based catalysts for the lean de-NOx with propene at higher temperatures, compared to Pt and Pd, is well known in the literature [e.g. 2, 20-23].

In respect, however, to the effect of H_2 on the Ir-catalyzed lean NOx conversion by propene (i.e., R#2: NO + C_3H_6 + O_2 + H_2) the following interesting aspects can be noted: H_2 does not practically affect the propene oxidation efficiency of iridium, notably enhancing however the NO reduction efficiency; the maximum NO conversion of 33% during R#1 is increased to ~70% during R#2, accompanied by a shift to notably lower temperatures (T= 280°C under R#2 instead of 340°C under R#1). Concentrating on the results of Fig. IV.5b, which shows the H_2-induced effect on the N-containing products, it is of worth to notice the pronounced effect of H_2 on the N_2 formation. On the other hand, its effect on the N_2O formation is less pronounced, whereas the production of NO_2 is significantly suppressed. All the above described specific features lead to a great enhancement in N_2-selectivity for the H_2-assisted lean NOx reduction with propene on Ir (Fig. IV.5b), which for temperatures higher than ~250°C goes beyond 90%. To gain insight into the specific role of each reducing agent (propene or H_2) on the lean SCR deNOx process, the NO + H_2 + O_2 reaction (R#3) was comparatively examined.
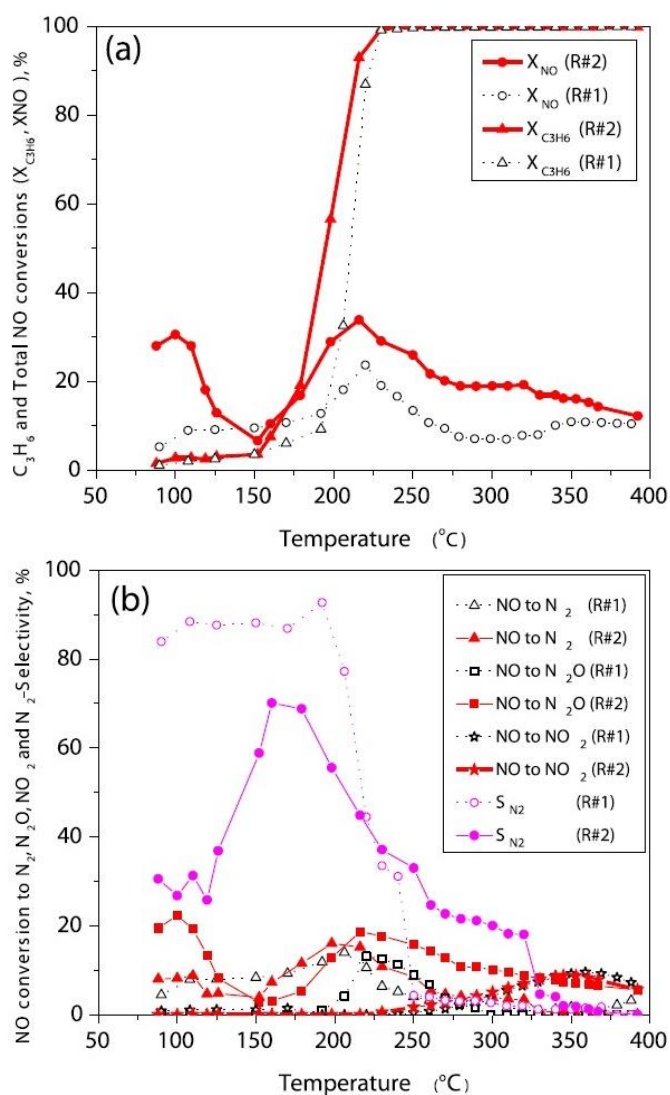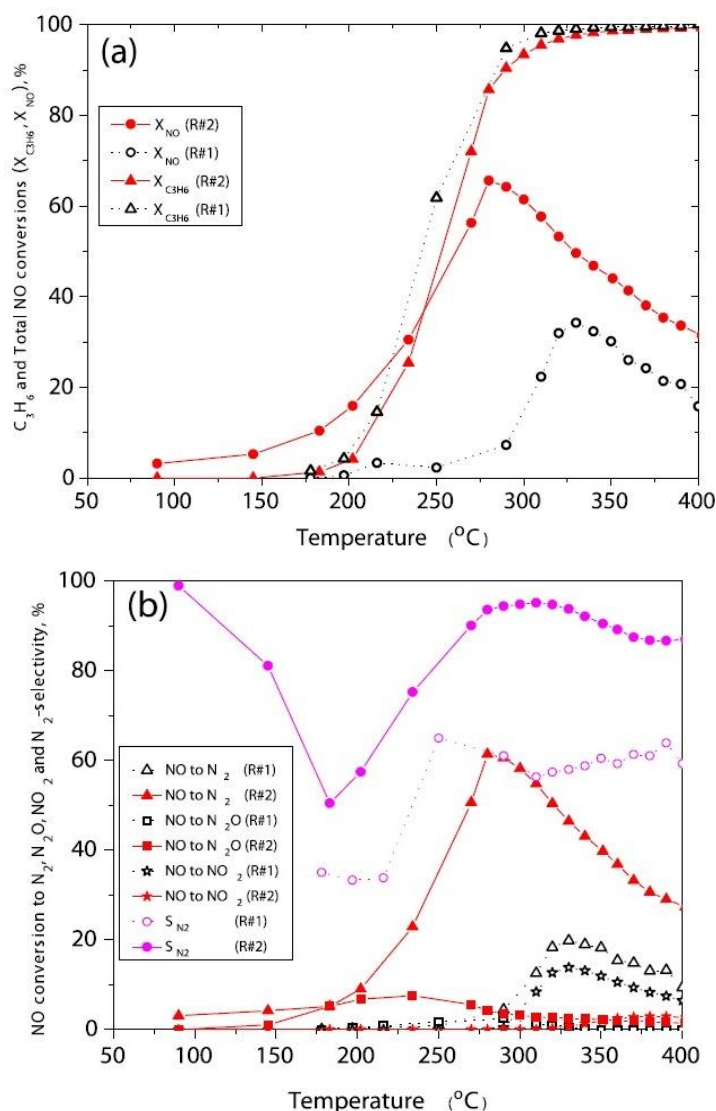
Figure IV.5: (a) The effect of temperature on the propene and total NO conversion performance of 0.5Ir/Al catalyst under R#1 and R#2 reactions; (b) the corresponding conversions and N$_2$-selectivity.

The comparison of all three reactions, R#1, R#2 and R#3 was at first performed on the Pt/ Al catalyst, which obeys significant promotional effects by H$_2$ (Fig. IV.3). As clearly evidenced from the results of Fig. IV.6, which comparatively represents the NO conversion profiles for the R#1 (NO + C$_3$H$_6$ + O$_2$), R#2 (NO + C$_3$H$_6$ + O$_2$ + H$_2$) and R#3 (NO + H$_2$ + O$_2$) reactions over 0.5Pt/Al catalyst at 50-400°C, the reactions R#2 and R#3, both involving H$_2$, follow very similar profiles. This suggests that H$_2$ contributes more significantly than propene in the lean SCR of NOx. In particular, at the low temperature region (50-190°C), the de-NOx efficiency can be fully ascribed to H$_2$. At elevated temperatures the hydrocarbon contributes also to the deNOx

efficiency, with its influence, however, to be notable at the intermediate temperature window of ca. 200-300°C (Fig. IV.6).

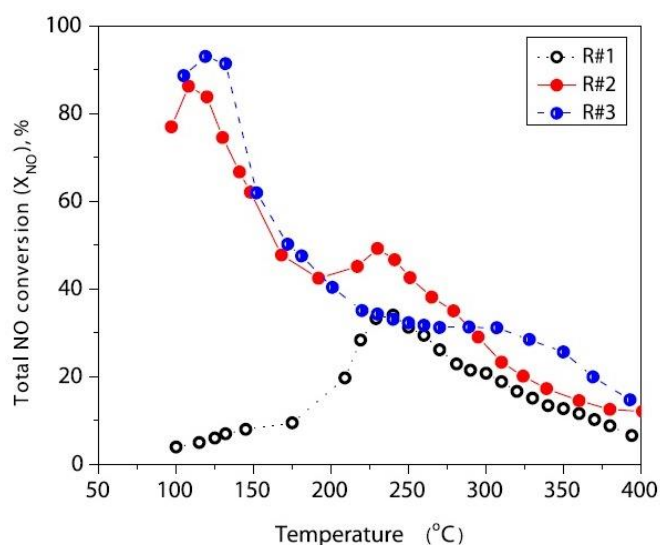**Figure IV.6:** The effect of temperature on NO conversion performance of 0.5Pt/Al catalyst under R#1, R#2 and R#3.

Fig. IV.7 depicts the N-containing products distribution under R#2 and R#3 reaction conditions, as well as the corresponding N$_2$- selectivity. Interestingly, although in the low temperature region the influence of propene on the total NO conversion is marginal (Fig. IV.6), its presence plays a crucial role on system's selectivity (Fig. IV.7). Indeed, at the low and intermediate temperature regions, the N$_2$ yield is similar or more pronounced during R#2 compared to R#3 reaction, while at the same time the N$_2$O yield is substantially depressed during R#2 in respect to that of R#3; both findings result to a superior N$_2$-selectivity of the former reaction R#2 (Fig. IV.7). Namely, the existence of both reductants in the Pt-catalyzed lean NOx reduction results in a more efficient (on both activity and selectivity) deNOx process.

Interestingly, comparison of the three reactions, i.e., NO + C$_3$H$_6$ + O$_2$ (R#1), NO + C$_3$H$_6$ + O$_2$ + H$_2$ (R#2) and NO + O$_2$ + H$_2$ (R#3) over iridium catalyst (Fig. IV.8) shows very different trends than those recorded on Pt. Indeed, contrary to 0.5Pt/Al (Fig. IV.6), the activity of 0.5Ir/Al during the lean SCR of NOx with H$_2$ (R#3, Fig. IV.8) is, more or less, similar to the SCR of NOx with propene (R#1, Fig. IV.8): in the case of H$_2$ a marginal, low temperature (~200°C), peak in NO conversion is evident (with X$_{NO}$< 10%), followed by a high temperature (T~330°C) peak of slightly better NO

conversion (X$_{NO}$~15%), whereas in the case of propene only the high temperature peak is evident with a slightly elevated NO conversion (X$_{NO}$~30%, Fig. IV.8).
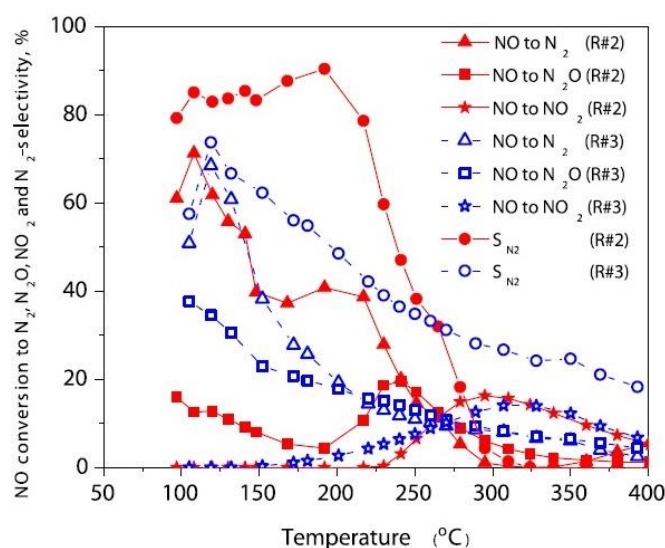

Figure IV.7: The N-containing products distribution (i.e., NO→N$_2$, NO→N$_2$O and NO→NO$_2$ conversions) and N$_2$-selectivity under the reactions R#2 and R#3 on 0.5Pt/Al catalyst.

When these two reductants are fed together (R#3), a synergistic effect on Ir-catalyzed lean de-NOx process is at work, resulting at a very pronounced increase in NO conversion, with a peak value of X$_{NO}$= 70% at 275°C (Fig. IV.8). As we have already noticed, the N$_2$-selectivity values of this interesting (H$_2$ + propene)-synergy are extremely high, approaching 100%, especially around the maximum NO conversion value (Fig. IV.5b).

To further elucidate the behavior of Ir during the H$_2$-assisted lean NOx reduction with propene, the following transient experiment was conducted (Fig.IV.9). The catalyst (0.5Ir/Al) was first pre-oxidized in the reactor at 500°C in air flow (50 cm^3/min) for 4 h. Then the temperature was fixed at the value of interest (T= 325°C), the gas phase of the reactor was cleaned by Ar flow for 5 min and the reactant mixture concerning the R#2 reaction was fed. The behavior of the as pre-oxidized catalyst was recorded as a function of time (ca. 3 h, Fig. IV.9). After this step, the reaction was interrupted and the catalyst was exposed to a hydrogen flow (50 cm^3/min) for 1 h, keeping the temperature constant at 325°C. Then, after cleaning with Ar flow (for 5 min), the behavior of the as pre-reduced catalyst in the same reaction (R#2) conditions was again recorded for about 3 h (Fig.IV.9).
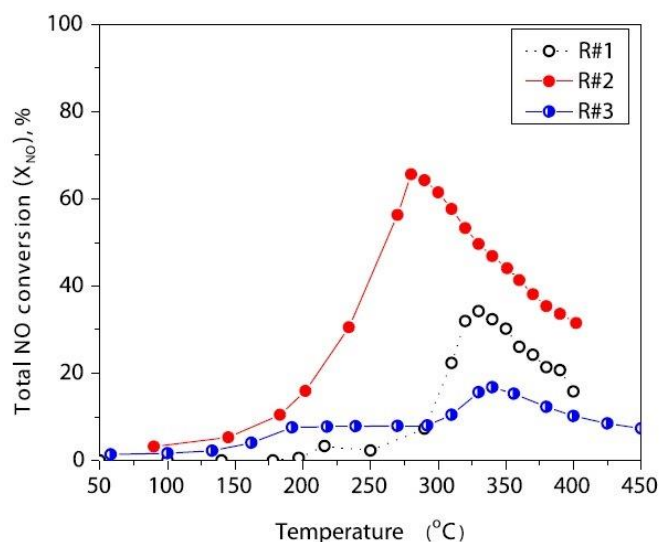
Figure IV.8: The effect of temperature on NO conversion performance of 0.5Ir/Al catalyst under R#1, R#2 and R#3.

Obviously, the pre-oxidized Ir has a completely different behavior than the pre-reduced one. The differences involve not only the values of the propene and the total NO conversions (Fig.IV.9a), but also the distribution of the N-containing products (Fig. IV.9b). Pre-oxidized Ir appeared to be more effective in NO reduction (almost two fold) but less effective in propene oxidation. Moreover, the NO reduction to N_2 (instead to N_2O) is superior in pre-oxidized samples. In respect to the aforementioned experiment however, it must be noticed, that deep iridium crystallites oxidation is not expected in the pre-oxidized (at $500^{o}C$, 4 h) sample; in accordance with Wögerbauer et al. [22], large Ir crystallites cannot be fully oxidized even up to $970^{o}C$. Therefore, at the beginning of the experiment of Fig. IV.9, we can assume a superficial overlayer of IrO_2 over the large particles together with isolated metallic iridium nanoentities, as detected by STEM (Fig. IV.2d).

The main experimental observations of the comparative catalytic study of Pt, Pd and Ir under the distinct reactions R#1 (NO + C_3H_6 + O_2) and R#2 (NO + C_3H_6 + H_2 + O_2) can be summarized as follows:

Reaction R#1: NO + C_3H_6 + O_2

(i) Pd > Pt > Ir is the sequence of catalytic performance in respect to hydrocarbon oxidation, since it is completed (X_{C3H6}= 100%) at 220, 250 and $325^{o}C$, respectively.

(ii)   In respect to NO conversion, all three metals display a similar inferior performance under SCR by propene (R#1), since maximum NO conversion values of less than 40% are achieved (Figs. IV.3a, IV.4a, IV.5a); these maxima are in all cases matching the temperature window of sharp increase in hydrocarbon conversion. Notably, the lean deNOx with propene is activated at significantly lower temperatures on Pt and Pd, compared to Ir (maximum NO conversions are ca. 237°C and 225°C, for Pt and Pd respectively and ca. 325°C for Ir).
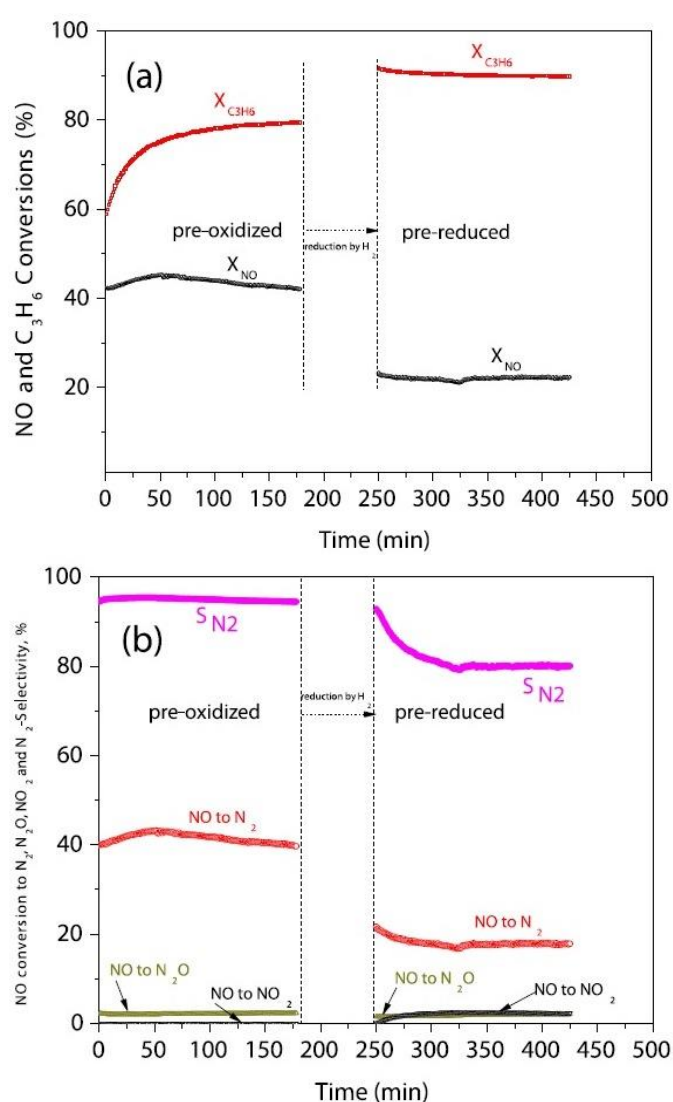

Figure IV.9: Transient behavior of 0.5Ir/Al catalyst during R#2 reaction after a pre-oxidation and a pre-reduction treatment: (a) NO and propene conversions versus time; (b) corresponding N-containing products distribution.

(iii)   In respect to the N-containing product distribution during R#1, Pt and Pd exhibit high selectivity values toward N_2 at the low temperature region, i.e. left to the maximum of NO conversion (ca. ~230°C), which are gradually declined up to zero upon increasing temperature (Figs. IV.3b and IV.4b). In contrast, Ir shows a good selectivity toward N_2 in all temperature intervals investigated, which moreover is improved upon increasing temperature even after X_{NO} maximum (Fig. IV.5b).

(iv)   Oxidation of NO to NO_2 is recorded in all cases only when propene conversion approaches 100% (Figs. IV.3b, IV.4b and IV.5b) and predominates upon increasing temperature.

Reaction R#2: NO + C₃H₆ + H₂ + O₂

(v)   Propene oxidation efficiency is slightly enhanced on Pt and Pd (not on Ir), when H_2 is introduced in the feed stream: a 10-15°C shift to lower temperatures of the propene conversion profiles is obvious in Figs. IV.3a and IV.4a during R#2 vs R#1 reaction; the sequence Pd > Pt > Ir in respect to hydrocarbon oxidation found for R#1 is still valid in the case of R#2.

(vi)   A strong improvement of the NO conversion efficiency is induced by H_2 co-feed in all cases (Figs. IV.3a, IV.4a and IV.5a). This H_2-assistance is obvious in the whole temperature interval investigated, significantly modifying the reaction pattern of NO, and is more substantial in the cases of Pt and Ir (Figs. IV.3a and IV.4a) compared to Pd. A two-maxima feature in NO conversion is observed in the cases of Pt and Pd, but not for Ir.

(vii) H_2-induced improvement in N_2-selectivity is practically obtained only in the case of Ir (Fig. IV.5b); for Pt and Pd, N_2-selectivity is similar or even worse to that recorded under R#1 conditions (Figs. IV.3b and IV.4b).

All (i)-(iv) features for the SCR of NO with propene (Reaction R#1) are well documented in the literature [e.g. 2,3,12–24] and in line to the following widely accepted reaction pathway on Pt-group metal surfaces which describes the formation of N_2 and N_2O products [1–4, 12, 14, 15, 17, 18]:

$$NO(g) \rightarrow NO_{ads} \qquad\qquad\qquad (1.1)$$

$$NO_{ads} \rightarrow N_{ads} + O_{ads} \qquad (1.2)$$

$$N_{ads} + N_{ads} \rightarrow N_2(g) \qquad (1.3)$$

$$NO_{ads} + N_{ads} \rightarrow N_2O(g) \qquad (1.4)$$

accompanied by scavenging of the adsorbed oxygen species by hydrocarbon reactant to form H$_2$O and CO$_2$. In case of H$_2$ co-feed, an additional hydrogen-assisted NO dissociation step could also be involved in the overall reaction scheme [31]:

$$NO_{ads} + H_{ads} \rightarrow N_{ads} + OH_{ads} \qquad (1.5)$$
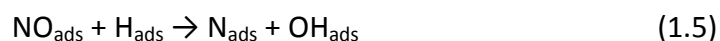
as well as a scavenging of the O$_{ads}$ by hydrogen to form H$_2$O.

The presence of NCO has been confirmed in several studies and has been considered as a possible reaction intermediate under SCR conditions [e.g. 16]. However, detailed mechanistic aspects to distinguish between the three reactions (R#1, R#2 and R#3) on the surfaces of the three metals (Pt, Pd and Ir) studied are beyond the scope of the present study.

In respect to Pt, due to the strong propene adsorption under reaction conditions, a substantial fraction of Pt sites could be in reduced state, even under the oxidizing (excess oxygen) conditions [2, 9, 12]. Recent in situ DRIFTS studies at stoichiometric reaction conditions have shown that the fraction of electron enriched Pt sites (i.e. metallic Pt^0 state) can be further increased via electropositive promotion [57]. These highly reduced sites are considered very active for NOx reduction process due to the facilitation of NO dissociation [58].

In the case of iridium based catalysts, both IrO$_2$ and Ir^0 entities are in equilibrium during the Ir-catalyzed lean NOx reduction by propene, and their ratio is strongly depended on O coverage and crystallite size [e.g., 19, 24, 25]. The presence of metallic iridium nanoparticles was indeed detected in our fresh catalyst by STEM imaging (Fig. IV.2d). In line with this, quantification of the H$_2$-TPR results implies that a significant amount of iridium may be in the metallic state (even after the strong oxidizing conditions imposed to the catalyst during preparation), since the amount of 19.6 mmol H$_2$ per gram of catalyst calculated from the TPR peak corresponding to the hydrogen consumed for the reduction of IrO$_2$, is significantly lower than the

value of 52 mmol H_2/g theoretically required in the case of the catalyst with a fully oxidized iridium phase.

Despite the intense interest on the H_2-assisted HC-SCR of NOx over Ag-based catalysts, following the pioneering work of Satokawa [43], the role of hydrogen is still unclear and to some extent contradictory. Some studies exclude the possibility of partial reduction of the silver surface as a result of H_2 presence in the reaction mixture [44]. Some other however provides evidence that H_2 promotes the reduction of Ag^+ ions to $Ag_n^{\delta+}$ clusters and metallic Ag [45]. There are no literature studies on the H_2-assisted HC-SCR of NOx over Pt-group metal based catalysts and our preliminary results do not provide any direct evidence for the exact role of H_2 on the observed promotional effects. Obviously, additional characterizations studies are required toward this direction. Nevertheless, based on the present results, and in particular on observation (v), a partial reduction of the noble metal phase due to H_2 can be considered. Although H_2 is a competitive to propene reducing agent and thus an inhibition of propene oxidation may be expected, the opposite is true. The latter is clear in the case of Pt and Pd (Figs. IV.3a and IV.4a), where the enhancement of propene oxidation by the H_2 co-presence is evident. This behavior can be explained by considering that the presence of H_2 in the reaction mixture favors the reduced state of the metal which is more active for hydrocarbons' oxidations [1-4, 20].

Similarly, in the case of Ir-based catalysts (Fig. IV.9) the pre-reduced phase is much more active for propene oxidation (X_{C3H6}= 90%) compared to the pre-oxidized one (X_{C3H6}= 60%). Moreover, it was clearly revealed that the propene oxidation efficiency of Ir/Al catalyst is gradually enhanced under reaction conditions, implying a progressive increase of Ir^0/IrO_2 ratio, which favors propene oxidation. The system, however, is balanced at an Ir^0/IrO_2 ratio between the pre-oxidized and pre-reduced modes, since it never achieves X_{C3H6} values similar to that obtained on the pre-reduced catalyst. It is also of interest, that a mixed Ir^0/IrO_2 phase, instead of a reduced one, seems to favors the NO reduction efficiency as well as the N_2-selectivity (Fig. IV.9).

The presence of H_2 in the feed has also a significant effect on NO conversion modifying its reaction pattern according to observation (vi). In the case of Pt and Pd (Figs. IV.3a and IV.4a), the NO conversion follows a two-maxima profile, due to the

distinguished role of H$_2$ (low temperature maximum) and C$_3$H$_6$ (high temperature maximum) as reductants. The results in Figs. IV.3a and IV.4a corresponding to Pt and Pd respectively, with two characteristic NO conversion maxima, imply that H$_2$ is the low temperature reductant of NO, while propene is activated (as NO reductant) at higher temperatures. However, a more complicated synergistic role of H$_2$ and C$_3$H$_6$ may be considered in order to explain the one maximum pattern in the case of Ir (Figs. IV.5 and IV.8).

IV.3 *Conclusions*

The Pt-, Pd and Ir-catalyzed C$_3$H$_6$-SCR of NOx are significantly promoted by H$_2$ on all these metals. These promotional effects are not limited to a specific temperature window, but are extended in the whole temperature interval of 50-400°C investigated. The H$_2$-assistance on C$_3$H$_6$-SCR of NOx is more substantial on Pt, then on Ir and less on Pd. The influence of H$_2$ on the oxidation state of the noble metals is considered to be a key factor for this promotion: an enhanced ratio of the metallic state of noble metal surface is presumably present under H$_2$ co-feed, which tracks the enhanced activity during Pt-, Pd- and Ir-catalyzed H$_2$-C$_3$H$_6$-SCR of NOx.

The characteristic two-maxima feature of NO reaction pattern obtained over Pt and Pd catalysts is indicative of the distinguished action of each reductant; H$_2$ is the low temperature reductant of NO, while propene is activated at higher temperatures, slightly lower to those obtained for the H$_2$-free, lean C$_3$H$_6$-SCR of NOx reaction. The different, one maximum pattern, of the NO reaction obtained on Ir catalyst, that showed a very effective H$_2$-assisted C$_3$H$_6$-SCR, is indicative of a possible synergy between the two reductants, and cannot be explained by the consideration of an enhanced Ir^0/IrO$_2$ ratio on catalyst surface, but most probably requires the cooperation of more than one factors for the explanation of this effective and selective (toward N$_2$) promotion.

REFERENCES

[1] Amiridis M.D., Zhang T., Farrauto R., "Selective catalytic reduction of nitric oxide by hydrocarbons", Applied Catalysis. B 10 (1996) 203-227.

[2] Burch R., Breen J.P., Meunier F.C., "A review on the selective reduction of NOx with hydrocarbons under lean burn conditions with non-zeolitic oxide and platinum group metal catalysts", Applied Catalysis B 39 (2002) 283-303.

[3] Burch R., Millington P.J., "Selective reduction of nitrogen oxides by hydrocarbons under lean-burn conditions using supported platinum group metal catalysts", Catalysis Today 26 (1995) 185-206.

[4] Granger P., Parvulescu V.I., "Catalytic NOx abatement systems for mobile sources: from three-way to lean burn after-treatment technologies", Chemical Reviews 111 (2011) 3155-3207.

[5] Parvulescu V.I., Granger P., Delmon B., "Catalytic removal of NO", Catalysis Today 46 (1998) 233-316.

[6] Burch R., "Knowledge and know-how in emission control for mobile applications", Catalysis Reviews 46 (2004) 271.

[7] Shelef M., McCabe R.W., "Twenty-five years after introduction of automotive catalysts: what next?", Catalysis Today 62 (2000) 35-50.

[8] Twigg M.V., "Catalytic control of emissions from cars", Catalysis Today 163 (2011) 33-41.

[9] Yentekakis I.V., Konsolakis M., Lambert R.M., Macleod N., Nalbandian L., "Extraordinary effective promotion by sodium in emission control catalysis: NO reduction by propene over Na-promoted Pt/γ-Al$_2$O$_3$", Applied Catalysis B 22 (1999) 123-133.

[10] Yentekakis I.V., Lambert R.M., Tikhov M.S., Konsolakis M., Kiousis V., "Promotion by Sodium in Emission Control Catalysis: A kinetic and spectroscopic study of the Pd-catalysed Reduction of NO by Propene", Journal of Catalysis 176 (1998) 82-92.

[11] Goula G., Katzourakis P., Vakakis N., Papadam T., Konsolakis M., Tikhov M., Yentekakis I.V., "The effect of potassium on the Ir/ C$_3$H$_6$+NO+O$_2$ catalytic system", Catalysis Today 127 (2007) 199-206.

[12] Yentekakis I.V., Tellou V., Botzolaki G., Rapakousios I.A., "A comparative study of the C$_3$H$_6$+NO+O$_2$, C$_3$H$_6$+O$_2$ and NO+O$_2$ reactions in excess oxygen over Na-promoted Pt/γ-Al$_2$O$_3$ catalysts", Applied Catalysis B 56 (2005) 229-239.

[13] Burch R., Watling T.C., "Kinetics of the reduction of NO by C3H6 and C3H8 over Pt based catalysts under lean-burn conditions", Studies in Surface Science and Catalysis 116 (1998) 199-211.

[14] Burch R., Millington P.J., Walker A.P., "Mechanism of the selective reduction of nitrogen monoxide on platinum-based catalysts in the presence of excess oxygen", Applied Catalysis B 4 (1994) 65-94.

[15] Burch R., Sullivan J.A., Watling T.C., "Mechanistic considerations for the reduction of NOx over Pt/Al$_2$O$_3$ and Al$_2$O$_3$ catalysts under lean-burn conditions", Catalysis Today 42 (1998) 13-23.

[16] Captain D.K., Amiridis M.D., "In situ FTIR studies of the selective catalytic reduction of NO by C$_3$H$_6$ over Pt/Al$_2$O$_3$", Journal of Catalysis 184 (1999) 377-389.

[17] Roberts K.L., Amiridis M.D., "Kinetic investigation of the Selective Catalytic Reduction of nitric oxide by propylene over Pt/Al$_2$O$_3$", Industrial and Engineering Chemistry Research 36 (1997) 3528-3532.

[18] Nikolopoulos A.A., Stergioula E.S., Efthimiadis E.A., Vasalos I.A., "Selective catalytic reduction of NO by propene in excess oxygen on Pt- and Rh-supported alumina catalysts", Catalysis Today 54 (1999) 493-450.

[19] Amiridis M.D., Mihut C., Maciejewski M., Baiker A.. "The selective catalytic reduction of NO by hydrocarbons over Pt- and Ir-based catalysts", Topics in Catalysis 28 (2004) 141-150.

[20] Nawdali M., Iojoiu E., Gelin P., Praliaud H., Primet M., "Influence of the pre-treatment on the structure and reactivity of Ir/γ-Al$_2$O$_3$ catalysts in the selective reduction of nitric oxide by propene", Applied Catalysis A 220 (2001) 129-139.

[21] Iojoiu E., Gelin P., Praliaud H., Primet M., "Reduction of NO by propene over supported iridium catalysts under lean-burn conditions: an in situ FTIR study", Applied Catalysis A 263 (2004) 39-48.

[22] Wögerbauer C., Maciejewski M., Baiker A., Gobel U., "Structural properties and catalytic behavior of Ir black in the selective reduction of NO by hydrocarbons", Journal of Catalysis 201 (2001) 113-127.

[23] Wögerbauer C., Maciejewski M., Baiker A., Gobel U., "Ir/H-ZSM-5 catalysts in the selective reduction of NOx with hydrocarbons", Topics in Catalysis 16–17(2001) 181-186.

[24] Wögerbauer C., Maciejewski M., Baiker A., "Structure sensitivity of NO reductyion over Iridium catalysts in HC-SCR", Journal of Catalysis 205 (2002) 157-167.

[25] Wögerbauer C., Maciejewski M., Schubert M.M., Baiker A., "Effect of sodium on the catalytic properties of iridium black in the selective reduction of NOx by propene under lean-burn conditions", Catalysis Letters 74 (2001) 1-7.

[26] Liu Z.-P., Jenkins S.J., King D.A., "Car Exhaust Catalysis from First Principles: Selective NO Reduction under Excess O_2 Conditions on Ir", Journal of Americal Chemical Society 126 (2004) 10746-10756.

[27] Ueda A., Nakao T., Azuma M., Kobayashi T., "Two conversion maxima at 373 and 573 K in the reduction of nitrogen monoxide with hydrogen over Pd/TiO_2 catalyst", Catalysis Today 45 (1998) 135-138.

[28] Machida M., Ikeda S., Kurogi D., Kijima T., "Low temperature catalytic NOx-H_2 reactions over Pt/TiO_2-ZrO_2 in an excess oxygen", Applied Catalysis B 35 (2001) 107-116.

[29] Costa C.N., Savva P.G., Andronikou C., Lambrou P.S., Polychronopoulou K., Belessi V.C., Stathopoulos V.N., Pomonis P.J., Efstathiou A.M., "An investigation of the NO/H_2/O_2 (lean De-NOx) reaction on a high active and selective $Pt/La_{0.7}Sr_{0.2}Ce_{0.1}FeO_3$ catalyst at low temperature", Journal of Catalysis 209 (2002) 456-471.

[30] Costa C.N., Efstathiou A.M., "Mechanistic aspects of the H_2-SCR of NO on a novel Pt/MgO-CeO_2 catalyst", Journal of Physical Chemistry C 111 (2007) 3010-3020.

[31] Costa C.N., Efstathiou A.M., "Low-temperature H_2-SCR of NO on a novel Pt/MgO-CeO_2 catalyst", Applied Catalysis B 72 (2007) 240-252.

[32] Polychronopoulou K., Efstathiou A.M., "NOx control via H_2-selective catalytic reduction (H_2-SCR) technology for stationary and mobile applications", Recent patents on Materials Science, 5 (2012).

[33] Burch R., Coleman M.D., "An investigation of promoter effects in the reduction of NO by hydrogen under lean-burn conditions", Journal of Catalysis 208 (2002) 435-447.

[34] Machida M., Watanabe T., Ikeda S., Kijima T., "A dual lean deNOx catalyst system consisting of NO-H_2-O_2 reaction and subsequent N_2O decomposition", Catalysis Communication 3 (2002) 233-238.

[35] Engelmann-Pirez M., Granger P., Leclercq G., "Investigation of the catalytic performances of supported noble meta based catalysts in the NO+H_2 reaction under lean conditions", Catalysis Today 107-108 (2005) 315-322.

[36] Hamada H., Haneda M., "A review of selective catalytic reduction of nitrogen oxides with hydrogen and carbon monoxide", Applied Catalysis A, 421-422 (2012) 1-13.

[37] Macleod N., Lambert R.M., "Lean NOx reduction with CO+H_2 mixtures over Pt/Al_2O_3 and Pd/Al_2O_3 catalysts", Applied Catalysis B 35 (2002) 269-279.

[38] Macleod N., Lambert R.M., "An in situ DRIFTS study of efficient lean NOx reduction with H_2+CO over Pd/Al_2O_3: the key role of transient NCO formation in the subsequent generation of ammonia", Applied Catalysis B 46 (2003) 483-495.

[39] Macleod N., Cropley R., Lambert R.M., "Efficient reduction of NOx by H_2 under oxygen-rich conditions over Pd/TiO_2 catalysts: an in situ DRIFTS study", Catalysis Letters 86 (2003) 69-75.

[40] Macleod N., Lambert R.M., "Low-temperature NOx reduction with H_2+CO under oxygen-rich conditions over a Pd/TiO_2/Al_2O_3 catalyst", Catalysis Communication 3 (2002) 61-65.

[41] Macleod N., Cropley R., Keel J.M., Lambert R.M., "Exploring the synergy of titania and alumina in lean NOx reduction: in situ ammonia generation during the Pd/TiO_2/Al_2O_3-catalysed H_2/CO/NO/O_2 reaction", Journal of Catalysis 221 (2004) 20-31.

[42] Konsolakis M., Vrontaki M., Augouropoulos G., Ioannides T., Yentekakis I.V., "Novel doubly-promoted catalysts for the lean NOx reduction by H_2+CO: Pd(K)/Al_2O_3-(TiO_2)", Applied Catalysis B 68 (2006) 59-67.

[43] Satokawa S., "Enhancing the NO/C_3H_6/O_2 reaction by using H_2 over Ag/Al_2O_3 catalysts under lean-exhaust conditions", Chemistry Letters 29 (2000) 294-295.

[44] Kannistro H., Ingelsten H.H., Skoglundh M., "Aspects of the role of hydrogen in H_2-assisted HC-SCR over Ag-Al_2O_3", Topics in Catasis 52 (2009) 1817-1820.

[45] Hernandez-Teran M. E., Fuentes G.A., "Enhancement by H_2 of C_3H_6-SCR of NOx using Ag/γ-Al_2O_3", Fuel 138 (2014) 91-97.

[46] Chaieb T., Delannoy L., Costentin G., Louis C., Casale S., Chantry R.L., Li Z.Y., Thomas C., "Insights into the influence of the Ag loading on Al_2O_3 in the H_2-assisted C_3H_6-SCR of NOx", Applied Catalysis B 156-157 (2014) 192-201.

[47] Mufti Azis M., Harelind H., Creaser D., "On the role of H_2 to modify surface NOx species over Ag-Al_2O_3 as lean NOx reduction catalyst: TPD and DRIFTS studies", Catalysis Science and Technology 5 (2015) 296-309.

[48] Chiang K.C., Chen K.L., Chen C.Y., Huang J.J., Shen Y.H., Yeh M.Y., Wong F.F., "Recovery of spent alumina-supported platinum catalyst and reduction of platinum oxide via plasma sintering technique", Journal of the Taiwan Institute of Chemical Engineers 42 (2011) 158-165.

[49] Babu N.S., Lingaiah N., Gopinath R., Sankar P.S. , Reddy, Sai Prasad P.S., "Characterization and Reactivity of Alumina-Supported Pd Catalysts for the Room-Temperature Hydrodechlorination of Chlorobenzene", Journal of Physical Chemistry C 111 (2007) 6447-6453.

[50] Iliopoulou E.F., Efthimiadis E.A., Nalbandian L., Vasalos I.A., Barth J.O, Lercher J.A., "Ir-based additives for NO reduction and CO oxidation in the FCC regenerator: Evaluation, characterization and mechanistic studies", Applied Catalysis B 60 (2005) 2277-288.

[51] Fiedorow R.M.J., Chahar B.S., Wanke S.E., "The sintering of supported metal catalysts. II. Comparizon of sintering artes of supported Pt Ir, and Rh catalysts in hydrogen and oxygen", Journal of Catalysis 51 (1978) 193-202.

[52] Balcon S., Mary S., Kappenstein C., Gengembre E., "Monopropellant decomposition catalysts II. Sintering studies on Ir/Al_2O_3 catalysts, influence of chloride anions", Applied Catalysis A 196 (2000) 179-190.

[53] Jehn H., Völker R., Ismail M.I., "Iridium losses during oxidation", Platinum Metals Review 22 (1978) 92-97.

[54] Vicerich M.A., Benitez V.M., Especel C., Epron F., Pieck C.L., "Influence of iridium content on the behaviour of Pt-Ir/ Al_2O_3 and Pt-Ir/ TiO_2 catalysts for selective ring opening of naphthenes", Applied Catalysis A 453 (2013) 167-174.

[55] Zhou R., Zhao B., Yue B., "Effects of CeO$_2$-ZrO$_2$ present in Pd/Al$_2$O$_3$ catalysts on the redox behavior of PdOx and their combustion activity", Applied Surface Science 254 (2008) 44701-4707.

[56] Berry F.J., Smart L.E., Sai Prasad P.S., Lingaiah N., Kanta Rao P., "Microwave heating during catalyst preparation: influence on the hydrodechlorination activity of alumina supported-palladium-iron bimetallic catalysts", Applied Catalysis A: General 204 (2000) 191-201.

[57] Matsuka V., Konsolakis M., Lambert R.M., Yentekakis I.V., "In situ DRIFTS study of the effect of structure (CeO$_2$-La$_2$O$_3$) and surface (Na) modifiers on the catalytic and surface behavior of Pt/γ-Al$_2$O$_3$ catalyst under simulated exhaust conditions", Applied Catalysis B 84 (2008) 715-722.

[58] Koukiou S., Konsolakis M., Lambert R.M., Yentekakis I.V., "Spectroscopic evidence for the mode of action of alkali promoters in Pt-catalyzed de-NOx chemistry", Applied Catalysis B, 76 (2007) 101-106.

CHAPTER V

Effect of Thermal Treatment on the Solid State Properties and N_2O Decomposition Performance of Ir/γ-Al$_2$O$_3$ Catalyst
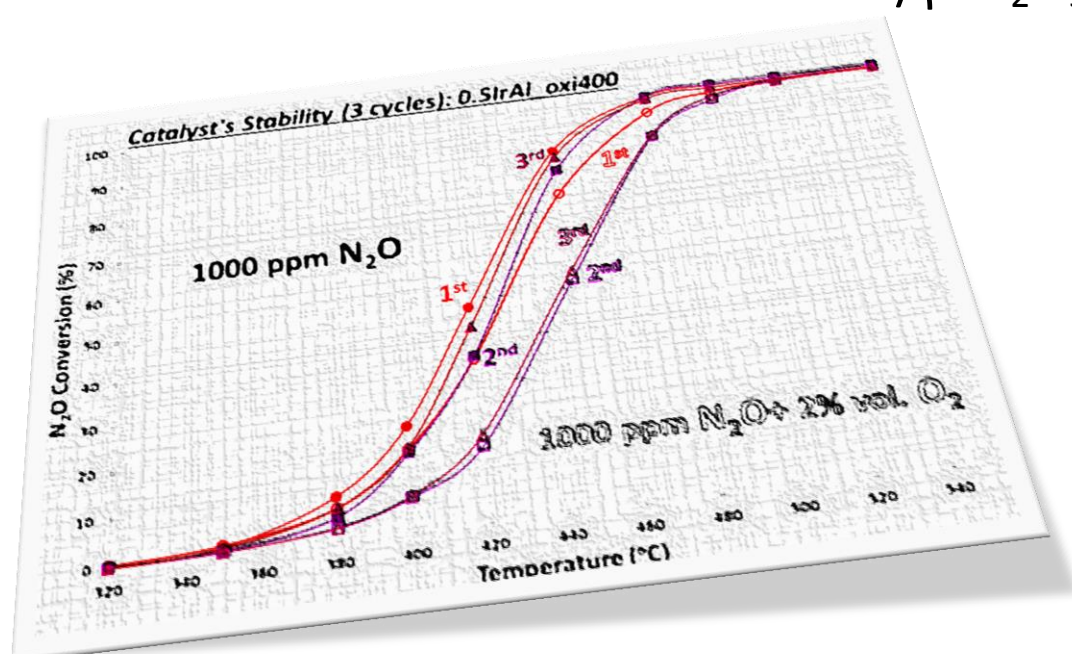
Taking into account the structural sensitivity of N_2O decomposition over Ir/Al$_2$O$_3$ catalysts, the present chapter aims at exploring the impact of thermal treatment/calcination temperature on the solid state properties and de-N_2O performance of Ir/γ-Al$_2$O$_3$ catalyst.

V EFFECT OF THERMAL TREATMENT ON THE SOLID STATE PROPERTIES AND N_2O DECOMPOSITION PERFORMANCE OF Ir/γ-Al$_2$O$_3$ CATALYST

INTRODUCTION

As mentioned in previous chapters, iridium based catalysts can be employed in various processes (i.e. reforming of hydrocarbons [1], selective catalytic reaction of NOx [2], N_2O decomposition [3], etc.), despite of Ir scarcity, the problems with Ir loss due to the formation of volatile iridium chlorides and oxychlorides, and the inferior stability (i.e. lack of resistance to sintering) under oxidizing conditions [4, 5]. However, recent studies have shown that these problems can be effectively overcome by means of metal-support interactions; supports with high oxygen ion mobility (e.g., CeO_2-containing materials), can provide Ir-based catalysts with exceptional catalytic performance for the decomposition of N_2O in the excess of O_2 [6]. On the other hand, the surface promotion with potassium notably prohibits the oxygen poisoning [7].

In addition, the thermal treatment, as well as the precursor salt used during the synthesis procedure are crucial factors for the physicochemical and morphological properties of the formed catalysts [8-14]. Iridium particles on metal oxide supports obey significant structural differences after calcination in air or after reduction in a hydrogen stream [8]. Heating in air facilitates the formation of large IrO_2, the reduction of which could result in Ir metal of low dispersion [9]. In addition, the residual Cl from the Ir precursor salt may be critical for the sintering process, notably affecting the particle size [10]. Huang et al. [11] reported that IrO_2 agglomeration did not occur above a critical Cl content. On the other side, Wögerbauer et al. [12] suggested that the presence of Cl suppressed the crystalline growth of Ir. Besides the effect of residual Cl to the Ir particle size, it has been also reported that the activity of N_2O decomposition is very sensitive to the presence of Cl [13]. Kim et al. [14] found that Rh catalyst prepared by nitrate precursor was more active for the decomposition of N_2O than the one prepared using a chloride precursor. In the latter case, the residual Cl on the catalyst surface covered the active Rh site, thus leading to a lower catalytic activity.

The present study investigates the effect of thermal treatment during synthesis of Ir/γ-Al$_2$O$_3$ catalysts (0.5IrAl_oxiT, where T is treatment temperature) on their solid state properties and N$_2$O decomposition performance. As a precursor salt of iridium, was used a Cl-free reagent (iridium acetylacetonate, Ir(O$_2$C$_5$H$_7$)$_3$). Three calcination temperatures were used for the catalysts treatment under air atmosphere: 400°C, 600°C and 800°C. All catalytic materials were characterized and tested for N$_2$O decomposition in the absence and presence of oxygen excess.

V.1 Experimental

Material Synthesis

The catalysts used in this chapter (0.5Ir/Al_oxi400, 0.5Ir/Al_oxi600, 0.5Ir/Al_oxi800) were obtained using the preparation process described previously in chapter II.1 (Materials Preparation). The catalytic materials of this section are presented in Table V.1.

Characterization Techniques

Complementary characterization studies involving N$_2$ physisorption (BET method), X-ray diffraction (XRD), hydrogen temperature programmed reduction (H$_2$-TPR) and Fourier Transform Infrared Spectroscopy (FTIR-pyridine) were carried out to gain insight into the solid state properties of Cl-free Ir/Al$_2$O$_3$ catalysts. The experimental conditions are described in chapter II.2 (Characterization Techniques).

Catalytic Activity Measurements

The catalytic decomposition of N$_2$O in the absence and presence of 2% vol. O$_2$ was tested over 0.5IrAl_oxiT catalysts, via typical light-off experiments (Chapter II.3: Catalytic Evaluation Studies). In order to investigate the stability of the catalysts, three successive reaction cycles were performed. The total gas flow rate during catalytic measurements was kept constant at 900cm^3/min, corresponding to GHSV~ 40,000 h^{-1}.

V.2 Results

Characterization Results

The physicochemical properties of catalytic materials are presented in Table V.1. Incorporation of Ir and the thermal treatment at 400°C (IrAl_oxi400) do not seem to affect the texture of the alumina support. Only a slight decrease of surface area is observed, possibly related to the blocking (or occupation) of small pores by iridium crystallites. However, as the calcination temperature increases, the total surface area decreases, whereas the average pore diameter increases. At high calcination temperature an obstruction of narrow pores can be occurred, resulting in a loss of surface area.

Table V.1: Physicochemical properties of 0.5IrAl_oxiT catalytic materials.

Catalyst	S_{BET} (m^2/g)	Pore Volume (cm^3/g)	Average Pore Diameter (nm)	Mean Ir Particle Size (nm)[1]	T_{max} (^{o}C) Reduction Peaks	
					IrO$_2$	IrAl$_x$O$_y$
γ-Al$_2$O$_3$	187	0.38	8.2	-	-	-
0.5IrAl_oxi400	184	0.38	8.4	14.7	223	650
0.5IrAl_oxi600	176	0.40	9.1	16.4	230	650
0.5IrAl_oxi800	131	0.38	11.7	14.1	230	650

[1] Calculated applying Scherrer equation;

The XRD patterns of IrAl_oxiT catalysts are presented in Figure V.1. Apart from the characteristics peaks of γ-Al$_2$O$_3$ at 37.7^o, 46° and 67° (2θ) (which are present in all catalytic materials), the diffraction peaks at 28°, 34.7^o and 54° (2θ) are attributed to the formation of IrO$_2$ phase [15]. It is worth noting that even at low calcination temperature (400°C), the IrAl_oxi400 catalyst presented peaks due to IrO$_2$. No other catalytic phases (metallic or oxide) were identified by XRD analysis. The mean Ir particle size was calculated applying Scherrer equation at 28° and 34.7^o (Table V.1). Despite the thermal treatment at different temperatures, the materials exhibit similar mean Ir particle size (~14-16 nm). This is very likely related with the relatively

low surface density of IrO_2 crystallites, as a result of the low metal loading (only 0.5% wt.), over a carrier with high surface area.
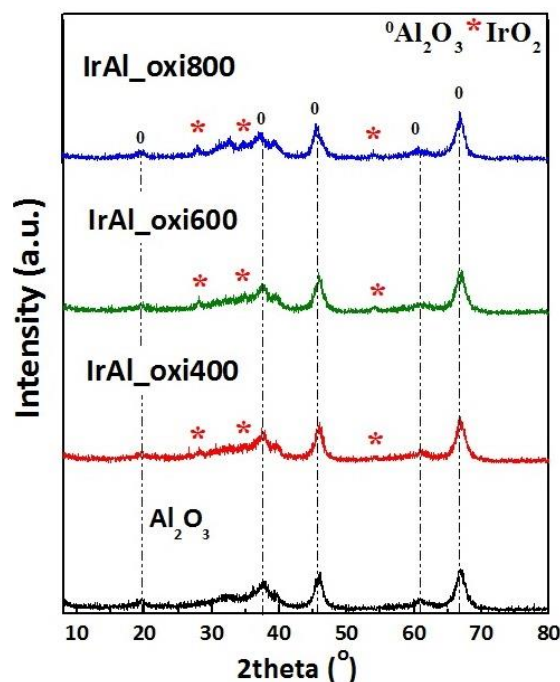

Figure V.1: XRD patterns of 0.5IrAl_oxiT catalytic materials.

H_2-TPR experiments were performed in order to investigate the impact of the thermal treatment on the reducibility of the supported Ir catalysts. A well-defined reduction peak at low temperature area (220-230°C) appeared for all three catalytic materials and is attributed to the reduction of IrO_2 phase [16-18]. The increase of calcination temperature shifted the maximum temperature (T_{max}) of the IrO_2 reduction peak (Table V.1). More specifically, the T_{max} was shifted from 223°C for IrAl_oxi400 catalyst to 230°C for the catalysts calcined at 600°C and 800°C (IrAl_oxi600, IrAl_oxi800), suggesting a slight decrease of reducibility. In addition, TPR profiles of all catalytic materials exhibit a broad peak at higher temperature area (T >500°C), with T_{max} at ca. 650°C. This peak can be attributed to the reduction of smaller Ir particles, interacting with the alumina carrier.

Recent studies based on H_2-TPR analysis of Ir/Al₂O₃ catalysts indicate the existence of a strong interaction between Al_2O_3 and IrO_x, under oxidative aging processes (airflow) at high temperatures (600-800°C), which lead to the formation of sub-surface $IrAl_xO_y$ entities. The reduction of these entities takes place at temperatures

between 400°C-700°C. This less active iridium phase was increased in proportion with increase of calcination temperature [1].

Table V.2 presents the surface acidity of all catalysts, as estimated by the FTIR-pyridine measurements. All catalysts presented only Lewis and no Brönsted acidity, as expected. The total acidity was significantly decreased, while the calcination temperature was increased. This can be attributed to the release of hydroxyl groups on catalyst surface upon the increase of calcination temperature [19]. Moreover, the total acidity can be divided into four types of acidic sites: very weak, weak, medium and strong acid sites. The incorporation of Ir over the alumina carrier, as well as the thermal treatment at 400°C did not cause any significant change of the total acidity of alumina.

Table V.2: Acidity of 0.5IrAl_oxiT catalysts.

Catalyst	Lewis Acidity (μmol/ g) [a]				
	Very Weak	Weak	Medium	Strong	Total
γ-Al$_2$O$_3$	43.99	26.14	12.16	33.64	115.93
0.5IrAl_oxi400	45.66	24.21	15.32	27.89	113.08
0.5IrAl_oxi600	39.77	20.42	13.62	28.67	102.48
0.5IrAl_oxi800	27.84	14.99	9.10	15.53	67.46

[a] Determined by FTIR-Pyridine method.

Catalytic Performance Evaluation

Figure V.2 presents the effect of thermal treatment on the N$_2$O decomposition performance of Ir catalysts, in the absence (continuous line) and presence of oxygen excess (dashed line). Typical sigmoid-type curves were observed in all samples. The catalyst calcined at 400°C (IrAl_oxi400) exhibited a superior performance in the absence, as well as in the presence of oxygen excess conditions. The increase of calcination temperature shifted the N$_2$O conversion curve to higher temperatures, while the presence of O$_2$ adversely affects the catalytic activity of the materials.

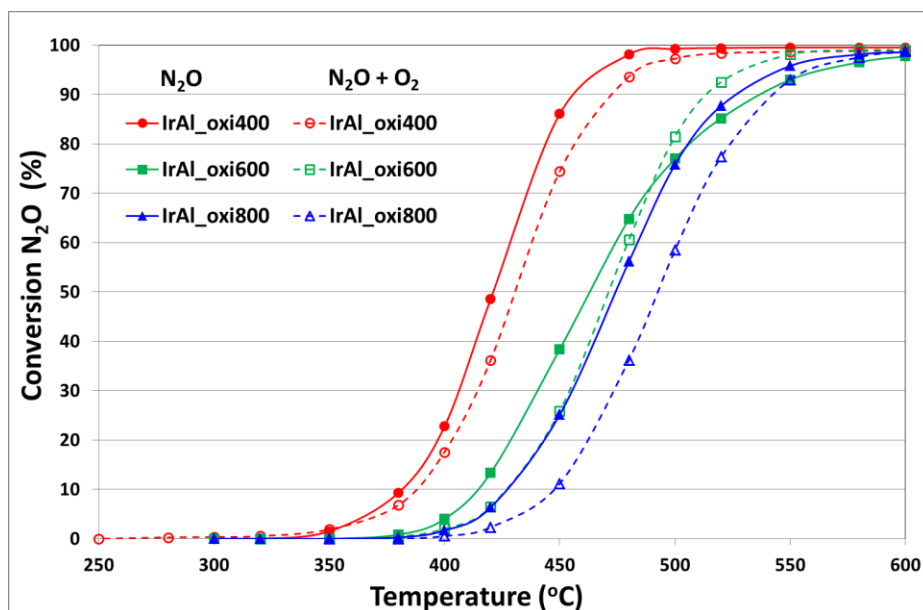Three successive reaction cycles were performed in order to examine catalysts stability.

Figure V.2: Effect of thermal treatment on N$_2$O decomposition in the absence and presence of O$_2$. Feed gas composition: 1000 ppm N$_2$O, zero or 2% vol. O$_2$ in He; GHSV~40,000 h^{-1}.

The results are shown in Figure V.3 (a, b), as the temperature required for 90% N$_2$O conversion (T$_{90}$) versus the reaction cycle. The most active and stable catalyst was the IrAl_oxi400 both in the absence and presence of 2% vol. O$_2$. The latter can be ascribed to the lower population of sub-surface inactive Ir species (IrAl$_x$O$_y$) compared to IrAl_oxi600 and IrAl_oxi800 catalysts, in agreement with other studies in the literature [1].
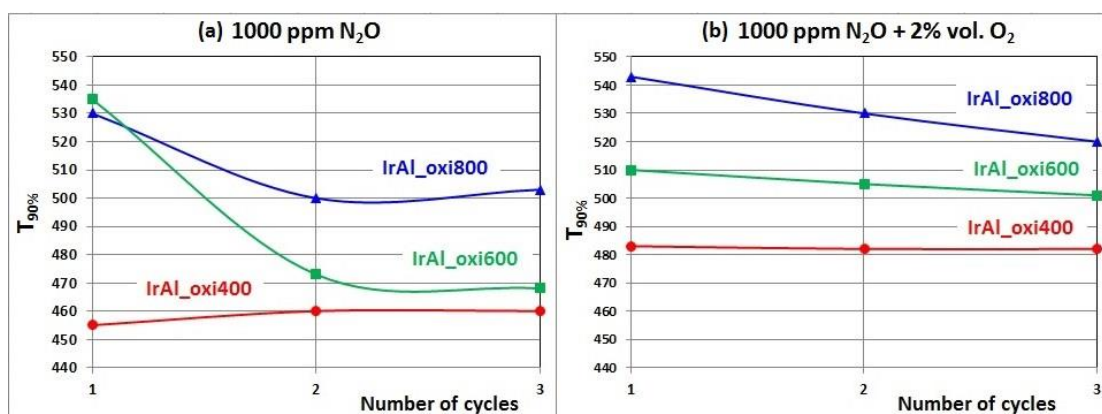

Figure V.3: Effect of thermal treatment on the stability of the 0.5IrAl_oxiT catalysts, after three successive reaction cycles. Feed gas composition: 1000 ppm N$_2$O (a), 1000 ppm N$_2$O and 2% vol. O$_2$ (b); GHSV~40,000 h^{-1}.

V.3 *Conclusions*

The influence of calcination temperature (400°C, 600°C and 800°C) on the solid state properties and the N_2O decomposition performance of Ir/γ-Al_2O_3 catalysts were explored in the present chapter. In all cases, Ir was identified in the form of IrO_2 phase of similar crystallite size. No agglomeration of the Ir particles was observed, even at high calcination temperatures. The optimum performance, in terms of activity and stability, was obtained for the IrAl_oxi400 catalyst. On the basis of characterization results, the superiority of the IrAl_oxi400 sample, as compared to IrAl_oxi600 and IrAl_oxi800, can be ascribed to the lowest population of inactive $IrAl_xO_y$ phase, which is favored at elevated temperatures.

REFERENCES

[1] Yentekakis I.V., Goula G., Panagiotopoulou P., Katsoni A., Diamadopoulos E., Mantzavinos D., Delimitis A., "Dry reforming of methane: Catalytic performance and stability of Ir catalysts supported on γ-Al_2O_3, $Zr_{0.92}Y_{0.08}O_{2-\delta}$ (YSZ) or $Ce_{0.9}Gd_{0.1}O_{2-\delta}$ (GDC) supports", Topics in Catalysis 58 (2015) 1228-1241.

[2] Amiridis M.D., Mihut C., Maciejewskiv M., Baiker A., "The selective catalytic reduction of NO by hydrocarbons over Pt- and Ir-based catalysts", Topics in Catalysis 28 (2004) 141-150.

[3] Ohnishi C., Iwamoto S., Inoue M., "Direct decomposition of nitrous oxide in the presence of oxygen over iridium catalyst supported on alumina", Chemical Engineering Science 63 (2008) 5076-5082.

[4] Wögerbauer C., Maciejewski M., Baiker A., "Structure sensitivity of NO reduction over iridium catalysts in HC-SCR", Journal of Catalysis 205 (2002) 157-167.

[5] Fiedorow R.M.J., Chahar B.S., Wanke S.E., "The sintering of supported metal catalysts: II. Comparison of sintering rates of supported Pt, Ir, and Rh catalysts in hydrogen and oxygen", Journal of Catalysis 51 (1978) 193-202.

[6] Yentekakis I.V., Goula G., Panagiotopoulou P., Kampouri S., Taylor M.J., Kyriakou G., Lambert R.M., "Stabilization of catalyst particles against sintering on oxide

supports with high oxygen ion lability exemplified by Ir-catalyzed decomposition of N$_2$O", Applied Catalysis B: Environmental 192 (2016) 357-364.

[7] Konsolakis M., Aligizou F., Goula G., Yentekakis I.V., "N$_2$O decomposition over doubly-promoted Pt(K)/Al$_2$O$_3$-(CeO$_2$-La$_2$O$_3$) structured catalysts: on the combined effects of promotion and feed composition", Chemical Engineering Journal 230 (2013) 286-295.

[8] Wang T., Schmidt L.D., "Morphology and Redispersion of Ir on SiO$_2$ in Oxidizing and Reducing Atmosphere", Journal of Catalysis 66 (1980) 301-315.

[9] Carter J.L., Cusumano J.A., Sinfelt J.H., "Hydrogenolysis of n-heptane over unsupported metals", Journal of Catalysis 20 (1971) 223.

[10] Cunha D.S., Cruz G.M., "Hydrogenation of benzene and toluene over Ir particles supported on γ-Al$_2$O$_3$", Applied Catalysis A 236 (2002) 55.

[11] Huang Y.J., Fung S.C., Gates W.E., McVicker G.B., "The effect of chloride and water vapor on the Pt-Ir interaction and IrO$_2$ agglomeration in bimetallic Pt-Ir reforming catalysts", Journal of Catalysis 131 (1991) 378.

[12] Wögerbauer C., Maciejewski M., Baiker A., Göbel U., "Ir/H-ZSM-5 catalysts in the selective reduction of NOx with hydrocarbons", Topics in Catalysis 16 (2001) 181–186.

[13] Yuzaki K., Yarimizu T., Aoyagi K., Ito S., Kunimori K., "Catalytic decomposition of N$_2$O over supported Rh catalysts: effects of supports and Rh dispersion", Catalysis Today 45 (1998) 129-134.

[14] Kim S., Lee S.J., Hong S.C., "A study on effect of Rh precursor and La addition on N$_2$O decomposition over Rh catalyst", Journal of Industrial and Engineering Chemistry 18 (2012) 1263-1266.

[15] Iliopoulou E.F., Efthimiadis E.A., Nalbandian L., Vasalos I.A., Barth J.O, Lercher J.A., "Ir-based additives for NO reduction and CO oxidation in the FCC regenerator: Evaluation, characterization and mechanistic studies", Applied Catalysis B 60 (2005) 277-288.

[16] Tian H., Zhang T., Sun X., Liang D., Lin L., "Performance and deactivation of Ir/γ-Al$_2$O$_3$ catalyst in the hydrogen peroxide monopropellant thruster", Applied Catalysis A: General 210 (2001) 55-62.

[17] Wang F., Cai W., Tana, Provendier H., Schuurman Y., Descorme C., Mirodatos C., Shen W., "Ageing analysis of a model Ir/CeO$_2$ catalyst in ethanol steam reforming", Applied Catalysis B: Environmental 125 (2012) 546-555.

[18] Chen P., Lu J., Xie G., Zhu L., Luo M., "Characterizations of Ir/TiO$_2$ catalysts with different Ir contents for selective hydrogenation of crotonaldehyde", Reaction Kinetics Mechanism and Catalysis 106 (2012) 419-434.

[19] Inmanee T., Pinthong P., Jongsomjit B., "Effect of Calcination Temperatures and Mo Modification on Nanocrystalline (γ-χ)-Al$_2$O$_3$ Catalysts for Catalytic Ethanol Dehydration", Journal of Nanomaterials 2017 (2017) 1-9.

[20] Kapteijn F., Rodriguez-Mirasol J., Moulijn J.A., "Review Heterogeneous Catalytic Decomposition of Nitrous Oxide", Applied Catalysis B: Environmental 9 (1996) 25-64.

SO$_2$ O$_2$
H$_2$O
HCs
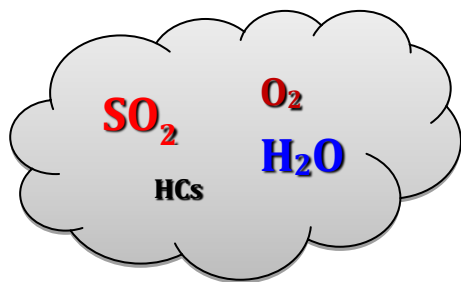
CHAPTER VI
Effect of Inhibitors on N$_2$O
Decomposition over Ir-based Catalysts
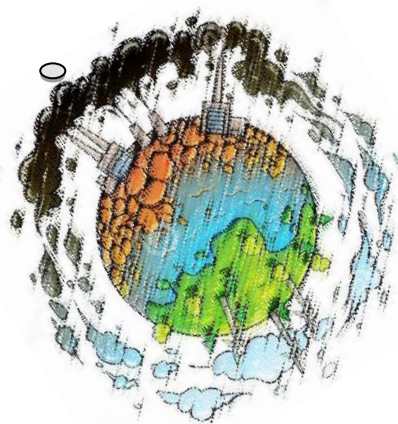
Chapter VI deals with the impact of various inhibitors (e.g. H$_2$O, SO$_2$), that typically exist in off-gases, on the de-N$_2$O performance of of Ir-based catalysts under different reaction conditions. Both "fresh" and "used" catalysts were characterized, in order to gain insight into the effect of the inhibitors on the solid state properties of the investigated catalytic materials and in turn on their de-N$_2$O efficiency.

INTRODUCTION

In chapter III, three different noble metals (Pt, Pd, Ir) supported on γ-Al_2O_3 were studied for the decomposition of N_2O. Among them Ir-based catalysts demonstrated the best de-N_2O catalytic performance. However, the co-existence of other gases inevitably present in the flue gas stream, such as H_2O and SO_2, significantly suppppresses the catalytic performance thus limiting the catalyst's applicability [1]. Thus, it is of major importance to investigate the catalytic conversion of N_2O in the presence of H_2O and SO_2.

Previous reports have shown that the deactivation caused by SO_2 was irreversible and attributed to the formation of stable sulfates on the surface of metal oxides and oxidic supports, while the inhibition effect of H_2O was reversible and the catalyst's initial activity was restored after removing H_2O from the feed [1-6]. Komvokis et al. [2] found that over Ru/Al_2O_3 catalyst, SO_2 formed stable sulfates on Ru active sites, which can be removed by regeneration under reducing (H_2 in He) atmosphere, at temperatures of ca. 500°C. The effect of H_2O on the other side, is attributed to the competitive adsorption of H_2O and N_2O molecules on the same active sites [2].

Marnellos et al. [3] studied the mechanism of the N_2O decomposition in the presence of SO_2. They have shown that the presence of SO_2 in the feed inhibited the N_2O decomposition reaction, without, however changing the reaction mechanism. In detail, oxidation of SO_2 to SO_3 takes place, which can then react with the support to form surface sulfates [3]. Lambert et al. [7] divided the supports in sulfating (like Al_2O_3) and non-sulfating (i.e. SiO_2, ZrO_2). The first group of supports can act as a sort of sink for SOx compounds, protecting the active phase from deactivation [7, 8].

In this regard, the present chapter investigates the effect of H_2O and SO_2 on N_2O decomposition over Ir-based catalysts under different experimental conditions.

EXPERIMENTAL

Material Synthesis

The un-promoted, the structurally/surface-promoted Ir catalysts (0.5Ir/Al, 0.5Ir/AlCe, 0.5Ir(0.5K)/Al), as well as the thermally treated Ir catalysts (0.5IrAl_oxi400,

0.5IrAl_oxi600, 0.5IrAl_oxi800) were obtained using the preparation procedure described in chapter II.1 (Materials Preparation).

Catalytic Performance Measurements

The effect of H$_2$O or SO$_2$ was studied under typical light-off and step-change experiments for the N$_2$O decomposition reaction in the absence and presence of 2% vol. O$_2$. The N$_2$O is continuously monitored, while the feed composition is switched from poison-free to poison-containing mixtures. The experimental procedures followed have been described in detail in chapter II.3 (Catalytic Evaluation Studies). The total gas flow during catalytic measurements was kept constant at 900cm^3/min, corresponding to GHSV~ 40,000 h^{-1}.

Characterization Techniques

The "used" catalysts (i.e. catalysts after N$_2$O decomposition reaction in the presence of poisons), were characterized via Hydrogen temperature-programmed reduction (H$_2$-TPR), X-ray Diffraction (XRD), as well as via temperature programmed desorption of SO$_2$ (SO$_2$-TPD). The experimental conditions are described in chapter II.2 (Characterization Techniques).

VI.1 EFFECT OF H$_2$O

VI.1.1 *Effect of H$_2$O on un-modified 0.5Ir/γ-Al$_2$O$_3$ catalyst*

Figure VI.1 presents the N$_2$O conversion as a function of temperautre at different H$_2$O concentrations (0, 5% and 10% vol.). It is evident that the 0.5Ir/Al catalysts performance is suppressed with the addition of H$_2$O in the feed. However, increasing H$_2$O content from 5% to 10%, did not lead to further deactivation of the catalyst performance. Similar behavior was observed by other research groups, who studied the catalytic decomposition of N$_2$O in the presence of water [3, 9, 10]. The N$_2$O light-off temperature is shifted to higher temperatures by ~100°C for 5% and 10% vol. H$_2$O, in respect to H$_2$O-free feed. The inhibition caused by the water presence in the feed is attributed to the competitive adsorption of H$_2$O with N$_2$O on the catalysts surface. Lin et al. [11] found that the influence is usually reversible and the activity

can be restored quickly after removing H_2O from the reaction mixture. These aspects will be further discussed below on the basis of the present findings.
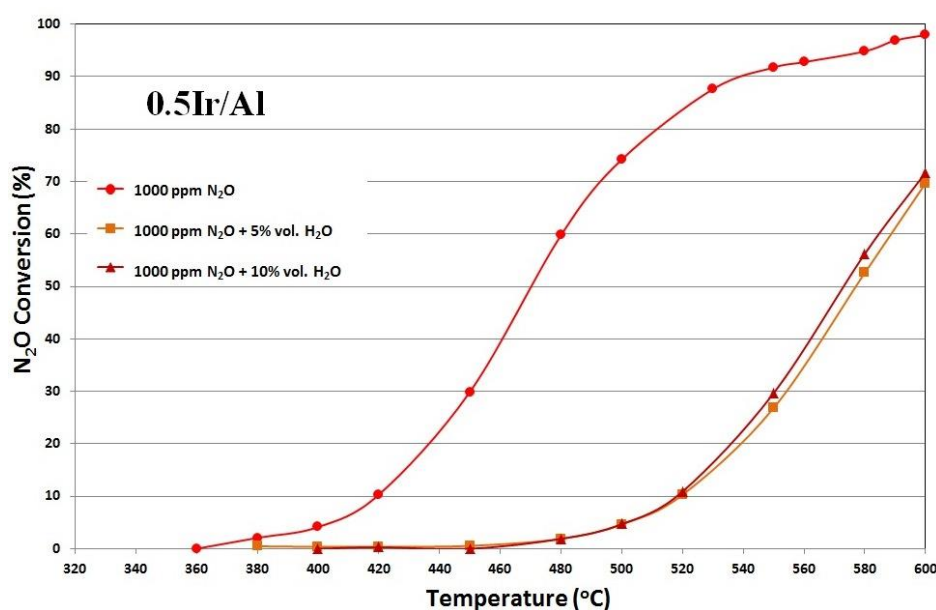

Figure VI.1: Effect of H_2O concentration N_2O decomposition over 0.5Ir/Al catalyst. Feed gas composition: 1000 ppm N_2O and 0, 5 and 10% vol. H_2O; Flow rate: 900cm^3/min; GHSV~40,000 h^{-1}.

VI.1.2 *Effect of H_2O on structurally modified 0.5Ir/AlCe catalyst*

The effect of 5% vol. H_2O on N_2O decomposition performance of structurally promoted Ir catalyst (0.5Ir/AlCe) is explored below (Figure VI.2). The catalyst performance was inhibited by H_2O, to a similar extent to that obtained over un-modified 0.5Ir/Al catalyst.

Step-change experiment was also performed to investigate the effect of 5% vol. H_2O on Ce-promoted Ir catalyst, in the presence of O_2. N_2O is continuously monitored, while the feed composition is switched from H_2O-free to H_2O-containing mixtures (Fig. VI.3). In the first step (t: 0-110 min), the catalyst is exposed only to N_2O and the N_2O conversion remains stable at ~100%. The addition of 2% vol. O_2 (t: 110-210 min) did not affect the catalyst's activity. The promotional effect of Ce on the deN$_2$O performance of 0.5Ir/Al catalysts in the presence of O_2 has been already discussed in chapter III.2.

However, addition of 5% vol. H_2O in feed (t: 210-310 min), causes a sudden drop on the N_2O conversion, from 100% to 20%.
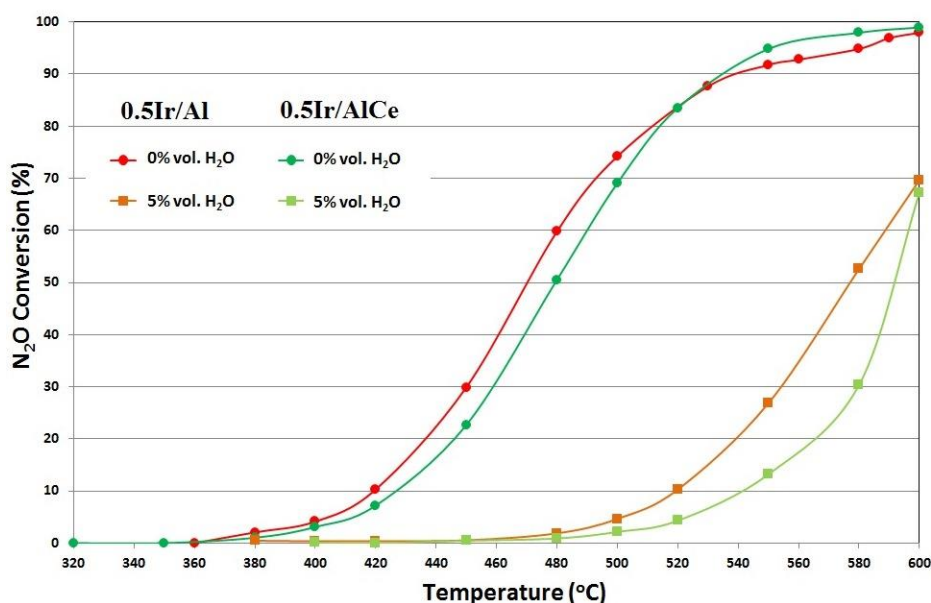
Figure VI.2: Effect of H$_2$O on N$_2$O decomposition over un-promoted and Ce-promoted Ir catalyst. Feed gas composition: 1000 ppm N$_2$O and 0%, 5% vol. H$_2$O; Flow rate: 900cm^3/min; GHSV~40,000 h^{-1}.

Figure VI.3: Effect of H$_2$O on N$_2$O decomposition over 0.5Ir/AlCe catalyst at 600°C. Feed gas composition-Step: (1) 1000 ppm N$_2$O; (2) 1000 ppm N$_2$O and 2% vol. O$_2$; (3) 1000 ppm N$_2$O, 2% vol. O$_2$ and 5% vol. H$_2$O; (4) 1000 ppm N$_2$O and 2% vol. O$_2$; (5) 1000 ppm N$_2$O, 2% vol. O$_2$ and 5% vol. H$_2$O; (6) 1000 ppm N$_2$O and 2% vol. O$_2$; Flow rate: 900cm^3/min; GHSV~40,000h^{-1}.

By removing H$_2$O the de-N$_2$O performance is totally recovered (t: 310-360 min). In the next H$_2$O-containing step (t: 360-460 min), the N$_2$O conversion was decreased at the same level to that obtained in previous step. Removing H$_2$O from the feed

stream at the last step (t: 460-510 min) the catalyst performance is recovered again to ~100% N_2O conversion. In light of the above, it can be concluded that H_2O has a detrimental influence on N_2O decomposition performance, which however is totally reversible due to its competitive adsorption on catalyst surface, without actually affecting the properties of the catalyst.

VI.1.3 *Effect of H_2O on surface-modified 0.5Ir(0.5K)/Al catalyst*

The effect of H_2O was also studied over surface promoted (K) Ir-based catalyst. The results of the step-change experiment are presented in Figure VI.4. The experimental procedure followed was the same to that, descibed above, for the structurally promoted catalyst. When H_2O was added in the N_2O and O_2 feed (t: 210-325 min), the N_2O conversion decreased to 20% from ~98% initial conversion. By removing H_2O from the feed stream (t: 325-360 min), the N_2O conversion was stabilized to ~92%, which is actually lower from the initial conversion performance (98%).
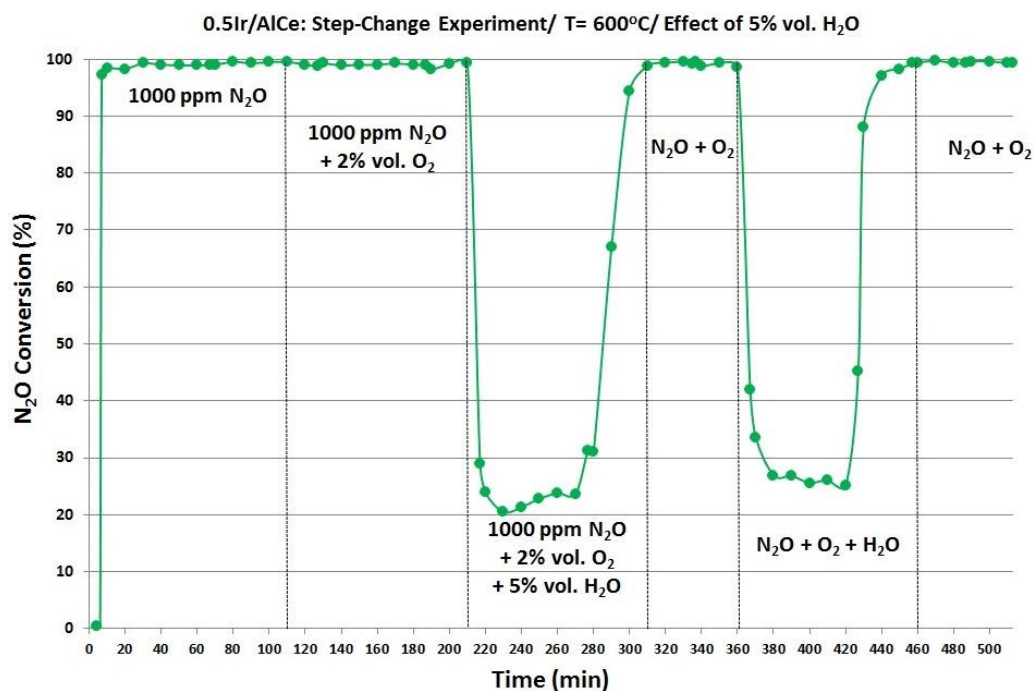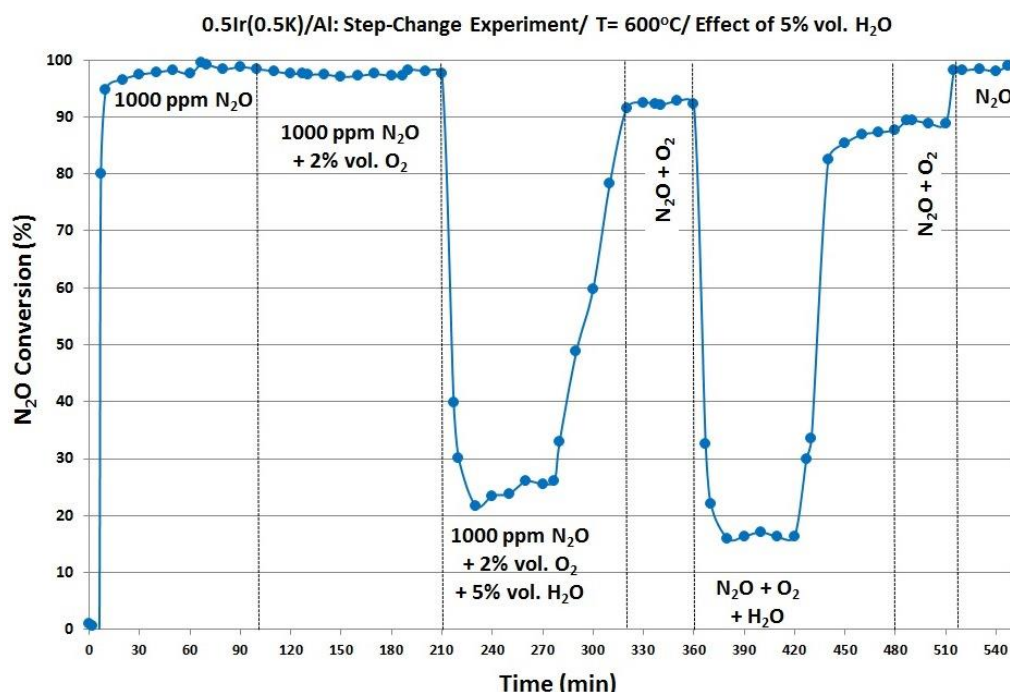

Figure VI.4: Effect of H_2O on N_2O decomposition over 0.5Ir(0.5K)/Al catalyst at 600°C. Feed gas composition-Step: (1) 1000 ppm N_2O; (2) 1000 ppm N_2O and 2% vol. O_2; (3) 1000 ppm N_2O, 2% vol. O_2 and 5% vol. H_2O; (4) 1000 ppm N_2O and 2% vol. O_2; (5) 1000 ppm N_2O, 2% vol. O_2 and 5% vol. H_2O; (6) 1000 ppm N_2O and 2% vol. O_2; (7) 1000 ppm N_2O; Flow rate: 900cm^3/min; GHSV~40,000 h^{-1}.

The second H$_2$O-containing step (t: 360-480 min) affected in a more severe manner the catalyst performance, resulting ~16% N$_2$O conversion. By removing H$_2$O from the feed stream (t=320-360 min), the N$_2$O conversion is again stablilized at ~90%. However, the initial performance (~98% N$_2$O conversion) was fully reached when both H$_2$O and O$_2$ were removed from the feed gas, at the last step (t: 515-550 min). The semi-reversible character of H$_2$O-poisoning obtained here cannot be solely ascribed to the competitive adsorption of H$_2$O. Only part of this inhibition, that actually corresponds to the sudden changes of N$_2$O conversion profile upon H$_2$O addition (or subsequent removal) in the feed stream, is consistent with this mechanism [12]. According with Konsolakis et al. [12], the addition of H$_2$O to the feed over Pt(K)/Al$_2$O$_3$-(CeO$_2$-La$_2$O$_3$) catalyst, can modify the oxidation state of active sites-though the formation of hydrohyl groups- which in turns hinders the N$_2$O adsorption/ decomposition [12, 13].

VI.2 EFFECT OF SO$_2$

VI.2.1 *Effect of SO$_2$ on un-modified (0.5Ir/Al) and structurally modified (0.5Ir/AlCe) catalysts*

The characterization results of fresh 0.5Ir/Al and Ce-modified catalyst (0.5Ir/AlCe) have been already presented and discussed in Chapter III.2. For discussion purposes, the textural and redox characteristics of Ir catalysts are included in Table VI.1, while the H$_2$-TPR and XRD profiles of the fresh catalysts are presented in Figure VI.6a, b.

Table VI.1: Textural and redox (H$_2$-TPR) characteristics of Ir catalysts.

Catalyst	S$_{BET}$ (m^2/g)	Pore Volume (cm^3/ g)	Pore Size (nm)	T$_{max}$ (^{o}C)^a IrO$_2$
0.5Ir/Al	160	0.34	8.6	232
0.5Ir/AlCe	159	0.31	7.9	233

^{a} Temperature at maximum reduction rate (H$_2$-TPR);

The main iridium phase over both catalysts is IrO$_2$. This is confirmed by the reduction peak at ~230°C in H$_2$-TPR profiles (Fig. VI.6a), as well as by the XRD patterns (Fig.

VI.6b) of the fresh catalysts, in which the IrO_2 peaks at 28°, 34.7^o and 54° (2θ) were observed.

In addition, the characterization results (i.e. HRTEM/STEM, CO-DRIFTS) that were presented in Chapter III.2, revealed that the un-modified Ir/Al_2O_3 catalyst exhibited both large and small IrO_2 crystallites, as well as iridium species with metallic character (Ir^0), dispersed all over the alumina support surface, while the incorporation of 20% wt. CeO_2 over Al_2O_3 brings upon a considerable increase in the particle size of IrO_2, accompanied by an improved surface dispersion of the metallic Ir nano-entities.

Figure VI.5 presents the effect of 50 ppm SO_2 on the N_2O decomposition of 0.5Ir/Al and 0.5Ir/AlCe catalysts at 600°C. During the first step (absence of SO_2), the % N_2O conversion is around 93-95% for both catalysts.
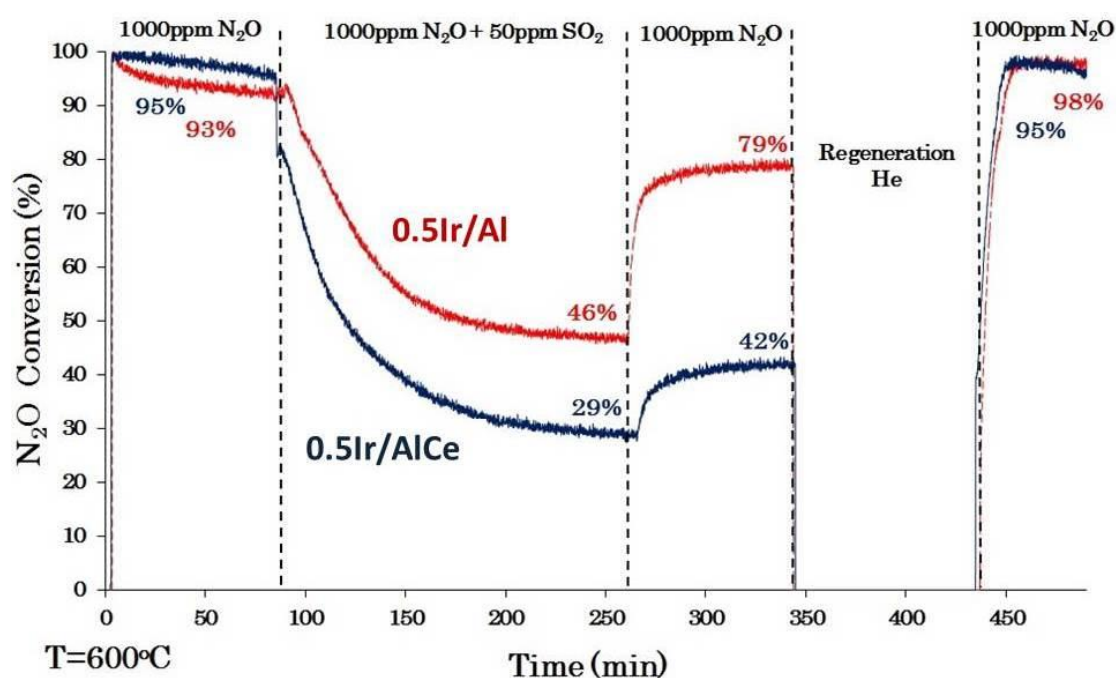
Figure VI.5: Effect of SO_2 on de-N_2O over 0.5Ir/Al and 0.5Ir/AlCe catalysts at 600°C. Feed gas composition-Step: (1) 1000 ppm N_2O; (2) 1000 ppm N_2O and 50 ppm SO_2; (3) 1000 ppm N_2O; (4) Regeneration under He flow at 850°C/ 1h; (5) 1000 ppm N_2O; GHSV~40,000 h^{-1}.

The addition of SO_2 to the feed (2nd step) reduces gradually the % N_2O conversion to 46% and 29% for the un-modified and Ce-modified Ir catalysts, respectively. After 3 h under N_2O and SO_2 gas stream, the SO_2 is removed and the de-N_2O catalytic performance was again tested. It is evident that the deactivation caused by SO_2 is

permanent and thus only a slight increase to the N$_2$O conversion was observed for both catalysts, i.e. 79% for 0.5Ir/Al and 42% for 0.5Ir/AlCe catalyst. It can be therefore inferred that the un-modified catalyst presents better resistance to sulfur poisoning. The 4th step includes regeneration of the catalysts under He flow at 850°C for 1 h. After regeneration, the N$_2$O conversion was increased for both catalysts, reaching the initial levels (~95-98%). The later, implies the effective removal of Sulphur species during the regeneration process, as will be further discussed in the following.

In order to investigate in depth the SO$_2$-induced deactivation mechanism, further characterization studies (i.e. SO$_2$-TPD, XRD and H$_2$-TPR) were performed over the used catalysts (i.e., the catalysts samples derived after the addition of SO$_2$ into the gas feed-2nd step) and regenerated catalysts (i.e., catalysts after the regeneration procedure-4th step).

Figure VI.6a presents the H$_2$-TPR profiles of used and regenerated catalysts. Fresh catalysts exhibit a peak at 232°C, ascribed already to the reduction of IrO$_2$. The low intensity peak at ca. 370°C over Ir/AlCe is attributed to ceria reduction. Both Ir/Al and Ir/AlCe used catalysts presented a wide reduction peak at ca. 400-500°C, which can be attributed to the reduction of sulphated compounds. In particular, over the Ir/Al used catalyst the formed Al$_2$(SO$_4$)$_3$ reduced at 495°C, while for the Ir/AlCe used sample the reduction of the formed Ce(SO$_4$)$_2$ took place at 370-480°C [14, 15]. Obviously, the regeneration step resulted in the desorption of sulfates that were formed over the catalyst surface.

The corresponding XRD patterns are presented in Figure VI.6b. Comparing the used and regenerated catalysts with the fresh ones, a significant decrease of the intensity of IrO$_2$ peaks can be observed. At the same time, new peaks appeared at the XRD patterns attributed to metallic Ir phase (2θ: 40.5^{o}). Haneda et al. [16, 17] reported that oxidized iridium surface can be reduced by introducing SO$_2$ into the reaction gas even in the presence of O$_2$. This was explained by the following model [18]: The disproportionation of SO$_2$ takes place on the Ir (111) surface: $3SO_{2(ads)} \rightarrow 2SO_{3(ads)} + S_{(ads)}$, where SO$_3$ is thermally desorbed and the remaining atomic sulfur reacts with surface oxygen on iridium, $S_{(ads)} + 2O_{(ads)} \rightarrow 2SO_{2\ (g)}$. The iridium surface, thus, reverts to metallic state. These findings are in agreement with the low intensity of IrO$_2$

reduction peaks in used catalysts (Fig. VI.6a). In addition, the intensity of Al_2O_3 and CeO_2 peaks was reduced due to the formation of sulfates over the catalysts surface.
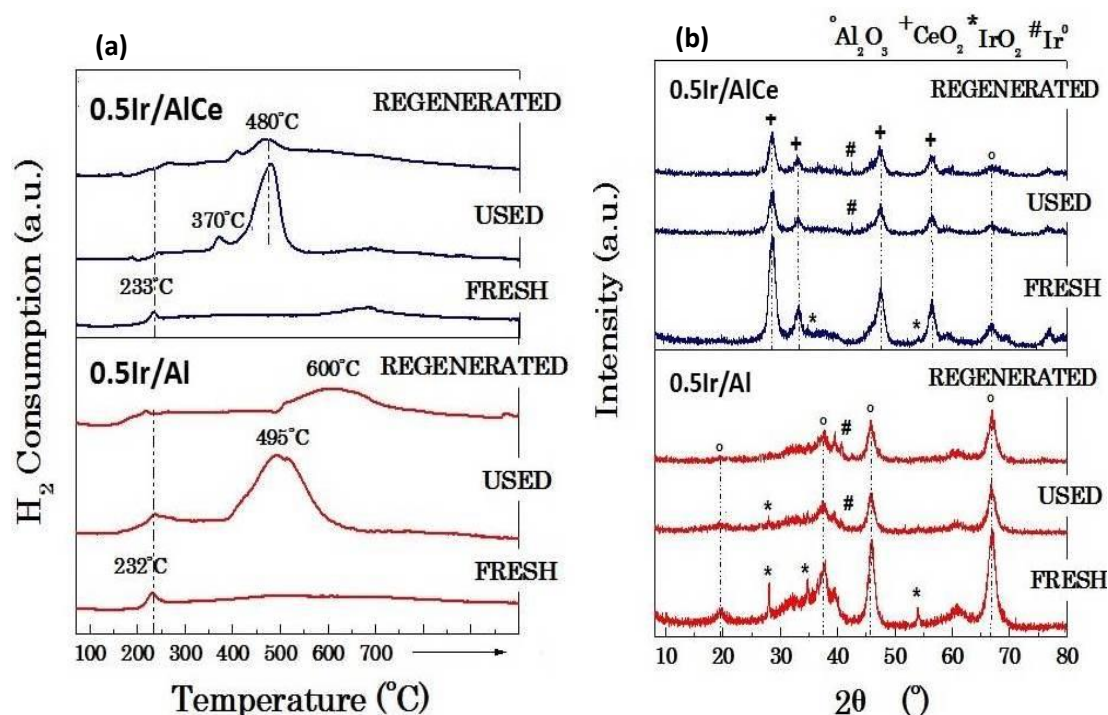

Figure VI.6: H_2-TPR (a) and XRD (b) profiles of fresh, used and regenerated catalytic materials.

Figure VI.7 presents the desorbed SO_2 form the used and regenerated catalysts. The fresh catalysts did not desorb any sulfates, as it was expected. 0.5Ir/AlCe catalyst desorbs more sulfates than 0.5Ir/Al, before and after the regeneration. This is probably related with the existence of CeO_2 which favored SO_x uptake and formation of sulfates [19]. The latter is in agreement with the presence of H_2-TPR peak at 370-480°C over the Ir/AlCe sample (Figure VI.6a), attributed to the reduction of $Ce(SO_4)_2$. It is interesting that even after the regeneration step SO_2 is desorbed from the catalysts. The latter implies the formation of stable sulfur species upon the SO_2 treatment, which are not completely removed during the regeneration process at 850°C. Temperatures higher than 700°C are required for the desorption of these compounds. However, these compounds did not affect the catalytic performance, taking into account the complete restoration of catalytic activity after the regeneration process (Fig. VI.5). The later can be probably related to the localization

of stable sulfur compounds to the bulk of supporting carriers rather than to catalyst surface [20].
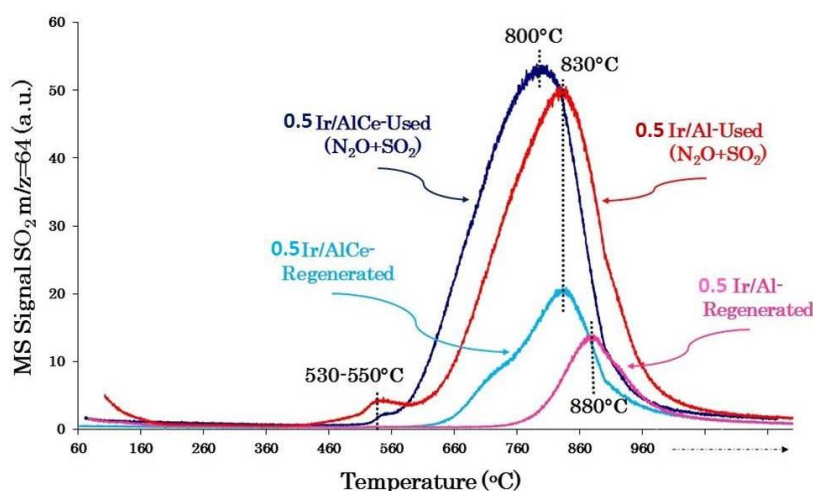
Figure VI.7: SO$_2$ desorption profiles of used and regenerated catalytic materials.

The impact of SO$_2$ on the durability of 0.5Ir/AlCe catalyst was also investigated in long-term stability tests for 9h at 600°C. Figure VI.8 illustrates the N$_2$O conversion as a function of time during the N$_2$O conversion in the presence or absence of 50 ppm SO$_2$.
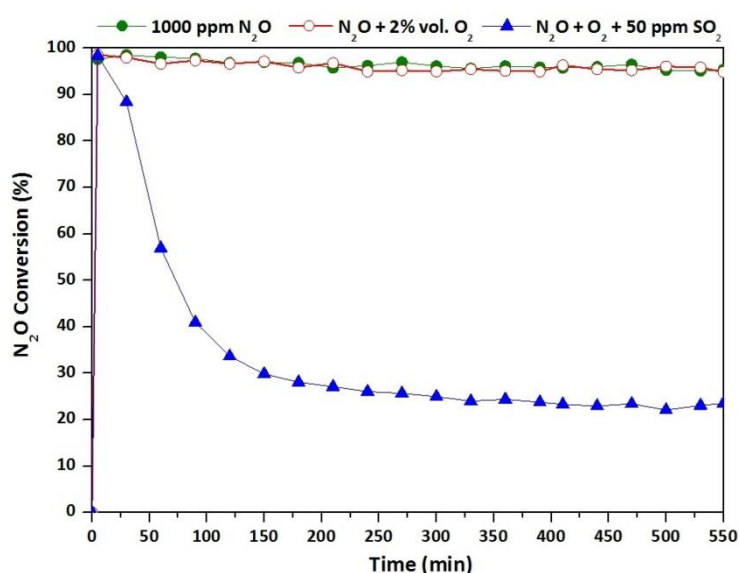
Figure VI.8: Response of N$_2$O conversion to long-term stability tests carried out under different feed gas compositions over 0.5Ir/AlCe catalyst; Flow rate: 900cm^3/min; GHSV~40,000 h^{-1}.

In the absence of SO_2, the N_2O conversion remains stable at ~97% over the whole time period, both in the absence and the presence of oxygen. However, SO_2 addition in the feed stream leads in a significant deactivation. In the first 3 h the N_2O conversion is dropped from 97% to 28%, whereas during the next 6 h a slight drop occurred, reaching a final N_2O conversion of ~22%.

VI.2.2 *Effect of SO_2 on the de-N_2O performance of thermally treated 0.5IrAl_oxiT catalysts*

The effect of SO_2 presence on the de-N_2O performance of 0.5IrAl_oxiT catalyst is depicted in Figure VI.9. The figure presents the % conversion of N_2O as a function of time for all three materials. SO_2 is added to the feed gas composition at t=60, 180 and 300 min. After 1 h, SO_2 is removed to check the reversibility of the catalyst deactivation. This procedure is repeated three times, consisting three subsequent cycles. During the first cycle the N_2O conversion is decreased from an initial activity (~90-100%) to 78%, 57% and 26% for 0.5IrAl_oxi400, 0.5IrAl_oxi600 and 0.5IrAl_oxi800, respectively.
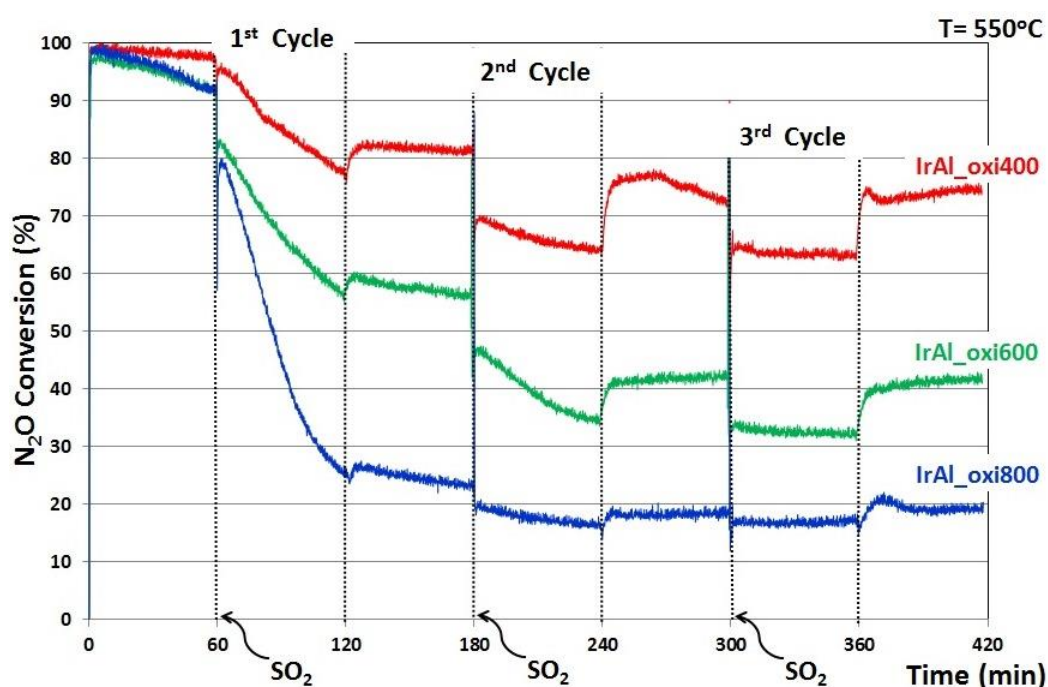

Figure VI.9: Effect of SO_2 (50 ppm) on the N_2O conversion over 0.5IrAl_oxiT catalysts. Feed gas composition: 1000 ppm N_2O and 2% vol. O_2; Temperature: 550°C; GHSV~40,000 h^{-1}.

The removal of SO$_2$ from the feed does not completely restore the initial catalytic performance, suggesting a permanent deactivation. In the next two cycles, a similar picture was recorded, with, however, the deactivation induced by SO$_2$ to be inferior as compared to first cycle. The latter can be related with the high accumulation of Sulphur compounds during the initial exposure of catalysts to SO$_2$-containing mixtures.

In any case, the superiority of the catalyst calcined at 400°C is obvious, both in SO$_2$-free and SO$_2$-containing mixtures, implying a better resistance to SO$_2$ poisoning as well as an improved regeneration ability. In particular, at the end of the 3rd cycle, the N$_2$O conversion of the best catalyst (0.5IrAl_oxi400) has reached the value of 74%, in contrast to 41% and 20% over the 0.5IrAl_oxi600 and 0.5IrAl_oxi800 samples, respectively.

The "used" catalysts (after exposure to SO$_2$ step-change experiments) were next characterized by temperature-programmed desorption of SO$_2$ (Figure VI.10). All catalytic materials exhibit one peak at high temperature area (~750-800°C) at the signal of SO$_2$ (m/z= 64).
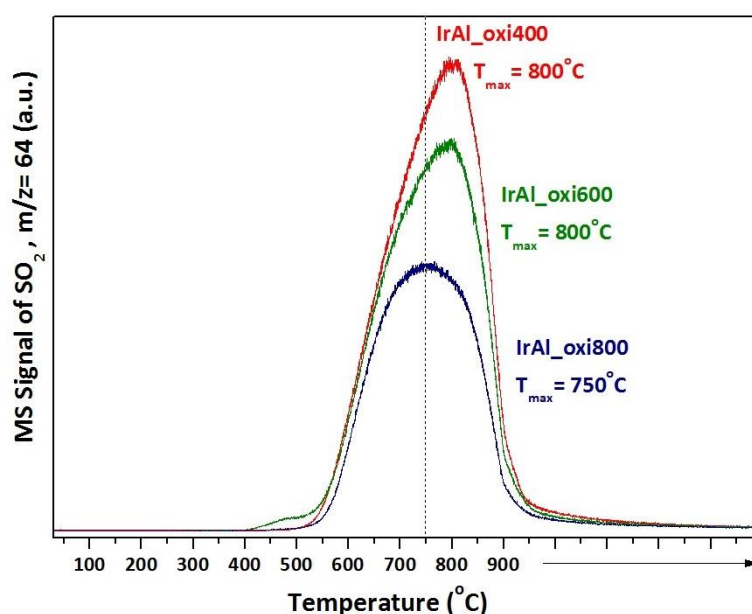

Figure VI.10: SO$_2$ desorption profiles of used catalytic materials.

The intensity of the 0.5IrAl_oxi400 peak is greater than the other two samples, while as the calcination temperature increased, a decrease of the peak intensity and thus

the desorbed SO_2 was observed. This variation is probably due to the different characteristics of the alumina substrate (surface area, as well as acidity/basicity properties which are associated with the sorption mechanism of SO_2 over γ-Al_2O_3 carrier). Chapter V presented the effect of thermal treatment on the acidity of Ir/Al_2O_3 catalysts (Fig. V.3 and Table V.2). The increase of calcination temperature resulted in a decrease of Lewis acidity. Hamzehlouyan et al. [20] revealed that SO_2 adsorption at Lewis acid sites gives rise to relatively weakly held SO_2. Notably, the optimum 0.5IrAl_oxi400 catalyst (Fig. VI.10), seems to have the highest relative population on SO_2 desorbed compounds. This apparently comes in contraction with its high SO_2 resistance behavior, most probably implying a selective accumulation of sulfur compounds into the alumina carrier rather than to the active IrO_x entities.

VI.3 *Conclusions*

The main conclusions that can be drawn from the present chapter can be summarized as follows:

- The inhibition caused by the water presence in the feed stream can be attributed to the competitive adsorption of H_2O with N_2O on the catalysts surface.

- The deactivation caused by SO_2 is a permanent phenomenon, with its extent to be strongly dependent on catalyst's composition and thermal treatment.

- The un-modified catalyst (0.5Ir/Al) presents the better resistance to sulfur poisoning.

- Among the Ir/Al_2O_3 catalysts thermally treated at different temperatures, the optimum performance as well as resistance to SO_2 poisoning was observed for the 0.5IrAl_oxi400 sample. The later can be ascribed to the largest population of IrO_x active phase and the selective accumulation of sulphur compounds into the Al_2O_3 carrier rather than to active entities.

REFERENCES

[1] Pekridis G., Athanasiou C., Konsolakis M., Yentekakis I.V., Marnellos G.E., "N$_2$O Abatement Over γ-Al$_2$O$_3$ Supported Catalysts: Effect of Reducing Agent and Active Phase Nature", Topics in Catalysis 52 (2009) 1880.

[2] Komvokis V.G., Marnellos G.E., Vasalos I.A., Triantafyllidis K.S., "Effect of pretreatment and regeneration conditions of Ru/γ-Al$_2$O$_3$ catalysts for N$_2$O decomposition and/or reduction in O$_2$-rich atmospheres and in the presence of NO$_X$, SO$_2$ and H$_2$O", Applied Catalysis B: Environmental 89 (2009) 627-634.

[3] Marnellos G.E., Efthimiadis E.A., Vasalos I.A., "Effect of SO$_2$ and H$_2$O on the N$_2$O decomposition in the presence of O$_2$ over Ru/Al$_2$O$_3$", Applied Catalysis B 46 (2003) 523.

[4] Kapteijn F., Rodriguez-Mirasol J., Moulijn J.A., "Heterogeneous catalytic decomposition of nitrous oxide", Applied Catalysis B 9 (1996) 25.

[5] Centi G., Perathoner S., Vazzana F., Marella M., Tomaselli M., Mantegazza M., "Novel catalysts and catalytic technologies for N$_2$O removal from industrial emissions containing O$_2$, H$_2$O and SO$_2$", Advances in Environmental Research 4 (2000) 325.

[6] Centi G., Galli A., Montanari B., Perathoner S., Vaccari A., "Catalytic decomposition of N$_2$O over noble and transition metal containing oxides and zeolites. Role of some variables on reactivity", Catalysis Today 35 (1997) 113.

[7] Lampert J.K., Kazi M.S., Farrauto R.J., "Palladium catalyst performance for methane emissions abatement from lean burn natural gas vehicles", Applied Catalysis B: Environmental 14 (1997) 211-223.

[8] Colussi S., Arosio F., Montanari T., Busca G., Groppi G., Trovarelli A., "Study of sulfur poisoning on Pd/Al$_2$O$_3$ and Pd/CeO$_2$/Al$_2$O$_3$ methane combustion catalysts", Catalysis Today 155 (2010) 59.

[9] Zeng H.C., Pang X.Y., "Catalytic decomposition of nitrous oxide on alumina-supported ruthenium catalysts Ru/Al$_2$O$_3$", Applied Catalysis B 13 (1997) 113.

[10] Wang X.F., Zeng H.C., "Decomposition of water-containing nitrous oxide gas using Ru/Al$_2$O$_3$ catalysts", Applied Catalysis B 17 (1998) 89.

[11] Lin Y., Meng T., Ma Z., "Catalytic decomposition of N$_2$O over RhOx supported on metal phosphates", Journal of Industrial and Engineering Chemistry 28 (2015) 138.

[12] Konsolakis M., Aligizou F., Goula G., Yentekakis I.V., "N$_2$O decomposition over doubly-promoted Pt(K)/Al$_2$O$_3$-(CeO$_2$-La$_2$O$_3$) structured catalysts: On the combined effects of promotion and feed composition", Chemical Engineering Journal 230 (2013) 286-295.

[13] Liu Z., He F., Ma L., Peng S., "Recent advances in catalytic decomposition of N$_2$O on noble metal and metal oxide catalysts", Catalysis Surveys from Asia 20 (2016) 121-132.

[14] Elbouazzaoui S., Courtois X., Marecot P., Duprez D., "Characterization by TPR, XRD and NOx storage capacity measurements of the ageing by thermal treatment and SO$_2$ poisoning of a Pt/Ba/Al NOx-trap model catalyst", Topics in Catalysis 30 (2004) 493.

[15] Zhang L., Li L., Cao Y., Yao X., Ge C., Gao F., Deng Y., Tang C., Dong L., "Getting insight into the influence of SO$_2$ on TiO$_2$/CeO$_2$ for the selective catalytic reduction of NO by NH$_3$", Applied Catalysis B: Environmental 165 (2015) 589.

[16] Haneda M., Fujitani T., Hamada H., "Effect of iridium dispersion on the catalytic activity of Ir/SiO$_2$ for the selective reduction of NO with CO in the presence of O$_2$ and SO$_2$", Journal of Molecular Catalysis A: Chemical 256 (2006) 143-148.

[17] Haneda M., Pusparatu, Kintaichi Y., Nakamura I., Sasaki M., Fujitani T., Hamada H., "Promotional effect of SO$_2$ on the activity of Ir/SiO$_2$ for NO reduction with CO under oxygen-rich conditions", Journal of Catalysis 229 (2005) 197.

[18] Fujitani T., Nakamura I., Kobayashi Y., Takahashi A., Haneda M., Hamada H., "Adsorption and reactivity of SO$_2$ on Ir (111) and Rh (111)", Surface Science 601 (2007) 1615-1622.

[19] Pereira H.B., Polato M.S., Monteiro J.L.F., Henriques C.A., "Mn/Mg/Al-spinels as catalysts for SOx abatement. Influence of CeO$_2$ incorporation and catalytic stability", Catalysis Today 149 (2010) 309.

[20] Hamzehlouyan T., Sampara C.S., Li J., Kumar A., Epling W.S., "Kinetic study of adsorption and desorption of SO$_2$ over γ-Al$_2$O3 and Pt/-Al$_2$O$_3$", Applied Catalysis B: Environmental 181 (2016) 587–598.

CHAPTER VII
General Conclusions-
Future Directions

GENERAL CONCLUSIONS

In the current thesis a series of Pt, Pd and Ir catalysts supported either on bare or rare earth (CeO_2, La_2O_3)-doped γ-Al_2O_3 were prepared, characterized and tested for the abatement of NOx and/ or N_2O. Moreover, the impact of surface promoters (K) as well as the influence of thermal pre-treatment on the de-N_2O performance of Ir-based catalysts, which exhibited the optimum behavior, was also examined. Finally, the effect of inhibitors, such as SO_2 and H_2O, on the activity and stability performance of Ir-based catalysts was explored. In all cases, an extended physicochemical characterization was carried out to reveal the underlying mechanism at atomic level, with particular emphasis on structure-property relationships. The following general conclusions can be drawn from the work presented in this thesis. For clarity purposes the conclusions are separately presented in relation to each reaction process and promotional route investigated in the current thesis.

N_2O decomposition over un-promoted γ- Al_2O_3 supported noble metals catalysts:
- The catalytic activity for N_2O decomposition follows the trend Ir > Pd > Pt, in the absence as well as in the presence of O_2 excess.
- The inferior performance of Pt catalyst is related with the sensitivity of metallic Pt^0 sites to oxygen poisoning.
- Pd catalyst is only slightly depressed by the presence O_2. The formed metal oxide phase (PdO) seems to be active towards N_2O decomposition.
- The superior performance of Ir catalyst is attributed to the existence of IrO_2 phase in conjunction to the establishment of a certain $Ir^{\delta+}/Ir^0$ ratio.

H_2 assisted C_3H_6-SCR of NO over un-promoted γ- Al_2O_3 supported noble metals catalysts:
- The H_2-assistance on C_3H_6-SCR of NO_x is more substantial on Pt, then on Ir and less on Pd.
- The key factor is considered to be the influence of H_2 on the oxidation state of the noble metals.

- H_2 co-presence promotes both the NO and C_3H_6 conversions, which is valid in the whole temperature interval investigated (50-400°C).

N$_2$O decomposition over structurally promoted (CeO$_2$, La$_2$O$_3$) γ- Al$_2$O$_3$ supported noble metals catalysts:

- Incorporation of Ce and La on Al_2O_3 carrier, notably enhances the de-N_2O performance of noble metal catalysts, following, however, the same trend as in the case of un-promoted alumina carrier (Ir > Pd > Pt).

- Incorporation of Ce and La on γ-Al_2O_3 results in a significant increase of Pt dispersion and the formation of electron enriched Pt sites ($Pt^{\delta-}$), located at metal-support interfacial area, which are highly active towards N_2O decomposition.

- The enhanced catalytic activity of doped Pd/ Al_2O_3 catalysts could be attributed to the creation of highly active PdO_x aggregates.

- Ir presented the optimum de-N_2O performance: The establishment of a certain $Ir^{\delta+}/Ir^0$ ratio and oxygen vacant sites (V_O) concentration in ceria around very small supported Ir particles under oxidative reaction conditions seem to largely promote a sustainable N_2O adsorption and decomposition into N_2 and O_2 over the CeO_2-promoted Ir/Al_2O_3 catalyst.

N$_2$O decomposition over Ir/γ- Al$_2$O$_3$ catalysts - Surface versus structural promotion:

- Addition of 0.5% wt. (optimal loading) of potassium (K) to Ir/Al_2O_3 in combination with oxygen excess, enhances the N_2O adsorption and its concomitant dissociation, whereas it promotes the formation of $Ir^{\delta+}$ species, in which desorption of adsorbed oxygen species is facilitated.

- The de-N_2O performance is negatively affected upon increasing K loading under oxygen deficient conditions.

- No further promotion can be achieved by combining structural and surface promoters, implying that the optimum surface chemistry, and in turn de-N_2O performance, can be achieved either by surface or structural modifiers.

Effect of thermal treatment on the de-N$_2$O performance of Ir/γ- Al$_2$O$_3$ catalysts:

- Increase of calcination temperature (600°C, 800°C) results in formation of inactive IrAl$_x$O$_y$ phase.

- Optimum de-N$_2$O performance, in terms of activity and stability, was obtained for the low temperature treated catalyst (400°C).

Effect of SO$_2$ and H$_2$O inhibitors on the de-N$_2$O performance of Ir-based catalysts:

- The deactivation caused by SO$_2$ is a permanent phenomenon, while the inhibition caused by H$_2$O is reversible.

- The accumulation of sulphur compounds into the catalyst surface is considered responsible for the SO$_2$-induced deactivation.

- The extent of SO$_2$ deactivation is strongly dependent on support composition, being more intense for Ir/AlCe rather than Ir/Al catalysts due to the formation of Al$_2$(SO$_4$)$_3$ and Ce(SO$_4$)$_2$ compounds.

- The inhibition caused by the water presence in the feed stream is attributed to the competitive adsorption of H$_2$O with N$_2$O on the catalysts surface.

In Table VII the de-N$_2$O performance of the most effective Ir-based catalysts, prepared in the present study, is compared with that of the literature reported noble metal-based catalysts.

Table VII: N$_2$O conversion performance (in the presence of O$_2$) of the optimum Ir catalysts in comparison to those reported in the literature.

Catalyst	Reaction Conditions	T$_{50}$ (^{o}C)	Ref.
2% wt. Rh/Al$_2$O$_3$	500 ppm N$_2$O + 5% vol. O$_2$; GHSV~ 30,000 cm^3 g^{-1} h^{-1}	350	[1]
2% wt. Ru/Al$_2$O$_3$	500 ppm N$_2$O + 5% vol. O$_2$; GHSV~ 30,000 cm^3 g^{-1} h^{-1}	370	[1]
2% wt. Ru/Al$_2$O$_3$	500 ppm N$_2$O + 5% vol. O$_2$; GHSV~ 56,000 h^{-1}	430	[2]
0.5% wt. Ir/Al$_2$O$_3$-CeO$_2$	1000 ppm N$_2$O + 2% vol. O$_2$; GHSV~ 40,000 h^{-1}	500	[3], *This work*
0.5% wt. Ir(0.5% wt. K)/Al$_2$O$_3$	1000 ppm N$_2$O + 2% vol. O$_2$; GHSV~ 40,000 h^{-1}	490	[4], *This work*
0.5% wt. Ir/Al$_2$O$_3$ (400°C)	1000 ppm N$_2$O + 2% vol. O$_2$; GHSV~ 40,000 h^{-1}	430	*This work*
0.5% wt. Ir/Al$_2$O$_3$ (600°C)	1000 ppm N$_2$O + 2% vol. O$_2$; GHSV~ 40,000 h^{-1}	470	*This work*
0.5% wt. Ir/Al$_2$O$_3$ (800°C)	1000 ppm N$_2$O + 2% vol. O$_2$; GHSV~ 40,000 h^{-1}	490	*This work*

The comparison is performed in terms of $T_{50\%}$, i.e., the temperature required for 50% conversion of N_2O. Although, the comparison is not straight forward due to the great variations in reaction conditions among the different research groups, a general overview can be obtained. It is evident that Rh and Ru-based catalysts, may demonstrate lower T_{50} temperatures, due to their excellent intrinsic characteristics. However, the lower cost of iridium metal, the lower metal loading (0.5% wt.) as compared to the particularly expensive Rh-based catalysts can counter balance their somehow inferior performance.

REFERENCES

[1] Christoforou S.C., Efthimiadis E.A., Vasalos I.A., "Catalytic Conversion of N_2O to N_2 over Metal-Based Catalysts in the Presence of Hydrocarbons and Oxygen", Catalysis Letters 79 (2002) 137.

[2] Komvokis V.G., Marnellos G.E., Vasalos I.A., Triantafyllidis K.S., "Effect of pretreatment and regeneration conditions of Ru/γ-Al_2O_3 catalysts for N_2O decomposition and/or reduction in O_2-rich atmospheres and in the presence of NO_X, SO_2 and H_2O", Applied Catalysis B: Environmental 89 (2009) 627-634.

[3] Pachatouridou E., Papista E., Delimitis A., Vasiliades M.A., Efstathiou A.M., Amiridis M.D., Alexeev O.S., Bloom D., Marnellos G.E., Konsolakis M., Iliopoulou E., "N_2O decomposition over ceria-promoted Ir/Al_2O_3 catalysts: The role of ceria", Applied Catalysis B 187 (2016) 259-268.

[4] Papista E., Pachatouridou E., Goula M.A, Marnellos G.E., Iliopoulou E., Konsolakis M., Yentekakis I.V., "Effect of alkali promoters (K) on nitrous oxide abatement over Ir/Al_2O_3 catalysts", Topics in Catalysis 59 (2016) 1020-1027.

FUTURE DIRECTIONS

The present thesis focused on the development of technologically advanced-in terms of design, composition, cost and efficiency-catalytic materials, which could abate N_2O and/or NO_x from combustion flue gases. Since the emission control is an important environmental issue, further investigation is required. In this regard, future extensions to the current presented work include the following:

- It is evident that in our days the simultaneous reduction of N_2O and NO_x is an issue of major environmental importance, comprising one of the most challenging fields in heterogeneous catalysis. Only a few studies are dealing with the simultaneous abatement both pollutants, especially under realistic exhaust conditions (e.g. excess oxygen, presence of unburned hydrocarbons, SO_2 and H_2O).
- Further surface chemistry and mechanistic studies by means of advanced characterization techniques (e.g., *in situ* DRIFTS studies) in order to gain insight into the impact of structural/surface promoters on the de-N_2O process over noble metals-based catalysts.
- Impact of preparation method (e.g., sol-gel, hydrothermal) and metal precursor salt (e.g., Cl-free precursor), on the solid state properties and the de-N_2O performance of as prepared catalysts.

APPENDIX
Basic Principles of Characterization Techniques
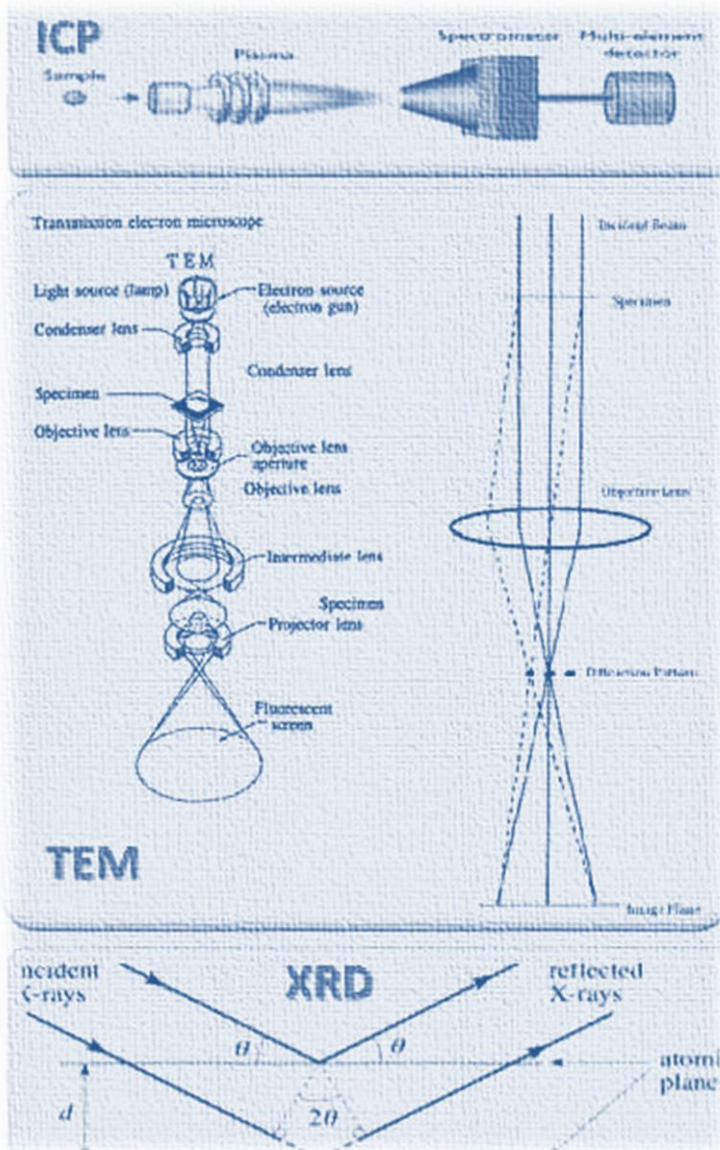
A.I.1 *Inductively Coupled Plasma- Atomic Emission Spectroscopy (ICP-AES)*

Plasma spectrometry techniques, namely Inductively Coupled Plasma-Atomic Emission Spectrometry (ICP-AES) and Inductively Coupled Plasma-Mass Spectrometry (ICP-MS), are widely used in the analytical laboratories, mainly because of their low limits of detection (LOD), high sensitivity, precision and analytical throughput. In these techniques, the analytical response depends directly on the number of analyte atoms present in the plasma and, therefore, on the analyte concentration in the sample. In ICP-AES, the radiation generated is finally measured using an appropriate detection system. In ICP-MS, analyte ions are extracted from the plasma and then directly registered [1].

Plasmas have been defined as highly ionized gases in which the number of free electrons is approximately equal to the number of positive ions. The inductively coupled plasma is a special type of plasma produced in a gas (usually argon) at atmospheric pressure, sustained by inductively coupling energy from a high frequency field. The field is typically applied by an induction coil with an accurrent at frequencies of about 30 MHz and power levels of 1000-2000 W. The temperature reached in the plasma ranges from 6000 to 10000 K, which is suitable for the atomization excitation and ionization of elemental species [2].

Inductively Coupled Plasma-Mass Spectrometry (ICP-MS) has become common practice in recent years for ultra-sensitive detection of trace metal- and metalloid-containing compounds. For identification of those compounds that are detected by ICP-MS, Electrospray Ionization-Mass Spectrometry (ESI-MS) has been gaining increasing popularity. Because traditional ESI-MS reveals only the molecular weight of a compound, Electrospray Ionization Tandem-Mass Spectrometry (ESI-MS/MS) has been increasingly used for structural characterization. ICP-MS, ESI-MS, and ESI-MS/MS provide complementary information, and when all three techniques are utilized for analysis of a sample, a complete picture of the species distribution for a given element within that sample can be obtained [3].

Inductively Coupled Plasma-Atomic Emission Spectrometry (ICP-AES) is one of the most common techniques for elemental analysis. Its high specificity, multi-element capability and good detection limits result in the use of the technique in a large variety of applications. All kinds of dissolved samples can be analyzed, varying from

solutions containing high salt concentrations to diluted acids. A plasma source is used to dissociate the sample into its constituent atoms or ions, exciting them to a higher energy level. They return to their ground state by emitting photons of a characteristic wavelength depending on the element present. This light is recorded by an optical spectrometer. When calibrated against standards the technique provides a quantitative analysis of the original sample. Fig. A.I.1 presents a schematic of an ICP-AES. In the ICP-AES a plasma source is used to make specific elements emit light, after which a spectrometer separates this light in the characteristic wavelengths [4].
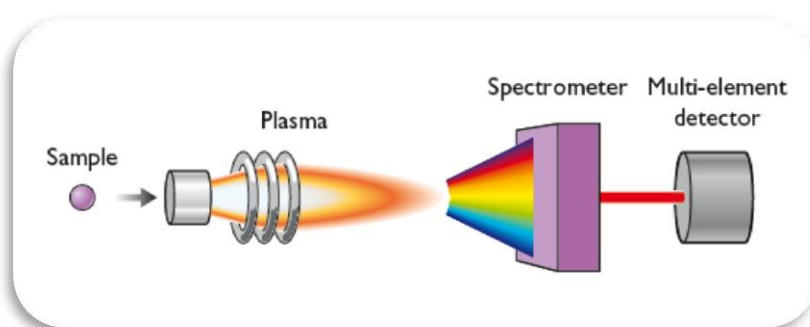

Figure A.I.1: Schematic of an ICP-AES [4].

Usually, the sample is supplied as a liquid solution because of its homogeneity, ease of handling and the possibility of preparing calibration standards. In this case, the main components of the sample introduction system are (Fig. A.I.2) [1, 4]:

(i) A nebulizer, which spreads out the liquid bulk generating an aerosol;

(ii) A spray chamber, which filters the aerosol and transports it to the plasma;

(iii) A desolvation system to reduce the mass of solvent reaching the plasma; and

(iv) An injector tube to introduce the aerosol into the plasma base.

A.I.2 N_2 Physisorption (BET)

Knowledge of morphological parameters allows understanding of catalyst evolution during preparation procedure and gives a feedback, useful for modifying the method to obtain the desired results. In the same way, knowledge of morphological

parameters is useful to comprehend the catalytic behavior in the reaction environment.
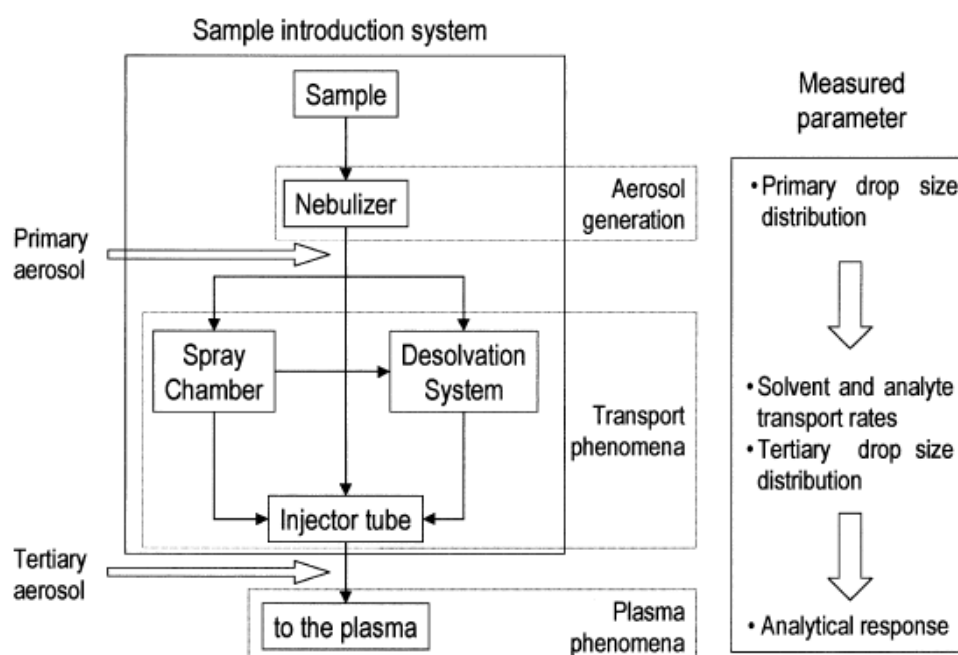

Figure A.I.2: Scheme of the sample-introduction system in plasma spectrometry [1].

On one hand the catalytic process takes place on the surface of the catalyst, and then its area strongly affects the catalytic activity. On the other hand, to reach the surface, the reagent molecules must run across the porous system, as well as the reaction products have to leave the catalyst. Mass transfer process inside the granules depends on pore size (bulk diffusion in macropores, Knudsen diffusion in mesopores and molecular diffusion in micropores) and tortuosity factor [5].

The International Union of Pure and Applied Chemistry (IUPAC) proposed to classify pores by their internal pore width (the pore width defined as the diameter in case of a cylindrical pore and as the distance between opposite walls in case of a slit pore). The pores are classified in three different classes depending on their size [5, 6]:

i. Micropores (size <2 nm), ultramicropores (size <0.7 nm);

ii. Mesopores (2 nm < size <50 nm); and

iii. Macropores (size >50 nm).

Pores can have a regular or, more commonly, an irregular shape. The most similar geometric form is used to represent pore shape: cylinders (in some oxides like

alumina and magnesia), slits (in activated carbons and clays) and voids between connected solid spheres (in silica and many solids obtained from gels). Cylinders (size diameter) and slits (size distance between walls) are the most widely used models being simple to handle. These models assume that each pore has a uniform size along the length, but very often they are ink-bottle shaped (pore body larger than pore mouth) or funnel shaped (the contrary): the physical meaning of the term pore size depends on the method used to investigate the porous texture. Last, catalyst granules contain generally pores of different size, so we must consider the pore size distribution that is the pore volume against pore size. Pores can be closed (not accessible from the external), blind (open at only one end), or through (open at both ends). Each pore can be isolated or, more frequently, connected to other pores to form a porous network [5].

IUPAC published in 1985 a classification of six sorption isotherms [6], based upon an extensive literature survey, and performed by Brunauer, Deming and Teller (BDDT) [7].

Nitrogen adsorption at boiling temperature (77 K) represents the most widely used technique to determine catalyst surface area and to characterize its porous texture. Starting point is the determination of the adsorption isotherm that is the nitrogen adsorbed volume against its relative pressure. Among these six sorption isotherms (Fig. A.I.3), only four are usually found in catalyst characterization; type I on microporous materials, type IV are typical for mesoporous materials, type II on non-porous or macroporous materials and type VI on uniform ultramicroporous materials [5, 6].

The model, developed by Brunauer, Emmet and Teller in 1940s [8, 9], still remains the most diffuse tool to determine the monolayer volume (V_m) of the adsorbate, and then the surface area (A_s) of solids by the equation A.1:

$$A_s = \left(\frac{V_m}{22414}\right) N_a \, \sigma \qquad \qquad \text{(A.1)}$$

Where N_a is Avogadro number and σ the area covered by one nitrogen molecule. The σ value generally accepted is 0.162 nm^2.
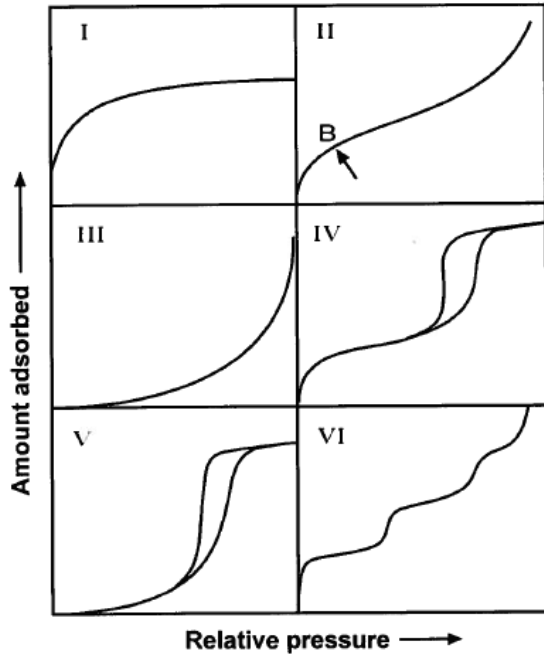
Figure A.I.3:

IUPAC classification of sorption isotherms [1].

V_m can be estimated by the three parameters BET equation, developed assuming that:

(i) The heat of adsorption of first monolayer is constant (the surface is uniform as concerns the adsorption);

(ii) The lateral interaction of adsorbed molecules is negligible;

(iii) The adsorbed molecules can act as new adsorption surface and the process can repeat itself;

(iv) The heat of adsorption of all monolayers but the first is equal to the heat of condensation.

According to the model the adsorbed volume (V_{ads}) depends on relative pressure (p/p_s), V_m, a parameter (c) related to heat of adsorption and liquefaction (high strong adsorbate - adsorbent interaction), a parameter (n) formally related to the mean number of layer that can be formed on the solid. The equation (A.2, three parameters BET equation) has the form:

$$V_{ads} = V_m \frac{cp/p_s}{1 - p/p_s} \frac{1 - (n+1)\,(p/p_s)^{\,n} + n\,(p/p_s)^{\,n+1}}{1 + (c-1)(p/p_s) - c\,(p/p_s)^{\,n+1}} \qquad (A.2)$$

If n → ∞, the equation assumes the following form, known as two parameters BET equation (A.3):

$$V_{ads} = V_m \frac{cp/p_s}{(1-p/p_s)\,(1+(c-1)p/p_s)}$$

(A.3)

Practically this equation is suitable for n>6 (macroporous and larger mesoporous solids): in this range the differences between the two forms of BET equation do not exceed the experimental error [5].

The methods that are used in order to determine the morphological characteristics of catalytic materials are [5]:

(i) BET method: for the measurement of total surface area;

(ii) T-plot: for surface area external to micropores, as well for total micropore volume;

(iii) Incipient wetness method, picnometry, Gurvitsch method (if applicable): in order to measure the total pore volume;

(iv) Gurvitsch volume method: to determine the total micropore and mesopore volume;

(v) BJH method, mercury porosimetry: to measure the mesopore volume and mesopore size distribution;

(vi) Mercury porosimetry: for the determination of macropore volume and macropore size distribution.

A.I.3 X-ray Diffraction (XRD)

X-ray Diffraction (XRD) is a powerful technique used to uniquely identify the crystalline phases present in materials and to measure the structural properties (strain state, grain size, epitaxy, phase composition, preferred orientation, and defect structure) of these phases. XRD is also used to determine the thickness of thin films and multilayers, and atomic arrangements in amorphous materials (including polymers) and at interfaces [10].

X-ray powder methods are based upon the fact that an X-ray diffraction is unique for each crystalline substance. It is the only analytical method that is providing qualitative and quantitative information about the compounds present in a solid sample. For analytical diffraction studies the sample is ground to a fine homogeneous powder. When an X-ray beam traverses the material a significant number of the particle can be oriented in such a way to fulfill Bragg condition for reflection. Diffraction patterns are obtained by automatic scanning. The identification of a species from its diffraction patterns is based upon the position of lines and their relative intensities [11].
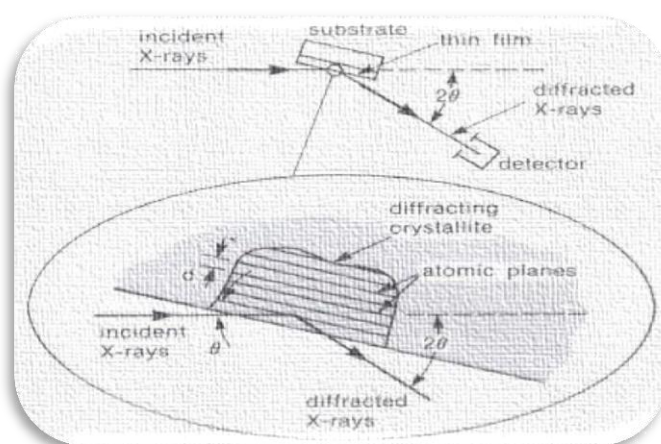

Figure A.I.4: Basic features of a typical XRD experiment [11].

Figure A.I.4 shows the basic features of an XRD experiment, where the diffraction angle 2ϑ is the angle between the incident and diffracted X-rays. In a typical experiment, the diffracted intensity is measured as a function of 2ϑ and the orientation of the specimen, which yields the diffraction pattern. The X-ray wavelength λ is typically 0.7-2 Å, which corresponds to X-ray energies (E=12.4 keV/λ) of 6-17 keV [11].

W.H. Bragg and his son W.L. Bragg developed a relationship in 1913 (A.4) to explain why the cleavage faces of crystals appear to reflect X-ray beams at certain angles of incidence (theta, ϑ) [12].

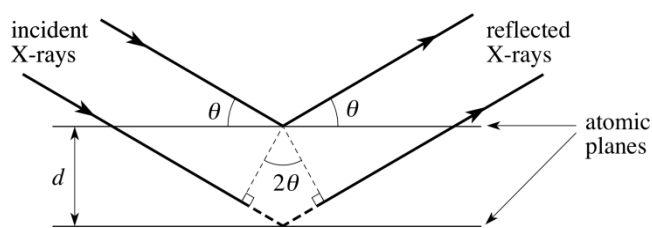$$n\lambda = 2d_{hkl}\sin\theta \qquad (Bragg's\ Law) \qquad\qquad (A.4)$$

Figure A.I.5: Bragg reflection.

The variable d_{hkl} is the distance between atomic layers in a crystal, the variable lambda λ is the wavelength of the incident X-ray beam and n is an integer [12].

The crystallinity of the sample can be deduced from the peaks position and peaks width, which decreases with increasing crystallinity. The Scherrer equation (A.5) can be used to determine the average size of the crystals (D) for the crystalline solid:

$$D = \frac{K\lambda}{\beta \cos\theta} \qquad\qquad (A.5)$$

Where K is the Scherrer constant or form factor and β is the peak width at half height [13].

A.I.4 Temperature Programmed Methods (TPM)

Temperature-programmed desorption (TPD), reduction (TPR) and oxidation (TPO) are thermo-analytical techniques for characterizing chemical interactions between gaseous reactants and solid substances, as well are considered as the most commonly used tools for characterizing heterogeneous catalysts. The data collected by these techniques are commonly interpreted on a qualitative basis or by utilizing simple, approximate kinetic methods. However, temperature-programmed techniques can also be regarded as transient response techniques and the experimental data can be utilized for dynamic modelling [14].

TPD was reported by Amonomiya and Cvetanovic [15] in 1963 and effectively was an extension to powdered solids of the flash desorption technique for the study of desorption of gases from heated metallic filaments in high vacuum. In TPD studies a solid previously equilibrated with an adsorbing gas is submitted to a programmed

temperature rise and the amount of desorbing gas is continuously monitored. TPR was inspired by the TPD technique and proposed in its present form by Robertson et al. [16] in 1975. In TPR the oxidic catalyst precursor is submitted to a programmed temperature rise under a flow of reducing gas mixture and the consumption of the reducing agent is continuously monitored. The temperature programmed techniques have also been extended to cover oxidation, sulphidation, methanation, hydrogenation, gasification, carburization and other catalytic surface reactions (TPO, TPS, TPM, TPH, TPG, TPC, and TPSR, respectively). Alongside catalyst characterization, temperature-programmed (TP) techniques can be applied to mimic pretreatment procedures related to the operation of catalytic processes [17]. The types of information obtainable from the most common TP techniques are summarized in Table A.I.1.

Table A.I.1: Types of information obtainable from TP techniques [15].

TPD: Temperature-Programmed Desorption
Characterization of adsorptive properties of materials
Characterization of surface acidity
Temperature range of adsorbate release, temperatures of rate maxima
Total desorbed amount, adsorption capacity, metal surface area and dispersion
Surface energetic heterogeneity, binding states and energies of adsorbed molecules
Mechanism and kinetics of adsorption and desorption
TPR: Temperature-Programmed Reduction
Characterization of redox properties of materials, 'fingerprint' of sample
Temperature range of consumption of reducing agent, temperatures of rate maxima
Total consumption of reducing agent, valence states of metal atoms in zeolites and metal oxides
Interaction between metal oxide and support
Indication of alloy formation in bimetallic catalysts

Mechanism and kinetics of reduction

TPO: Temperature-Programmed Oxidation
Characterization of redox properties of metals and metal oxides
Characterization of coke species in deactivated catalysts
Total coke content in deactivated catalysts
Mechanism and kinetics of oxidation reactions

In TP techniques a small catalyst sample (typically 10-500 mg) is placed in a reactor system equipped with a programmable furnace. The reactor is a quartz tube fixed bed (i.d. typically 2-6 mm). In TP runs the pretreated sample is exposed to continuous flow of inert or reactive gas mixture, while the temperature is raised according to a predetermined program. The sample temperature and the outlet gas composition are continuously monitored. Typical detectors for TP are the thermal conductivity detector (TCD) and mass spectrometer (MS). Use and calibration of the TCD is straightforward, but it is applicable only for binary mixtures of gases. MS provides total monitoring of the outlet gas composition. Careful selection of the experimental conditions is essential for novel samples to ensure sufficient detector sensitivity and well-defined mass and heat transfer. Intraparticle diffusion limitations are avoided if possible, the reactor is preferably operated in differential reactor mode and gas-phase reactant exhaustion is prevented [15].

A.I.5 Transmission Electron Microscopy (TEM)

The transmission electron microscope is a very powerful tool for material science (Fig. A.I.6a). A high energy beam of electrons is shone through a very thin sample, and the interactions between the electrons and the atoms can be used to observe features such as the crystal structure and features in the structure like dislocations and grain boundaries. Chemical analysis can also be performed. TEM can be used to study the growth of layers, their composition and defects in semiconductors. High resolution can be used to analyze the quality, shape, size and density of quantum wells, wires and dots.

The TEM operates on the same basic principles as the light microscope but uses electrons instead of light. Because the wavelength of electrons is much smaller than that of light, the optimal resolution attainable for TEM images is many orders of magnitude better than that from a light microscope. Thus, TEMs can reveal the finest details of internal structure - in some cases as small as individual atoms.
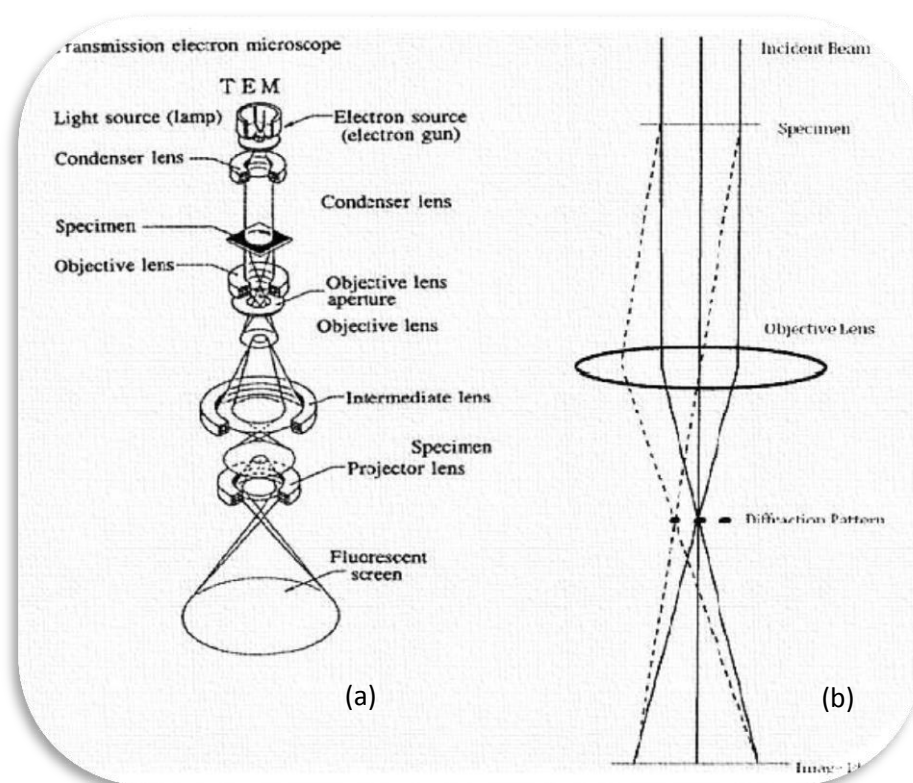

Figure A.I.6: (a) General layout of a TEM describing the path of electron beam in a TE (Taken from JEOL 2000FX Handbook); (b) A ray diagram for the diffraction mechanism in TEM.

The beam of electrons from the electron gun is focused into a small, thin, coherent beam by the use of the condenser lens. This beam is restricted by the condenser aperture, which excludes high angle electrons. The beam then strikes the specimen and parts of it are transmitted depending upon the thickness and electron transparency of the specimen. This transmitted portion is focused by the objective lens into an image on phosphor screen or charge coupled device (CCD) camera. Optional objective apertures can be used to enhance the contrast by blocking out high-angle diffracted electrons. The image then passed down the column through the intermediate and projector lenses, is enlarged all the way. The image strikes the

phosphor screen and light is generated, allowing the user to see the image. The darker areas of the image represent those areas of the sample that fewer electrons are transmitted through while the lighter areas of the image represent those areas of the sample that more electrons were transmitted through.

Fig. A.I.6b shows a simple sketch of the path of a beam of electrons in a TEM from just above the specimen and down the column to the phosphor screen. As the electrons pass through the sample, they are scattered by the electrostatic potential set up by the constituent elements in the specimen. After passing through the specimen they pass through the electromagnetic objective lens which focuses all the electrons scattered from one point of the specimen into one point in the image plane. In addition, Fig. A.I.6b presents a dotted line where the electrons scattered in the same direction by the sample are collected into a single point. This is the back focal plane of the objective lens and is where the diffraction pattern is formed.

A TEM specimen must be thin enough to transmit sufficient electrons to form an image with minimum energy loss. Therefore specimen preparation is an important aspect of the TEM analysis. For most electronic materials, a common sequence of preparation techniques is ultrasonic disk cutting, dimpling, and ion-milling.

Dimpling is a preparation technique that produces a specimen with a thinned central area and an outer rim of sufficient thickness to permit ease of handling. Ion milling is traditionally the final form of specimen preparation. In this process, charged argon ions are accelerated to the specimen surface by the application of high voltage. The ion impingement upon the specimen surface removes material as a result of momentum transfer [18, 19].

A.I.6 *Infrared Spectroscopy (FTIR, DRIFTS)*

Infrared spectroscopy is certainly one of the most important analytical techniques available to today's scientists. One of the great advantages of infrared spectroscopy is that virtually any sample in virtually any state may be studied. Liquids, solutions, pastes, powders, films, fibers, gases and surfaces can all be examined with a judicious choice of sampling technique. As a consequence of the improved instrumentation, a variety of new sensitive techniques have now been developed in order to examine formerly intractable samples. Infrared spectrometers have been

commercially available since the 1940s. At that time, the instruments relied on prisms to act as dispersive elements, but by the mid-1950s, diffraction gratings had been introduced into dispersive machines.

Infrared spectroscopy is a technique based on the vibrations of the atoms of a molecule. An infrared spectrum is commonly obtained by passing infrared radiation through a sample and determining what fraction of the incident radiation is absorbed at a particular energy. The energy at which any peak in an absorption spectrum appears corresponds to the frequency of a vibration of a part of a sample molecule [20].

The most significant advances in infrared spectroscopy have come about as a result of the introduction of Fourier-transform spectrometers. This type of instrument employs an interferometer and exploits the well-established mathematical process of Fourier-transformation. Fourier-transform infrared (FTIR) spectroscopy has dramatically improved the quality of infrared spectra and minimized the time required to obtain data. In addition, with constant improvements to computers, infrared spectroscopy has made further great strides [20].

However, in some cases IR technique is currently limited to the analysis of samples transparent to IR radiation and formed into the shape of a self-supported pellet. Some samples cannot be analyzed due to the lack of mechanical strength and/or transmission. This applies in particular to hydrated samples or certain catalysts used to combat automotive pollution. The use of a diffuse reflection accessory and the associated DRIFTS (Diffuse Reflectance Infrared Fourier Transform Spectroscopy) technique helps to circumvent these obstacles and to analyze materials under reactive atmosphere [21].

Fourier Transform Infrared Spectroscopy (FTIR)

Fourier-transform infrared (FTIR) spectroscopy is based on the idea of the interference of radiation between two beams to yield an interferogram. The latter is a signal produced as a function of the change of path length between the two beams. The two domains of distance and frequency are interconvertible by the mathematical method of Fourier-transformation.

The basic components of an FTIR spectrometer are shown schematically in Fig. A.I.7. The radiation emerging from the source is passed through an interferometer to the sample before reaching a detector. Upon amplification of the signal, in which high-frequency contributions have been eliminated by a filter, the data are converted to digital form by an analog-to-digital converter and transferred to the computer for Fourier-transformation.
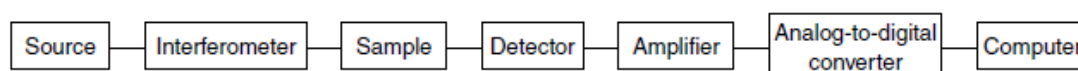

Figure A.I.7: Basic components of an FTIR spectrometer [20].

FTIR spectroscopy of adsorbed probe molecules is one of the most available and well developed methods for studying the composition and structure of the surface functional groups of supported metal catalysts. As the vibrational spectrum reflects both the properties of the molecule as a whole and the characteristic features of separate chemical bonds, FTIR spectroscopy offers the fullest possible information on the perturbation experienced by a molecule on contact with the solid surface, and often determines the structure of adsorption complexes and of surface compounds. Examination of supported metal catalysts deals with two types of surfaces strongly differing in their properties: surface of a support and surface of a metal-containing particle. Various species can reside on the support surface: hydroxyl groups of different nature; Lewis acid sites (coordinately unsaturated surface cations); base sites (bridging oxygen atoms or oxygen atoms of OH groups); structures formed by impurity anions that remain after the synthesis (sulfate, nitrate and ammonia groups) or form upon contacting with air (carbonate-carboxylate structures).

Various spectroscopic probe molecules are widely used for characterization of Lewis and Brønsted acid sites on the surfaces of oxide catalysts. Among such probes are strong bases: amines, ammonia and pyridine, and weak bases: carbon oxide, carbon dioxide and hydrogen. Being a weaker base than ammonia, pyridine interacts with the sites widely varying in acidity. However, within each type of Lewis acid site, which is determined with pyridine as a probe molecule, there are distinctions in

acidity that cannot be revealed with the use of strong bases. In this connection, very advantageous is the adsorption of weak bases like CO. The application of such probe molecules as CO or pyridine makes it possible to estimate both the concentration and the acid strength of OH groups and Lewis acid sites in zeolites, oxide and other systems. Concentration of the surface groups accessible for identification by FTIR spectroscopy is above 0.1 μmol/g [22].

Diffuse Reflectance Fourier Transform Infrared Spectroscopy (DRIFTS)

DRIFTS is a versatile technique for analyzing nontransparent samples, powders, roughened surfaces and coating. It offers the advantages of easy sample preparation and applicability to analyze samples at elevated temperature and pressure [21]. Diffuse reflectance relies upon the focused projection of the spectrometer beam into the sample where it is reflected, scattered and transmitted through the sample material (shown in Fig. A.I.8). The back reflected, diffusely scattered light (some of which is absorbed by the sample) is then collected by the accessory and directed to the detector optics. Only the part of the beam that is scattered within a sample and returned to the surface is considered to be diffuse reflection.
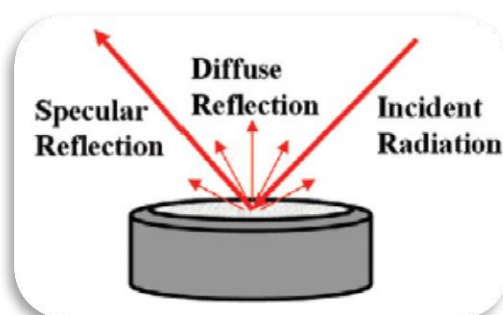
Figure A.I.8: Mechanisms generating the diffuse reflection of a powder [23].

Some powders may be analyzed by diffuse reflectance as neat samples (coal samples, soil samples, diffuse coatings on a reflective base). Usually, the sample must be ground and mixed with a non-absorbing matrix such as KBr. The sample to matrix ratio should be between 1 to 5% (by weight). Diluting ensures a deeper penetration of the incident beam into the sample which increases the contribution of the scattered component in the spectrum and minimizes the specular reflection

component. The specular reflectance component in diffuse reflectance spectra causes changes in band shapes, their relative intensity, and, in some cases, it is responsible for complete band inversions (Restrahlen bands). Dilution of the sample with a non-absorbing matrix minimizes these effects (particle size and sample loading mechanics also play an important role) [23].

REFERENCES

[1] Mora J., Maestre S., Hernandis V., Todoli J.L., "Liquid-sample introduction in plasma spectrometry", Trends in Analytical Chemistry 22 (2003) No. 3.

[2] Ponce de Leòn C.A., Montes-Bayòn M., Caruso J.A., "Review: Elemental speciation by chromatographic separation with inductively coupled plasma mass spectrometry detection", Journal of Chromatography A 974 (2002) 1-21.

[3] Rosen A.L., Hieftje G.M., "Review: Inductively coupled plasma mass spectrometry and electrospray mass spectrometry for speciation analysis: applications and instrumentation", Spectrochimica Acta Part B 59 (2004) 135-146.

[4] Philips Innovation Services-Materials Analysis "Inductively Coupled Plasma-Atomic Emission Spectrometry (ICP-AES)", Technical Note 12, September (2013).

[5] Leofanti G., Padovan M., Tozzola G., Venturelli B., "Surface area and pore texture of catalysts", Catalysis Today 41 (1998) 207-219.

[6] Sing K.S.W., Everett D. H., Haul R.A.W., Moscou L., Pierotti R.A., Rouquerol J., Siemieniewska T., "Reporting Physisorption Data For Gas/Solid Systems with Special Reference to the Determination of Surface Area and Porosity", Pure & Applied Chemistry 57, (1985) 603-619.

[7] Brunauer S., Deming L.S., Deming W.E., Teller E., "On a theory of the van der Waals adsorption of gases", Journal of The American Chemical Society 62 (1940) 1723-1732.

[8] Brunauer S., Emmett P.H., Teller E., "Adsorption of Gases in Multimolecular Layers", Journal of the American Chemical Society 60 (1938) 309-319.

[9] Brunauer S., "The Adsorption of Gases and Vapors", University Press, Oxford, (1945).

[10] Brundle C.R., Evans C.A., Wilson S., "Encyclopedia of materials characterization", Chapter 4, (1992).

[11] Klug H.P., Alexander L.E., "X-ray Diffraction Procedures for Poly Crystalline and Amorphous Materials", 2nd Edition, John Wiley & Sons, New York (1974).

[12] Bragg W.H., Bragg W.L., "X rays and crystal structure", London (1915).

[13] Langford J.I., Wilson A.J.C., "Scherrer after Sixty Years: A Survey and Some New Results in the Determination of Crystallite Size", Journal of Applied Crystallography 11 (1978) 102-113.

[14] Kanervo J., "Kinetic analysis of temperature-programmed reactions", PhD Thesis, Helsinki University of Technology (2003).

[15] Amenomiya Y., Cvetanovic R.J., "Application of flash-desorption method to catalyst studies. III. Propylene alumina system and surface heterogeneity", Journal of Physical Chemistry 67 (1963) 2705-2708.

[16] Robertson S.D., McNicol B.D., De Baas J.H., Kloet S.C., Jenkins J.W., "Determination of reducibility and identification of alloying in copper-nickel-on-silica catalysts by temperature-programmed reduction", Journal of Catalysis 37 (1975) 424-431.

[17] Kapteijn F., Moulijn J.A., Tarfaoui A., "Catalyst characterization and mimicking pre-treatment procedures by temperature-programmed techniques. In Catalysis: An Integrated Approach", Studies in Surface Science and Catalysis 123 (1999) 525-541.

[18] Williams D.B., Carter C.B., "Transmission electron microscopy", Plenum (1996).

[19] Hirsch P., "Electron microscopy of thin crystals", Butterworths (1965).

[20] Stuart B., "Infrared Spectroscopy: Fundamentals and Applications", Wiley (2004).

[21] Armaroli T., Bécue T., Gautier S., "Diffuse Reflection Infrared Spectroscopy (DRIFTS): Application to the *in situ* Analysis of Catalysts", Oil & Gas Science and Technology 59 (2004) 215-237.

[22] Belskaya O.B., Danilova I.G., Kazakov M.O., Mironenko R.M., Lavrenov A.V., Likholobov V.A., "FTIR Spectroscopy of Adsorbed Probe Molecules for Analyzing the Surface Properties of Supported Pt (Pd) Catalysts", Chapter 7, Infrared Spectroscopy-Materials Science, Engineering and Technology (2012) 149.

[23] Pike Technologies, "Diffuse Reflectance-Theory and Applications", Application Note (2011).

Curriculum Vitae
Pachatouridou Eleni

Personal Information

First Name: Eleni   _Phone:_ +302310498352 (office)   _Address:_ Filellinon 24
Last Name: Pachatouridou   +306989784349 (mobile)   54645, Martiou 25th
Date of Birth: August 6, 1988   _E-mail:_ elenipachat@gmail.com   Thessaloniki, Greece

Education

_2014-2017_   **PhD: "Structure-Property Relationships and Stability Studies on Multi-Promoted Catalytic Systems for NOx and/or N_2O Abatement"**
School of Production Engineering & Management, Technical University of Crete (TUC)/ Chemical Process and Energy Resources Institute (CPERI), Centre for Research and Technology Hellas (CERTH)

_2012-2014_   **Master in Processes & Advanced Materials Technology: "Deactivation of FCC Catalysts from Ni"**
Faculty of Chemical Engineering, Aristotle University of Thessaloniki (AUTH)/
Chemical Process and Energy Resources Institute (CPERI-CERTH)

_2006-2012_   **Diploma in Chemistry**
Department of Chemistry, University of Ioannina (UOI)

Work Experience

Nov 2015- Today
     CPERI-BASF Collaboration Agreement
     Chemical Process and Energy Resources Institute (CPERI-CERTH)

Mar 2015-Oct 2015
     National Research Project **KREPIS**
     Chemical Process and Energy Resources Institute (CPERI-CERTH)

Jan 2013- Feb 2015
     National Research Project **Thales**
     Department of Production Engineering & Management (TUC)/
     Chemical Process and Energy Resources Institute (CPERI-CERTH)

Jan 2012- Dec 2012
     Trainee/ Internship
     Chemical Process and Energy Resources Institute (CPERI-CERTH)

Research Experience

Aug 28-Sep 9, 2014
     University of South Carolina
     Department of Chemical Engineering, Carolina, US
     Characterization of catalysts for the reduction of N_2O and/or NOx emissions from the flue gases of stationary or/and mobile sources, via X-Ray Photoelectron Spectroscopy (XPS), Diffuse Reflectance Infrared Fourier Transform Spectroscopy (DRIFTS) and Scanning Transmission Electron Microscopy (STEM)

Feb 10-Feb 21, 2014
     University of Cyprus
     Department of Chemistry, Nicosia, Cyprus
     Characterization of catalysts for the reduction of N_2O and/or NOx emissions from the flue gases of stationary or/and mobile sources, via Diffuse Reflectance Infrared Fourier Transform Spectroscopy (DRIFTS)

Research Skills

Synthesis of Catalytic Materials- Techniques:
Co-precipitation
Impregnation
Hydrothermal

Characterization of Catalytic Materials- Methods:
Temperature Programmed Reduction/ Oxidation/ Desorption (TPX)
Thermogravimetric Analysis (TGA/DSC)
Fourier Transform Infrared Spectroscopy- Pyridine Adsorption (FTIR-Pyridine)
Diffuse Reflectance Infrared Fourier Transform Spectroscopy (DRIFTS)
And Conventional Methods: N_2 Physisorption (BET method), X-Ray Diffraction (XRD)

Catalysts Evaluation Tests:
Reduction/ Decomposition of SOx and NOx Emissions in a Bench-Scale Unit (DeSOx/ DeNOx Unit)

Other Research Areas:
Kinetics study of two different coked catalysts via Thermogravimetric Analysis (TGA) and Temperature Programmed Oxidation (TPO)

Languages

Greek: Native
English: Excellent reading and writing, very good oral skills (Cambridge 1st Certificate)
German: Basic Knowledge (1st Zertifikat Deutsch)
Russian: Good reading and writing, excellent oral skills

Other Skills

Computer Skills: ECDL Certificate, Excellent knowledge of Microsoft office (Excel, Word, PowerPoint)
Personal Skills: Analyzing and investigating nature, hardworking, team working, organization skills under pressure of deadlines

Publications in Scientific Journals

2017   **Impact of synthesis parameters on the solid state properties and the CO oxidation performance of ceria nanoparticles**
Maria Lykaki, **Eleni Pachatouridou**, Eleni Iliopoulou, Sonia A.C. Carabineiro, Michalis Konsolakis, *RSC Advances 7 (2017) 6160-6169*

2016   **Effect of alkali promoters (K) on nitrous oxide abatement over Ir/Al$_2$O$_3$ catalysts**
E. Papista, **E. Pachatouridou**, M.A. Goula, G.E. Marnellos, E. Iliopoulou, M. Konsolakis, I.V. Yentekakis, *Topics in Catalysis 59 (2016) 1020-1027*

A comparative study of the H$_2$-assisted selective catalytic reduction of nitric oxide by propene over noble metal (Pt, Pd, Ir)/γ-Al$_2$O$_3$ catalysts
M.A. Goula, N.D. Charisiou, K.N. Papageridis, A. Delimitis, E. Papista, **E. Pachatouridou**, E.F. Iliopoulou, G. Marnellos, M. Konsolakis, I.V. Yentekakis, *Journal of Environmental Chemical Engineering 4 (2016) 1629-1641*

N$_2$O decomposition over ceria-promoted Ir/Al$_2$O$_3$ catalysts: The role of ceria
E. Pachatouridou, E. Papista, A. Delimitis, M.A. Vasiliades, A.M. Efstathiou, M.D. Amiridis, O.S. Alexeev, D. Bloom, G.E. Marnellos, M. Konsolakis, E. Iliopoulou, *Applied Catalysis B 187 (2016) 259-268*

2015   **Nitrous Oxide Decomposition over Al$_2$O$_3$ Supported Noble Metals (Pt, Pd, Ir): Effect of Metal Loading and Feed Composition**
E. Pachatouridou, E. Papista, E.F. Iliopoulou, A. Delimitis, G. Goula, I.V. Yentekakis, G.E. Marnellos, M. Konsolakis, *Journal of Environmental Chemical Engineering 3 (2015) 815-821*

Nickel on alumina catalysts for the production of hydrogen rich mixtures via the biogas reforming reaction: Influence of the synthesis method
M. A. Goula, N. Charisiou, K. Papageridis, A. Delimitis, **E. Pachatouridou**, E. Iliopoulou
International Journal of Hydrogen Energy 40 (2015) 9183-9200

2014   **Comparing calcined and un-treated olivine as bed materials for tar reduction in Fluidized Bed gasification**
C. Christodoulou, D. Grimekis, K.D. Panopoulos, **E.P. Pachatouridou**, E.F. Iliopoulou, E. Kakaras, *Fuel Processing Technology 124 (2014) 275-285*

Citations: 42
H-index: 4

International Conferences

2017   Impact of synthesis parameters on the solid state properties and the CO oxidation performance of ceria nanoparticles
Maria Lykaki, **Eleni Pachatouridou**, Eleni Iliopoulou, Sonia A.C. Carabineiro, Michalis Konsolakis, EuropaCat, August 27-31, 2017, Florence, Italy (Submitted)

2016   Application of hierarchical bi-functional ZSM5 based catalysts to catalytic pyrolysis of biomass
E. Kantarelis, R. Javed, S. Stefanidis, **E. Pachatouridou**, A. Psarras, K. Kalogiannis, E. Iliopoulou, A. Lappas, *International Symposium on Catalysis for Clean Energy and Sustainable Chemistry, September 7-9, 2016, Madrid, Spain*

2015   Effect of alkali promoters (K) on nitrogen oxides abatement over Ir/Al$_2$O$_3$ catalysts
E. Papista, **E. Pachatouridou**, K.N. Papageridis, N.D. Charisiou, M.A. Goula, E. Iliopoulou, G. Marnellos, M. Konsolakis, I.V. Yentekakis, 10th International Congress on Catalysis and Automotive Pollution Control, October 2015, Brussels, Belgium

Effect of SO$_2$ on N$_2$O decomposition over iridium catalysts supported on ceria modified alumina
E. Pachatouridou, E.F. Iliopoulou, M. Konsolakis, I. Yentekakis, *EuropaCat, August 2015, Kazan, Russia*

2014   The effect of Ce$_{0.8}$La$_{0.2}$O$_{1.9}$ support modifiers on the microstructure and N$_2$O decomposition (de-N$_2$O) performance of γ-Al$_2$O$_3$ supported Ir catalysts
A. Delimitis, **E. Pachatouridou**, E. Papista, E.F. Iliopoulou, , G.E. Marnellos, M. Konsolakis, I. Yentekakis, *18th International Microscopy Congress, September 7-12, 2014, Prague, Czech Republic.*

Hydrogen production via biogas reforming over nickel-alumina catalysts. Effect of catalysts' synthesis method
M.A. Goula, O.A. Bereketidou, N.D. Charisiou, K.N. Papageridis, **E. Pachatouridou**, E.F. Iliopoulou, *8th International Conference on Environmental Catalysis, August 2014, Asheville, North Carolina, USA*

N_2O Decomposition over Structurally Promoted Ir/Al_2O_3 Catalysts
E.F. Iliopoulou, **E. Pachatouridou**, E. Papista, A. Delimitis, G.E. Marnellos, M. Konsolakis, I. Yentekakis, *8th International Conference on Environmental Catalysis, August 2014, Asheville, North Carolina, USA*

CO_2 effect on the performance of SOx reduction additives in Fluid Catalytic Cracking (FCC) regenerator
E. Pachatouridou, E.F. Iliopoulou, D.K. Iatridis, A.A Lappas, *12th International Conference: Protection and Restoration of the Environment, June-July 2014, Skiathos, Greece*

Nitrous oxide decomposition over Al_2O_3 supported noble metals (Pt, Pd, Ir): Effect of metal loading and feed composition
E. Papista, **E. Pachatouridou**, E.F. Iliopoulou, A. Delimitis, G. Goula, I.V. Yentekakis, G.E. Marnellos, M. Konsolakis, *13th International Conference on Clean Energy (ICCE-2014), June 2014, Istanbul, Turkey*

National Conferences

2017 **Ε. Παχατουρίδου**, Ε.Φ. Ηλιοπούλου, Μ. Κονσολάκης, Ι.Β. Γιεντεκάκης, *«Επίδραση θερμοκρασίας πύρωσης στην καταλυτική συμπεριφορά καταλυτών $Ir/γ-Al_2O_3$ κατά την διάσπαση του N_2O»*, 11ο Πανελλήνιο Συνέδριο Χημικής Μηχανικής, Μάιος 25-27, 2017, Θεσσαλονίκη.

Μ. Λυκάκη, **Ε. Παχατουρίδου**, Ε. Ηλιοπούλου, S. Carabineiro, Μ. Κονσολάκης, *«Υδροθερμική σύνθεση νανοσωματιδίων CeO_2: επίδραση στις φυσικοχημικές και καταλυτικές ιδιότητες μικτών οξειδίων CuO/CeO_2»*, 11ο Πανελλήνιο Συνέδριο Χημικής Μηχανικής, Μάιος 25-27, 2017, Θεσσαλονίκη.

2016 Μαρία Λυκάκη, **Ελένη Παχατουρίδου**, Ελένη Φ. Ηλιοπούλου, Sonia A.C. Carabineiro, Μιχάλης Κονσολάκης, *"Επίδραση της μεθόδου σύνθεσης στην επιφανειακή και καταλυτική συμπεριφορά νανο-δημητρίας"*, 14ο Πανελλήνιο Συμπόσιο Κατάλυσης, Οκτώβριος 13-15, 2016, Πάτρα.

2015 Ε. Πάπιστα, **Ε. Παχατουρίδου**, Ν. Κακλίδης, Τ. Κράια, Ε. Ηλιοπούλου, Ι. Γεντεκάκης, Γ.Ε. Μαρνέλλος και Μ. Κονσολάκης, *"Καταλυτική Διάσπαση του N_2O σε Καταλύτες Ir/Al_2O_3: επί της Επίδρασης των Δομικών Ενισχυτών και των Συνθηκών Αντίδρασης"*, 10ο Πανελλήνιο Συνέδριο Χημικής Μηχανικής, Ιούνιος 4-6, 2015, Πάτρα.

Ε. Πάπιστα, **Ε. Παχατουρίδου**, Ν. Κακλίδης, Α. Δελημήτης, Ε. Ηλιοπούλου, Γ. Γούλα, Ι. Γεντεκάκης, Γ.Ε. Μαρνέλλος και Μ. Κονσολάκης, *"Καταλυτική Διάσπαση Του N_2O σε Δομικά Ενισχυμένους Καταλύτες Ευγενών Μετάλλων"*, 10ο Πανελλήνιο Συνέδριο Χημικής Μηχανικής, Ιούνιος 4-6, 2015, Πάτρα.

Ε. Παχατουρίδου, Ε.Φ. Ηλιοπούλου, Μ. Κονσολάκης, Ι. Γιεντεκάκης, *«Επίδραση SO_2 κατά την καταλυτική διάσπαση N_2O σε καταλύτη Ir/Al_2O_3 ενισχυμένο με Ce»*, 10ο Πανελλήνιο Συνέδριο Χημικών Μηχανικών, Ιούνιος 2015, Πάτρα.

2014 **Ε. Παχατουρίδου**, Ε. Πάπιστα, Α. Δελημήτης, Μ. Βασιλειάδης, Α.Μ. Ευσταθίου, Ε. Ηλιοπούλου, Μ. Κονσολάκης, *«Επίδραση της προσθήκης CeO_2 στην επιφανειακή και καταλυτική συμπεριφορά καταλυτών Ir/Al_2O_3 κατά την διάσπαση του N_2O»*, 13ο Πανελλήνιο Συμπόσιο Κατάλυσης, Οκτώβριος 2014, Παλαιός Άγιος Αθανάσιος, Πέλλα.

Μ.Α. Γούλα, Ν. Χαρισίου, Κ. Παπαγερίδης, **Ε. Παχατουρίδου**, Ε.Φ. Ηλιοπούλου, *«Επίδραση της φύσης του φορέα στηριζόμενων καταλυτών Pt, Ir, Pd για την αντίδραση της εκλεκτικής καταλυτικής αναγωγής (SCR) οξειδίου του αζώτου (NO) με χρήση*

προπυλενίου (C$_3$H$_6$) ως αναγωγικό μέσο», 13ο Πανελλήνιο Συμπόσιο Κατάλυσης, Οκτώβριος 16-18, 2014, Παλαιός Άγιος Αθανάσιος, Πέλλα.

Α. Δελημήτης, **Ε. Παχατουρίδου**, Ε. Πάπιστα, Γ.Ε. Μαρνέλλος, Μ. Κονσολάκης, Ι. Γεντεκάκης, Ε.Φ. Ηλιοπούλου, «*Μελέτη της μικροδομής καταλυτών Ir υποστηριγμένων σε δομικά ενισχυμένη γ-Al$_2$O$_3$ για διεργασίες καταλυτικής διάσπασης N$_2$O με μεθόδους ηλεκτρονικής μικροσκοπίας*», 13° Πανελλήνιο Συμπόσιο Κατάλυσης, Οκτώβριος 16-18, 2014, Παλαιός Άγιος Αθανάσιος, Πέλλα.

Ε. Πάπιστα, **Ε. Παχατουρίδου**, Ε.Φ. Ηλιοπούλου, Ι. Γεντεκάκης, Γ. Γούλα, Γ.Ε. Μαρνέλλος, Μ. Κονσολάκης, «*Καταλυτική διάσπαση N$_2$O σε δομικά ενισχυμένους (CeO$_2$, La$_2$O$_3$) καταλύτες ευγενών μετάλλων (Pt, Pd) υποστηριγμένους σε αλούμινα*», 13° Πανελλήνιο Συμπόσιο Κατάλυσης, Οκτώβριος 16-18, 2014, Παλαιός Άγιος Αθανάσιος, Πέλλα.

2012   Α.Χ. Ψαρράς, **Ε. Παχατουρίδου**, Ε.Φ. Ηλιοπούλου, Α.Α. Λάππας , «*Επίδραση αλουμίνας στην παθητικοποίηση δηλητηριωδών μετάλλων (Ni) σε καταλύτες καταλυτικής πυρόλυσης (FCC)»*, 9° Πανελλήνιο Συνέδριο Χημικών Μηχανικών, 2012, Αθήνα.